NASA CR-72363

LIGHTWEIGHT MULTILAYER INSULATION SYSTEM

by

C. R. Lindquist and G. E. Nies

Prepared for

PACE ADMINISTRATION

-7953

UNION CARBIDE
LINDE DIVISION

NASA CR-72363

FINAL REPORT

LIGHTWEIGHT MULTILAYER INSULATION SYSTEM

by

C. R. Lindquist and G. E. Nies

Prepared for

NATIONAL AERONAUTICS AND SPACE ADMINISTRATION

February 23, 1968

CONTRACT NAS 3-7953

Technical Management
NASA Lewis Research Center
Cleveland, Ohio
James R. Faddoul

LIGHTWEIGHT MULTILAYER INSULATION SYSTEM

by

C. R. Lindquist and G. E. Nies

Union Carbide Corporation, Linde Division

ABSTRACT

The development work necessary to achieve low thermal conductivity and good gas conductance in self-evacuating multilayer insulation (SEMI) panel systems for liquid hydrogen space tankage is described. Tests of a prototype system applied to a 30-inch diameter calorimeter tank resulted in a heat flux in liquid hydrogen service of 0.63 Btu/hr. ft.^{2} for an in space condition and only 10 Btu/hr-ft^2 during ground hold. Conceptual designs for insulation systems for various shaped tanks and specifically a preliminary design for an 82.6 inch diameter spherical tank are presented.

TABLE OF CONTENTS

TABLE OF CONTENTS (Cont'd)

LIST OF FIGURES

LIST OF FIGURES (Cont'd)

LIST OF TABLES

LIGHTWEIGHT MULTILAYER INSULATION SYSTEM

C. R. Lindquist and G. E. Nies

Union Carbide Corporation, Linde Division

1.0 SUMMARY

It was the goal of this program to develop a lightweight, self-evacuating multilayer insulation (SEMI) panel concept for liquid hydrogen space tankage and determine its performance on a 30-inch diameter calorimeter tank. The concept was also to be used for the preliminary design of an insulation system for an 82.6-inch diameter liquid hydrogen tank. The insulation was to consist of shingled panels having rigid open cell polyurethane spacers and double aluminized Mylar radiation shields. Each panel would be filled with carbon dioxide gas which would cryopump to the desired vacuum level upon cooling the cold end to liquid hydrogen temperature.

Based on thermal conductivity measurements, gas transmittance measurements, and cost estimates, the conclusion was reached that the spacer system within the multilayer insulation should consist of three layers of foam: one solid layer and two with square punched holes. Requirements for storage of the system in air indicated that a laminate of Mylar/aluminum/aluminum/ Mylar would be suitable for the external portion of the shingled panels and that a carbon dioxide purge would be required for the area behind the panels where a laminate of aluminized Mylar was used. Analysis and test work indicated that carbon dioxide would be the best gas to use for cryopumping.

Conceptual designs were determined for spherical, cylindrical and ellipsoidal tanks utilizing the shingled panel approach. A more detailed preliminary design was made for an 82.6-inch diameter tank for which, based on the measured thermal conductivity, the heat flux would be 0.7 Btu/hr.ft.sq.

Gas transmittance tests of a perforated Mylar honeycomb indicate a much better gas transmittance than has been experienced with the foam. It is, therefore, recommended that some initial development work be performed to learn how to incorporate this Mylar honeycomb within the multilayer insulation in order to take advantage of this better transmittance and attempt to reduce the time needed for a SEMI panel system to reach equilibrium (about 40 hours is required as presently designed). This concept should then be applied to the calorimeter tank to evaluate its performance and then the 82.6-inch diameter tank should be insulated to demonstrate its applicability to space craft tankage.

2.0 INTRODUCTION

For proper thermal performance, multilayer insulation systems must maintain a vacuum in the sub-micron range. One method to achieve this degree of vacuum which has been evaluated (see Reference 1, CR-72017) is to fill the insulation system with a condensible gas which will cryopump when a portion of the insulation system is cooled to the temperature of liquid hydrogen. This concept, when applied to insulation installed in discreet panels is referred to as the self-evacuating multilayer insulation (SEMI) panel concept.

In order for the SEMI panel concept to be effective, it is necessary that a part of each individual sealed panel be in contact with a surface maintained at the temperature of the stored cryogen. One means of accomplishing this while keeping edge effects (solid conduction through the jacket material, etc.) to a minimum is to install the panels in a shingle arrangement. The basic conceptual design for SEMI panels is illustrated in Figure 1. The shingle concept as it might be applied to a cylindrical tank is shown in Figure 2.

In previous work with the SEMI panel concept described in Reference 1 there were apparently some problems with self-evacuation by cryopumping. It seemed that the contained gas (carbon dioxide) was not transmitted through the panel to the cold surface at a sufficiently high rate so that the indicated residual gas pressure was too high. Although the achieved thermal performance (a heat flux of 0.88 Btu/hr.ft.^{2} was measured) was considered attractive, it was felt that further improvement could be made if better gas transmittance through the insulation system could be effected. Early test results also indicated a possibility that the vacuum jacket did not fully recover dimensionally with the insulation panels evacuated and the external pressure reduced from atmospheric pressure to vacuum to simulate a vehicle launch into space, thereby resulting in a further degradation in thermal performance. Concepts to achieve a reduced contact area between the spacers and the radiation shields and jacket material were proposed to alleviate this condition as well as to improve gas transmittance by the introduction of physical irregularities into the system.

It was the goal of this present program to evaluate these solutions by development testing and to demonstrate the results on a 30-inch diameter calorimeter tank. An application design was to be developed for spherical, ellipsoidal and cylindrical tankage in a general way and specifically the design of a SEMI panel insulation system was to be generated, based on these principles for an 82.6-inch diameter spherical tank as a practical application of the concept to space tankage.

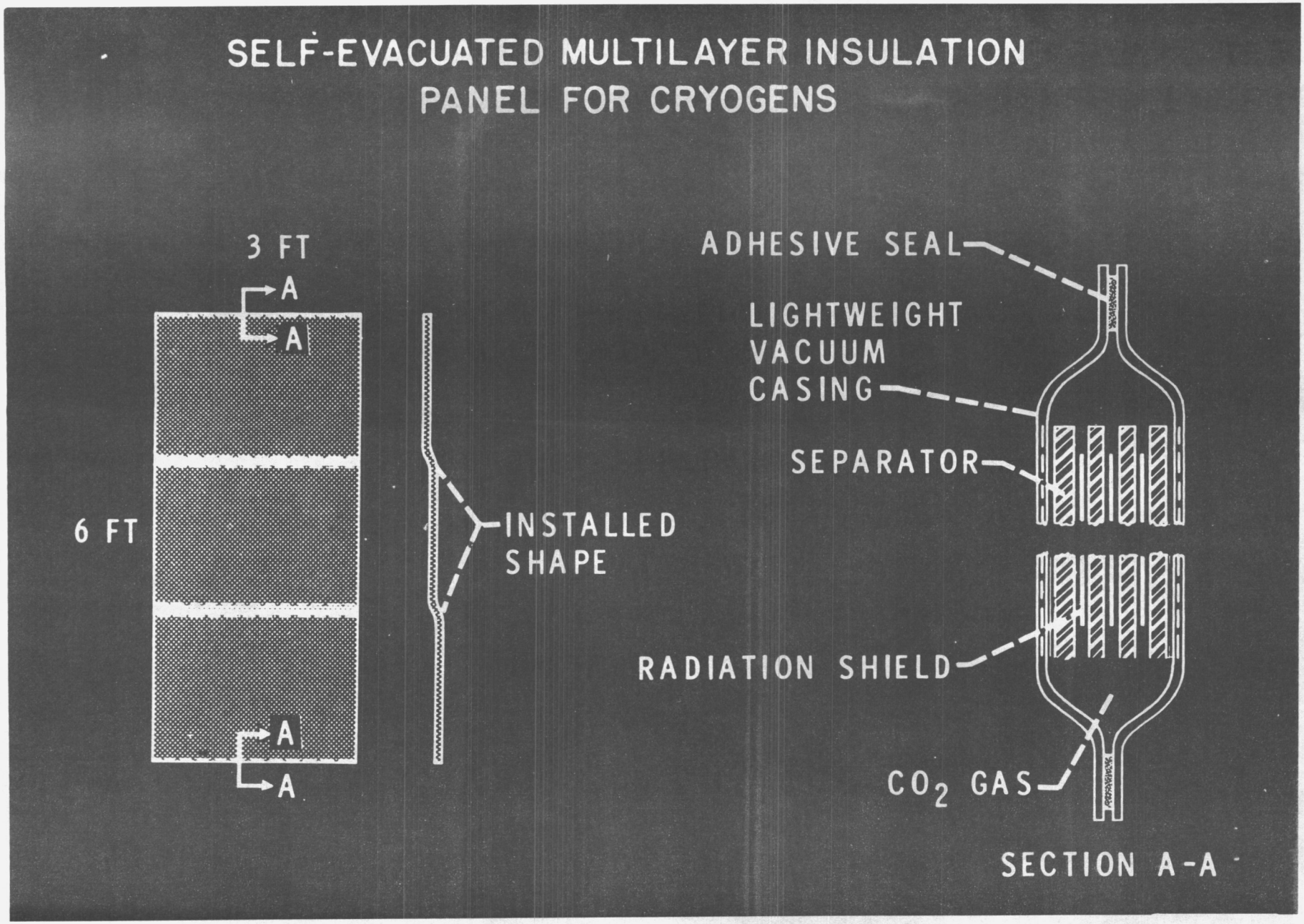
SELF-EVACUATED MULTILAYER INSULATION
PANEL FOR CRYOGENS
3 FT
A
A
6 FT
A
A
INSTALLED
SHAPE
ADHESIVE SEAL
LIGHTWEIGHT
VACUUM
CASING
SEPARATOR
RADIATION SHIELD
CO_2 GAS
SECTION A-A

Figure 1

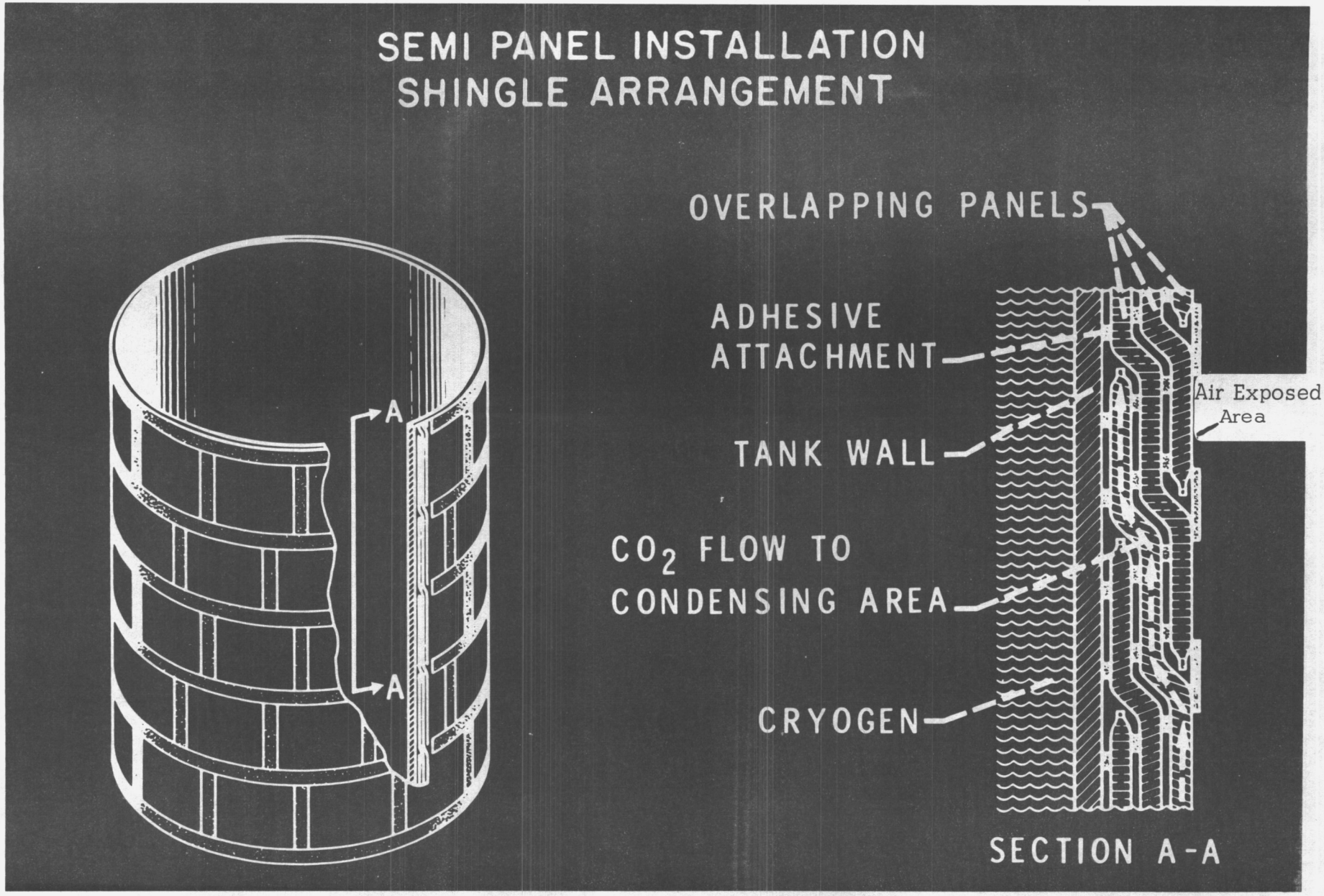
SEMI PANEL INSTALLATION
SHINGLE ARRANGEMENT
A
A
OVERLAPPING PANELS
ADHESIVE ATTACHMENT
TANK WALL
CO_2 FLOW TO CONDENSING AREA
CRYOGEN
Air Exposed Area
SECTION A-A

Figure 2

3.0 RESULTS AND CONCLUSIONS

During the course of this work, an improved spacer concept that resulted in better thermal performance and more rapid evacuation was evolved. Panel storage time in air up to 30 days was demonstrated. A heat flux of only 0.63 Btu/hr-ft.^{2} was demonstrated on a 30-inch diameter calorimeter tank insulated with three shingle systems in the space condition. The ground hold heat flux approached 10 Btu/hr-ft.^{2}. A preliminary design for an 82.6-inch diameter spherical tank was conceived.

A brief discussion of the results and conclusions of the self-evacuating multilayer insulation development program are given in this section. Detailed results are given in Section 4. Tabulated data, detailed analyses, etc. are included in the Appendices, referenced in Section 4.

3.1 Foam Spacer Configuration

3.1.1 Analytical Study and Screening

Previous work with self-evacuating multilayer insulation systems indicated that there was some residual compression of the insulation when the compressive load of the atmosphere was removed. In an effort to reduce the support area for solid conduction and thus minimize the effect of residual compression, four concepts were chosed for screening. These included spacers having punched holes, spacers utilizing strips of foam material, foam maze on a silk net spacer configuration and dimpled casings. The first two were chosen for further thermal and gas transmittance testing on the basis of effectiveness and cost as well as experience gained from pressure deflection tests of small (18" x 12") sample test panels. No mechanical failure of the foam was noted with the compression loads up to 1 atm.

3.1.2 Thermal Tests

In an effort to determine the effects of support area and a method of support, a series of thermal tests were conducted at NASA, Lewis Research Center, using a flat plate calorimeter. Compressive loads from 0.001 psi to 1 atm. were imposed on samples. While the results were not conclusive, a spacer configuration consisting of two layers of foam with 1-1/4" square holes on 2" centers and one solid layer of foam was chosen for further work. At the minimum load of 0.001 psi this configuration gave a heat flux of 0.04 Btu/hr.sq.ft.

3.1.3 Gas Transmittance Tests

Transmittance tests were performed for a number of spacer configurations in panels 1 ft. wide by 3 ft. long. The data are summarized in Figure 3. While there was considerable scatter in the data, especially on the low end, it is apparent that the punched hole spacer configuration offers somewhat better gas transmittance than do stripped spacers. However, it is interesting to note that the panel made up with double layers of solid foam in each layer

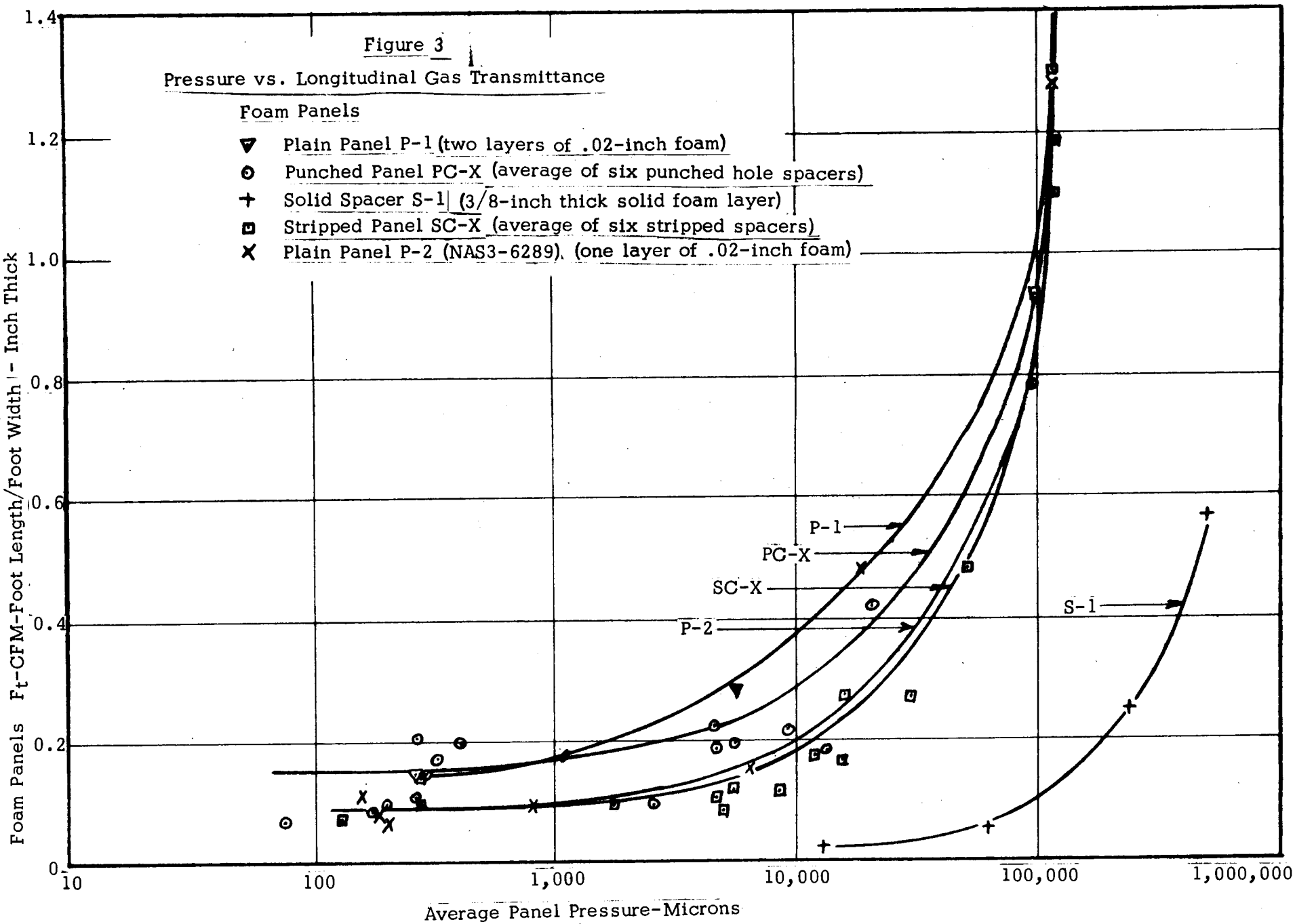
Figure 3
Pressure vs. Longitudinal Gas Transmittance
Foam Panels
Plain Panel P-1 (two layers of .02-inch foam)
Punched Panel PC-X (average of six punched hole spacers)
Solid Spacer S-1 (3/8-inch thick solid foam layer)
Stripped Panel SC-X (average of six stripped spacers)
Plain Panel P-2 (NAS3-6289), (one layer of .02-inch foam)
P-1
PC-X
SC-X
P-2
S-1
Foam Panels Ft-CFM-Foot Length/Foot Width - Inch Thick
1.4
1.2
1.0
0.8
0.6
0.4
0.2
0
10
100
1,000
10,000
100,000
1,000,000
Average Panel Pressure-Microns

have about the same transmittance as do the punched hole panels. Similarly, panels made up with a single layer of foam have very much the same transmittance as do the stripped panels. The solid 3/8" thick foam panel (designated S-1) has much poorer transmittance than any of the others. This may indicate that the gas transmittance that is present is due to saw marks in the foam resulting from the slicing operation. On the basis of these data it was decided to proceed with the punched hole spacer configuration.

Data were also obtained for a Mylar honeycomb material pierced through the cell walls to provide a path for gas. This material exhibited a gas transmittance much higher than any of the foam configurations as can be seen on Figures 3 and 4. Since this honeycomb material exhibits such a good transmittance it is recommended that tests be performed with a system utilizing this honeycomb within an insulation panel made up of foam spacers and aluminized Mylar radiation shields. It is probable that the honeycomb material will have to be faced on one side to prevent longitudinal collapse when the atmospheric pressure load is applied, and that the radiation shields will have to be perforated in some manner to permit gas to flow from the foam layers to the honeycomb and hence to the vacuum source.

3.1.4 Foam Compression Tests

As a quality assurance procedure, the new foam buns obtained for this program were subjected to compression tests and density measurements. The density of the four buns ranged between 2.0 and 2.1 lbs./cu.ft. The compressive strength was well above 20 psi. Therefore all of the foam material was considered usable for application to spacers in SEMI panels.

Figure 4

Pressure vs. Longitudinal Gas Transmittance

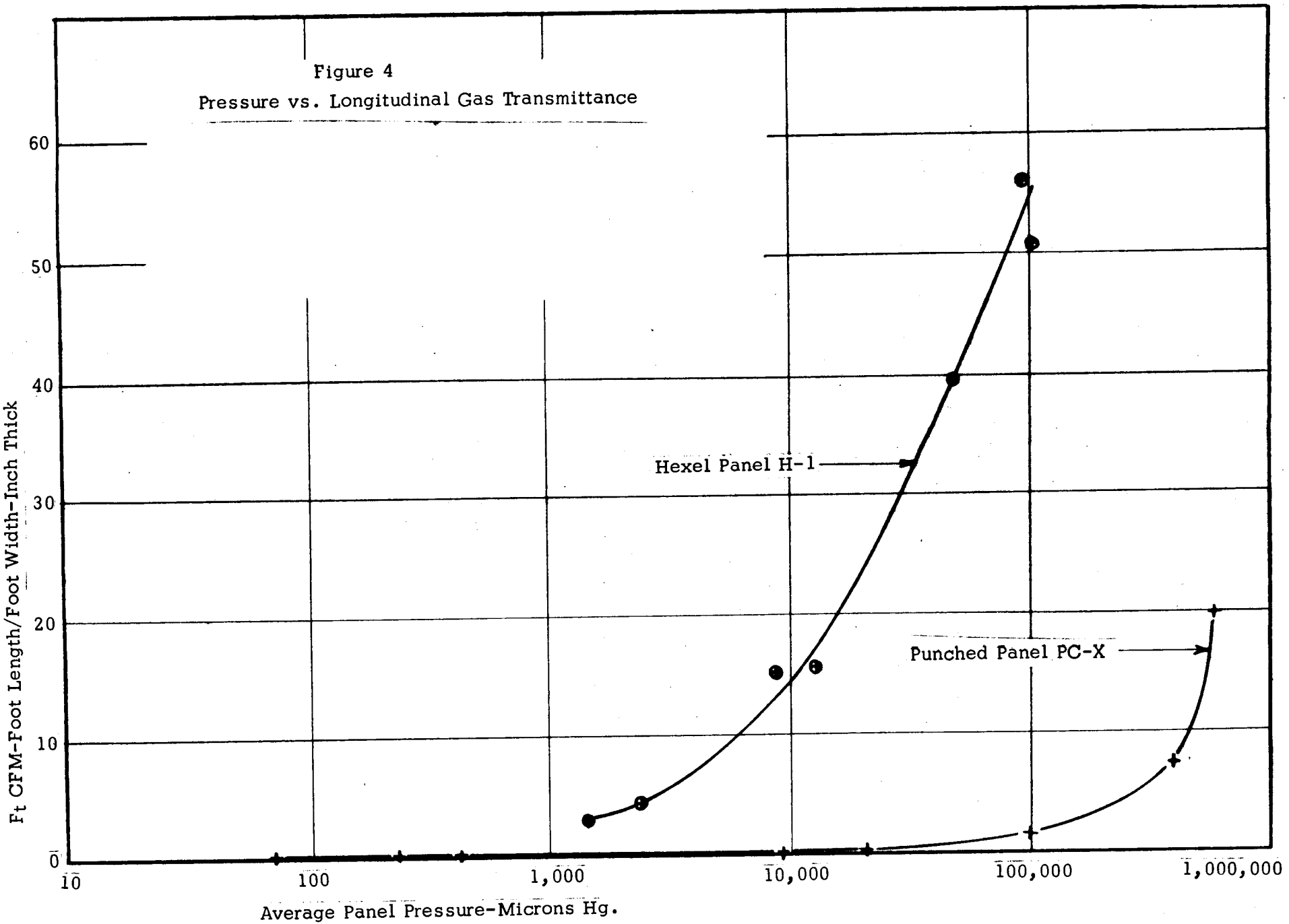

3.2 Panel Storage

3.2.1 Analytical Study of Panel Storage

A number of concepts were investigated to permit storage of insulation panels after filling with CO_2. The panels must be capable of cryopumping to a pressure of 1×10^{-4} torr at liquid hydrogen temperature 30 days after the initial installation on a vehicle. It was determined that a quantity of 0.5 grams of palladium oxide getter* would be needed to react with the hydrogen off-gassing from the materials within the panels. The recommended method of preventing permeation of air gases into the panels is to make the exposed area of each panel (that portion exposed to the atmosphere which makes up one-sixth of the total panel area for a three layer shingle arrangement) of an impermeable material. A Mylar/aluminum/aluminum/Mylar laminate is recommended and was employed on the calorimeter tank. It was recommended that the area behind and between the panels be purged with CO_2. This approach of the impermeable outer casing was the lightest weight and simplest method of maintaining the CO_2 atmosphere within the panels.

3.2.2 Permeability Tests

Permeability tests were conducted on both 4-ply aluminized Mylar and Mylar/aluminum/aluminum/Mylar (MAAM) casing materials. The aluminized Mylar laminate in the as received, wrinkled and drawn conditions, exhibited a permeability rate in the order of .3 to $.5 \times 10^{-5}$ atm cc helium/sec.ft.^{2} atmosphere. The MAAM laminate permeability was less than 4×10^{-8} atm. cc helium/sec.ft.^{2}.atm, the low limit of the apparatus. The former material was used for those portions of the paneled jackets exposed to the carbon dioxide atmosphere (5/6 of the total panel area) and the latter was used for the air exposed side of the panels.(1/6 of the total panel area).

3.2.3 Storage Life Test

Two concepts to obtain storage of self-evacuating insulation panels for extended periods of time were tested utilizing a 40-inch square flat plate test apparatus. The concepts were impermeable outer casing and carbon dioxide purge. Two panels embodying these concepts were placed side by side and shingled with dummy panels for simulataneous test purposes. The panels, filled with carbon dioxide, were chilled to liquid hydrogen temperature and the cryopumping effects noted. After one week of storage the cryopumping test was repeated.

It may be concluded from these tests that either the impermeable outer casing concept or the carbon dioxide purge system could be workable.

* Union Carbide patent No. 3,108,706

However, it was found that the carbon dioxide purge bag had to have a reasonable low permeability value, because air could permeate through it into the carbon dioxide atmosphere and thence into the panel. The impermeable outer casing approach, therefore, is simpler, results in a lighter weight system and was recommended for the calorimeter tank application.

3.3 Cryopumping

3.3.1 Theoretical Pumpdown Characteristics of Cryopumped Panel

In order to develop criteria for the satisfactory operation of a cryopumped panel, it is desirable to be able to predict the time necessary to obtain the low pressure required for optimum thermal performance. Although the complexity of the problem prohibits an exact analytical solution, an approximate numerical solution has been obtained that generates a theoretical pumpdown curve. This solution also was used to assess the performance of the panel when filled with gases other than carbon dioxide.

A numerical solution for this combined heat and mass transfer problem was developed and results were obtained on an IBM 360 computer. The solution combines an analytical expression for the transient temperature profile with numerical computations for the mass transfer.

Results were obtained on the basis of two different heat and mass transfer mechanisms, i.e. flow longitudinally along the shingled panel and flow perpendicular to the panel layers. The real case is a combination of these (the perpendicular mass flow occurring around the edges of the radiation shields), and the results bracket the real case. Ammonia, N-butane, carbon dioxide, N-propane, methane, nitrogen and oxygen were investigated. Considering mass flow perpendicular to the layers, neglecting the barriers caused by the radiation shields, which assumption would be expected to result in lower than actual pumpdown time, all gases will cryopump down to less than 0.1 micron mercury in less than forty minutes. Considering flow parallel to the layers, the pumpdown time for methane, oxygen and nitrogen appears to be excessively long (over six hours.)

3.3.2 Cryopumping Tests

In order to verify the analysis and make a selection of the cryopumping gas to be used in later work, a demonstration test was conducted utilizing the flat plate tester. As predicted by theory, the carbon dioxide filled panel reached a lower vacuum level in a shorter period of time than did the same panel when it was filled with nitrogen gas. On this basis, carbon dioxide gas is recommended for self-evacuating insulation panels. A temperature distribution for both cases is given in Section 4.3.2.

3.3.3 Vacuum Gauge Tests

Throughout the program, considerable difficulty was experienced in measuring the degree of vacuum achieved by cryopumping CO_2. After test work with a number of different arrangements of apparatus, utilizing both cold cathode ionization gauges and hot cathode ionization gauges with carbon dioxide and nitrogen gas as the cryopumped medium, the conclusion reached was that the problem was offgassing the gauges themselves. Indications were that this gas was hydrogen. The degree of vacuum indicated by the gauge depends upon the gas transmittance between the gauge and the vacuum source. Palladium oxide getter should be used in the vicinity of the gauge. This getter material chemically reacts with the hydrogen to form water. The water in turn, depending upon the transmittance, will be cryopumped on the cold surface. It is probable in most of the tests because the gauges were gas transmittance limited even though the gauges read a high pressure level or were off scale, that the vacuum in the insulation system itself was adequate.

3.4 Calorimeter Tank

In order to demonstrate the feasibility of the self-evacuating multilayer insulation panel concept, a double guarded calorimeter, 30 inches in diameter, was insulated with a shingled panel system.(see Fig. 5) The insulation consisted of alternate layers of foam and double aluminized Mylar encased within a Mylar laminate jacket. A triple shingled arrangement was employed and the air exposed 1/6 of each panel a casing constructed of Mylar/aluminum/aluminum/Mylar laminate designed to be impermeable. The area behind the panels was purged with carbon dioxide and the panels were carbon dioxide filled. Each spacer layer consisted of a solid sheet of foam and two punched hole sheets of foam in the configuration described in 3.1.2.

The insulation panels were fabricated and installed on the calorimeter tank at the Linde facility in Tonawanda, New York, Testing was performed in a test chamber at NASA-Plumbrook Station, Ohio. Two series of tests were conducted simulating ground hold launch and space storage. These were separated by a 30-day period during which time the insulated calorimeter tank was stored in air to simulate ground storage after application of SEMI panels. A final test was conducted with the chamber evacuated and the panels vented to the chamber. Test results of all three tests were quite similar. The measured heat flux was 0.63 Btu/hr.ft.^{2}.

After cooldown, the ground hold heat flux approached 10 Btu/hr./ft.^{2}. The data for the space condition are shown in Figure 6. Here the weight penalty due to thermal effects, expressed as weight of the insulation plus integrated weight of the hydrogen boil-off after launch, all on a per square foot basis, versus elapsed time is shown. It will be seen that the first two tests where the insulation panels actually cryopumped were practically identical. Steady-state rate was reached after about 40 hours of flight. Steady state was reached somewhat earlier in the third test with the panels vented to the chamber, probably because of a better vacuum within the panels at initial fill. It is to shorten this transient period that further work with the perforated Mylar honeycomb is recommended.

The test results indicate that any effect of gas transmittance in the semi-panels was eliminated. Order of magnitude calculations indicate that 64% of the heat flux is due to solid conduction, 11% is due to radiation and 25% is due to edge effects (i.e., conduction along the jacket material and radiation shields). In view of this breakdown, any additional development should be directed toward reducing the solid conduction. It is possible that some of the effect is due to residual compression, and this should be investigated.

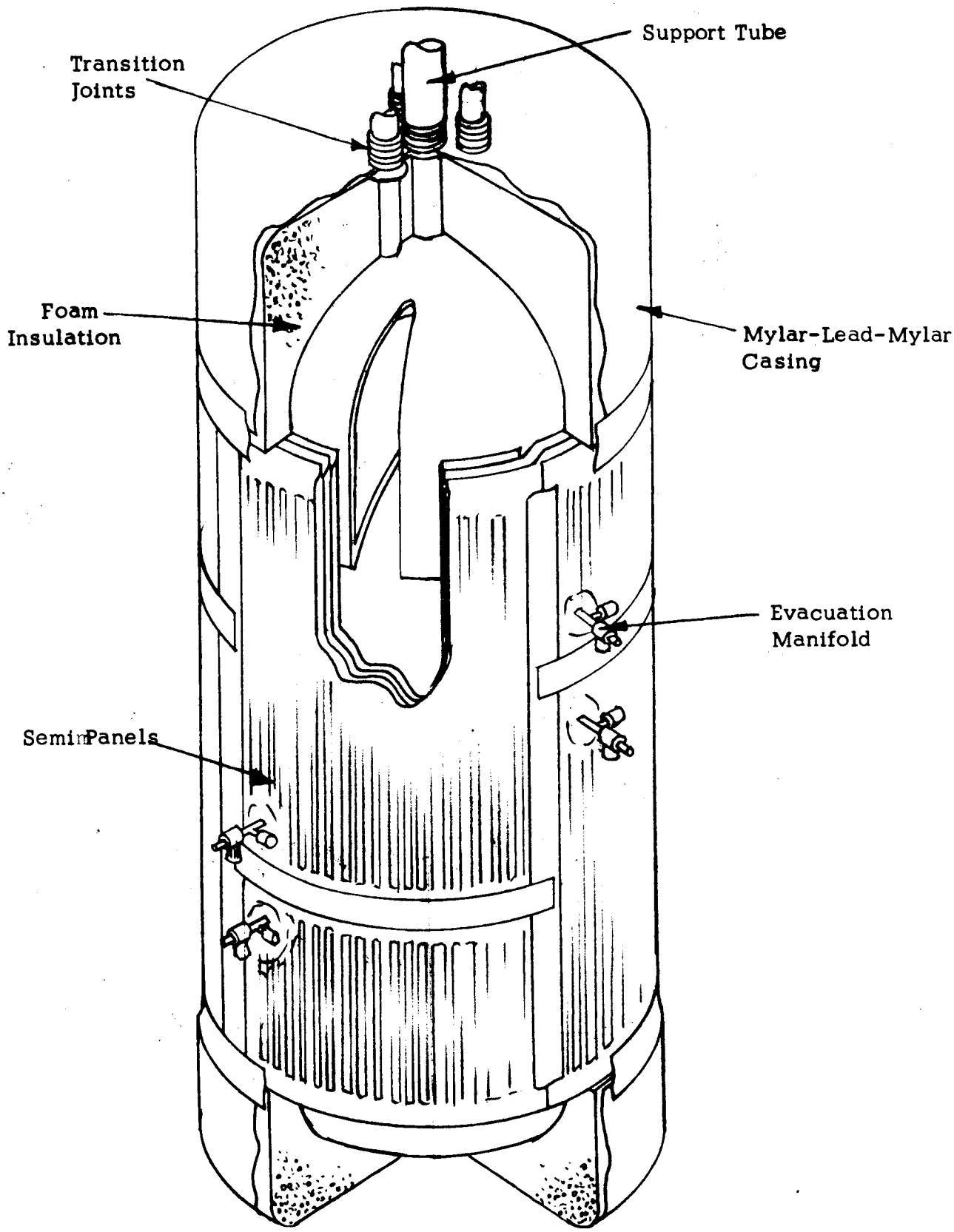

Figure 5 Calorimeter Tank Insulation System

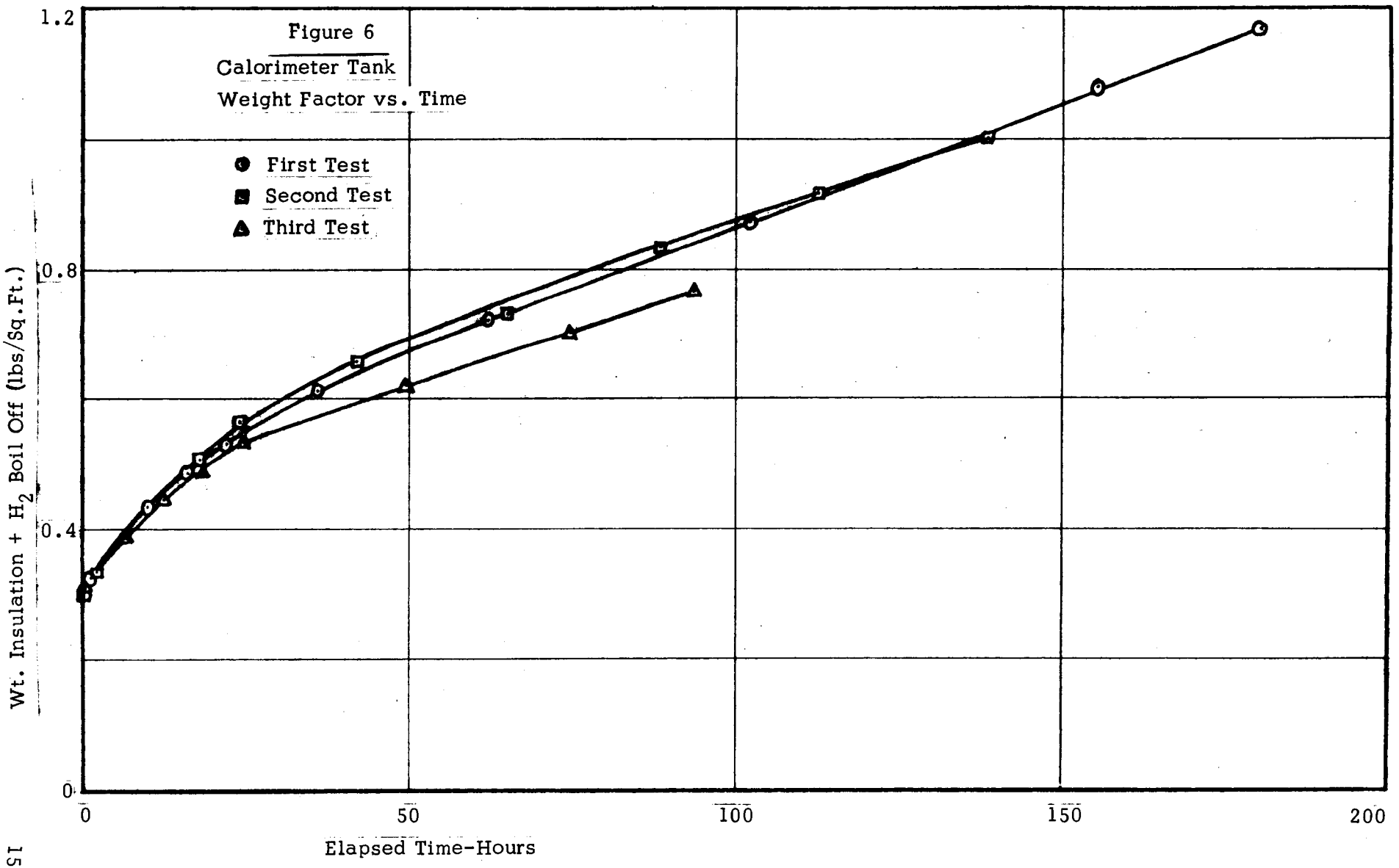
Figure 6
Calorimeter Tank
Weight Factor vs. Time
First Test
Second Test
Third Test
1.2
0.8
0.4
0
Wt. Insulation + H_2 Boil Off (lbs/Sq.Ft.)
0
50
100
150
200
Elapsed Time-Hours

3.5 Application

A general investigation and analysis was made for various sizes and shapes of aerospace tankage to which the self-evacuating panel concept could be applied. Spherical, cylindrical, and ellipsoidal tanks were considered. It was concluded that a shingled pattern similar to that used on the calorimeter tank was most applicable. Specific panel dimensions were worked out for three sizes of spherical tankage in this preliminary investigation.

Upon completion of the preliminary investigation a more detailed design analysis was conducted for an 82.6 inch diameter hydrogen tank supported by a cone at its girth. The specific design recommended called for three pole cap panels at the top and bottom and a total of 42 panels around the girth (21 above the support cone and 21 below it). The performance was predicted for this design utilizing a Fortran computer program for the IBM 360/40 computer. Based on the data obtained by testing the calorimeter tank, the total heat leak into the tank would be about 190 Btu/hr. including provision for the support. This latter figure results in a net heat flux of 0.67 Btu/hr.ft.^{2} for this particular design. This could be improved significantly by using larger individual panels or perhaps by breaking the radiation shields at each shingled layer. The performance could also be improved significantly by using additional spacer layers or inclusion of the Mylar honeycomb. It is recommended that after some development with the interrupted shields and the Mylar honeycomb, this design be detailed and the tank insulated and tested.

3.6 Recommendations

It is quite probable that the insertion of one or more sheets of Mylar honeycomb will significantly accelerate the approach to thermal equilibrium by enhancing gas flow to the cryopumping surface. It is, therefore, recommended that its application to shingled panels be developed and the concept tested on the calorimeter tank. The new design should then be applied to the 82.6 inch diameter tank, and that tank insulated as a practical demonstration of the SEMI panel concept.

Application of Mylar honeycomb will reduce the overall heat flux, but its effect and the effect of cutting the radiation shields to enhance gas transmittance and reduce lateral heat flow should be evaluated. Other means to reduce solid conduction should be sought. It is also recommended that the effects of residual compression of the insulation be investigated and any effects of residual gas within the cellular structure evaluated.

A program aimed at getting a better knowledge of the vacuum gauging problem is recommended.

4.0 Foam Spacer Configuration

4.1.1 Foam Spacer Configuration Study and Screening

One objective of this program was to develop a spacer configuration which has a reduced support area (area of compression) such that the resulting panel demonstrates an improved heat flux under low loads. The materials used were .02 in. thick rigid polyurethane foam and double aluminized Mylar radiation shields. Thermal testing of lightly loaded multilayered insulation samples by NASA, Lewis Research Center, indicated improved insulation system performance for spacers having a contact area of 10 to 30 percent of the sample area. Therefore, an investigation of the effects of variables such as strip width and support area was undertaken to determine the optimum spacings and web widths necessary to achieve both thermal and gas transmittance improvements. Strips were limited to .02 inch thickness, over a range of 1/16 to 9/16 square inches at support areas. All spacers in any particular test specimen were identical in strip width and support area.

In order to select two panel configurations for thermal and gas transmittance optimization studies, small sample panels of four different configurations were fabricated and subjected to compressive tests. Preliminary test panels consisted of spacers and aluminized Mylar radiation shields enclosed in 4-ply aluminized Mylar casing material. A support area of 13% composite spacer was used for these tests.

The four sample panels fabricated and tested used (1) spacers of foam maze over silk netting; (2) a dimpled casing material; (3) two layers of crisscrossed foam strips bonded to a .02-inch thick foam sheet; and (4) spacers of .02 -inch thick foam with punched holes and a solid .02-inch thick solid sheet. A test panel consisted of seven layers of spacers and six radiation shields encased within a jacket of four-ply double aluminized Mylar. The panels were 18" x 12".

The panel utilizing the foam maze over silk net spacers consisted of one aluminized Mylar radiation shield with two foam maze over silk net spacers on either side. Each spacer consisted of .020 inch thick by .25 inch wide open cell foam strips bonded to a .0035 inch thick 100% silk net, having a mesh of approximately 14 threads per inch in both directions. Foam strips on adjacent foam maze spacers were mismatched by one half space (See Figures 7 and 8) in order to achieve minimum support area. The foam strips, located on 1-1/16 inch centers were bonded to the silk net using small patches of a heat sealable Mylar film at numerous points.

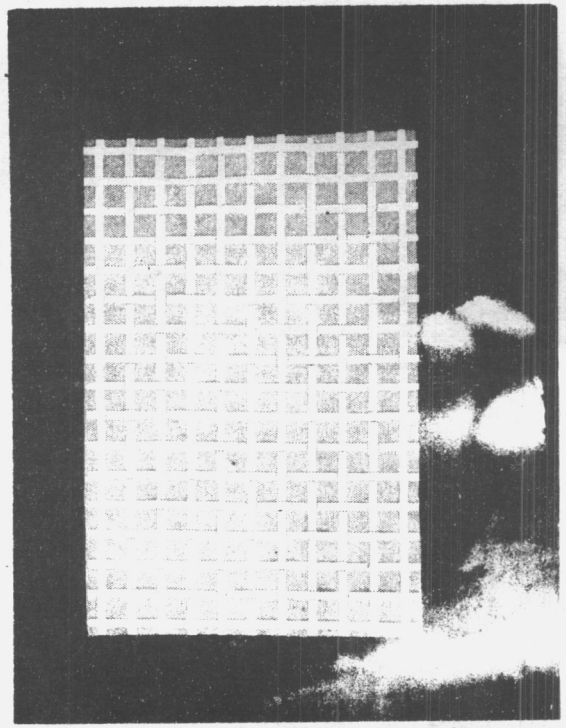

Figure 7 Foam Maze On Silk Net Spacer

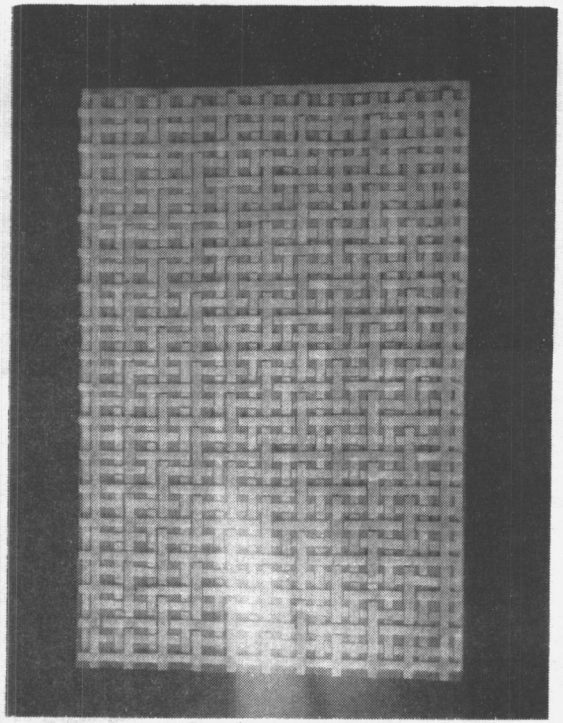

Figure 8 Two-Layer Maze On Silk Net Spacer

The dimpled casing material panel consisted of 7 layers of .20 inch thick foam with six radiation shields. The dimpled casing material was obtained by thermo-vacuum forming the 4-ply aluminized Mylar material over a form constructed of 7/8" diameter metal washers thumbtacked to a board in a 60° pattern. The center-to-center distance of the dimples was 1-1/2 inches.

The third panel configuration, illustrated in Figure 9 consisted of spacers comprised of two layers of .020 inch thick foam strips crisscrossed on a .020 inch thick foam sheet. A total of seven of these composite spacers and six aluminized Mylar shields were used. The 3/4 inch wide strips, located on 2-1/4 inch centers, were bonded at right angles to each other and subsequently bonded to the foam sheet with Miracle Contact Cement. (Actual panels would use Narmco 7343/7139 adhesive.)

The fourth compression test panel contained 7 composite spacers with 6 aluminized Mylar radiation shields. Each composite spacer consisted of three .020 inch thick foam sheets. However, to reduce the support area, two of the three sheets contained 13/16" square punched holes located in straight rows, 5/16 inches apart. The sheets with holes were assembled mismatched by one-half space (See Figure 10), and adjacent to each other to obtain the minimum support area.

The spacers were tested by evacuating the sealed panel to obtain various compressive loads. The panel thickness was then measured at four separate support locations and averaged. This procedure was repeated at several pressure levels. The averaged data is plotted on Figure 11. Compressive cycling data between atmospheric pressure and vacuum is also presented in Appendix 1.

The dimpled casing material method, although in a somewhat limited fashion, might also offer improvement to the thermal and transmittance properties of the insulation system. The advantage of this method is limited by the fact that any improvements are available only for the recovered insulation system. Figures 12 and 13 respectively show the compressed and recovered dimpled panels. The compression tests indicated that the dimples started to compress at .3 psi and were completely flattened at 5.0 psi compressive load.

All of these reduced support area configurations appear feasible. Any of the three foam spacer configurations appear to offer sufficient strength such that handling is not a problem. Side slip, noted previously in tests involving .040 inch thick spacers, was not observed in these tests using the

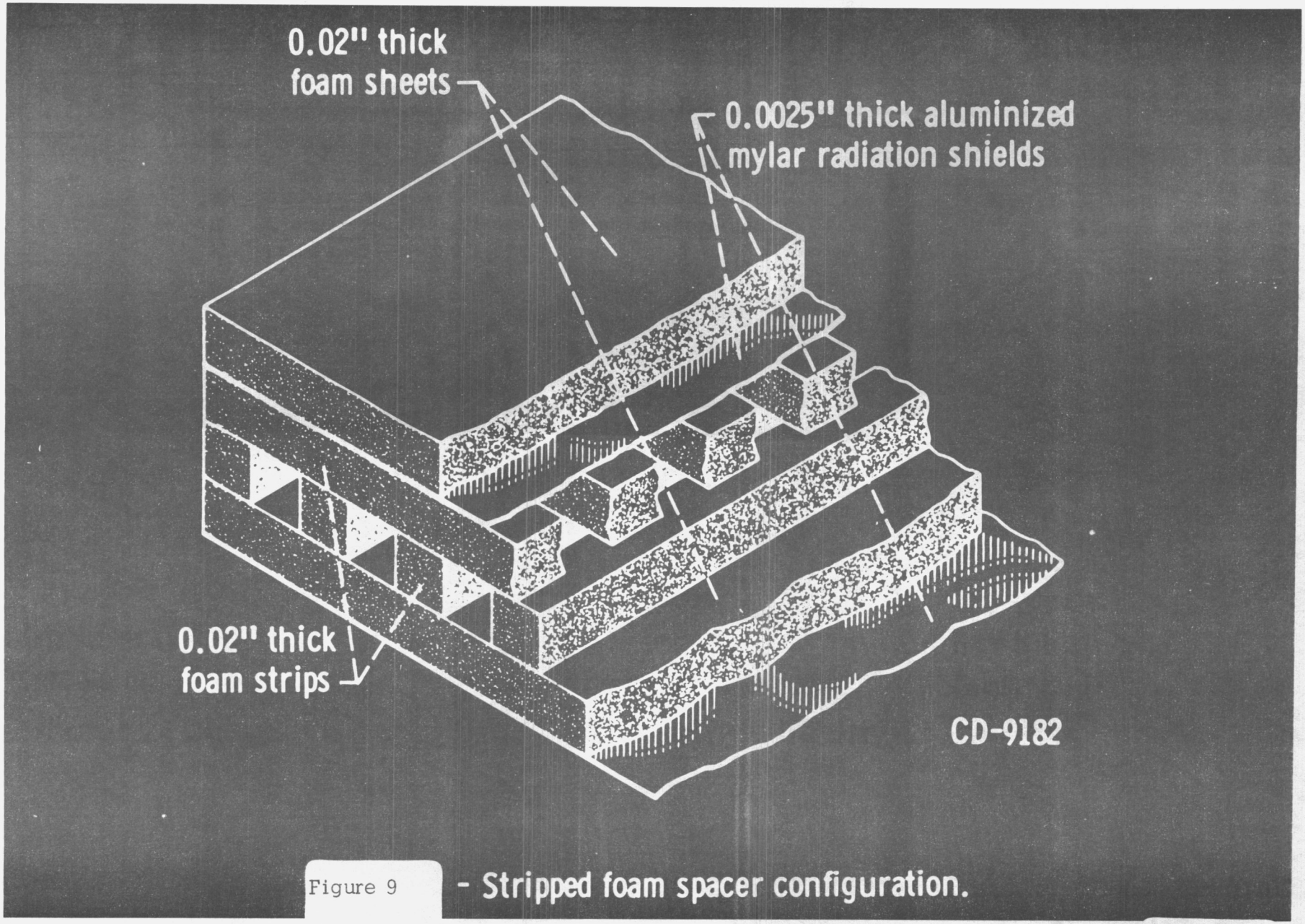

Figure 9 - Stripped foam spacer configuration.

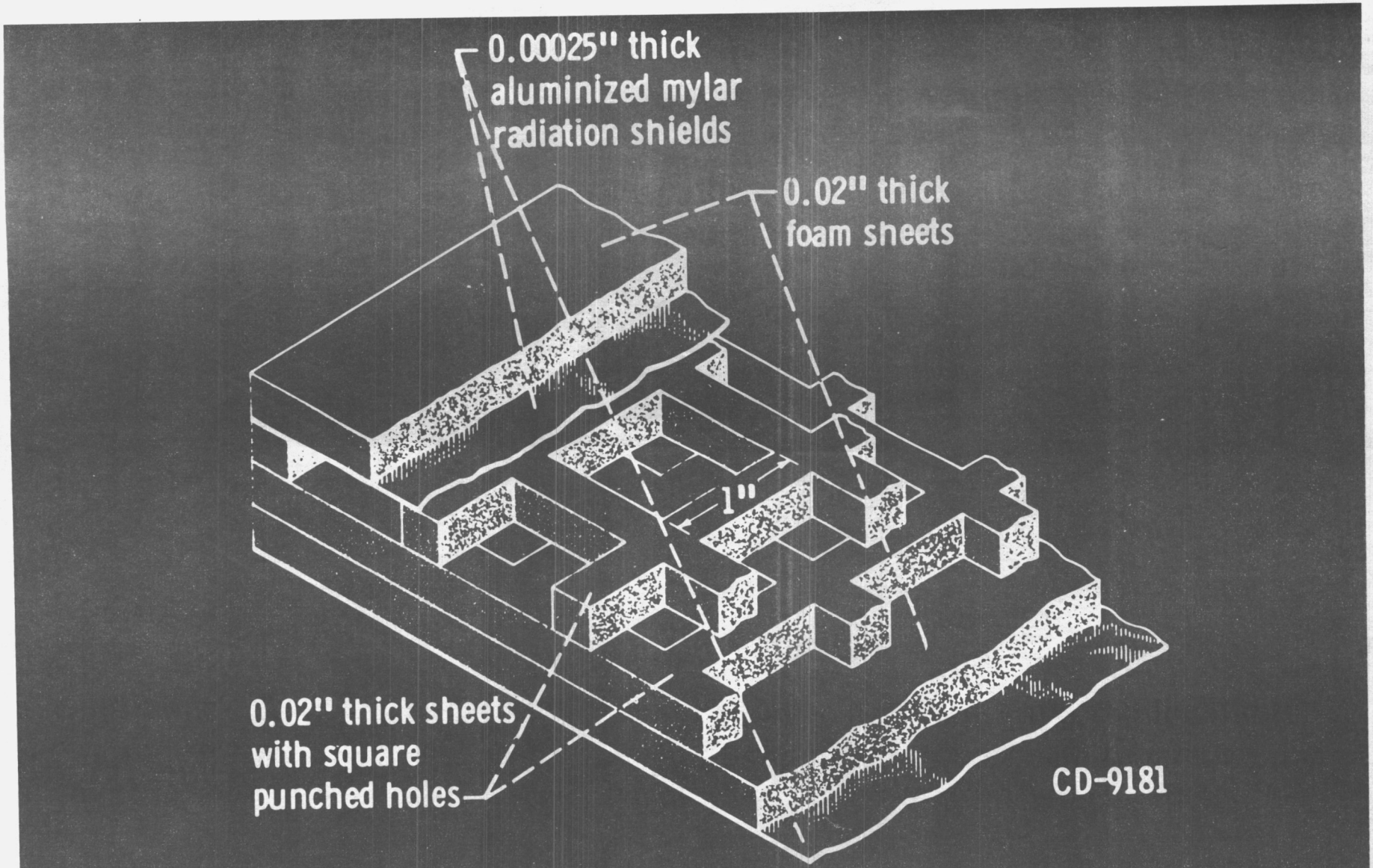

Figure 10 - Punched hole spacer configuration.

Figure 11

PRESSURE DEFLECTION CURVE
PRELIMINARY PANEL TEST
(TASK I) ROOM TEMPERATURE
(SEE Appendix 1 FOR DATA)

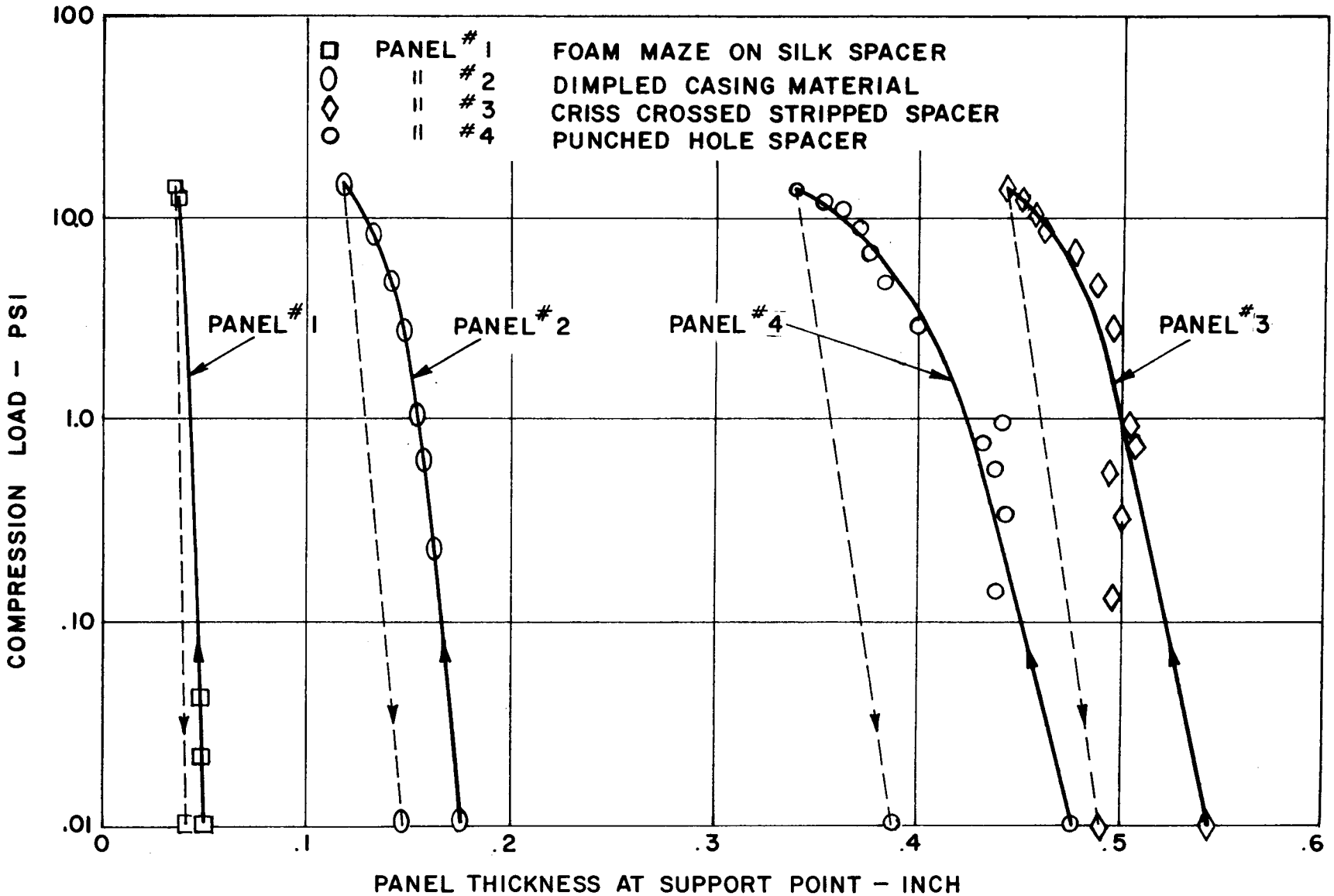

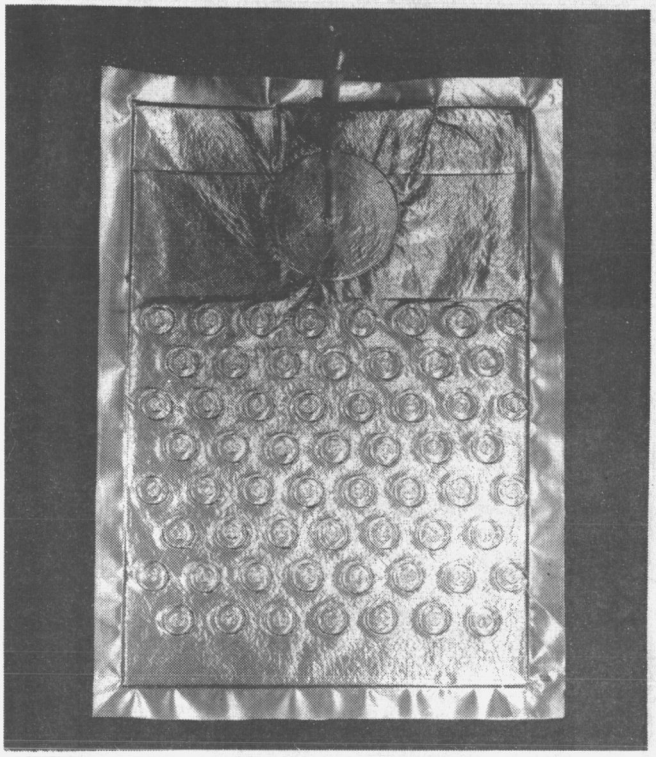

Figure 12 Dimpled Panel Compressed At One Atmosphere

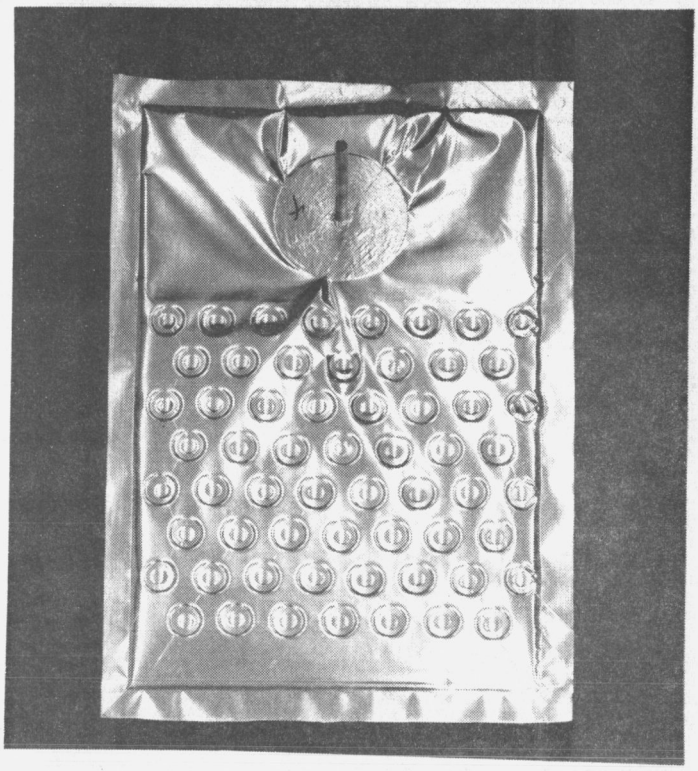

Figure 13 Dimpled Panel Recovered

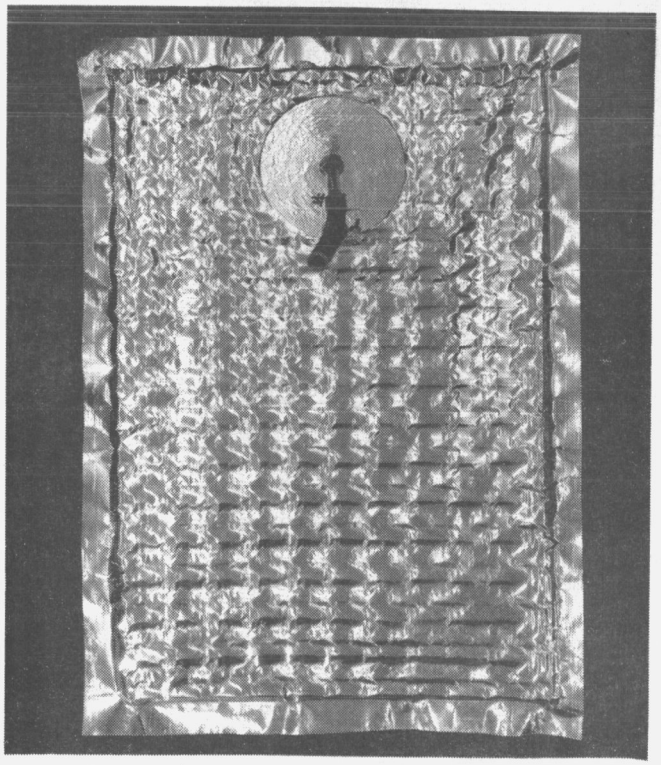

Figure 14 Compressed Panel Using Punched Hole Spacers

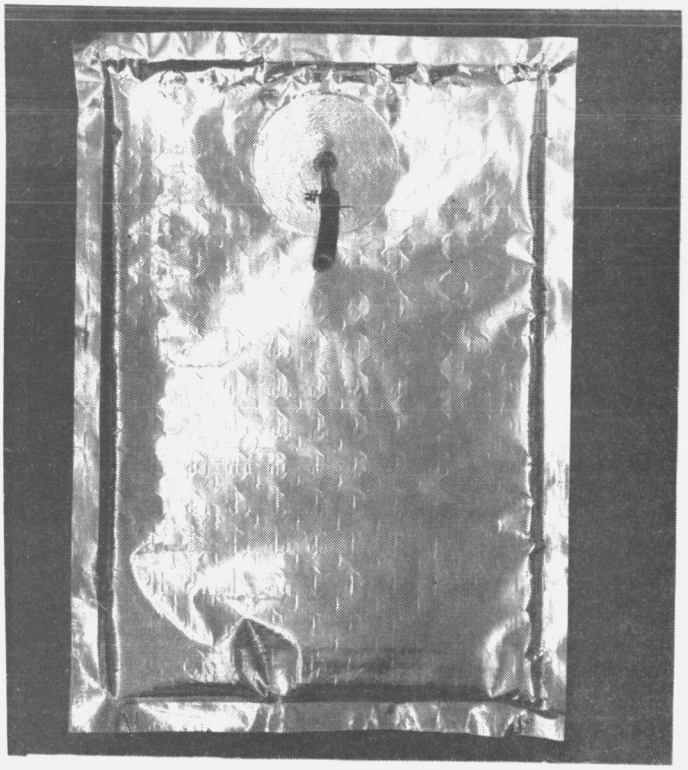

Figure 15 Recovered Panel Using Punched Hole Spacers

.020 inch thick spacer. Likewise, the panels did not distort and warp during these tests to the degree that was observed during previous tests performed under Contract NAS 3-6289. Finally, from the presented data it is observed that any of the three spacer configurations would be acceptable from a load bearing standpoint, as indicated by the similarity of the slopes of the curves. Panel #3 is believed to be thicker than Panel #4 because of the additional thickness of the adhesive and the increased rigidity of the foam at the support points due to the adhesive. Panel #3 and Panel #4 contain the same number of foam thicknesses. Therefore, since all satisfy the recovered and compressed load conditions, it appears that economic considerations are in order to determine which two of the three configurations should be further investigated. In terms of cost of materials, the foam maze on silk net costs approximately twice as much as the punched hole spacer and three times the cost of the double stripped foam spacer. In terms of labor, the cost to fabricate the foam maze on silk net approaches 15 hours per square foot of spacer. (Each one foot of spacer consists of two layers of crossed foam strips, individually bonded to the silk.)

The labor to fabricate the remaining two spacer configurations was determined to be one square foot per man hour for the punched hole spacer (consists of a total of 3 layers of foam, two of which contain punches holes) and also one square foot per man hour for the stripped spacer (consists of one foam spacer, with two layers of foam strips bonded at right angles to each and in turn bonded to the parent spacer.) Figure 14 and 15 respectively show the compressed and recovered condition of a panel using the punched hole spacer. Figures 16 and 17 respectively show the compressed and recovered condition for a panel using crisscrossed strips and Figure 18 shows the compressed condition of a panel using the foam maze on silk.

In view of the somewhat limited improvement possibility of the dimpled panel, the high costs involved in fabricating the foam maze on silk, it was decided that panels for thermal and gaseous conductance investigations be conducted on the stripped and the punched hole spacer.

Dimensions as indicated by an asterisk in Table 1 were used in the thermal and gas transmittance test specimens. Spacers with web widths of 3/4 of an inch with spacings appropriate to achieve the desired open areas of 70, 80, and 90 percent were used for both configurations.

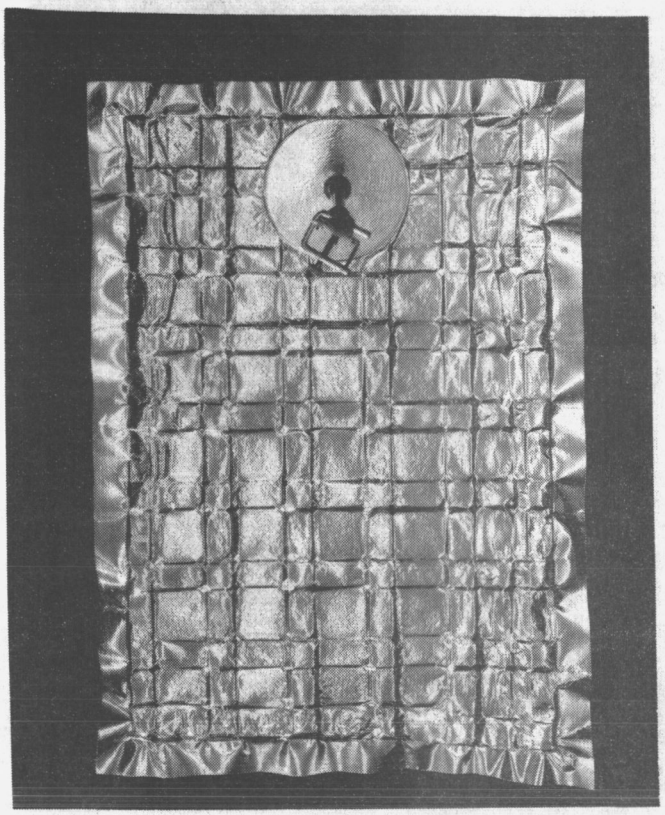

Figure 16 Compressed Panel Using Double Stripped Spacers

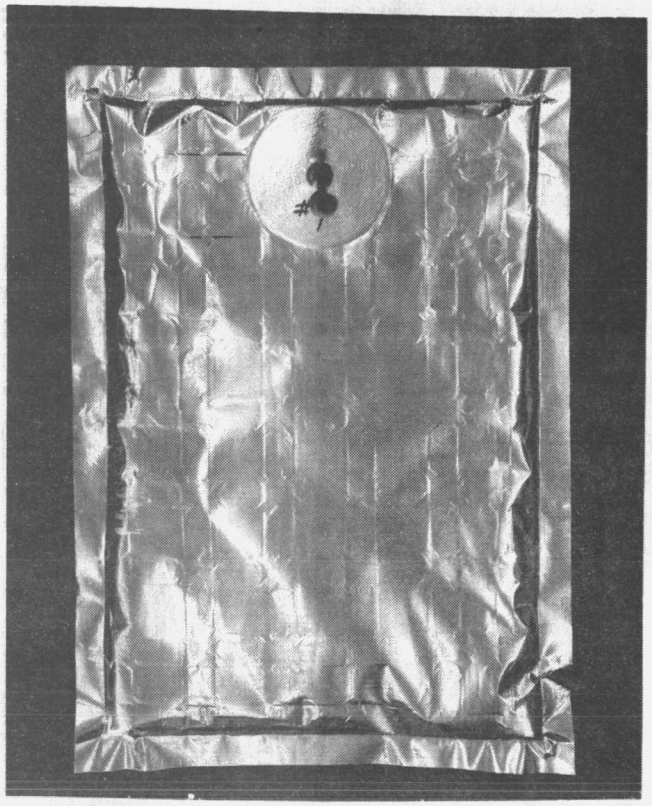

Figure 17 Recovered Panel Using Double Stripped Spacers

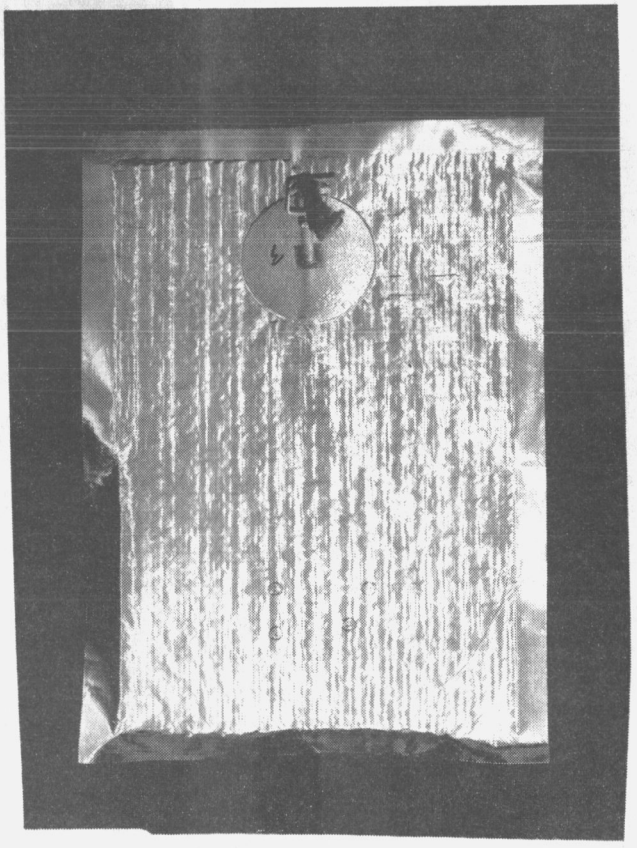

Figure 18 Compressed Panel Using Foam Maze On Silk Spacers

TABLE 1

SPACER DESCRIPTION FOR VARIOUS SUPPORT AREAS AND WEB THICKNESSES

DESCRIPTION	WEB WIDTH (t) INCHES	HOLE SIZE (s) INCHES	% SUPPORT AREA (2 LAYERS)	THERMAL SPECIMEN CODE NO.**
Punched hole spacer (one .02-inch layer of foam plus two .02-inch layers with punched holes per composite spacer)	1/4	7/16	30	--
		1/2	22*	PT-1
		3/4	12	--
	1/2	3/4	32	--
		1-1/8	19*	PT-2
		1-3/4	10	--
Support Area $= \frac{2t^2}{(s + t)^2}$	5/8	1	30	--
		1-3/8	20*	PT-3
		2	11	--
	3/4	1-1/4	28*	PT-6
		1-5/8	20*	PT-5
		2-3/8	11*	PT-4
Stripped Spacer (one .02-inch layer of foam plus two layers of .02 inch strips per composite spacer)	1/4	3/16	34	--
		5/16	20	--
		1/2	11*	ST-1
	1/2	7/16	30	--
		5/8	20	--
Support Area $= \frac{t^2}{(s + t)^2}$		1	11*	ST-2
	5/8	1/2	31	--
		13/16	20	--
		1-1/4	11*	ST-3
	3/4	5/8	30*	ST-6
		15/16	20*	ST-5
		1-9/16	10*	ST-4

* Utilized for thermal and gas transmittance testing

** Refer to Table 2

To achieve the maximum amount of information with the minimum number of samples it was decided to use a 20% support area configuration for the three remaining punched square hole panels, and 10% support area for the three remaining stripped panels.

4.1.2 Thermal Test

As a result of the spacer configuration study, both stripped spacers and punched hole spacers were determined to offer the greatest advantages for improved panel heat flux. Therefore, in order to determine and subsequently optimize the effect of stripped spacers and punched hole spacers on the thermal performance of multilayer insulation panels, six samples of each type were fabricated for evaluation using a cold guarded flat plate calorimeter at NASA, Lewis Research Center. The samples differed by web width and spacing configuration. (Refer to Tables 1 and 2)

Each thermal sample simulated an insulation system three panels thick. Each panel contained seven composite spacers, six aluminized Mylar radiation shields, and two pieces of four ply aluminized Mylar casing material placed one on either side. All twenty-one of the composite spacers of any particular sample were identical.

Each stripped spacer was a composite of two layers of .020-inch thick strips bonded at right angles to each other and subsequently spot bonded to a single layer of .20-inch thick foam using Narmco 7343/7139 adhesive.

Each punched hole spacer was a composite of three layers of .02-inch thick foam. Two of the three layers contained punched holes to reduce the support area. These two sheets with punched holes were assembled mismatched by one-half space and adjacent to each other to obtain the minimum support area. The punched hole spacer composite was assembled without using an adhesive.

The results of the thermal tests are shown on Table 2 with a description of each. The data for a sample having solid sheets of foam as a spacer are included for comparison. These data for the control sample were taken from reference 2 which describes the test apparatus and procedures in detail.

The thermal tests were conducted on flat plate tester at NASA, Lewis Research Center which is capable of imposing compressive loads on the sample from 15 psi (1 atm) to 0.001 psi. The cold plate temperature was maintained at that of liquid hydrogen in both the guard and test areas. Heat flux was determined by measuring the amount of hydrogen boil off.

TABLE 2

THERMAL PERFORMANCE DATA

Sample No.	Spacer Configuration	Percent Support Number of Support Points and Support Width	Heat flux, But/(ft^2) (hr); compressive load, psi					
			15	5	1	0.1	0.01	0.001
3082 (ref. 1)	Control - Full sheets of foam	100%	6.65	4.50	2.15	0.57	0.141	0.052
PT1	Punched holes	22%, 350 PTS 1/4"	6.86	5.05	2.99	1.79	-----	----
PT2	Punched holes	19%, 64 PTS 1/2"	7.51	5.33	3.44	1.33	-----	----
PT3	Punched holes	20%, 47 PTS 5/8"	7.91	6.02	3.91	3.67	-----	----
PT4	Punched holes	11%, 17 PTS 3/4"	8.56	4.27	2.98	0.52	0.14	0.05
PT5	Punched holes	20%, 31 PTS 3/4"	8.97	6.66	1.79	0.45	0.28	0.15
PT6	Punched holes	28%, 47 PTS 3/4"	6.47	4.00	2.06	0.45	0.13	0.04
ST1	Strips	11%, 190 PTS 1/4"	8.42	5.71	2.70	0.72	-----	----
ST2	Strips	11%, 50 PTS 1/2"	7.30	3.88	1.93	0.30	-----	----
ST3	Strips	11%, 31 PTS 5/8"	8.41	5.50	4.24	----	-----	----
ST4	Strips	10%, 20 PTS 3/4"	9.40	2.85	2.44	0.3	-----	----
ST5	Strips	20%, 40 PTS 3/4"	7.69	5.39	2.83	1.70	-----	----
ST6	Strips	30%, 60 PTS 3/4"	7.07	5.11	3.60	0.74	-----	----

It is evident from the data that thermal performance does not depend on the support area alone. Sample PT-6 (1-1/4" square holes on 2" centers) exhibited thermal performance superior to the control sample and since the punched hole spacers exhibit better gas transmittance (see Section 4.1.3 below) than either the stripped or plain spacers, this configuration was chosen for use in the full scale SEMI panels for test on the calorimeter tank.

4.1.3 Gas Transmittance Tests

The results of previous vacuum transmittance and cryopumping tests indicated a need for improved gas transmittance through the spacer layers and/or around the edges of the spacers. As a result of the spacer configuration study, (see Section 4.1.1), stripped spacers as well as punched hole spacers were determined to be most beneficial. In view of this, a total of thirteen gas transmittance test panels were fabricated and tested in an effort to optimize gaseous transmittance through the panels, particularly in the pressure regime below 1000 microns average panel pressure. Each of the thirteen gas transmittance specimens measuring one ft. wide by three ft. long, were composed of seven foam spacers (composites or plain) and six aluminized Mylar radiation shields, enclosed in a flexible vacuum jacket of Mylar laminate. Manifolds, attached on either end of the three foot long panel, contained a pressure tap and an evacuation port.

Twelve of the thirteen samples consisted of composite spacers, six punched hole spacer samples and six stripped spacer samples, while the thirteenth transmittance sample employed plain sheet foam spacers to serve as a control panel. Except for the size the sample configurations were the same as those provided for thermal testing. In addition a solid block of 3/8" thick open cell foam was incorporated in a panel and and evaluated in the transmittance apparatus. A brief description of each of the thirteen samples is given in Table 3 including an identification number for each specimen, the web widths and spacings and also the percent open area.

In order to estimate the optimum support area arrangement of the foam separators as regards the self evacuation rate of the panels, a series of transmittance measurements were performed on each of the thirteen panels. As a general procedure, carbon dioxide gas was admitted at the upstream end of the panel, while maintaining the downstream end of the panel at a low pressure by means of a vacuum pump. Full width manifolds were employed at both ends of the panel to assure a uniform gas flow across the full three foot length of the panel. The flow rate (transmittance) was determined by one of two methods, depending on the pressure level and flow rate involved. High flow rates were measured by means of a totalizing wet drum gas meter attached to the exhaust of the vacuum pump, while low flow rates were calculated from observations made of the changes in pressure of a known volume of gas over a specific time interval. For

TABLE 3

GAS TRANSMITTANCE PANEL SPECIMENS

CONTRACT NAS 3-7953

Dimensions Foam Spacer 12" x 36"
Radiation Shield 12" x 36"
7 Foam Composite Spacers
6 Aluminized Mylar Shields

Description	Code No.	Strip Width (inch)	Strip Spacing (inch)	Support Area Percent
Stripped Spacer	SC-1	1/4	1/2	11
(One .02 inch layer of	SC-2	1/2	1	11
foam plus two layers of .02 inch	SC-3	5/8	1 1/4	11
strips per composite spacer)	SC-4	3/4	1 9/16	10
	SC-5	3/4	15/16	20
	SC-6	3/4	5/8	30
		Spacing	Hole Size	
Punched Hole Spacer	PC-1	1/4	1/2	22
(One .02 inch layer of foam	PC-2	1/2	1 1/8	19
plus two .02 inch layers	PC-3	5/8	1 3/8	20
with punched holes per	PC-4	3/4	2 3/8	11
composite spacer)	PC-5	3/4	1 5/8	10
	PC-6	3/4	1 1/4	28
Plain Spacer	P-1	---	---	---
(Two .02 inch layers of foam per composite spacer)				
Solid 3/8 inch Thick Foam	S-1	---	---	---
(no shields)				

CONTRACT NAS 3-6289

Dimensions Foam Spacer 24" x 30"
Radiation Shield 24" x 30"
4 Foam Layers
3 Aluminized Mylar Shields

Plain Spacer	P-2	---	---	---
(One .02 inch layer of foam per composite spacer)				

both cases, the panel average pressure was controlled by adjusting bellows sealed needle valves at either end of the panel. Attempts were made to limit the pressure drop across the panel to 25 mm Hg and 300 microns in the high and low pressure ranges respectively.

A schematic of the test apparatus is shown in Figure 19. An example of the data reduction method and transmittance data are presented in the Appendix 2. The average or weighted thickness was determined by adding the product fractions of support area and open area times the respective number of layers of open cell foam at either location. Panel descriptions are shown in Table 3. Review of the transmittance data plotted on Figures 20 and 21 indicates that there is considerable scatter in the data which seems to mask any correlation between transmittance and support area on configuration. As mentioned previously, however, the transmittance level seems better for the punched hole panels than the stripped panels. It also appears that gas transmittance is independent of the differential pressure across a panel as would be expected in the molecular flow regime.

Transmittance tests performed on a small sample of pierced Hexcel Mylar honeycomb material indicate that the material exhibits an increased gas conductance of approximately 15 times that of a punched foam panel or 30 times that of a stripped panel for average panel pressures of 1800 microns as shown on Figure 4. At an average panel pressure of 100,000 microns, the gas transmittance increased by as much as 50 times the transmittance measured for any of the foam panels. The test panel consisted of one layer (0.109 inch thick) of hexagonal Mylar honeycomb material enclosed within a Mylar/lead/Mylar jacket. The Hexcel material, which measured 12 inches wide by 20 inches long, consisted of a 5/16" hexagonal honeycomb in which the 10 mil walls of each cell contained small holes (.04 inch diameter) to provide escape paths for gas during evacuation.

This material exhibited sufficient compression strength in the direction of panel thickness. However, very little collapse strength was noted in the longitutional direction, which could lead to installation and recovery problems if this material were used in SEMI panel unless a facing sheet were used. The panel length was greatly reduced (accordion fold) during evacuation unless the ends of the panel were restrained.

Aside from the mechanical problems involved with using this material in panels, approximate thermal calculations indicate that the

FIGURE 19

SCHEMATIC-VACUUM SYSTEM LONGITUDINAL GAS TRANSMITTANCE APPARATUS

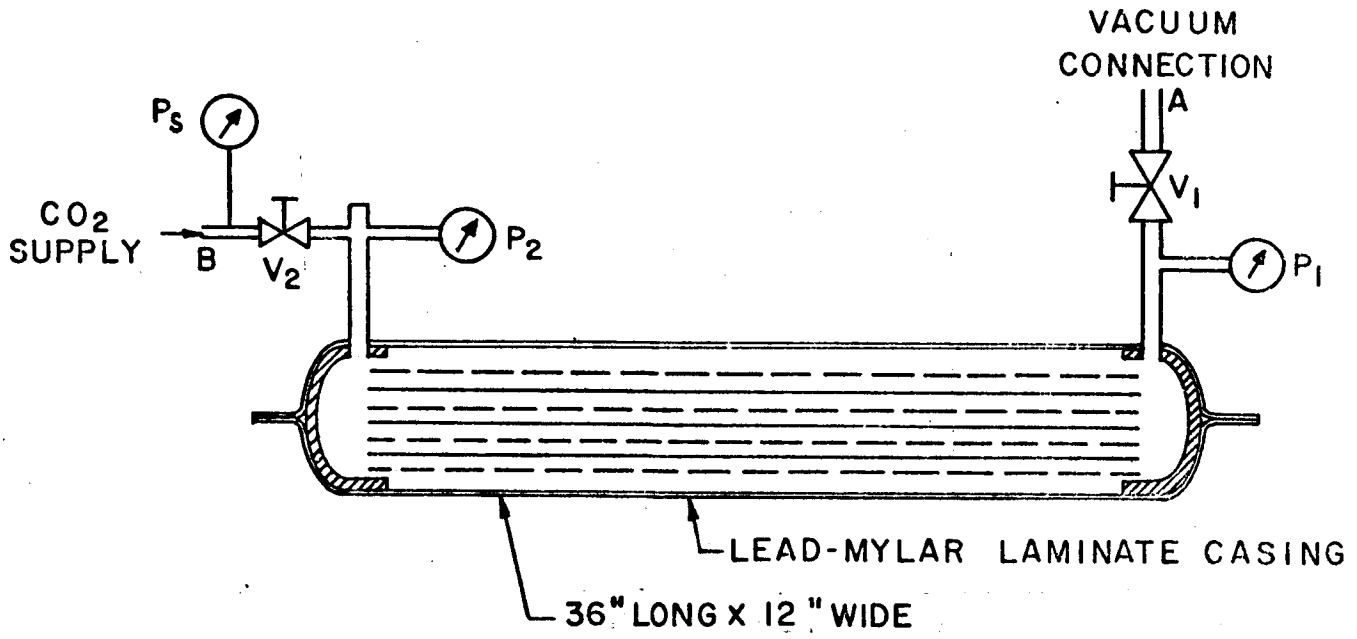

VOLUMETRIC MEASUREMENT METHOD

A. ABOVE 1000 μ AVERAGE PRESSURE
WET DRUM ON PUMP EXHAUST

B. BELOW 1000 μ AVERAGE PRESSURE
KNOWN VOLUME SUPPLY

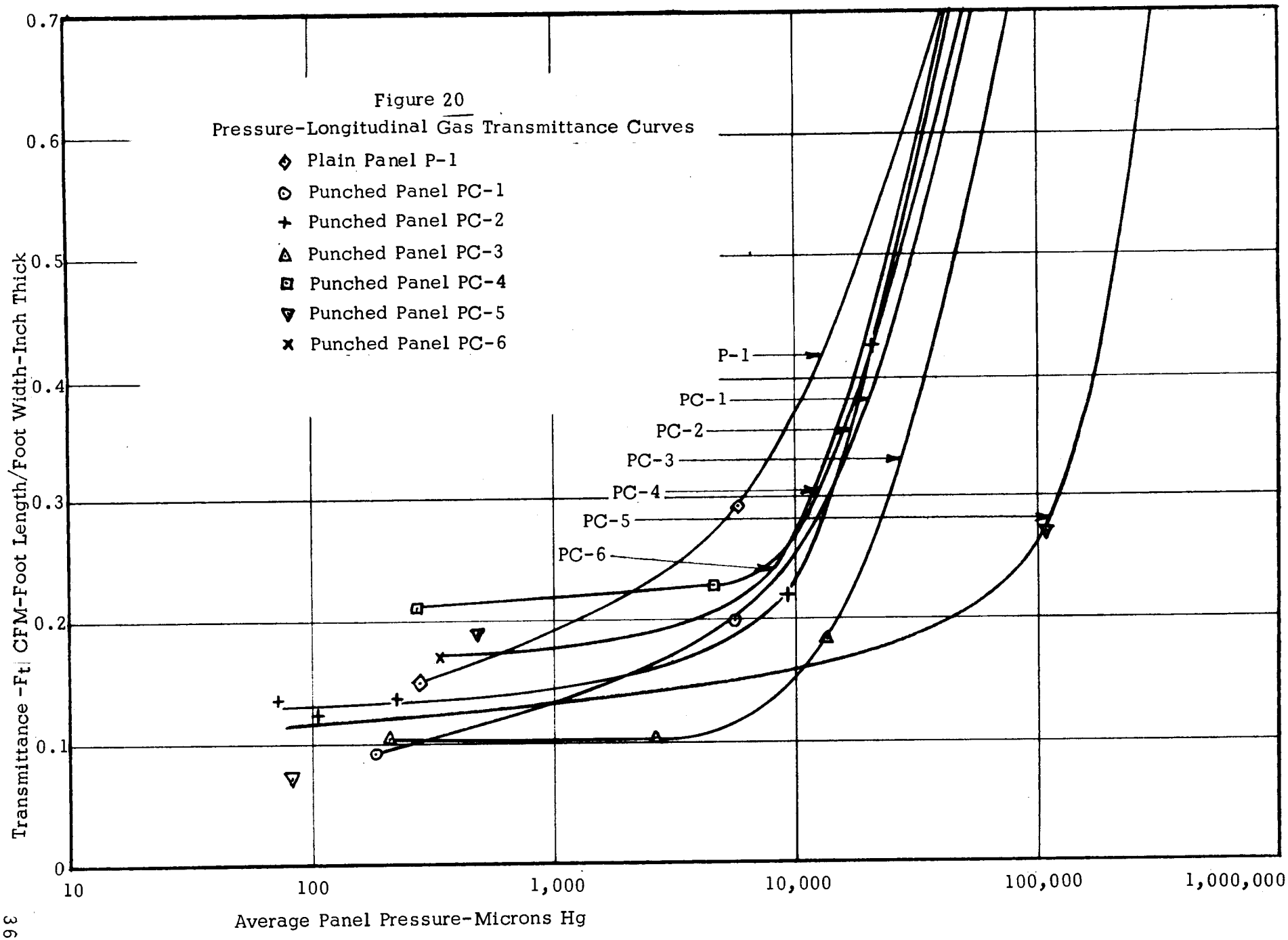
Figure 20
Pressure-Longitudinal Gas Transmittance Curves
Plain Panel P-1
Punched Panel PC-1
Punched Panel PC-2
Punched Panel PC-3
Punched Panel PC-4
Punched Panel PC-5
Punched Panel PC-6
P-1
PC-1
PC-2
PC-3
PC-4
PC-5
PC-6
Transmittance -Ft³ CFM-Foot Length/Foot Width-Inch Thick
0.7
0.6
0.5
0.4
0.3
0.2
0.1
0
10
100
1,000
10,000
100,000
1,000,000
Average Panel Pressure-Microns Hg

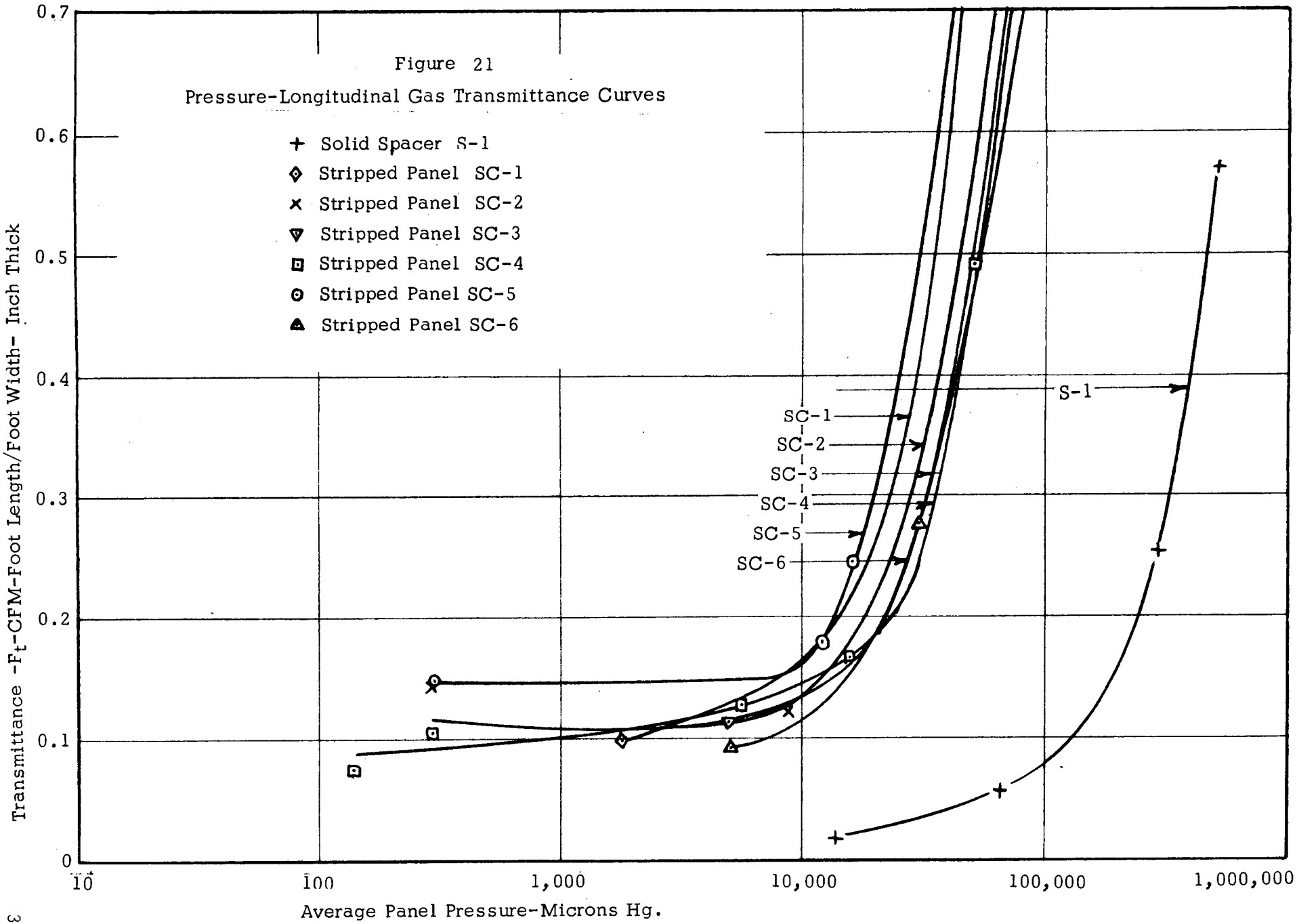
Figure 21
Pressure-Longitudinal Gas Transmittance Curves
Solid Spacer S-1
Stripped Panel SC-1
Stripped Panel SC-2
Stripped Panel SC-3
Stripped Panel SC-4
Stripped Panel SC-5
Stripped Panel SC-6
S-1
SC-1
SC-2
SC-3
SC-4
SC-5
SC-6
Transmittance -Ft-CFM-Foot Length/Foot Width- Inch Thick
0.7
0.6
0.5
0.4
0.3
0.2
0.1
0
10
100
1,000
10,000
100,000
1,000,000
Average Panel Pressure-Microns Hg.

apparent lateral thermal conductivity of this material is approximately the same as a single 0.026 inch thick open cell rigid foam sheet and thus probably would not affect the overall thermal performance of the panel.

4.1.4 Foam Compression Tests

To assure that the open cell rigid polyurethane foam specially obtained for this program was of sufficient strength for use in continuation of the SEMI panel development program, compression tests were performed on 2 inch cube samples. Two foam cube samples were obtained from each bun for a total of four tests. As can be observed in Figure 22 , the compressive yield strength is greater than 20 psi and therefore these foam buns are of sufficient strength and meet the quality assurance requirements.

The foam was produced by Union Carbide Chemicals Division according to the following formula:

TABLE 4 - Foam Components

NIAX Polyol T-221	100.0 PBW
Ucon-11	30.0
L-5320	4.0
TMBDA	.6
Aluminum No. 422	1.0
NIAX AFPI	103.0
Stannous Octoate	0.2

To determine the foam density, the samples were measured with a vernier-type caliper and the volume calculated. The weight of each sample was determined on a beam balance type scale. The density was calculated by dividing the sample weight by the volume. The compressive strength was determined with the use of a pressure deflection tester as shown in Figure 23 . Force on the compression plate is provided by compressed gas operating on a piston. The dial indicator operated by the movement of the piston rod inciates the deflection of the test sample.

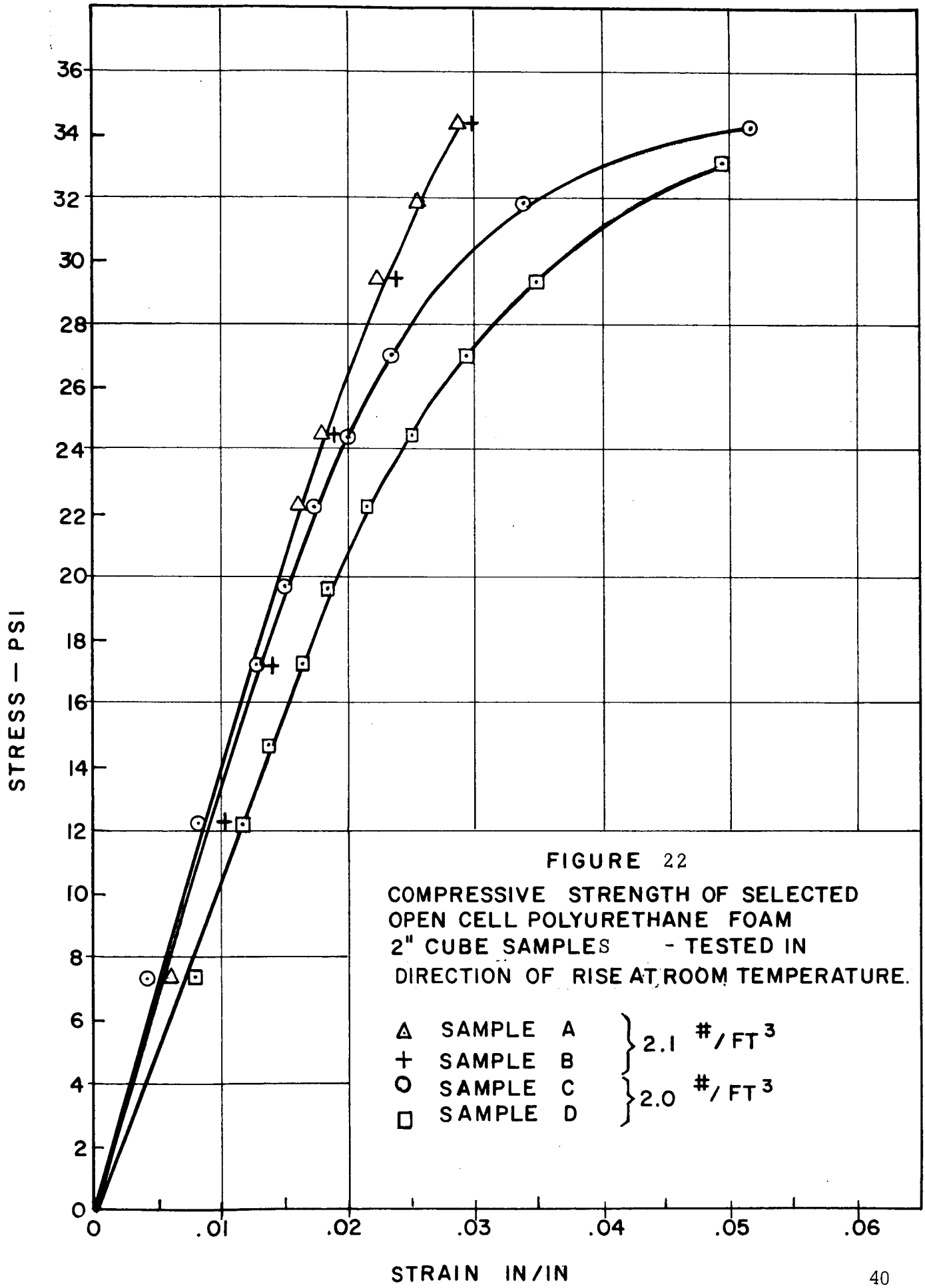

FIGURE 22

COMPRESSIVE STRENGTH OF SELECTED OPEN CELL POLYURETHANE FOAM 2" CUBE SAMPLES - TESTED IN DIRECTION OF RISE AT ROOM TEMPERATURE.

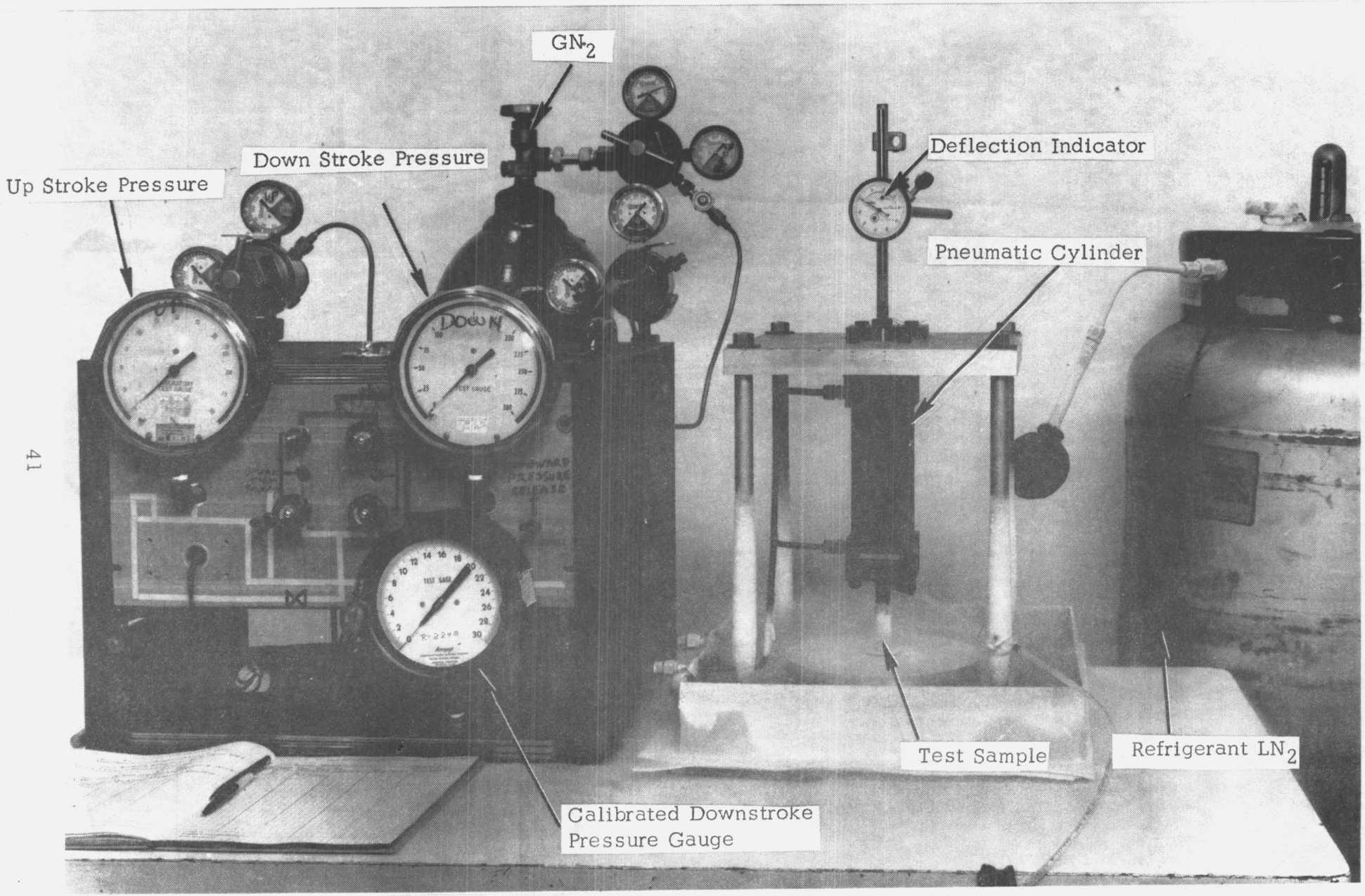

PRESSURE DEFLECTION TEST APPARATUS FIGURE 23

4.2 Panel Storage

4.2.1 Analytical Study of Storage Problems Associated With Permeability and Offgassing of Insulation Materials

Development of a cryopumped panel system that will perform satisfactorily after an extended period of time requires that various factors such as total material offgassing, casing material permeability, and installation procedures be considered from a system standpoint. In the critical phases of this program, this involved an analytical study of the various items using data derived from Contract NAS3-6289, and did not require additional development work. Only after completion of the analytical study was limited testing of samples performed in an attempt to support the analytical findings with experimental results.

The panels are required to be capable of cryopumping to a pressure of 1×10^{-4} torr at liquid hydrogen temperature 30 days after the initial insulation installation. Various techniques to attain this goal were suggested for investigation such as:

1. Removal of hydrogen gas by use of a getter.
2. Fabrication of panels having the outside exposed areas composed of an impermeable casing material.
3. Enclosing the installed system completely in an impermeable bag.
4. Enclosing the installed system in an external bag filled with carbon dioxide or other condensible gas.
5. Enclosing the installed system in an external bag and purging constantly with carbon dioxide or other condensible gas.
6. Backfilling or purging the space between panels with carbon dioxide or other condensible gas.
7. Combinations of above.

This investigation has revealed that to achieve the required storage life the panels fabricated of 4-ply aluminized Mylar laminate will require a hydrogen getter, and will also require that either the outer exposed area of the panels be fabricated of a highly impermeable material (permeability of the material to be in the order of 5×10^{-9} atm. cc helium per sec.-ft.^{2} was shown to be a practical figure based on the work done during this effort as described in Section 4.2.2 below) or that the external purge bag technique be employed to limit the exposure to ambient air. In addition to this, the space between the panels (83% of the total panel area) must be maintained in a carbon dioxide or vacuum environment. Final choice on the proposed method of an impermeable panel jacket versus an external purge bag is dictated by mission requirements as both methods have merit depending on allowable weight penalties, system

complexities, and time limits. A word of caution though is in order on the use of the purge bag concept. Since gas transfer by permeation is dependent on partial pressures rather than total pressure, it is necessary to maintain a sufficient flow rate of purge gas to sweep away undesirable gases or to limit the concentration of these gases by using a relatively leak tight purge bag.

Concurrent with the investigation of the fabrication and storage techniques necessary to achieve the required cryopumped pressure of 1×10^{-4} torr after a thirty-day storage period, calculations were made to reduce the lateral heat conduction through the panels by using a thinner casing material (subsequently offering a lower heat leak at a sacrifice of permeability) for the internal portions of the panel in conjunction with a impermeable material for the exposed portion of the panel.

As mentioned above, the investigation indicated the need for a hydrogen getter. The presence of hydrogen gas results from air permeation through the casing material, and offgassing of the insulation materials. The hydrogen gas that permeates the casing material from the atmosphere is of no consequence in comparison to the amount of hydrogen gas evolved from the panel materials. The calculated gas load, for a thirty-day period, considering a 40-inch by 72-inch panel composed of 14 layers of open cell foam and six aluminized Mylar radiation shields, amounted to $\sim$47 atmospheric cubic centimeters of hydrogen gas. (This volume of gas would theoretically cause a final panel pressure of 2.5 torr after thirty days.) Of this total gas load, hydrogen gas attributed to air permeation through the 4-ply aluminized Mylar casing material was only 4×10^{-3} atm. cc for the thirty-day period. This was calculated on the basis that the hydrogen gas permeability rate is 1.67 times that of helium gas permeability rate (sq. root of the ratio of molecular weights), resulting in a combined helium plus hydrogen permeability rate of 2.67 times that of the measured helium leak rate of the casing material. The concentration of helium in atmospheric air is six parts helium per million parts of air.

The hydrogen gas due to materials offgassing was calculated based on offgassing rate data for each material as derived from pressure rise tests performed under contract NAS 3-6289. Offgassing rates as determined by the settle out method, rather than rates determined by pump down tests, were used in order that the gas compositions of the sample (published in Contract NAS 3-6289 reports) would be available, thus making it possible to calculate the expected partial pressure of the hydrogen gas in the panels.

Based on these calculations, and the hydrogen capacity of Linde Palladium Oxide getter*, a minimum of 5 grams of getter are required to achieve a cryopumped pressure of 1×10^{-4} torr after a thirty-day storage period. Additional life requirement beyond the thirty-day time period will require proportionally larger amounts of getter.

The investigation of panel capabilities also included calculations to determine cryopumped panel pressures that would be achieved after certain periods of time if various panel areas are exposed to atmospheric air. In all calculations, the initial panel pressure was assumed to be 5×10^{-5} torr of non-condensible gases. This pressure level was assumed to be realistic, and one that is measurable within a vacuum panel. The time period for the panel to achieve a cryopumped pressure of 1×10^{-4} torr for 100% panel area exposed to atmospheric air was also calculated.

For calculations it was assumed that the panels would undergo two exposure periods. Initially 100% of the panel area would be exposed to ambient air for a maximum time period of five days, during which time the panels and a carbon dioxide purge system would be installed on the tankage. The second exposure period considered the outer 1/6 of the shingled panel to be exposed to atmospheric air for twenty-five days, while the remaining 5/6 of the panel beneath other panels was maintained for a carbon dioxide purged atmosphere. The purge system is required to reduce the panel area exposed to the atmosphere, and to assume that the space behind the panels achieves a low cryopumped pressure, i.e. contains only condensible gasses.

A brief description of the various concepts and the results achieved are presented in Table 5 . It can be seen that a panel fabricated entirely of 4-ply laminate of aluminized Mylar material will not meet the thirty-day pressure requirement without the use of a getter. Similarly the use of the Mylar trilaminate (.5 mil Mylar x .5 mil Mylar metalized both sides x.5 mil Mylar) does not meet the specified thirty-day hold time. This tri-laminate was investigated in an attempt to reduce the lateral thermal conductivity of the casing material yet still maintain the required vacuum integrity of the panel.

It does appear, however, that a panel fabricated of the 4-ply Mylar casing material, with the outer exposed area of the panel laminated with an impermeable material such as Mylar/lead/Mylar laminate (MLM) or Mylar/aluminum/aluminum /Mylar Laminate (MAAM) will meet the thirty-day requirement if used in conjunction with a hydrogen getter. In fact

TABLE 5

SUMMARY - PANEL STORAGE

Description*	Cryopumped Panel Capabilities: Time To Achieve 1×10^{-4} torr (Initial Pressure 5×10^{-5} torr for 100% Panel Exp. to air	Pressure - Torr (Initial Press 5×10^{-5} Torr): 5 Days @ 100% Exp.	25 Days @ 1/6 Exp.	After 30 Days Exposure, 5 Days @ 100% + 25 Days @ 1/6 Area
4-Ply Aluminized Mylar Laminate w/o H_2 Getter-hydrogen plus helium permeability equals 2.67 times helium permeability. Assume no hydrogen offgassing.	--	--	$.96 \times 10^{-4}$	1.5×10^{-4}
Same As Above	4.5 Days	1.05×10^{-4}	--	1.5×10^{-4}
4-Ply Aluminized Mylar Laminate with H_2 Getter	--	6.9×10^{-5}	--	8.5×10^{-5}
4-Ply Aluminized Mylar Laminate, outer exposed area covered with Mylar Lead Mylar, H_2 Getter.	--	6.5×10^{-5}	--	6.5×10^{-5}
Same As Above	15.7 Days	1×10^{-4}	--	1×10^{-4}
Mylar Tri Laminate, H_2 Getter Perm. = $1.22 \times 10^{-5} \frac{\text{atm. cc helium}}{\text{sec. ft.}^2 \text{ atm.}}$	3.7 Days	1.19×10^{-4}	--	1.75×10^{-4}
Mylar Tri Laminate, outer exposed area covered with Lead-Mylar, H_2 Getter.	4.4 Days	1.07×10^{-4}	--	1.07×10^{-4}

* All panels contain 14 layers of open cell regid polyurethane foam (.020 inch thick) and 6 aluminized Mylar radiation shields.
Panel Dimensions - 40 inches x 72 inches.

Air contains 6 PPM helium or $P_{max_{he}} = 4 \times 10^{-3}$ torr

it appears likely that because of the highly impermeable exposed area of the casing and the carbon dioxide purge on the enclosed 5/6 of the panel, the installed system could be stored without loss of allowable installation time to 15 days before beginning the carbon dioxide purge, yet still retain the capability of achieving 1×10^{-4} torr after one year of storage. Either material is satisfactory, but the Mylar/aluminum / aluminum/Mylar laminate offers a weight advantage over the Mylar/ lead/ Mylar laminate without incurring serious thermal or permeability penalties. For example, the weight savings using MAAM on the 82.6 inch diameter sphere rather than MLM amounts to eight pounds. (10 pounds for MLM outer casing versus two pounds for MAAM casing.)

An alternate method for achieving the required storage life is to enclose the completed panel insulation system in an external bag and constantly pressurize (purge) with carbon dioxide gas . A purge rather than simple pressurization is needed to remove the air gases that would permeate through the casing. The use of the purge bag versus impermeable outer casing would be mission dependent as mentioned previously based on weight penalty versus launch complexity involved. However the estimated weight of a purge bag for the 82.6-inch diameter tank is 3.5 pounds, which means that the purge bag must be removable to be competitive on a weight basis with panels having an impermeable outer exposed area of casing since the estimated weight of the impermeable jacket is two pounds. The external purge bag would most likely be fabricated of 4-ply aluminized Mylar laminate and a contact adhesive with the intent to make as tight a bag as is practical, approaching the permeation through the basic material.

Since a purge system is required for the space behind the panels for either system, the external purge bag technique is not penalized because of additional ground support equipment. Fabrication and installation costs and complexity of the purge bag versus use of impermeable outer casings would likely favor the impermeable casings.

The use of a purge bag as a technique to reduce the helium content of the panels because of permeation of residual helium in the panels out to a pure CO_2 purge gas atmosphere while in storage does not appear to be feasible. Calculations indicate that although the helium gas within the panel will permeate out into the purge bag, the rate at which this transpires is so slow that the process is ineffective.

Enclosing the installed insulation system within an impermeable bag pressurized with CO_2 appears less practical than the approach of a more permeable bag with a continuous purge because of the time and cost associated with fabrication, installation and leak checking.

Calculation methods for the various techniques are presented in Appendix 5.

4.2.2. Casing Permeability Tests

To evaluate preformed and plain casing materials in the unwrinkled (as received) and wrinkled condition, helium permeability tests were performed on test samples using a Veeco MS-9 helium mass spectrometer leak detector. Low helium permeability for the casing materials is required to insure that the insulation panels can be cryopumped to a suitably low pressure for optimum insulation performance.

Materials tested included 4-ply aluminized Mylar and Mylar-aluminum-aluminum-Mylar (MAAM) casing material. The results of these tests, shown in Table 6 , are comparable to results achieved previously for the 4 ply material under contract NAS3-6289, i.e. in the range of 0.3×10^{-5} atm. cc helium per sec. ft.^{2} atm. helium, while the MAAM casing material was determined to have a helium permeability rate equal to or lower than the capability of the leak detector, i.e. 5×10^{-9} atm.cc. helium per second ft.^{2} atm. The MAAM was leak checked to investigate its possible use as an impermeable 1/3 air exposed area of the casing and not as a substitute for the 4-ply casing material. MAAM, although offering a very low permeability, is unacceptable as a casing material because of its high lateral thermal conductivity.

Permeability tests of the 4-ply aluminized Mylar laminate material were performed on both wrinkled and unwrinkled test specimens using a 3-inch diameter permeability tester (See Fig. 24). The wrinkled samples were obtained from the casing of evacuated panels containing three layers of glass insulation material. Samples of drawn casing were obtained by thermo-vacuum forming the 4-ply material over a form constructed of 7/8" diameter by .080 inch thick washers thumbtacked to a board in a 60° pattern on 1-1/2 inch centers.

The test procedure was as follows. A sample of the subject material was clamped between two "O" ring sealed cavities. One side of the tester was then evacuated to a low pressure via the leak detector; helium at one atmosphere pressure was then admitted to the second cavity and a steady state helium indication obtained on the leak detector. This number was then compared to the indicated reading obtained for the fixed standard leak to yield the specimen permeability. The standard leak and permeability were equated by the formula,

$$\frac{\text{Steady State Detector Scale Reading (Units)} \times \text{Standard Leak (Atm.cm}^3\text{/sec. units)}}{\text{Standard Leak Detector Scale Reading (Units)} \times \text{Area of test sample (ft}^2\text{ units)}}$$

TABLE 6

MEASURED PERMEABILITY OF CASING MATERIALS

	Permeability Rate*
I. Mylar-Aluminum-Aluminum-Mylar (MAAM) - 1/2 mil Mylar .35 Aluminum	4×10^{-8}**
II. 4-Ply Aluminized Mylar Ma/aMa+ aMa/aM M - 1/4 Mil Mylar a - Aluminizing / - Bond Line	
a. Unwrinkled 1.	$.3 \times 10^{-5}$
2.	$.3 \times 10^{-5}$
b. Wrinkled 1.	$\times 10^{-5}$
2.	$.3 \times 10^{-5}$
3.	$.3 \times 10^{-5}$
4.	$.3 \times 10^{-5}$
c. Drawn 1.	$\times 10^{-5}$
2.	$.5 \times 10^{-5}$
3.	$.5 \times 10^{-5}$

* Permeability $\frac{\text{Atm cc helium}}{\text{sec.-ft.}^2\text{-atm.}}$

** Limit of leak detector

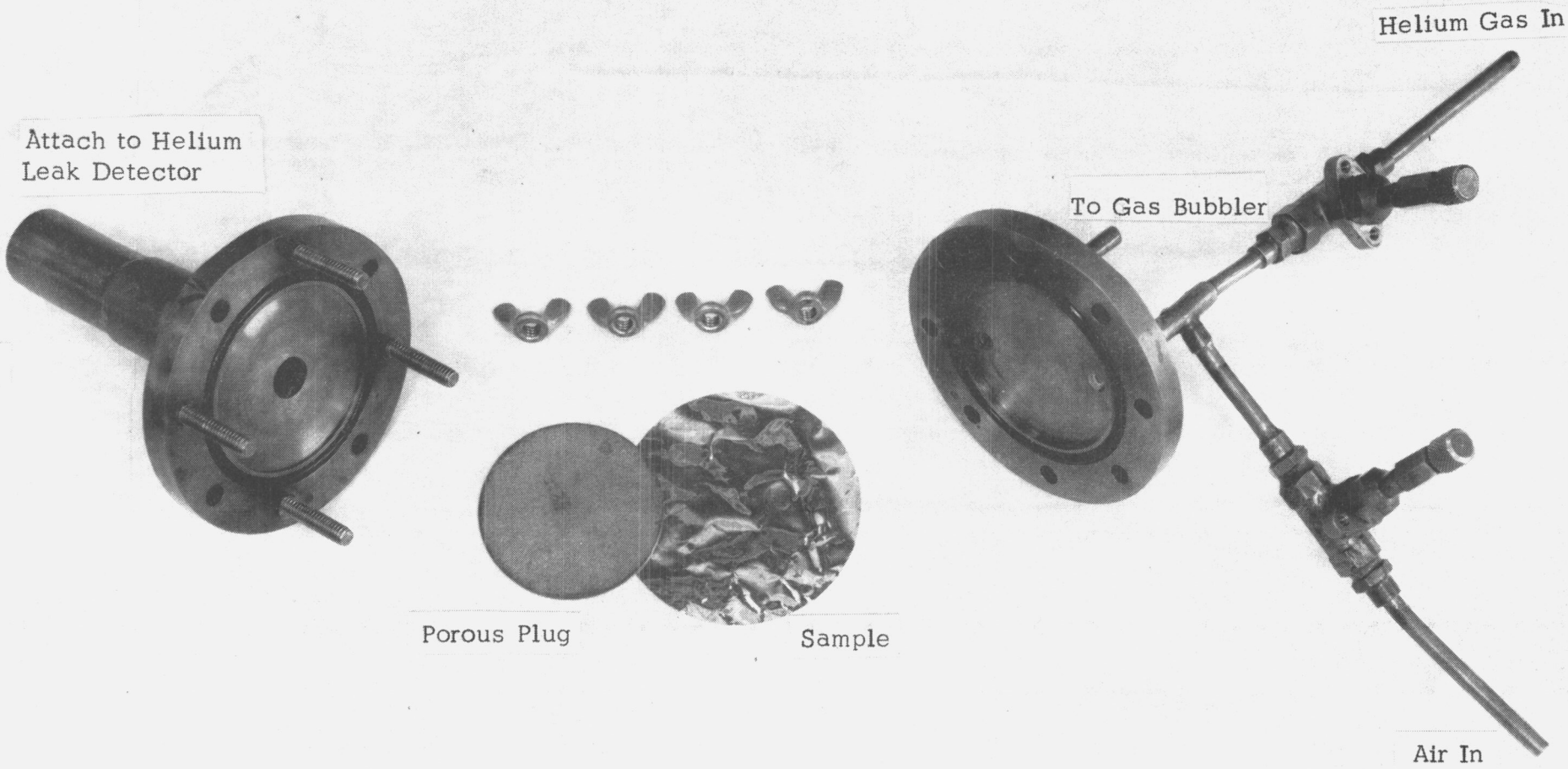

Figure 24 Permeability Tester Disassembled

4.2.3 Storage Life Tests

Two 18 x 36 in. test panels, composed of 14 layers of .02 inch thick open cell foam spacers and six aluminized Mylar radiation shields enclosed in a four-ply aluminized Mylar casing assembled with NARMCO 7343/7139 adhesive were fabricated. These were applied to a flat wall test tank for storage life tests. Both panels contained 0.5 grams of Palladium Oxide hydrogen getter.

In order to evaluate the effect of air exposure on casing permeability, panel No. 1 employed an impermeable casing of Mylar/Aluminum/Aluminum/Mylar laminate (MAAM) on the outer 1/3 of the jacket surface which was exposed to the air atmosphere, while the outer exposed area of panel No. 2 was protected from air exposure by a carbon dioxide purge bag. The net effect of these two systems was to eliminate panel exposure to the air, as the remaining area of each panel was already protected from air exposure by virtue of the panels being sealed to the flat wall tester and purged with CO_2. Two dummy panels, each measuring 24 x 36 inches were used, one on either side of the demonstration panels, to provide a two-layered shingled insulation system.

Preconditioning of panel materials was limited to heating the aluminized Mylar radiation shields in air at 200°F for 24 hours. This procedure of heating the shields in air was found particularly helpful in reducing hydrogen offgassing. Residual hydrogen in the panel was removed with hydrogen getter located on the outer most spacer, at the warm (ambient) end of the panel. Efforts to improve gaseous conductance of these panels were limited to one 1/2-inch diameter hole in each aluminized Mylar radiation shield. Each hole, located on a 1-inch radius using the evacuation port at origin, was indexed 120° from the hole in the adjacent radiation shield.

The outer casing for each panel was vacuum formed to obtain the necessary depth required to enclose the insulation without preload. These casings were vacuum formed over a mandrel which consisted of a 3/8 inch stack of art board and one conductance layer of dexiglas. The "MAAM" material was laminated to the 4-ply material after the casing was formed but prior to removing the casing from the vacuum forming fixture. Goodyear G-207 heat sealable resin was used to laminate the MAAM and 4-ply material. NARMCO adhesive was used to bond the casing joints and also to bond the instrumentation manifold to the casing. The manifold included a cold cathode ionization gage, a thermocouple type vacuum gage, and a 0-30 inch Hg Bourdon tube gage. In addition, the manifold also included a connection to obtain a sample of the residual gases at cryogenic temperature and a thermocouple to record the temperature of the manifold.

The completed panels were evacuated for 96 hours using a LN_2 cold trap and diffusion pump prior to helium leak checking. The panel leak rates, as determined by a helium leak detector were as follows:

Panel No. 1- 4 -Ply Casing Plus outer exposed area laminated with MAAM	$.28 \times 10^{-5} \frac{\text{atm cc hel.}}{\text{sec ft}^2}$
Panel No. 2- 4-Ply Casing W/O Impermeable outer casing	$.34 \times 10^{-5} \frac{\text{atm cc hel.}}{\text{sec ft}^2}$

These leak rates are comparable to previously measured rates for the basic material. The difference in measured helium leak rate between panel No. 1 and panel No. 2 is attributable to reduced permeable panel area. Panel No. 1 had 1/6 of its area laminated with MAAM. The leak rate of panel No. 1 based on a corrected area (area of 4-ply casing only) was $.34 \times 10^{-5} \frac{\text{atm cc hel.}}{\text{sec ft}^2}$

After leak checking, the panels were backfilled to one atmosphere with Coleman grade carbon dioxide gas and installed on the LH_2 flat wall tester in a shingled manner as follows. A dummy panel, covering the upper 2/3 of the LH_2 test surface, was installed to establish the first shingled layer. The two test panels were then installed with the lower portion of the panels contacting the remaining 1/3 exposed area of LH_2 test surface. A second dummy panel was then positioned on the outer-lower 2/3 of the test area to establish a minimum two layer panel thickness insulation system.

All panels were attached to each other and to the test tank by applying Goodyear G-207 contact adhesive in a one inch wide pattern around the outer most edges of the test area. The space between the panels was then made vacuum tight using the BFF - (Johns Manville Co.) three inch wide pressure sensitive tape applied at the edges of the panel to tank joints and panel to panel joints. A .040 inch thick polyethylene bag for the carbon dioxide purge was fabricated to cover the exposed outer 1/6 area of the plain 4-ply panel. The purge bag and the space behind the panels were constantly maintained with a CO_2 atmosphere during simulated panel storage life tests. During hydrogen testing, only the purge bag was maintained with a CO_2 atmosphere.

In addition to the CO_2 panel purge, it was necessary to maintain a helium purge on the test vessel guard insulation in order to preclude the possibility of cryopumping air. Upon completion of the installation of the panel system and purges the test panels were re-evacuated using a LN_2 cold trap and diffusion pump for another 72 hours and finally backfilled with Coleman grade carbon dioxide gas.

The purpose of these tests was to demonstrate the storage life capability of the panels. This was accomplished by recording the cryopumped pressure and analysis of the residual gas in the panels at liquid hydrogen temperature. The panels were then allowed to warm-up and stored at room temperature for approximately two weeks, at which time the cryopump test was repeated in order to compare the pressures achieved and the gas analysis obtained from both tests.

Figure 25 is a plot of the cryopumped pressure achieved within the panels for the tests. Figure 26 shows the installed storage life panels during hydrogen testing. Manifold temperature recorded during this test ranged from a high of 48°F to a low of 22°F. (Room temperature ranged from 55°F to 35°F during the test). Test data are presented in Appendix 4.

Although the thermocouple type vacuum gages indicated a pressure of less than 1 micron (1×10^{-3} torr) for the first test, the cold cathode gages were not operative. Analysis of the residual gas at this pressure within the panel is shown in Table 7.

From observation of the results of the gas analysis and a plot of the thermal history for the first test, it appears that the "N_2 + CO" is most likely nitrogen, due to the rapid panel pressure decay after the admission of liquid hydrogen to the test vessel. Failure of the panels to achieve the desired 1×10^{-4} torr was probably due to gas transmittance limitations of the panel rather than gas composition.

These panels, with the original carbon dioxide backfill were retested following a two week interval, during which time the carbon dioxide purge was continuously maintained in the space behind the panels, and on the exposed outer 1/3 of Panel No. 2. This second cryopumping test resulted in achieving panel pressures in the order of 100 microns. (See Figure 27). Analysis of the 100 micron plus residual gas, indicated a high helium background which was attributable to a leak into the space behind the panels from the helium purged tank insulation. Both panels were found to contain helium gas. Apparently the high helium background of the panels after this test was caused by seal leakage around the panel edges from the helium purged guard insulation and was not due to any real leaks in the panels. The helium gas entered the space behind the panels via small pin hole type leaks which developed in the seal between the panels and the aluminum face plate on the flat plate tests. This was borne out by the fact that the measured leak plus permeability rates of the panels after this second test were $.25 \times 10^{-5}$ and $.24 \times 10^{-5}$ atm. cc helium/ft.^{2} for panels No. 1 and 2 respectively.

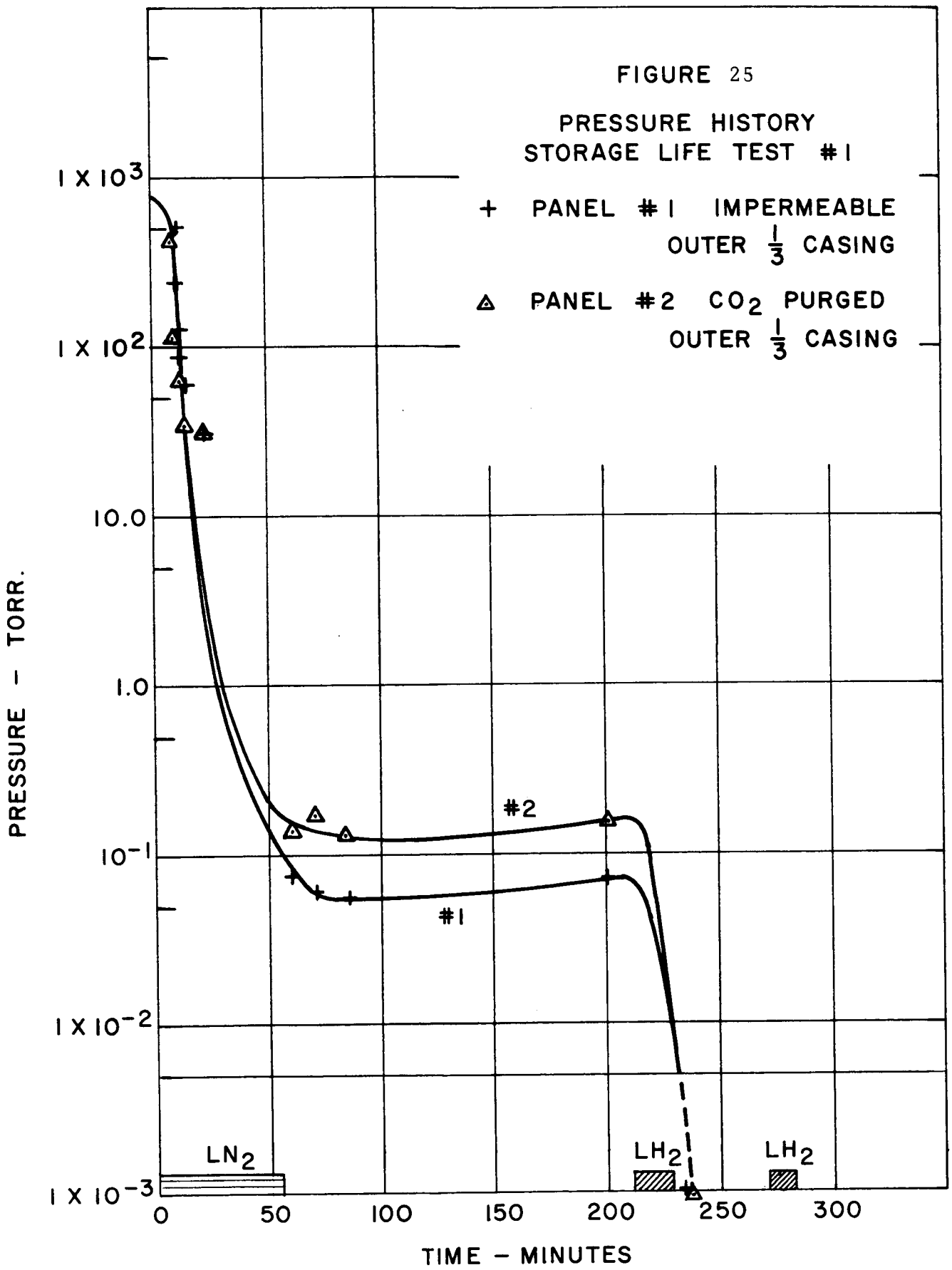
FIGURE 25
PRESSURE HISTORY
STORAGE LIFE TEST #1
+ PANEL #1 IMPERMEABLE OUTER 1/3 CASING
△ PANEL #2 CO2 PURGED OUTER 1/3 CASING
1 X 10^3
1 X 10^2
10.0
1.0
10^-1
1 X 10^-2
1 X 10^-3
PRESSURE - TORR.
#2
#1
LN2
LH2
LH2
0
50
100
150
200
250
300
TIME - MINUTES

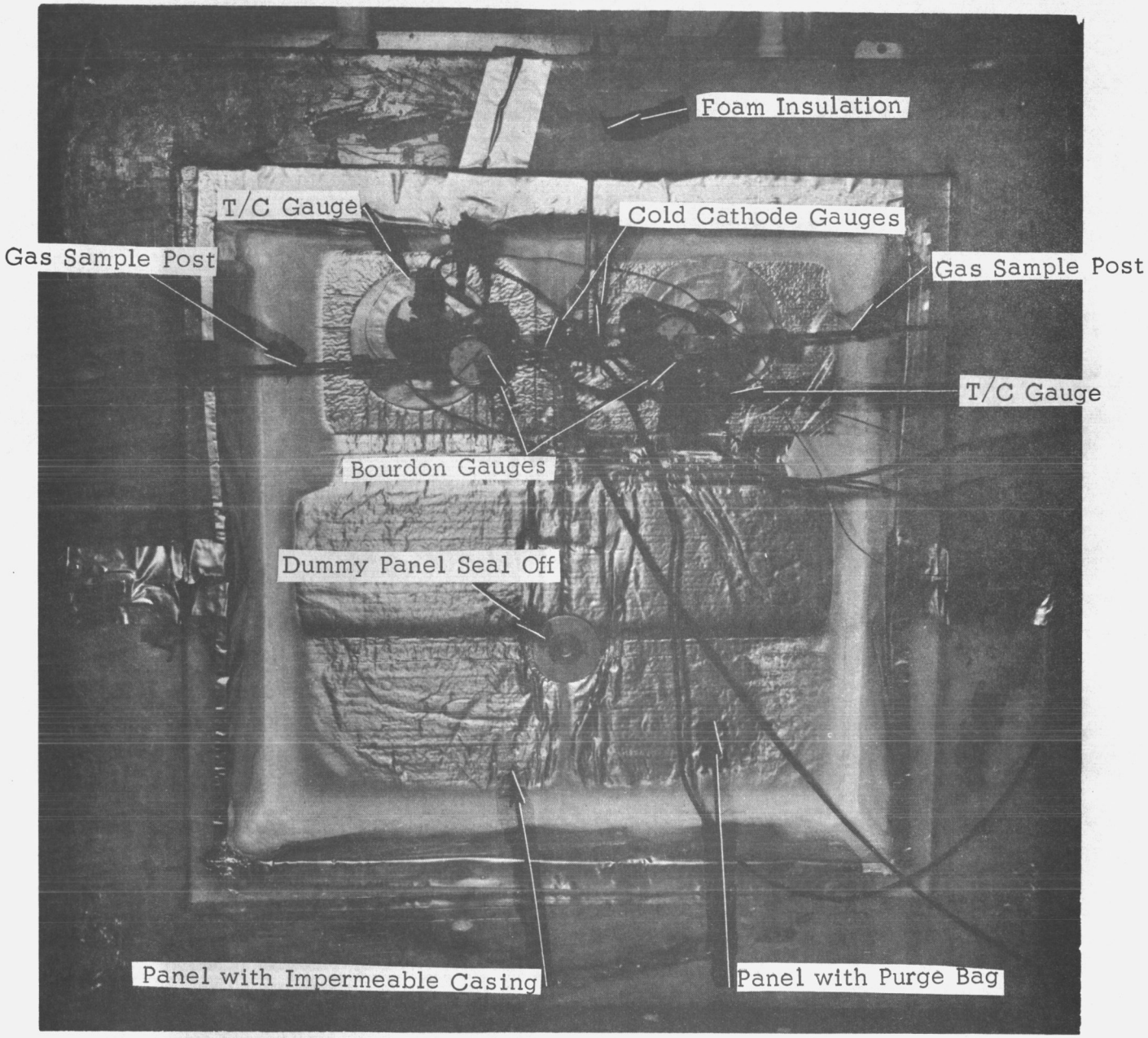

STORAGE LIFE DEMONSTRATION PANELS DURING LH_2 TEST

Figure 26

TABLE 7

Residual Gas Analysis - Panel Settleout
Panel # 1 4 ply casing, hydrogen getter with MAAM on outer 1/3 area
Panel #2 4 ply casing, hydrogen getter outer 1/3 exposed to air
Sample # 1 and # 2 (CO_2 Filled Panels at LH_2 temperature after 96 hrs of pumping (Test No. 1 and 2)
Sample # 3 (Evacuated Panels at Ambient Temperature after additional 961 hrs of pumping.) (1057 total hrs pumping)
Sample # 4 (Evacuated Panels at ambient temperature after additional 552 hrs of pumping.) (1609 total hrs pumpint)
Sample # 5 (CO_2 filled panels at LH_2 temperature after additional 69 hrs. of pumping (1678 total hrs pumping) and one week of CO_2 storage-Test # 4)

	Component									
	Argon	Carbon Dioxide	Methane	Hydrogen	Oxygen	N_2 & CO	Water	Helium	Ucon-11	Panel Pressure microns (thermocouple gage)
PANEL #1										
Sample # 1	.52*	14.7	0.37	N.D.	N.D.	14.7	M.C.	N.D.	N.D.	<5
Sample # 2	N.D.	1.7	N.D.	N.D.	.3	1.6	0.76	M.C.	N.D.	150
Sample # 3	.23	58.0	N.D.	N.D.	2.9	10.8	N.D.	N.D.	28.0	75
Sample # 4	.24	50.8	N.D.	N.D.	2.5	15.1	.08	N.D.	31.2	90
Sample # 5	- -	- -	- -	No	Sample	-	- -	- -	-	-
PANEL # 2										
Sample # 1	0.3*	3.0	N.D.	N.D.	5.6	M.C.	0.1	N.D.	N.D.	<5
Sample # 2	1.0	0.39	N.D.	N.D.	15.6	M.C.	0.15	18.1	N.D.	80
Sample # 3	.3	57.0	N.D.	N.D.	6.9	14.9	N.D.	N.D.	21.0	60
Sample # 4	N.D.	54.8	N.D.	N.D.	1.7	15.7	1.7	N.D.	26.0	70
Sample # 5	N.D.	51.2	N.D.	N.D.	N.D.	14.6	34.7	N.D.	N.D.	<5

* % Volume
N.D. Not Detected
M.C. Major Component

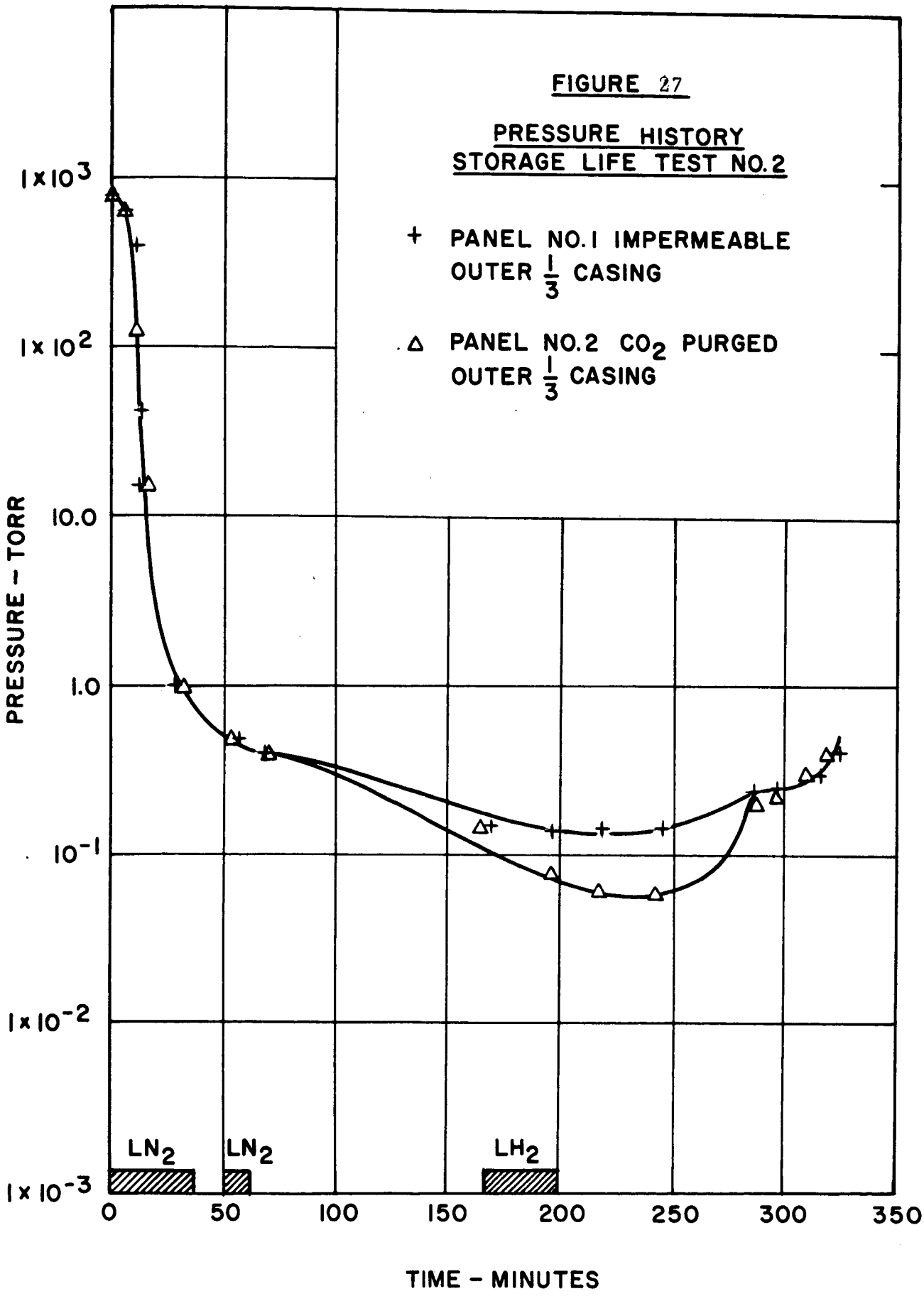
FIGURE 27
PRESSURE HISTORY
STORAGE LIFE TEST NO. 2
+ PANEL NO. 1 IMPERMEABLE OUTER 1/3 CASING
△ PANEL NO. 2 CO_2 PURGED OUTER 1/3 CASING
PRESSURE - TORR
1 x 10^3
1 x 10^2
10.0
1.0
10^-1
1 x 10^-2
1 x 10^-3
LN2
LN2
LH2
0
50
100
150
200
250
300
350
TIME - MINUTES

The difference in these readings before and after testing may be attributed to experimental accuracy in leak testing.

The ultimate cryopumped panel pressures during the second test were 150 and 80 microns for Panels No. 1 and 2 respectively. Of this, 95% of the 150 microns in Panel No. 1 was helium, while Panel No. 2 contained 15 microns of helium in the 80 micron total pressure. It is believed that the reason that Panel No. 1 contained the higher helium contamination is due to the positions of the panels relative to the location of the helium purge port, coupled with the fact that more leaks were found in the immediate area around the purge port. Because of the limited conductance behind the panels, Panel No. 2 was therefore not exposed to as great a helium concentration as Panel No. 1.

To preclude a similar failure of this seal on later storage life tests, a Mylar/lead/Mylar laminate casing was bonded directly to the aluminum face plate using NARMCO 7343/7139 adhesive, and this flap was in turn bonded to the outside of the foam guard.

The cryopumped pressure achieved in Panel No. 2, the panel which was covered with a carbon dioxide filled bag, was not satisfactory in either test, since in addition to helium a significant buildup in air pressure between tests was noted. The gas analysis during the second test indicated that a significant portion of the 80 microns was due to oxygen, nitrogen, and argon. Apparently, although there was leakage of carbon dioxide out of the polyethylene "purge bag", it was not sufficient to sweep out the air permeating through the bag material and resulted in an air partial pressure sufficient to cause air constituent permeability into the panel. Therefore, the polyethylene purge bag was replaced with a Mylar purge bag.

The two storage life panels, after an additional evacuation time of about 1580 hours since the previous test, were again backfilled with Coleman Grade carbon dioxide immediately prior to the first of two cryopump tests. The panels cryopumped to 1×10^{-4} torr during test No. 3 (See Figure 28) as measured on a cold cathode type vacuum gage. After a one week storage time, the second test of these same panels (test No. 4) achieved a pressure of less than 1×10^{-3} torr(1 micron) as measured by a thermocouple type vacuum gage, with the cold cathode vacuum gages reading greater than 5×10^{-3} torr.

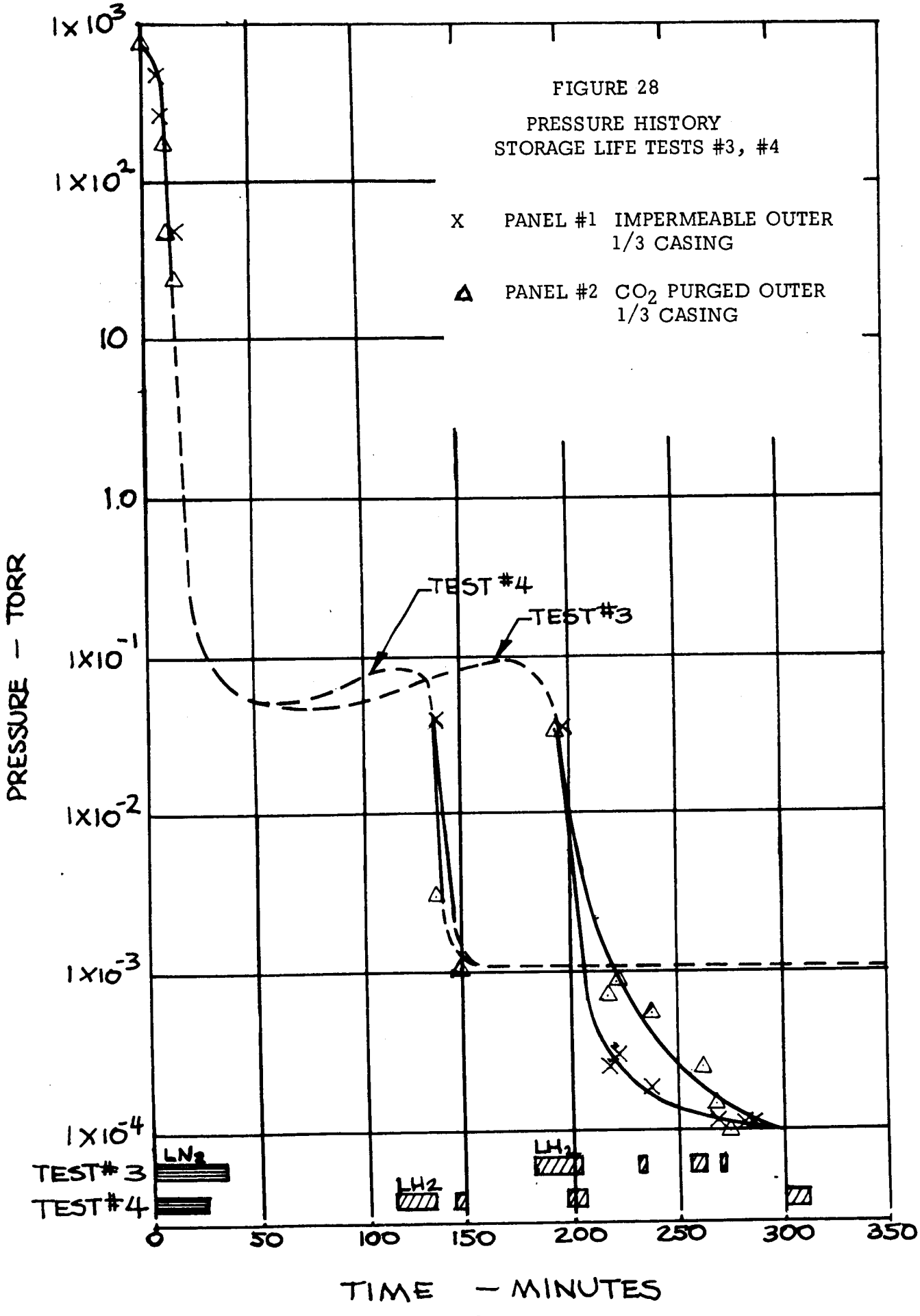
FIGURE 28
PRESSURE HISTORY
STORAGE LIFE TESTS #3, #4
X PANEL #1 IMPERMEABLE OUTER 1/3 CASING
Δ PANEL #2 CO_2 PURGED OUTER 1/3 CASING
TEST #4
TEST #3
PRESSURE - TORR
1X10^3
1X10^2
10
1.0
1X10^-1
1X10^-2
1X10^-3
1X10^-4
LN2
LH2
LH2
TEST #3
TEST #4
0
50
100
150
200
250
300
350
TIME - MINUTES

It is reasoned that the low pressure measured in the first test was attributable to the fact that the cold cathode gages had been thoroughly outgassed by the long evacuation period. After a one week soak, however, a high pressure was indicated because of outgassing from the gages and relatively poor gas transmittance from the gages to the cryopumping surface. The pressure at the gages was in the order of several microns which was water. It appeared that since the thermocouple gage was indicating a pressure of less than 1×10^{-3}, the cryopumped pressure of the CO_2 filled panel itself was most likely lower than indicated by the ionization gages. For this reason it is felt that the data indicated a successful demonstration of the ability of these panels to withstand the one week storage life.

Evacuation of the storage life panels was continued for a total of ~1580 hours between the previous cryopumping tests (No. 1 and 2) and cryopumping tests (No. 3 and 4). During this period, several residual gas samples at ambient temperature were obtained. In addition to panel evacuation, the space behind the panels was also evacuated to determine the effect on panel pressure rise and gas analysis of the settleout components. The results of these gas analyses, presented in Table 5 indicates little advantage in long term pumping after the initial evacuation of noncondensibles. Gas sample No. 4 taken after 552 hours of additional pumping beyond the time that gas sample No. 3 was obtained, is observed to differ only slightly from sample No. 3. Also, the effect of permeation and/or leakage through the casings in the space behind the panels does not contribute significantly if at all to the panel gas load.

Sample No. 5 from Panel No. 2 was obtained after the 4th cryopump test. However, because of a leak in the glass stop cock on the sampling bulb, a gas sample was not obtained from Panel No. 1 during test No. 4. No gas samples were taken during cryopump test No. 3. It was considered wise to avoid a possibility of contaminating the vacuum space. Also since the observed pressure was 1×10^{-4} torr it is highly unlikely that a gas analysis would have displayed any meaningful information.

4.3 Cryopumping

4.3.1 Theoretical Pumpdown Characteristics of a Cryopumped Panel

The analytical transient temperature profile is obtained from a general solution obtained by Carslaw and Jaegar[3]. The linear transient heat conduction equation is:

$$\frac{\partial t}{\partial \theta} = \alpha \frac{\partial^2 t}{\partial x^2} \tag{1}$$

where:

t = temperature, °R
θ = time, hr.
x = distance from cold end of panel, ft.
α = thermal diffusivity, ft. 2/hr.

To simplify the boundary conditions, we let

$$T = t - t_i \tag{2}$$

where:

t_i = initial temperature of the insulation before cooldown i.e. ambient temperature, °R.

(1) then becomes:

$$\frac{\partial T}{\partial \theta} = \alpha \frac{\partial^2 T}{\partial x^2} \tag{3}$$

The boundary conditions are:

$$\begin{aligned} T &= T_o \text{ when } x = O \\ T &= O \text{ when } x = L \\ T &= O \text{ when } \theta = O \end{aligned} \tag{4}$$

where:

T_o = cold side temperature, °R

L = length of heat path, ft.

To solve (3) subject to boundary conditions (4), we let

$$T = u + w \tag{5}$$

where u and w satisfy the following equations:

$$\frac{d^2 u}{d x^2} = 0 \qquad (0 < x < L) \tag{6}$$

$$u = T_o \qquad \text{when } x = 0$$

$$u = 0 \qquad \text{when } x = L$$

and

$$\frac{\partial w}{\partial t} = \alpha \frac{\partial^2 w}{\partial x^2} \qquad (0 < x < L) \tag{7}$$

$$w = 0 \qquad \text{when } x = 0 \text{ and } x = L$$

$$w = -T \qquad \text{when } \theta = 0$$

Solving (6) and (7) we find

$$u = T_o \left(1 - \frac{x}{L}\right) \tag{8}$$

$$w = \sum_{1}^{\infty} a_n \sin \frac{n \pi x}{L} e^{-\frac{\alpha_n^2 \pi^2 \theta}{L^2}} \tag{9}$$

where:

$$a_n = \frac{2\,T_o}{L} \int_o^L \left(\frac{x}{L} - 1\right) \sin \frac{n\pi x^1}{L}\, dx^1 \qquad (10)$$

Integrating (10), we obtain

$$a_n = -\frac{2\,T_o}{n\pi} \qquad (11)$$

(11) into (9) thus gives:

$$w = -\frac{2T_o}{\pi} \sum_1^\infty \frac{1}{n} \sin \frac{n\pi x}{L}\, e^{-\frac{\alpha n^2 \pi^2 \theta}{L^2}} \qquad (12)$$

(8) and (12) into (5) gives the final solution for T.

$$T = T_o \left\{ 1 - \frac{x}{L} - \frac{2}{\pi} \sum_1^\infty \frac{1}{n} \sin \frac{n\pi x}{L}\, e^{-\frac{\alpha n^2 \pi^2 \theta}{L^2}} \right\} \qquad (13)$$

The mass transfer is calculated numerically by dividing the panel into twenty linear grids. The mass transfer between successive units is determined by the following equation:

$$\Delta N_{ij} = \frac{M\,F\,W\,(\theta_j - \theta_{j-1})\,(P_{i+1} - P_i)}{L\,R\,T_{avg,\,i}} \qquad (14)$$

where:

ΔN_i = mass than entered element i from element i + 1 during time $\theta_j - \theta_{j-1}$, lb. moles.

M = number of divisions, e.g. 20.

F = gas transmittance of the panel, CFM ft. length/ft. width.

W = panel width, ft.

L = panel length, ft.

θ_j = current time, min.

θ_{j-1} = time at previous iteration.

P_{i+1} = pressure of element i + 1, mm Hg.

P_i = pressure of element i, mm Hg.

$T_{avg,i}$ = average temperature of element i and element i + 1, °K.

R = universal gas constant, (mm Hg) ($ft.^3$) / (lb.mole)(°K.)

From previous experimental data the following empirical correlation was derived for the conductance.

$$\log F = 0.86744 \log P + 1.1783 \quad P > 50 \text{ mm Hg} \tag{15}$$

$$F = 40 \quad P \leq 50 \text{ mm Hg} \tag{16}$$

The pressure in a given element was determined in the following manner. A pressure P_1 was calculated by the ideal gas law by the equation:

$$P_1 = \frac{N_i R T_i}{V} \tag{17}$$

where:

N_i = mass in the element, lb.moles.

V = volume of the element, $ft.^3$

T_i = temperature of the element, °R.

The vapor pressure, P_o, of the substance at T_i was then determined by an empirical equation. The program then selects the smaller of P_1 and P_o which is then taken as P, the pressure of the element. This procedure thus automatically takes into account the solidifcation of the gas at low temperatures.

Dushman[4] gives an equation for the vapor pressure of CO_2.

$$\log P_o = 8.882 + 0.8702 \log T - 0.003891 T - 1408/T \tag{18}$$

where P_o is in mm Hg and T is in K.

For the other gases of interest, data from several sources [4, 5, 6, 7] was plotted on a semi-log plot versus 1/T and was found to yield a straight line. Using a least squares fit on the computer, constants were then determined for the following equation.

$$\log P_o = A - B/T \tag{19}$$

where P_o and T have the units of mm Hg and °K, respectively. Values of A and B resulting from the program are given in Table 8.

The computer calculations proceed as follows. The system is initialized by assigning t_i (ambient temperature) to all the elements in the panel. The initial mass in each element is then calculated using equation (17). The analytical solution then assumes that the cold side temperature instantaneously reaches the temperature of the liquid in the tank (20.4°K for liquid hydrogen). Heat transfer then proceeds as the time is incremented. The temperature at any time and at any location in the panel is determined by equation (13). As an element cools, its pressure is lowered as calculated by (17) or a vapor pressure equation. Mass then flows out of an into the element as determined by equation (14). The new amount of mass in the element is calculated by (20).

$$N_{i,j} = N_{i,j-1} - \Delta N_{i-1,j} + \Delta N_{i,j} \tag{20}$$

where:

$N_{i,j}$ = new amount of gas in element i after time j, lb. moles.

$N_{i,j-1}$ = previous amount of gas in element i at time j-1, lb. moles.

Whenever equation (14) indicates that more mass flows out of the element than is actually present, then the amount leaving is assigned the amount of mass present. When equation (20) indicates zero mass in the element, then the element takes on the pressure of the nearest colder element that does contain mass. A pressure versus time relationship is thus established.

The most important prerequisite for a successful application of this computer solution to the cryopumped panel is a good understanding of the heat transfer mechanisms and heat flow paths in the transient condition. There are three possible controlling heat transfer modes that apply during the pumpdown and cooldown period. In the early stages of the cooldown, the panel is entirely filled with the gas phase. The high thermal diffusivity of the gas phase is then controlling and the profile therefore develops due to gas transmittance. However,

TABLE 8

Constants For Vapor Pressure Correlation

Gas	A	B
Nitrogen	7.8508	372.63
Ammonia	9.9703	1631.7
Methane	7.2762	491.62
Oxygen	7.8293	431.15
Propane	7.5299	1072.26
N-Butane	7.624	1290.46

as the gas begins to solidify at the cold end of the panel, the density of the gas phase decreases, heat is then transferred at a slower rate, and solid conduction along the aluminized Mylar must then be considered. Thus the two remaining possibilities for the controlling heat transfer mechanism are gas conduction at a low pressure (approximately 0.1 micron of mercury) and solid conduction along the aluminized Mylar.

Examination of (13) shows that the rate at which the temperature profile is established is determined by

$$\frac{\alpha \pi^2}{L^2} .$$

Therefore, the group $\frac{\alpha \pi^2}{L^2}$ not α should be examined to determine the controlling heat transfer mechanism. Table 9 gives the values of α and $\frac{\alpha \pi^2}{L^2}$ for the three mechanisms. Since the normal gas conduction at atmospheric pressure has the highest value of $\frac{\alpha \pi^2}{L^2}$, it appears that this mechanism would be controlling. The mechanism would only be effective while a continuous gas phase is present in the panel which, of course, is not true after the panel has cryopumped to a low pressure. But, the period after this low pressure has been attained is not of practical interest. Another point worth mentioning is that this continuous phase could also be interrupted by the stratified nature of the panel, for example, if gas in the upper layers separated from the lower layers of the panels by impervious Mylar could not somehow migrate to the lower levels. However, if gas tight seals existed between the layers then a panel containing a gas such as nitrogen could not possibly be cryopumped since the temperature in the upper layers, one third of the way through the stock of three shingled panels, would be considerably above the solidifcation point of such a gas. Experimental evidence indicates that such is not thecase and a nitrogen filled panel will indeed cryopump. Therefore, there must be sufficient communication between the layers (probably at the outside edges) for the gas to flow to the lower sections. Thus the normal gas conduction at a high pressure during the early stages of the pumpdown is probably the controlling mechanism.

Even though the initial gas conduction is probably controlling in this problem, the third mechanism of conduction longitudinally along the aluminized Mylar was also investigated in order to bracket the actual heat transfer mechanism.

Table 9

Thermal Parameters in Transient Temperature Profile

Mechanism	α (Ft.^{2}/Hr.)	L (in.)	$\frac{\alpha \pi^2}{L^2}$ (Hr.$^{-1}$)
Normal gas conduction at atmospheric pressure (CO_2)	0.383	1.25	35.4
Normal panel conduction at vacuum	0.000320	1.25	0.291
Longitudinal conduction at vacuum	0.1576	36	0.160

The panel investigated in this analysis which will be used for the cryopump tests had the following characteristics.

Panel length - 36 in.
Panel width - 36 in.
Panel thickness - 0.40 in.
Cold side temperature - 294.4°K

For the normal gas transmittance mechanism, the gases investigated were ammonia, n-butane, carbon dioxide, methane, and nitrogen. For the longitudinal panel transmittance mechanism, propane and oxygen were also tried. The transient temperature profile for CO_2 is given in Figure 29 while the transient for the longitudinal panel transmittance mechanism is given in Figure 30. The theoretical pumpdown curves for both mechanisms for various gases are given in Figures 31 & 32. As can be seen from the curves, the normal gas transmittance predicts that all the gases investigated would give satisfactory performance with nitrogen giving the longest pumpdown time to 0.1 micron (40 minutes.) The longitudinal panel transmittance mechanism predicts that ammonia, n-butane, carbon dioxide, and propane would all pump down in a reasonably short time (20-40 minutes). Methane, oxygen and nitrogen would not pump down to 0.1 micron for at least six hours and therefore would probably be unsatisfactory for this application. However, as discussed earlier, some form of the normal gas transmittance mechanism is probably controlling. All of the gases investigated therefore probably would give satisfactory performances in the cryopumped panel.

The most critical assumption in the computer analysis was that of the controlling transient heat transfer mechanism. The actual mechanism has probably been bracketed by considering two possible mechanisms but experimental data was needed in order to select the correct mechanism. If the transient experimental data obtained was in disagreement with both of these mechanisms, then the program could be modified to accept the experimental temperature - time data. A pumpdown curve could then be generated on the computer based upon the actual heat transfer mechanism.

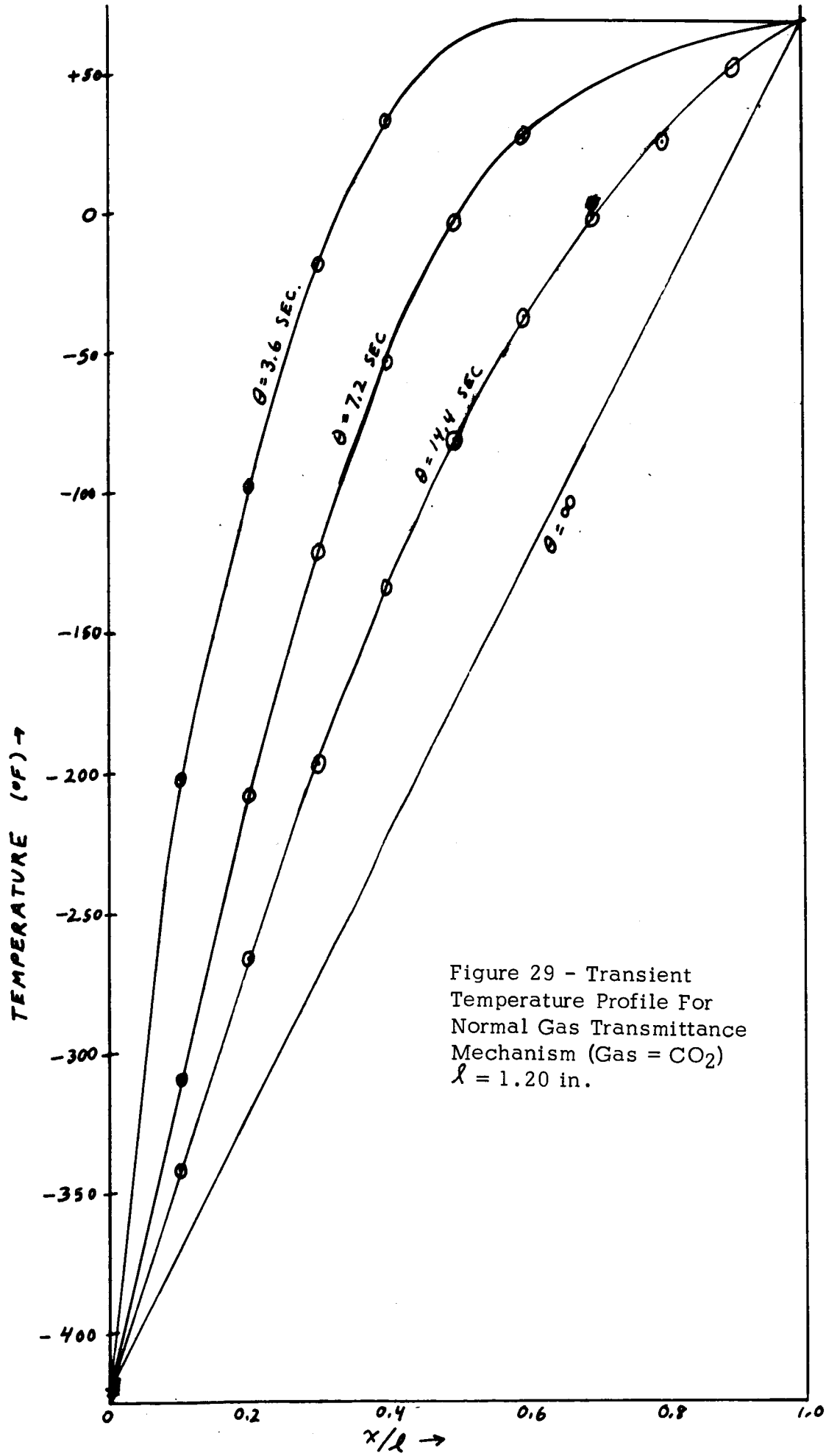

Figure 29 - Transient Temperature Profile For Normal Gas Transmittance Mechanism (Gas = CO_2)
ℓ = 1.20 in.

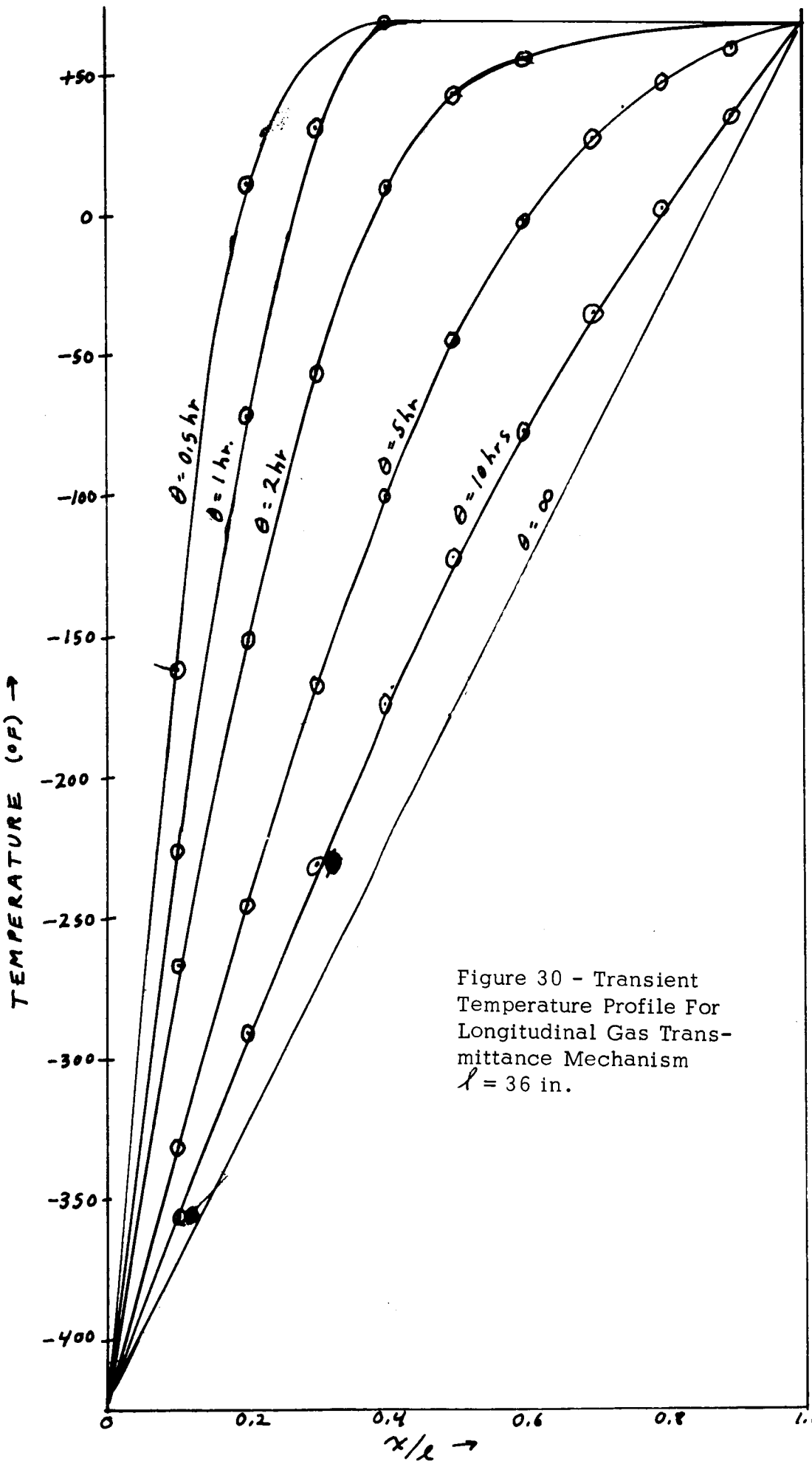

Figure 30 - Transient Temperature Profile For Longitudinal Gas Transmittance Mechanism
ℓ = 36 in.

FIGURE 31 Theoretical Pumpdown Curves For Various Gases In a 36" x 36" 7 Layer SEMI Panel at LH_2 Temperatures

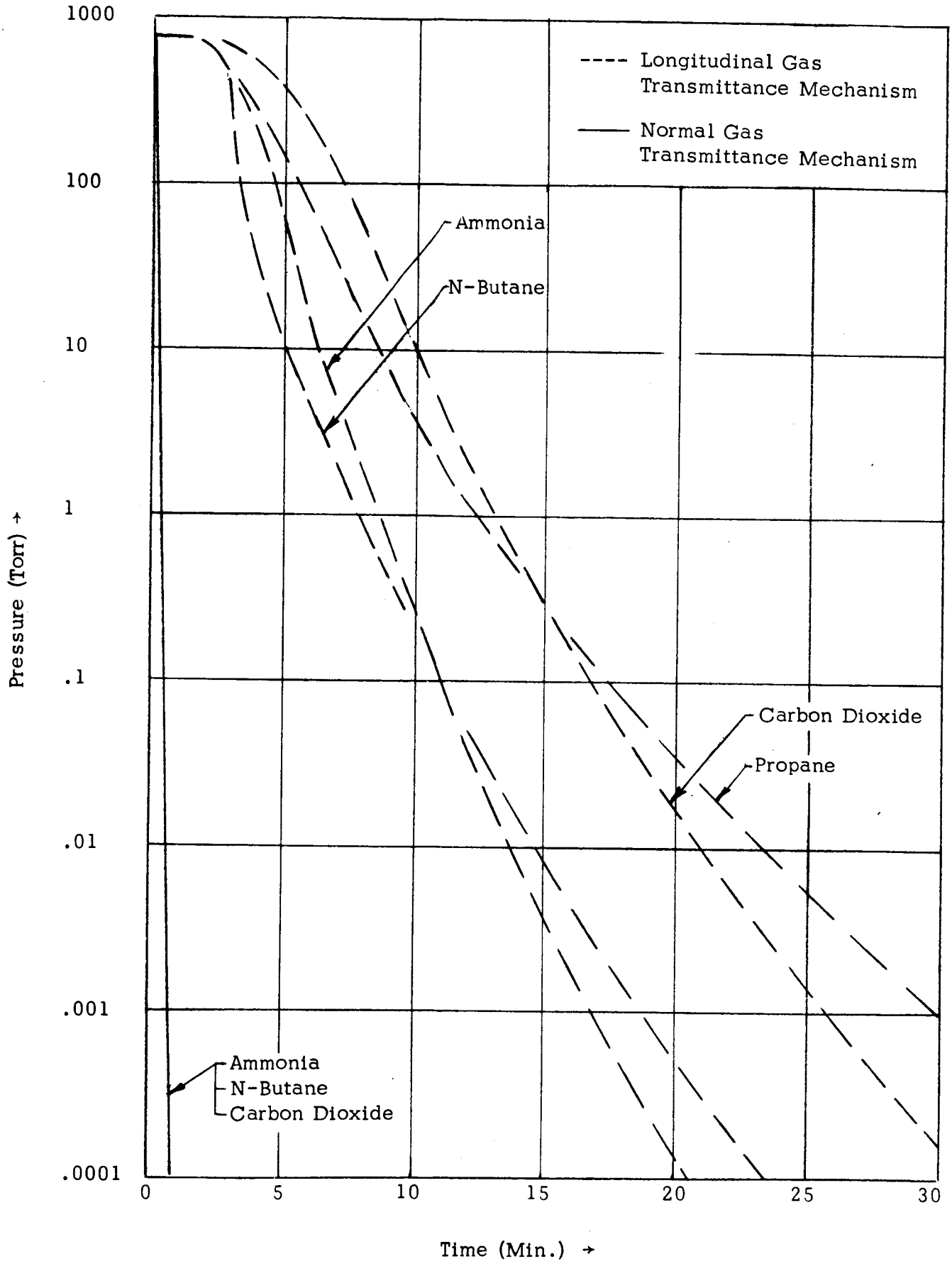

FIGURE 32 Theoretical Pumpdown Curves For Various Gases In A 36" x 36" 7 Layer SEMI Panel at LH_2 Temperatures

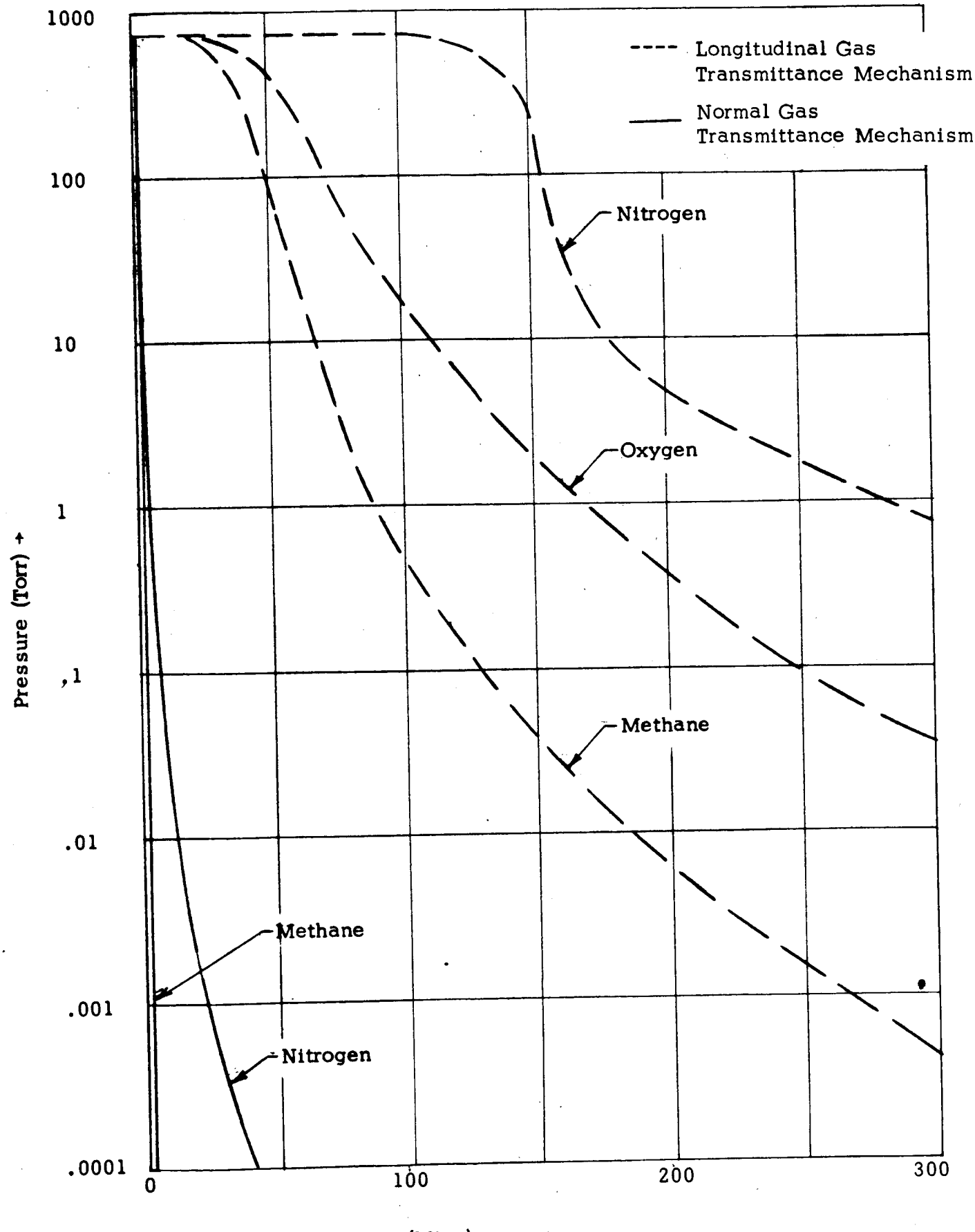

4.3.2 Cryopumping Tests

In order to verify the analysis and make an intelligent choice of the cryopumping gas, a simulated panel system was installed on the 40 inch square flat plate tester. The schematics for the test panel and for the apparatus are shown in Figures 33 and 34. The test panel was built using two layers of 0.02 inch rigid open cell polyurethane foam with each of the six double aluminized Mylar radiation shields. The dummy panels were fabricated with 1/10-inch thick foam sheets stacked up to the required thickness. The as-built system had a test panel .35-inch thick versus 0.2-inches thick for the evacuated dummy panels. Thermocouples were located, as shown in Figure 35, within the test panel, on the face of the tank, on the evacuation manifold, and the various gauges.

In initial testing it was found very difficult to get the dummy panels leak tight. However, since both the dummy panels and the area behind the test panel are all to be purged with the test panel purge gas, it was decided to put one lead Mylar jacket over the entire apparatus and bond it directly to the face plate of the tester. Thus, the dummy panels and the area behind the panels had a common vacuum system.

NRC cold cathode gauges were used to measure the vacuum level in the test panel both at the warm end and at the cold end. A thermocouple gauge was also attached to the warm end.

It was decided to test the two gases which covered the extremes of pumpdown as determined by a theoretical analysis. These were carbon dioxide and nitrogen.

Because of the mass and high heat leak of the test apparatus, it was necessary to cool it down with liquid nitrogen prior to initiating the liquid hydrogen fill. Thus, the tank cooldown took a finite time whereas the analysis reported above assumed an instantaneous cooldown. For this reason it would not be expected that the test results plotted as vacuum level versus time would agree exactly with the predicted. Figure 36 shows a comparison between the actual vacuum time history as measured on the thermocouple gauge, and the predicted curve. These data have been adjusted to account for the time the pressures were coming to equilibrium during the nitrogen cooldown. However, the curve as shown is considered to be representative of what would occur if the cooldown could have been affected with liquid hydrogen alone. It will be noted that the evacuation curve is longer in time than predicted but that the ultimate pressure of something less than 1/10 of a micron appears to have been achieved in about one hour after LH_2 fill.

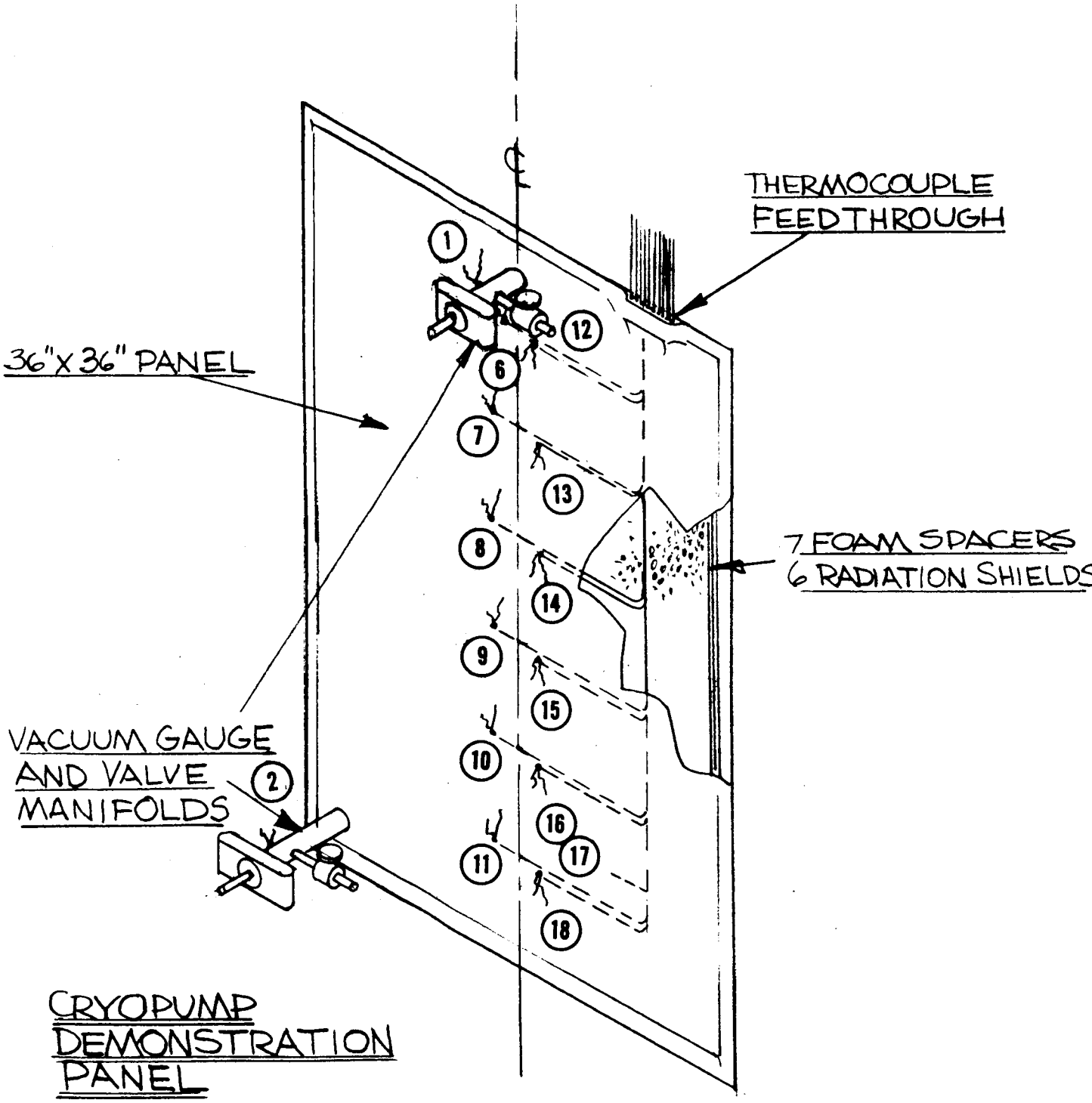

CRYOPUMP DEMONSTRATION PANEL

FIGURE 33

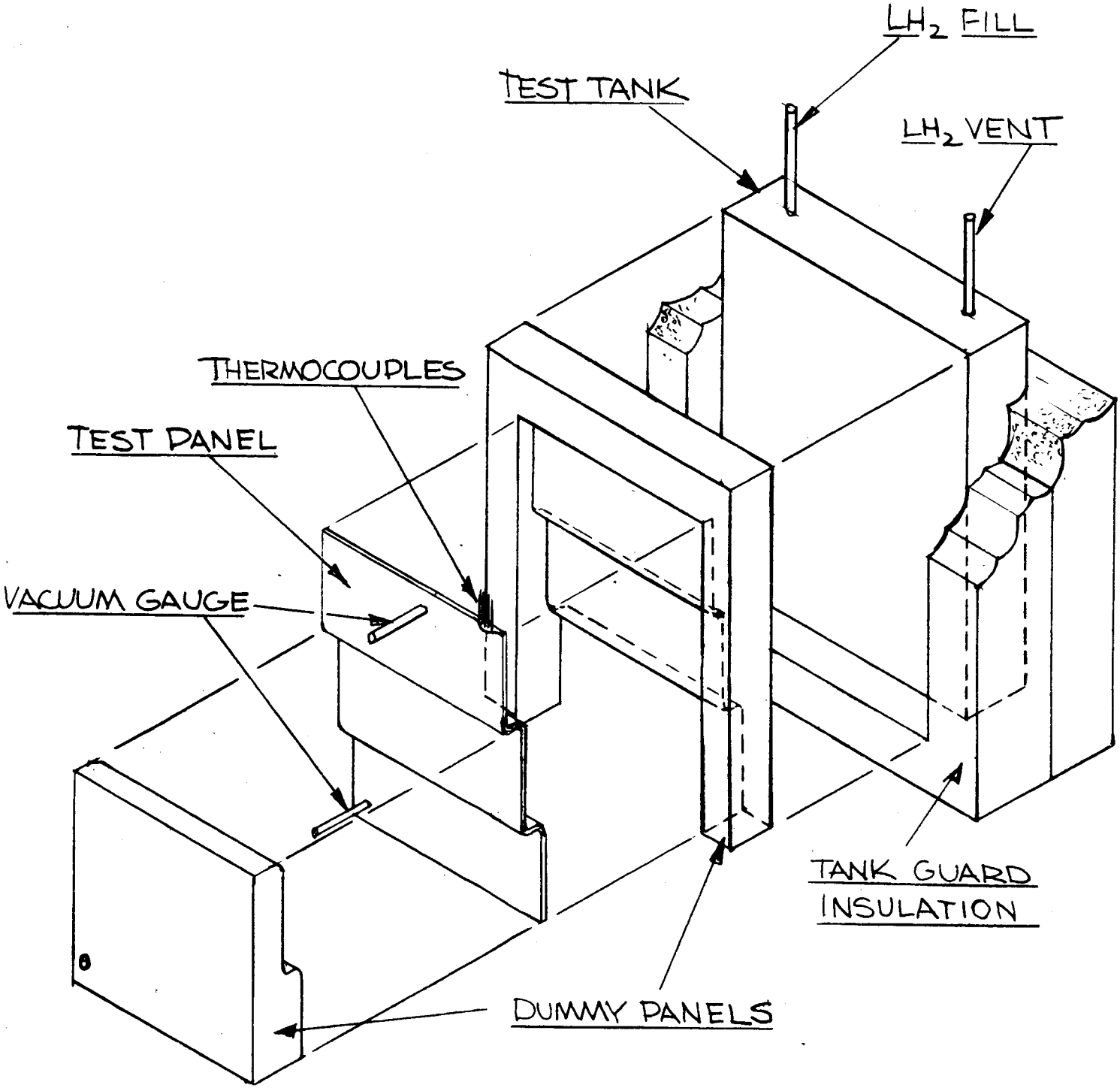

CRYOPUMP PANEL TEST SETUP

FIGURE 34

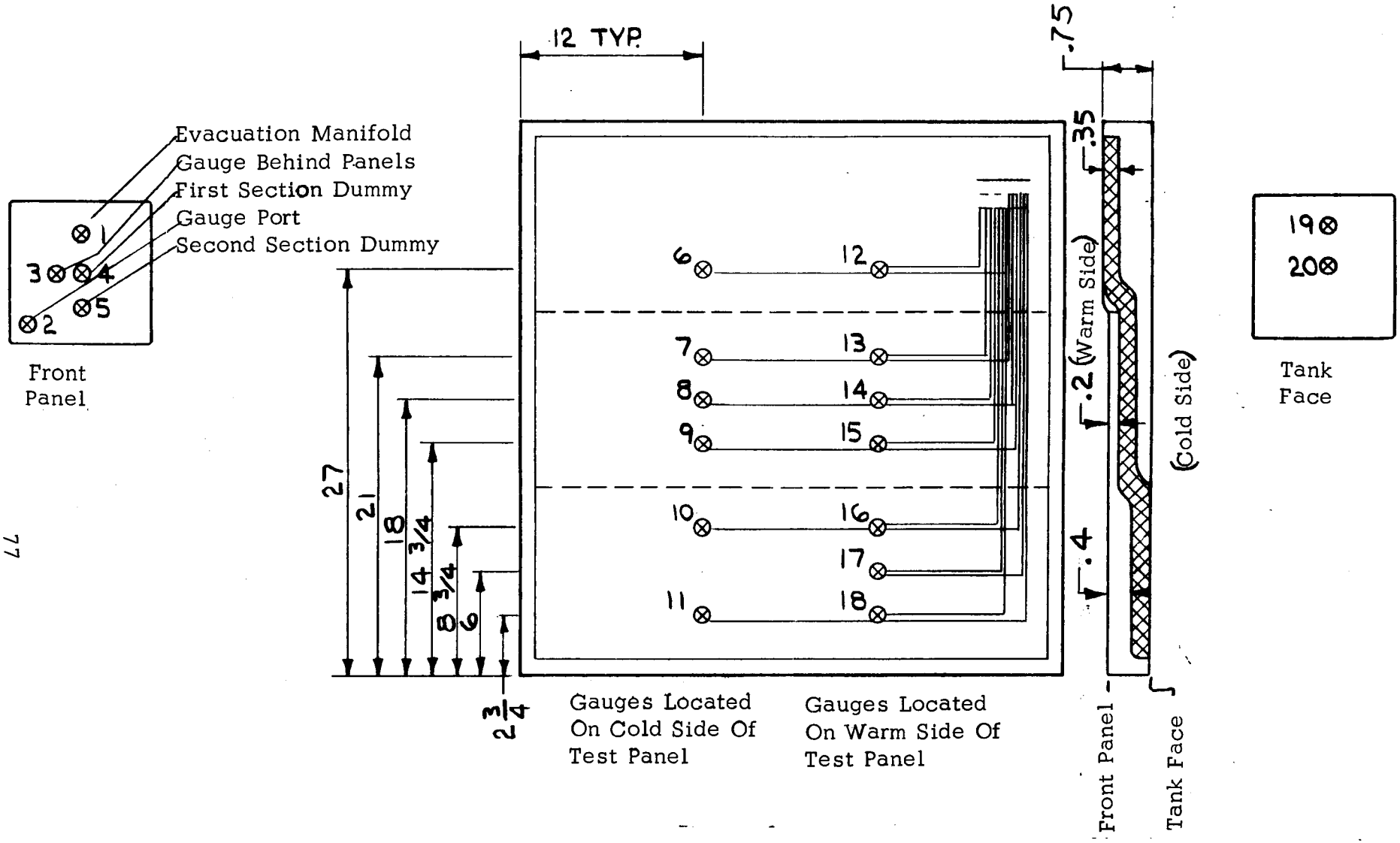

NOTE: Thermocouples inside test panels located one layer in from warm side and cold side respectively

THERMOCOUPLE LOCATION
36"x36" 1 LAYER SEMI-PANEL

FIGURE 35

FIGURE 36

VACUUM HISTORY FOR CARBON DIOXIDE IN A

36" x 36", 7 LAYER SEMI PANEL

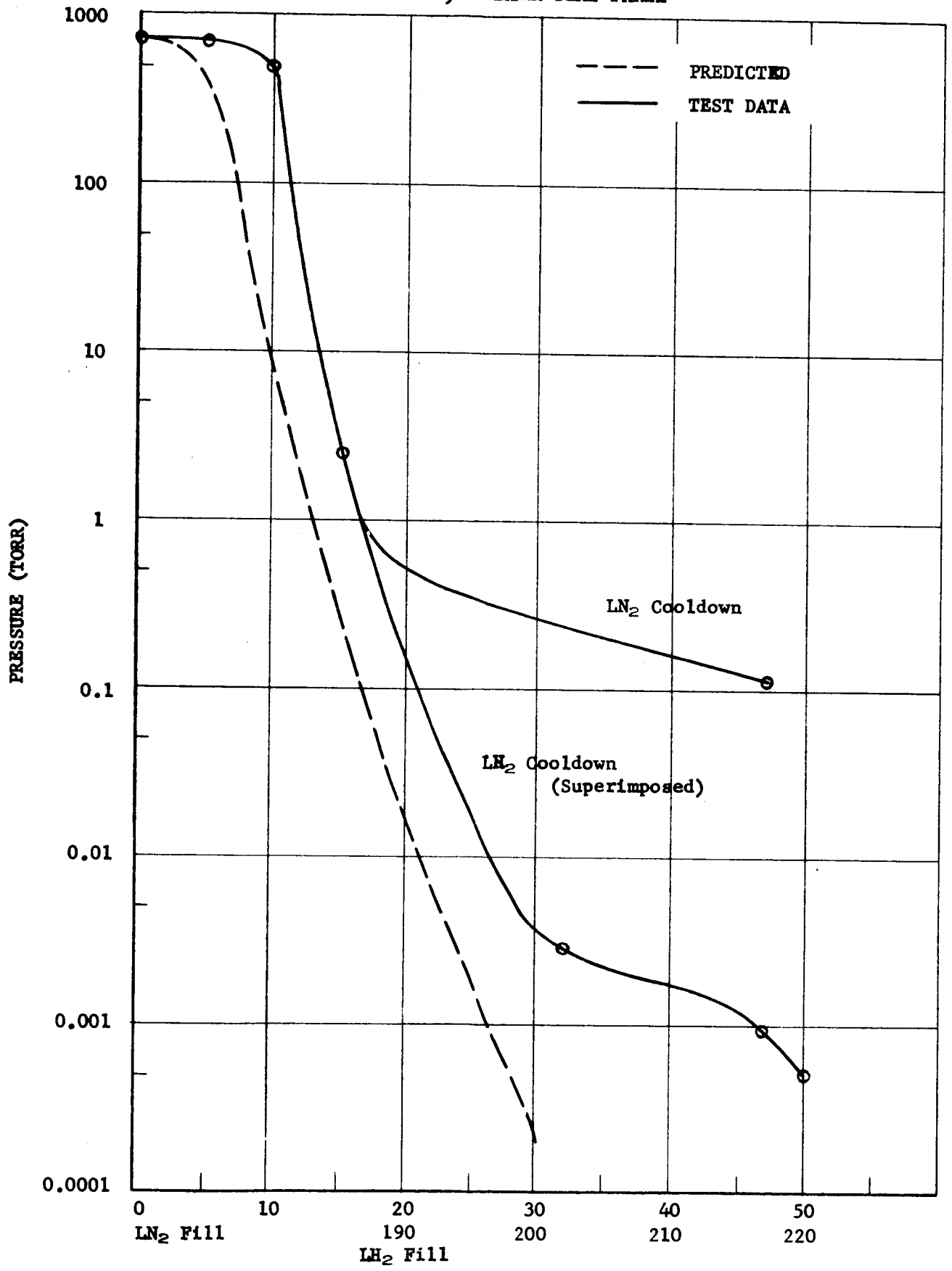

The warm end cold cathode gauge never did come on scale, whereas the cold end cold cathode gauge recorded about 1/10 of a micron about one hour after the liquid hydrogen fill. While these data certainly are not conclusive, it is felt that the high pressure reading of the cold cathode gauges is due to hydrogen offgassing of the gauges themselves. A getter capsule was located in the proximity of these gauges. The hydrogen evolved thus formed water rapidly, however, the conductance between the getter package and a cold cryopumping surface would be quite low for water. Thus, it is believed that high water pressure in the vicinity of the gauges themselves caused the high reading.

The thermocouples within the test panel were located on the inside and the outside radiation shield with one layer of foam separating the thermocouples from the panel casing. The temperature measurements recorded at steady state for the carbon dioxide purged system are shown on Table 10. Review of these data will indicate that each shingle layer of the panel is essentially isothermal, and that there is a greater temperature drop both across the panels and at those positions where the shingling goes from one layer to another. The large temperature drop from the warm side to the cold side at any given location tends to indicate that a respectable degree of vacuum was achieved. The fact that most of the temperature drop occurs across the test panel as compared with the dummy panel is possibly due to the fact that the dummy panel was thinner, and also may indicate that the dummy panel had a higher vacuum level (70μ Hg was measured). This high residual gas in the dummy panel could possibly be helium gas leakage from around the edges. (Helium gas was used to purge the foam insulation and the area outside the test panels.)

At the completion of the carbon dioxide test, the test panel and dummys were evacuated and back filled with evaporated liquid nitrogen and the test procedure repeated. As predicted by theory, it took much longer for the nitrogen gas to cryopump than the carbon dioxide, (three hours versus one hour to approach a steady state) and the final vacuum level apparently was higher. The pressure time history compared with the theoretical is shown in Figure 37. Although neither of the cold cathode gauges were indicating, it is probable that a pressure somewhere in betweem 0.1 and 1 micron was the best that was achieved.

The temperature distribution achieved at steady state during the gaseous nitrogen test is also shown in Table 10. It will be seen that lower temperature levels were experienced with the nitrogen purge gas than had been noted when CO_2 was used. This is probably due to the fact that essentially no vacuum was available during the nitrogen cooldown. It will also be noted that the temperature gradient across the panel is greatest on the cold leg of the shingle system. This may be due to the effects of subcooling of the insulation or it may indicate a greater degree of vacuum on the cold end than on the warm end.

TABLE 10

STEADY STATE TEMPERATURE MEASUREMENTS (°C)

Thermocouple No.	Location	CO_2 Test	N_2 Test
1	Evac. Manifold	+ 15	0
2	Gauge Port	+ 15	- 18
3	Gauge Behind Panels	+ 20	0
4	First Section Dummy	+ 12	- 10
5	Second Section Dummy	+ 10	- 15
6	Cold Side Warm Section	- 66	- 130
7	Cold Side Middle Section	- 105	- 150
8	Cold Side Middle Section	- 105	- 155
9	Cold Side Middle Section	- 110	- 160
10	Cold Side Cold Section	- 120	- 160
11	Cold Side Cold Section	Inoperative	Inoperative
12	Warm Side Warm Section	+ 5	- 20
13	Warm Side Middle Section	0	- 20
14	Warm Side Middle Section	0	- 25
15	Warm Side Middle Section	0	- 8
16	Warm Side Cold Section	- 75	- 65
17	Warm Side Cold Section	- 80	- 65
18	Warm Side Cold Section	- 90	- 75
19	Tank Wall Top	- 90	- 75
20	Tank Wall Middle	<- 230	<- 230
Time After LH_2 Fill		80 Min.	465 Min.

FIGURE 37

VACUUM HISTORY FOR NITROGEN IN A

36" x 36", 7 LAYER SEMI PANEL

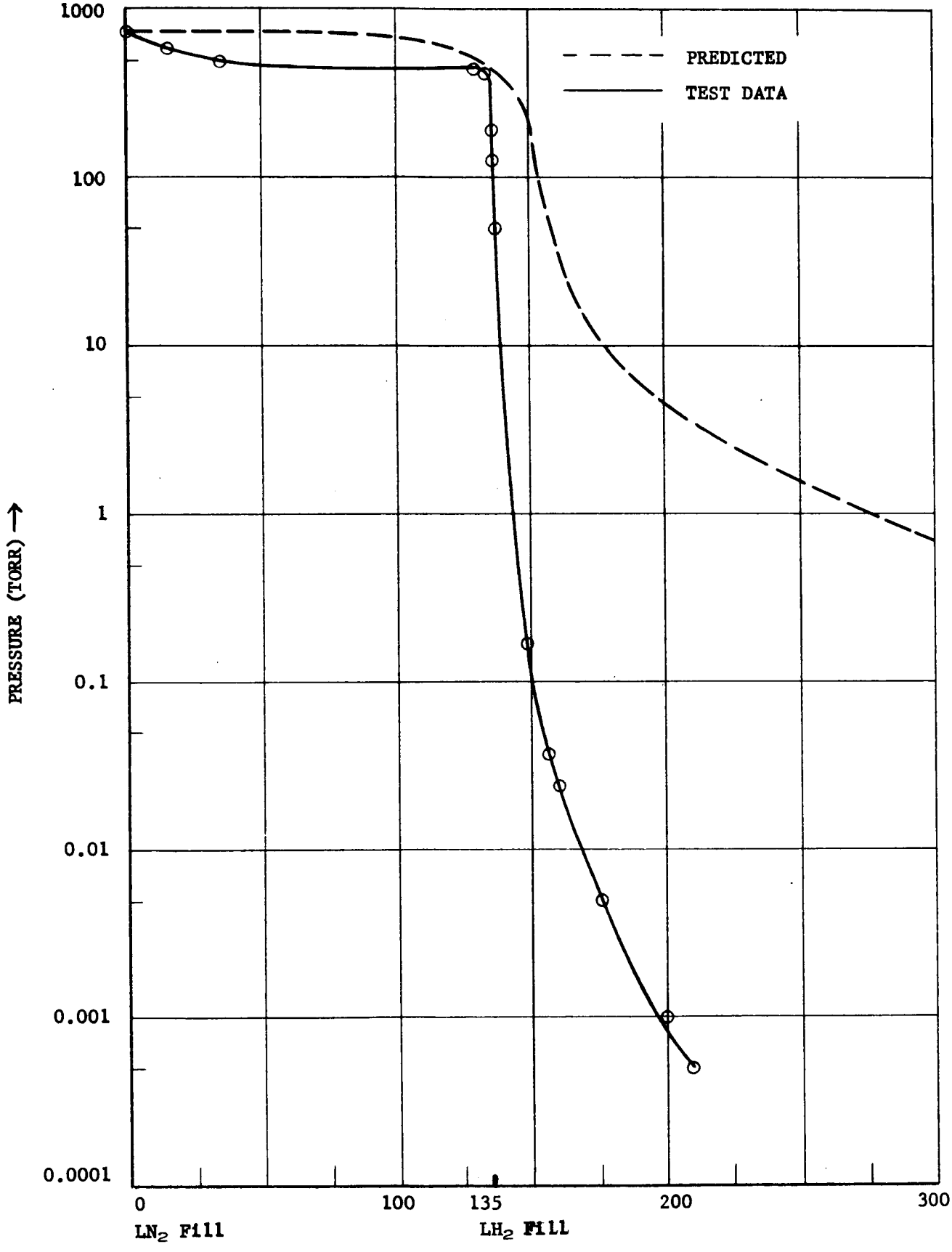

Since the relative performance of the self evacuating characteristics of the insulation between carbon dioxide and nitrogen gas are as predicted by theory, carbon dioxide was used as the purge gas for the panels applied to the calorimeter tank.

4.3.3 Vacuum Gauge Tests

Throughout the work with carbon dioxide filled insulation systems, problems with accurate vacuum gauging were present. The desired vacuum level (10^{-4}torr) is below the range for thermocouple type gauges and near the upper limit for ionization gauges. Additional difficulty was attributed to gauge off-gassing and possible dissociation of the carbon dioxide. A number of attempts to investigate this dilemma were made on various types of apparatus. All consisted of a piping manifold connected to a liquid nitrogen or hydrogen cold trap and a vacuum pump. As shown on Table 11 each had a different gas transmittance between the test gauge and vacuum source.

Arrangement number 8 is shown in Figure 38. This had the highest gas transmittance of the arrangements tested. Three ports located on the right end next to the NRC readout are available for gauge tests. In the photograph two NRC type 524 cold cathode gauges are shown installed. Provision is made for valving off one of the gauges and including a getter package with it. The cold trap is shown at the center. The Equibar 120 capacitance type differential pressure gauge is attached across a valve to the vacuum pumping station.

Three series of tests were conducted on this apparatus as shown on Table 12; two with the two cold cathode gauges using used and fresh getter material, and one with a CVC GIC017 hot cathode ionization gauge. It will be seen that in all cases the gauges agreed with each other. An improvement in residual gas pressure by a factor of two is indicated by installing fresh getter. Since the original getter material was not subjected to sufficient hydrogen to use it up, it is surmised that there may be some poisoning action due to the carbon dioxide. More development work will be needed to determine the effects of long-term exposure to carbon dioxide for the getter.

When the test apparatus was originally charged with CO_2, it was found that only relatively high pressures could be obtained by cryo-pumping, indicating either severe offgassing or impurities in the Coleman grade CO_2. It was therefore the practice to condense the carbon dioxide on the cold trap and then evacuate the system for some time through a diffusion pump in order to remove noncondensables. This had to be repeated two or three times. Even after cleaning up of the CO_2, however, it was noted that the dynamic pumping produced lower residual pressures than did cryopumping. This is an indication that there was offgassing in the system somewhere.

TABLE 11

SUMMARY - VACUUM GAUGE TEST DATA - CRYOPUMPING TESTS

Carbon Dioxide Gas

Arrangement	Calculated Gas Transmittance Atm cc/sec.		Volume to Area Ratio (cm)	Dynamic Pressure (Torr) Gauge No. 1		Dynamic Pressure (Torr) Gauge No. 2		Cryopumped Pressure (Torr) Gauge No. 1		Cryopumped Pressure (Torr) Gauge No. 2		Cryogen
1	27.5		.98	1.75×10^{-5}	(0)	5×10^{-5}	(0)	1×10^{-3}	(8×10^{-4})	3×10^{-2}	(3×10^{-2})	LN_2
2	27.5		.98	-		2×10^{-4}	(0)	-	(-)	2×10^{-3}	(3.5×10^{-3})	LN_2
3	500.0		1.1	-	(-)	1×10^{-5}	(0)	-	(-)	1×10^{-3}	(4.1×10^{-3})	LN_2
4	2,900	(Gettered Gauge)	1.3	9×10^{-5}	(-)	-	(-)	4×10^{-5}	(-)	-	(-)	LN_2
	3,300	--		3×10^{-5}	(-)			1.5×10^{-4}	(-)	-	(-)	
5	410	(Gettered Gauge)	1.03	3.5×10^{-4}	(0)	-	(-)	1.5×10^{-4}	(-)	-	(-)	LN_2
	410	--		2.5×10^{-4}	(0)			2×10^{-4}	(-)	-	(-)	
6	775	(Gettered Gauge)	1.2	9×10^{-5}	(0)	-	(-)	1.5×10^{-4}	(-)	-	(-)	LN_2
	775	--		8×10^{-5}	(0)			1.3×10^{-4}	(-)	-	(-)	
7	670	(Gettered Gauge)	1.03	8×10^{-5}	(-)	-	(-)	4×10^{-4}	(-)	-	(-)	LH_2
	705	--		8×10^{-5}	(-)			4.5×10^{-4}	(-)	-	(-)	
8	6,130	(Gettered Gauge)	1.24	3×10^{-6}	(-)	-	(-)	3.5×10^{-5}	(-)	3.6×10^{-5}**	(-)	LN_2
	11,000	--		-				1.6×10^{-5}	(-)	1.7×10^{-5}**	(-)	

Nitrogen Gas

7	670	(Gettered Gauge)	1.03	$>5 \times 10^{-3}$		-	(-)	$>5 \times 10^{-3}$		-	(-)	LH_2
	705			$>5 \times 10^{-3}$	(-)			$>5 \times 10^{-3}$	(-)			

Gauge No. 1 NRC-524 Cold Cathode Ionization Gauge

Gauge No. 2 General Electric 22 GT-103 Hot Ionization Gauge

* Pressure indicated in parenthesis was measured using a Equibar 120 capacitance type differential pressure meter.

** Indicates CVC hot ionization gauge.

Figure 38
Gauge Test Arrangement No. 8

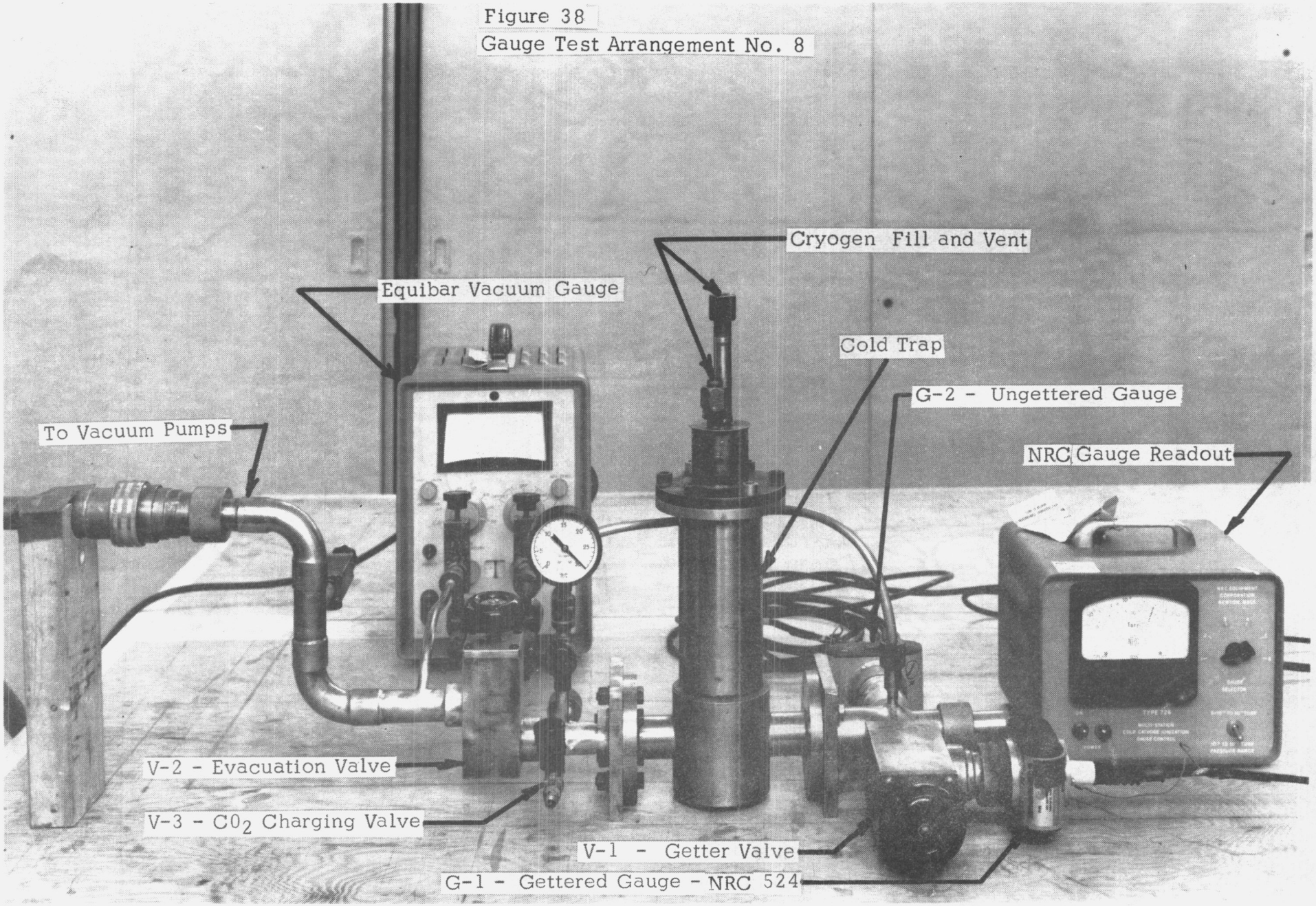

TABLE 12

VACUUM GAUGE TESTS - ARRANGEMENT NO. 8

Method of Pumping	Getter	NRC Cold Cathode No. 1	NRC Cold Cathode No. 2	CVC Hot Cathode	Remarks
Dynamic	In system		1.5×10^{-5} Torr	Not installed	Used getter
	Out of system				
Cryopumped	In system		2.1×10^{-5}		
	Out of system		1.1×10^{-5}		
Dynamic	In system	3×10^{-6} Torr	3×10^{-6}	Not installed	Fresh getter
	Out of system				
Cryopumped	In system		6.8×10^{-6}		
	Out of system		1.1×10^{-5}		
Cryopumped	In system		3.5×10^{-5}	3.6×10^{-5} Torr	CVC gauge
	Out of system		1.6×10^{-5}	1.7×10^{-5}	installed

The Linde Palladium Oxide getter material was installed to convert hydrogen, which was suspected as the offgassing material from the gauges, to water. The experience gained in these tests and previous ones indicates that the getter does react satisfactorily with offgassed hydrogen; however, the system gas transmittance for water is worse than is the transmittance for hydrogen. Thus in some cases the pressure at the gauge throat was higher with the getter in the system. This water vapor, however, will condense on the cryopumping surface while the offgassed hydrogen will not. Therefore, the use of getter is recommended.

There was speculation that the offgassing was due to the system rather than just the vacuum gauges. In order to get an indication of the affect, 21 sq. in. of copper foil were rolled and inserted into the system at the plug shown on the right in Figure 38. The total surface area of the system was thus increased by about 20%. No change in the indicated pressure levels could be detected, however, and it is felt that this is an indication that the offgassing load from the system other than the gauges is small.

In order to get an indication of any dissociation of the carbon dioxide atmosphere by firing the gauges at high pressure, gas analyses were made before and after gauge firing with and without getter in the system. These data are shown on Table 13. Unfortunately, there was an air leak into the sample bottle when the sample without the getter was taken after gauge firing. Prior to taking any samples, the system was pressurized to 1000 microns with Coleman grade carbon dioxide and valved off. After valving it was found that the pressure continued to rise to about 1700 microns as measured by the Equibar. This rise may be attributed to poor transmittance through the piping to the Equibar. It will be noted that firing of the gauge in both tests caused an increase in the oxygen concentration of the residual gas. This may be an indication of carbon dioxide dissociation. The data for water and hydrogen do not appear to be accurate enough to draw any conclusions regarding the operation of the getter material. Gauge tests with nitrogen in place of carbon dioxide resulted in gauge readings about the same as with carbon dioxide tending to indicate that dissociation does not occur.

A tabulation of all gauge tests made is shown in Table 12. Apparatus Number 8 was designed for high transmittance to compare it with previous data to determine the effect of transmittance on the ultimate cryopumped or vacuum-pumped pressure. The data for cryopumped pressure versus transmittance are shown Figure 39. As would be expected, because of the many variables

TABLE 13

GAUGE TEST GAS ANALYSES

	Without Getter		With Getter	
Component	Background Sample	After Firing	Background Sample	After Firing
H_2	Not detected		N.D.	0.03%
CH_4	N.D.		N.D.	0.01
H_2O	0.48%		0.02%	0.02
N_2 + CO	< 1		< 1	< 1
O_2	0.02		0.02	6.6
Ar	N.D.		N.D.	N.D.
CO_2	Major component		M.C.	M.C.
Pressure	1600 μ		1700 μ	1700 μ

No Data - Air Leak

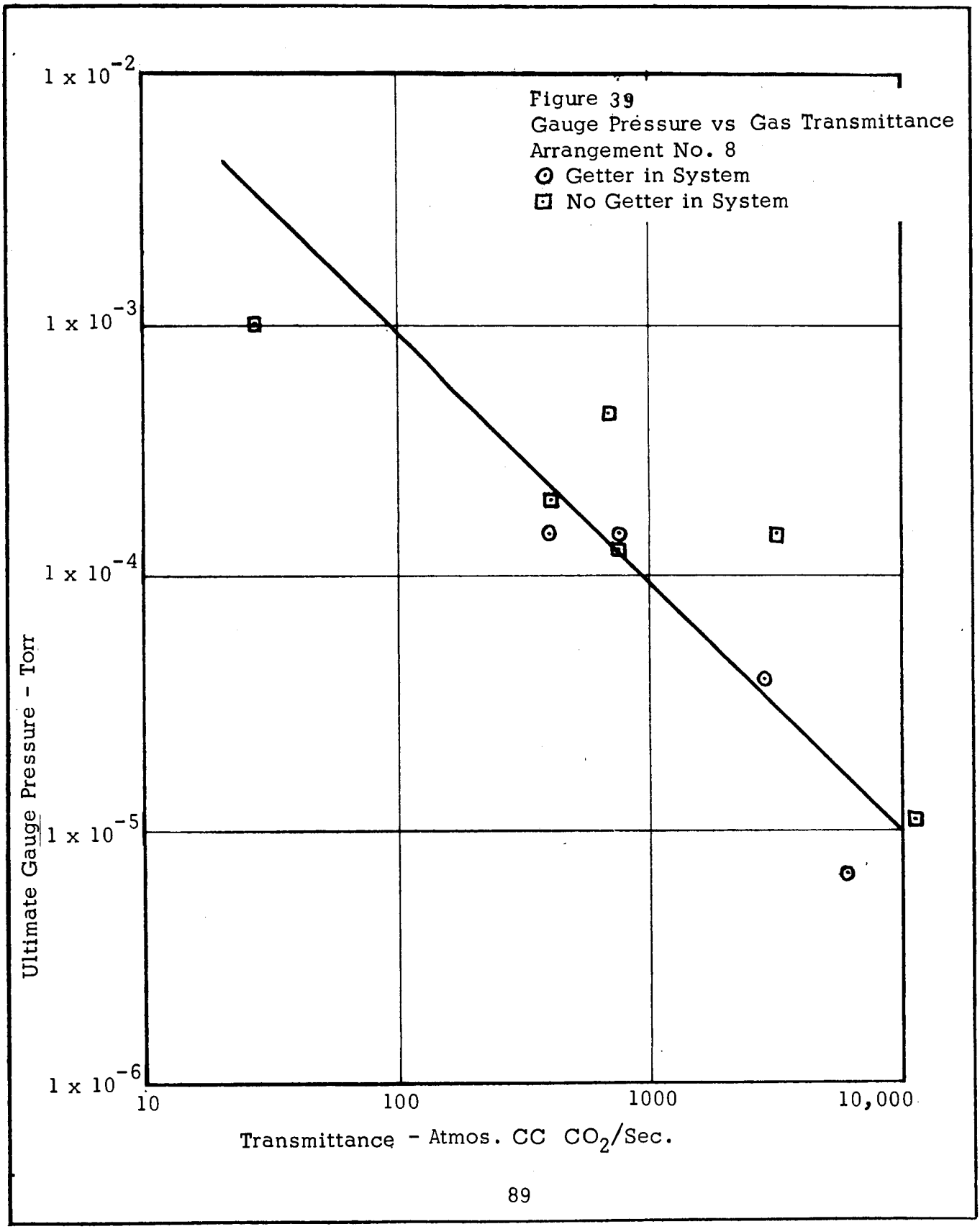
Figure 39
Gauge Pressure vs Gas Transmittance
Arrangement No. 8
Getter in System
No Getter in System
1 x 10-2
1 x 10-3
1 x 10-4
1 x 10-5
1 x 10-6
Ultimate Gauge Pressure - Torr
10
100
1000
10,000
Transmittance - Atmos. CC CO2/Sec.

involved other than just transmittance, there is considerable scatter in the data. Among the variables which would influence these data, assuming that the gas load is primarily from offgassing of the gauge, are past history of the gauge, inaccuracies in estimating the actual transmittance and the gas composition. Past history of the gauge is probably the most important.

If one assumes that the pressure at the cryopumping surface is low relative to the pressure at the vacuum gauge and that the offgassing rate is constant over an extended period of time (this is no doubt quite an oversimplifying assumption), the relationship between the pressure achieved and the transmittance should be linear when plotted on a log-log scale since the flow rate is proportional to the product of the transmittance and the pressure difference in the molecular flow regime. As can be seen on Figure 39, there is some indication that this is occurring, and the data indicate that the gauge readings may be attributable to the flow of off-gassed gas through the system to the vacuum source. Similarly, if one estimates the transmittance of an insulation panel as applied to the calorimeter tank and compares it to these gauge test data, one would predict a pressure in the micron range. The pressure actually measured during testing was in fact in this range until about 40 hours into the test.

While these data are anything but conclusive, it may be reasoned that much of the difficulty in measuring low pressures in cryopumped panels may be attributable to offgassing of the gauges. It would seem that the gauges are indicating the pressure in their throats but not necessarily the pressure near the cold surface or elsewhere in a panel.

Operation of a NRC-524 cold cathode ionization gauge at low ambient temperature causes the gauge to read only very slightly lower than actual pressure. In a test conducted using an ungettered NRC gauge surrounded by dry ice, a gettered NRC gauge located in the same vacuum system but in an ambient temperature zone and an Equibar Capacitance Type Vacuum gauge used as the vacuum reference, the gauges read as noted in Table 14 after cryopumping Coleman grade carbon dioxide on a liquid nitrogen cold trap. The gauge test manifold pressure increase noted in the Table was attributed to a probable "O" ring failure on either the gauge itself or on the vacuum coupling holding the gauge, since no leakage was detected after warm-up.

TABLE 14

NRC-524 Cold Cathode Gauge Tests

Low Temperature Operation

Coleman Grade Carbon Dioxide Cryopumped at LN_2 Temperature

	Ambient Temperature		Low Temperature
Time Minutes	Gettered NRC-524 Pressure (Torr)	Equibar Pressure (Torr)	Ungettered NRC-524 Pressure (Torr)
0	-	-	- @ 24°C
5	1.6×10^{-3}	0.2×10^{-3}	1.5×10^{-3} @ 24°C
7	1.6×10^{-3}	0.2×10^{-3}	1.3×10^{-3} @ -5°C
9	1.5×10^{-3}	0.1×10^{-3}	1.2×10^{-3} @ -26°C
12	1.3×10^{-3}	-	1.1×10^{-3} @ -38°C
15	$> +5.0 \times 10^{-3}$	400.0×10^{-3}	$>+5.0 \times 10^{-3}$ @ -43°C

4.4. Calorimeter Tank

4.4.1 Calorimeter Tank Panel Design

The GFE calorimeter tank on which SEMI panels were installed for test is double guarded. It is a vertically mounted cylinder with a guard on top, measuring tank in the center, and a guard on the bottom. The assembly is supported by a central support tube which is suspended from the chamber dome for test purposes and which is supported at both ends for horizontal or vertical handling in its shipping dolly.

The SEMI panel insulation system is shown on Figure 40 (Drawing D/SK-102626). The shingled panels were installed in three layers, shingled horizontally. Two sets of panels were installed to simulate seams that would be experienced on a flight tank. A total of eight panels were installed on the calorimeter tank. They extended over the guard tanks to preclude lateral heat flow which would mask the test results.

In order to predict the thermal performance of the SEMI panel insulated calorimeter tank, the computer program originally written under Contract NAS3-6289 was revised to account for the variations between the calorimeter tanks and subsequent variations in panel sizes, for various values of insulation thermal conductivity. The results are indicated in Table 15.

TABLE 15

Thermal Analysis - Computer Program

3 Layered Semi Panel Insulated Calorimeter Tank

Predicted Heat Flux	Assumed Insulation Thermal Conductivity*
Btu/hr.ft.^{2}	Btu/hr.ft.°R
.26	1.5×10^{-5}
.3.2	2.5×10^{-5}
.39	3.5×10^{-5}
.45	4.5×10^{-5}

*Values assumed for parametric study

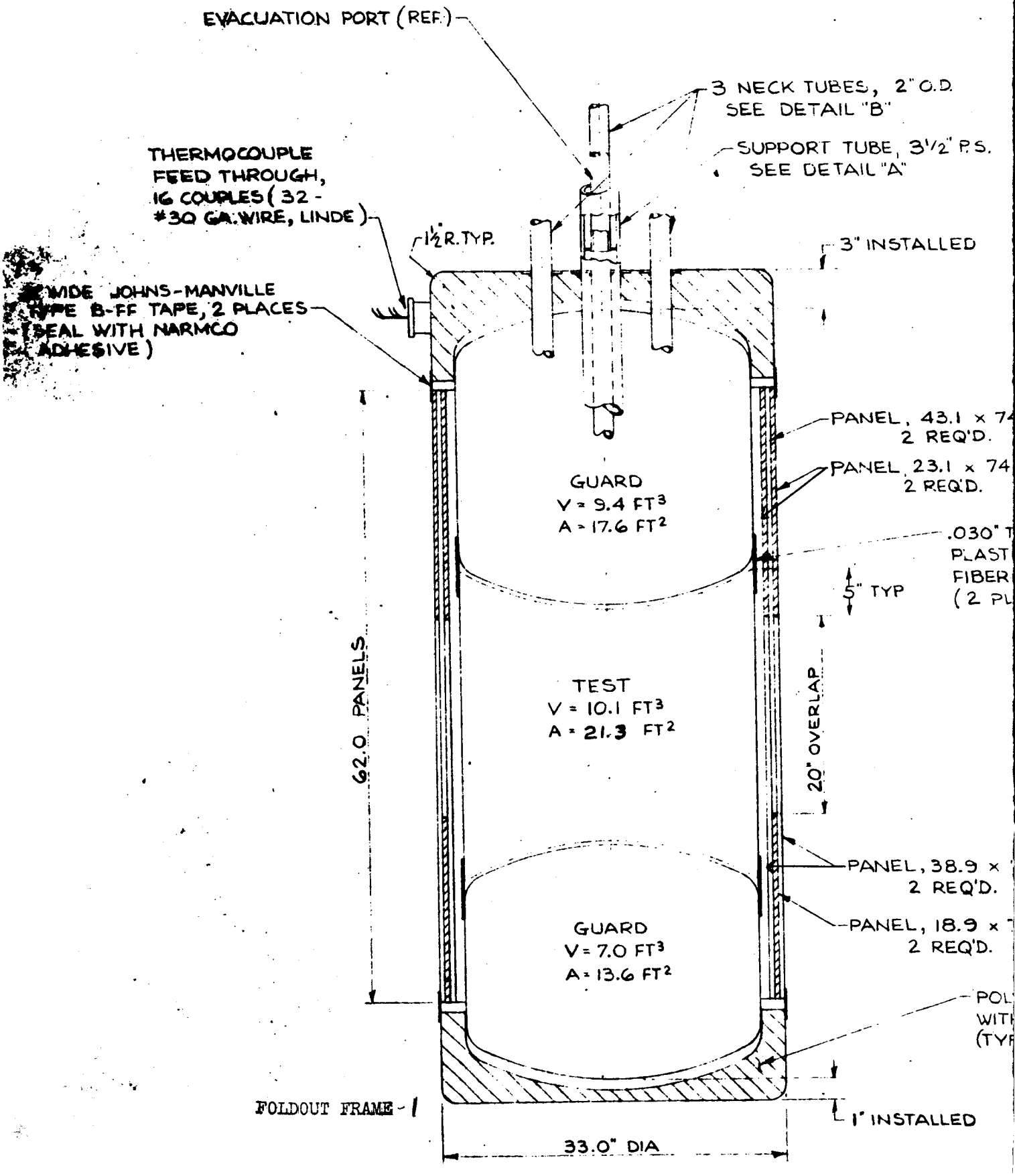

FOLDOUT FRAME - 1

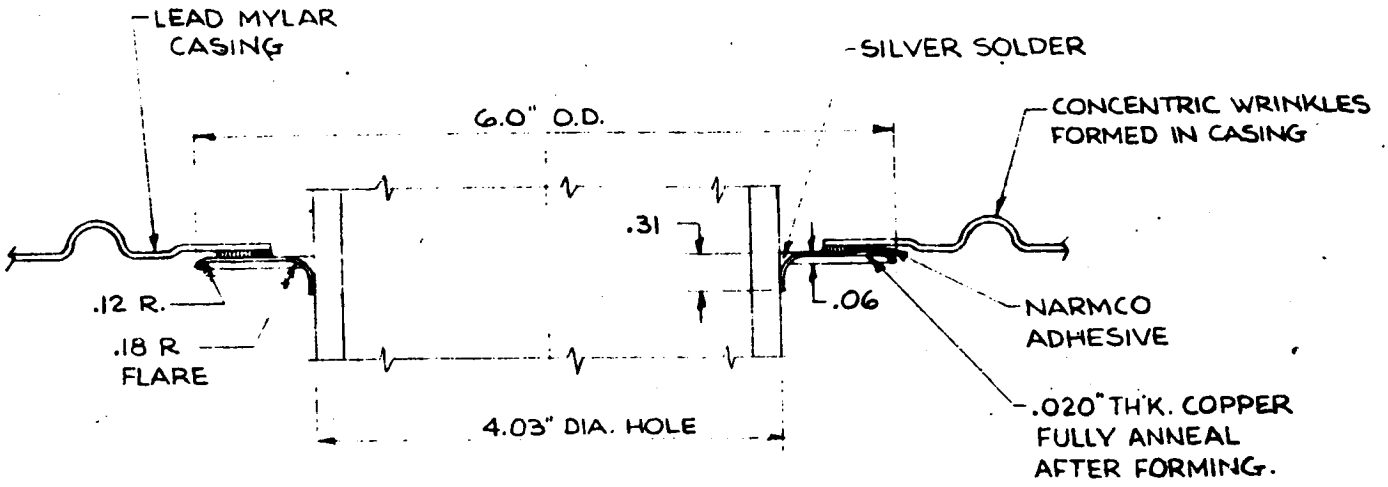

DETAIL "A"
SCALE : FULL
(NASA - LeRC)

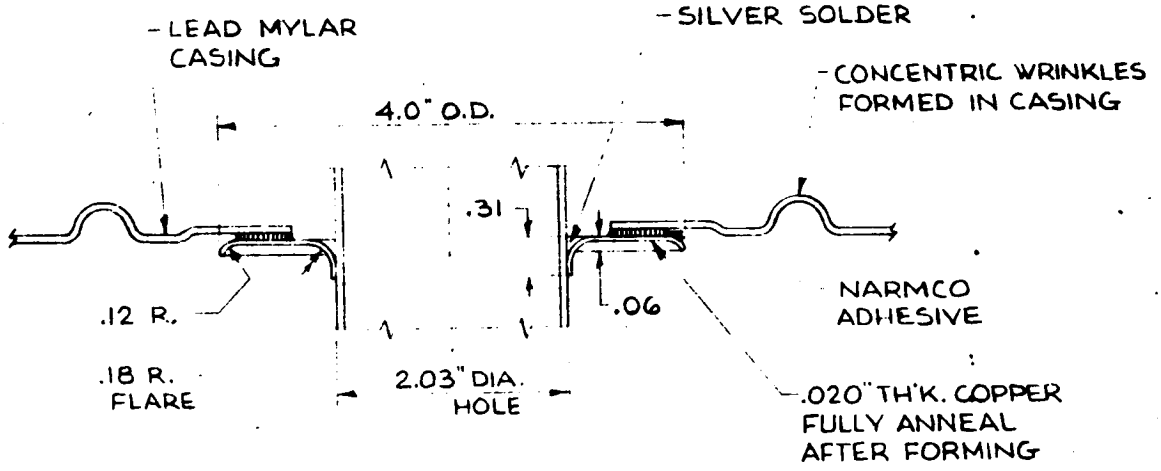

DETAIL "B"
SCALE : FULL
(NASA - LeRC)

1.0

O

H'K. x 6" WIDE
C IMPREGNATED
GLASS WRAP
ACES)

74.0

74.0

YURETHANE FOAM, COVERED
H LEAD MYLAR CASING MATERIAL.
P. BOTH HEADS)

TITLE: CALORIMETER INSULATION SYSTEM 3 LAYERED SEMI PANELS TASK V NAS3-7953	WORK ORDER
UNION CARBIDE CORPORATION LINDE DIVISION ENGINEERING DEPARTMENT TONAWANDA, NEW YORK	REPRODUCED FROM ALT. SCALE 1½"=1'-0" DRAWN REH CHK'D DATE 7/66 SHEET — SHEETS — LAYOUT ALT. LTR. DSK-102626

FOLDOUT FRAME

FOLDOUT FRAME - 2 93

FIGURE 40

4.4.2 Calorimeter Panel Fabrication

Panel fabrication was done by a two man team. In some operations, such as foam punching and panel lay-up, two men worked together. Other operations such as foam cleaning, casing forming and adhesive application were one man operations. Proper indexing of fabrication operations provided for best utilization of personnel and facilities. Thus, panel lay-up, adhesive curing, evacuation and leak detection became simultaneous operations on different panels.

Panel fabrication encompassed several operations:

1. Preprocessing the aluminized Mylar radiation shields by heating in air for 24 hours at 150°F.

2. Punching the foam spacers including vacuum cleaning of the foam to remove the foam dust generated during the bun slicing operation.

3. Vacuum forming both casings to obtain the required pleats and recovered panel thickness without residual compression.

4. Getter installation and adhesive application (Narmco 7343/7139 preceded by a prime coat of Goodyear G-207 solution) with pressure cure.

5. Panel evacuation and helium leak checking.

Each of the above mentioned operations will be discussed briefly in the following sections.

Results of development work performed under a previous SEMI panel contract (NAS3-6289) indicated that pre-conditioning of the aluminized Mylar radiation shield was necessary to alleviate hydrogen offgassing. Furthermore, it was determined that heating the aluminized Mylar in warm circulating air for 24 hours would sufficiently remove the hydrogen, and that subsequent vacuum pumping of the panel would adequately clean-up the insulation materials.

The foam spacer used for the calorimeter panels was a three layer composite consisting of two 0.02 inch thick open cell rigid polyurethane foam layers containing punched holes (PT-6 configuration) and one 0.02 inch thick layer of unpunched open cell rigid polyurethane foam. The two punched hole layers were positioned relative to each other such that support was achieved only at the intersection of the two webs, as shown in Figure 41.

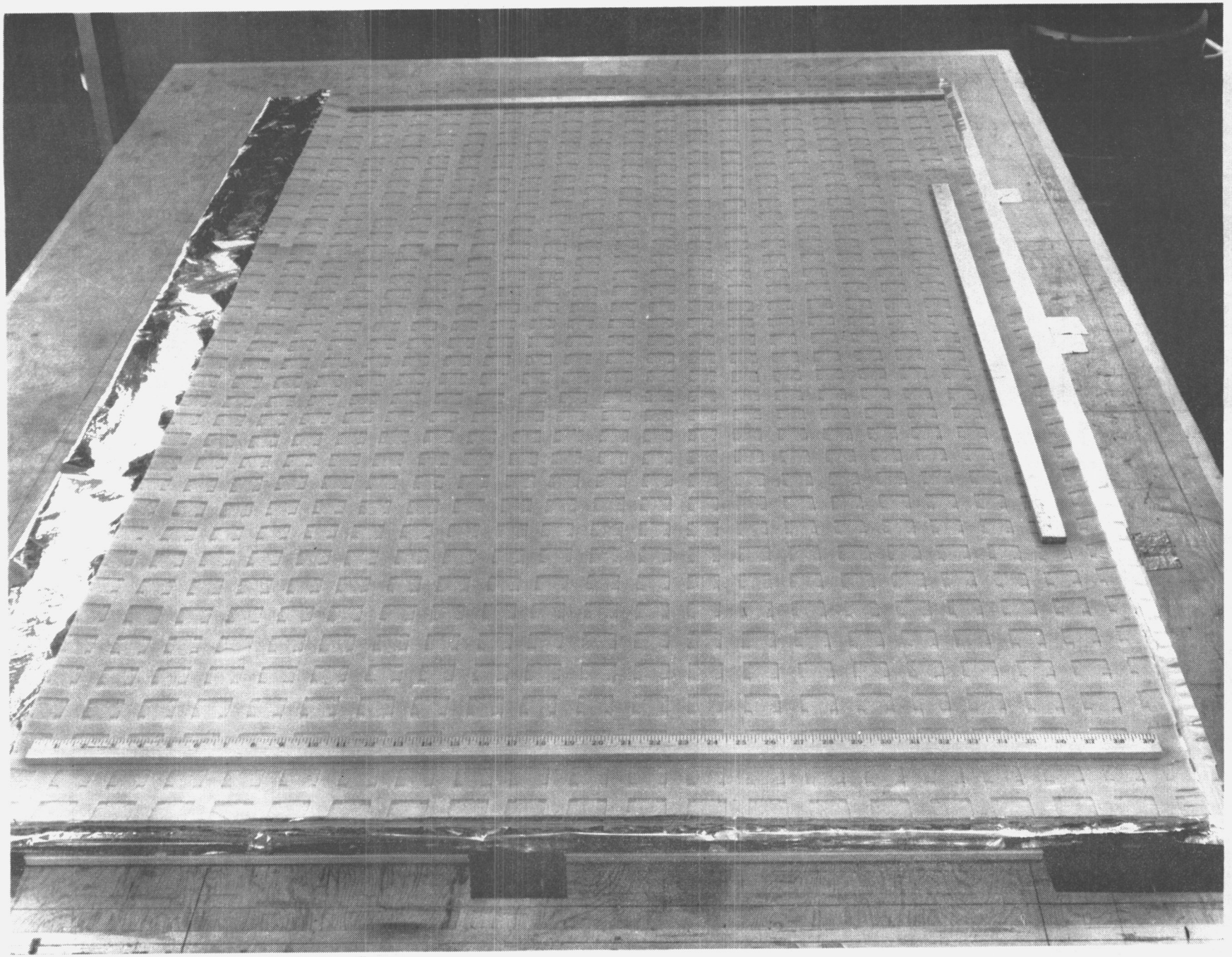

FIGURE 41 PT-6 SPACER PATTERN

Several single layers of punched foam are shown in Figure 42. Also apparent in this figure is a bar containing a row of 21 cutters which was traversed along the punching table, with indexing pins to locate each row of punched holes properly. With this method, seven layers of foam could be punched satisfactorily at one time. Panel casings were constructed of a composite casing material consisting of an impermeable outer air exposed section of Mylar/aluminum/aluminum/Mylar (MAAM), and 4-ply aluminized Mylar laminate which was used for the remaining 5/6 of the panel area. This combination was designed to achieve a casing with a highly impermeable surface that is exposed to air, yet allowing the remainder of the panel to exhibit a low thermal conductivity to enhance thermal performance.

After bonding the two materials together with the Narmco 7343/7139 adhesive and Goodyear G-207 prime, the composite casing was vacuum formed (stretched) to provide the required panel thickness. Three-eighths inch wide pleats on 1-inch centers were formed in the casing at the same time, to allow for additional material to account for the difference in diameter as the panels were curved around the tank. The casing pleats are readily apparent in Figure 43. This photograph was made prior to assembling the panel. A completed panel is shown being evacuated in Figure 44. The somewhat mottled appearance of the panel is due to surface irregularities caused by the crisscrossed foam webs. Prior to panel assembly, one gram of palladium oxide getter was placed in the foam spacer in the immediate area surrounding the evacuation manifold. Panel adhesive joints were then made in the following sequence: After degreasing the Mylar bond surfaces with Methyl Ethyl Ketone (MEK) and allowing the casing to air dry, the surfaces were primed with a solution of G-207 formulation and oven dryed for 24 hours. The prime consisted of the following:

Goodyear 207 B	100 gms
Toluene	63 gms
MEK	27 gms
Goodyear 207 C	4 gms

After the prime had cured, the Narmco adhesive was applied in the normal manner, which consists of the following:

Narmco 7343	100 gms
7139	11 gms

Room temperature cure @ 2-3 psi for 24 hours
followed by Room Temperature cure for 6 days.

FIGURE 42
FOAM PUNCHING OPERATION

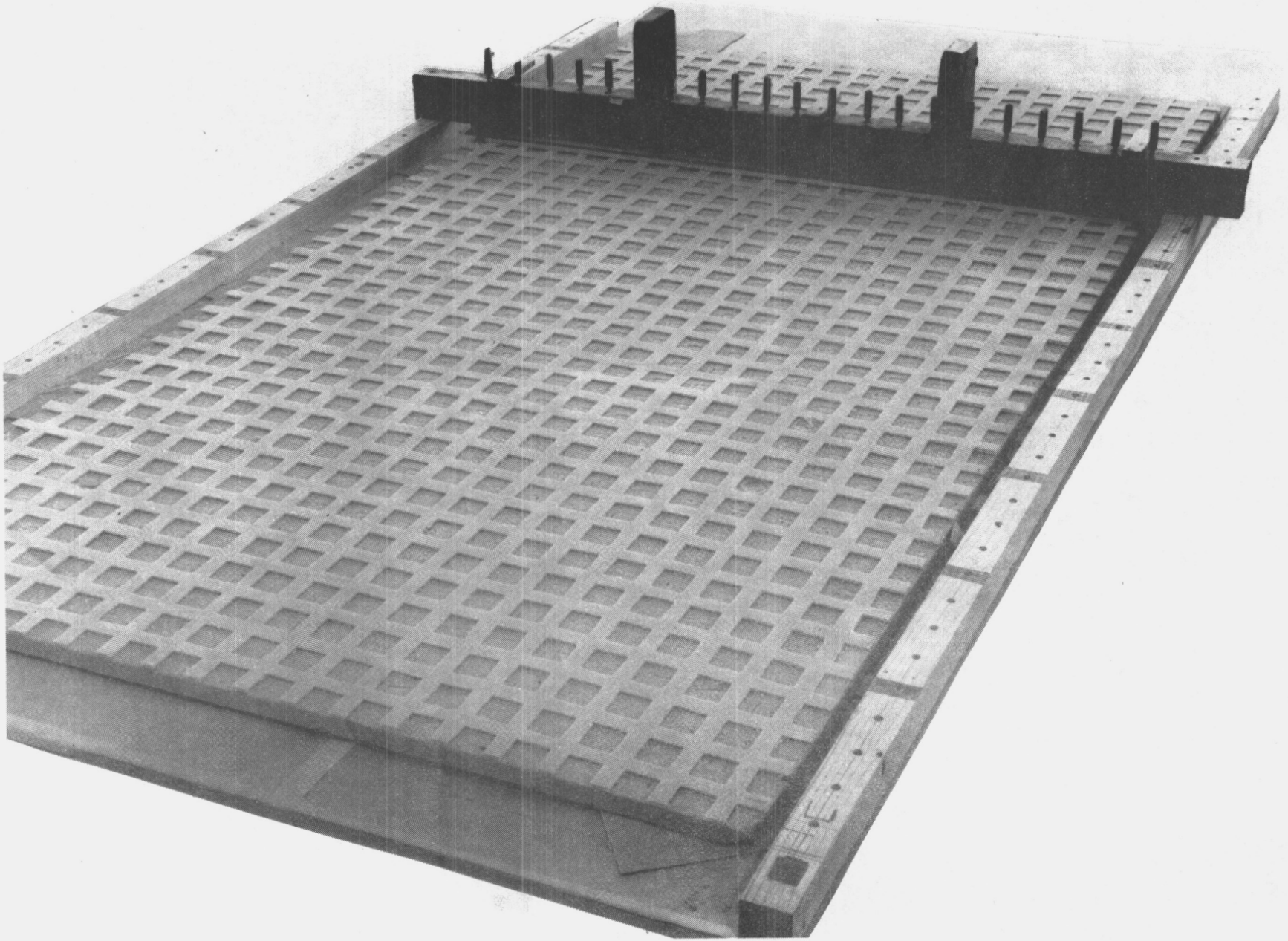

FIGURE 43

VACUUM FORMED CASING

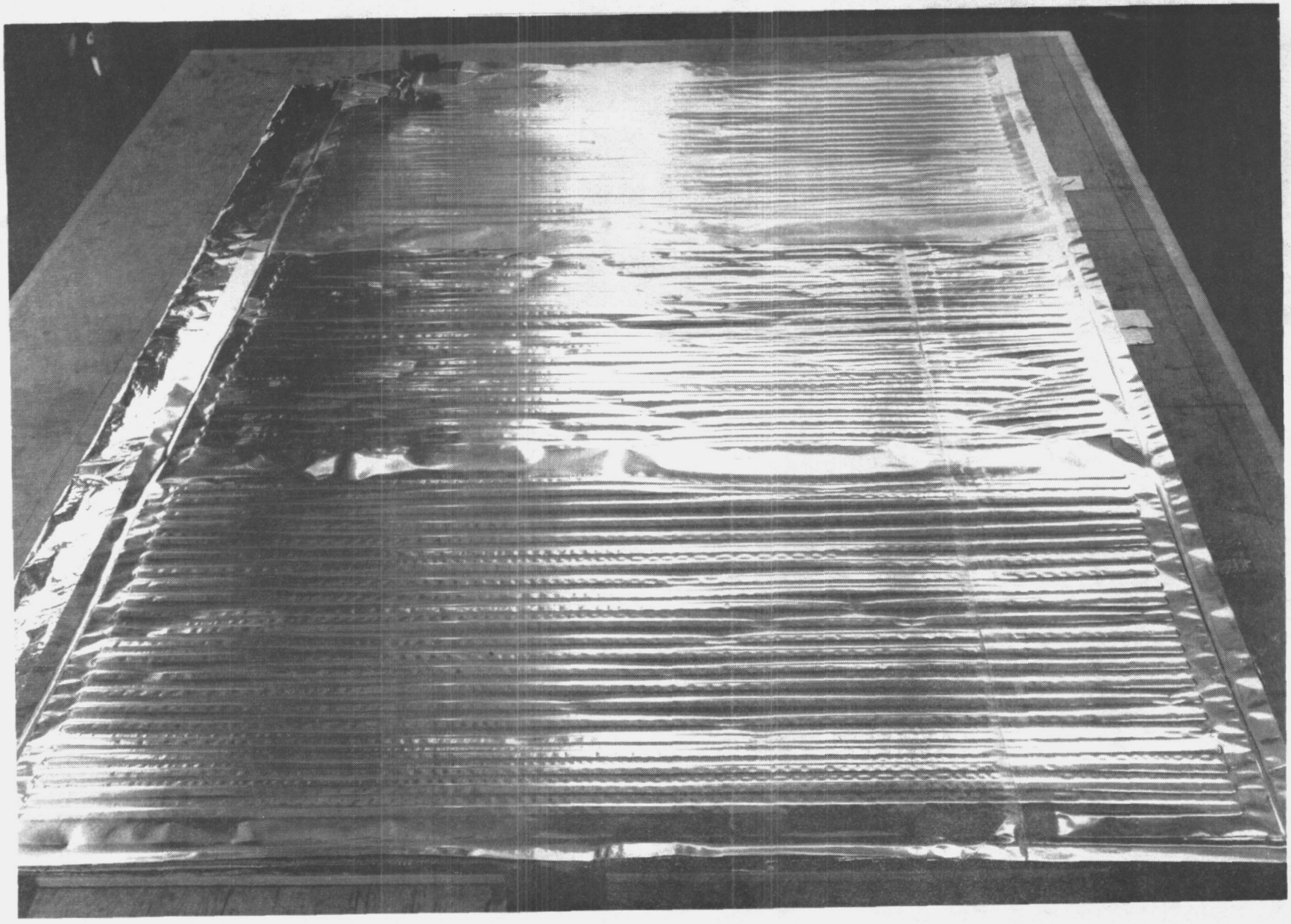

FIGURE 44

COMPLETED PANEL

Evacuated

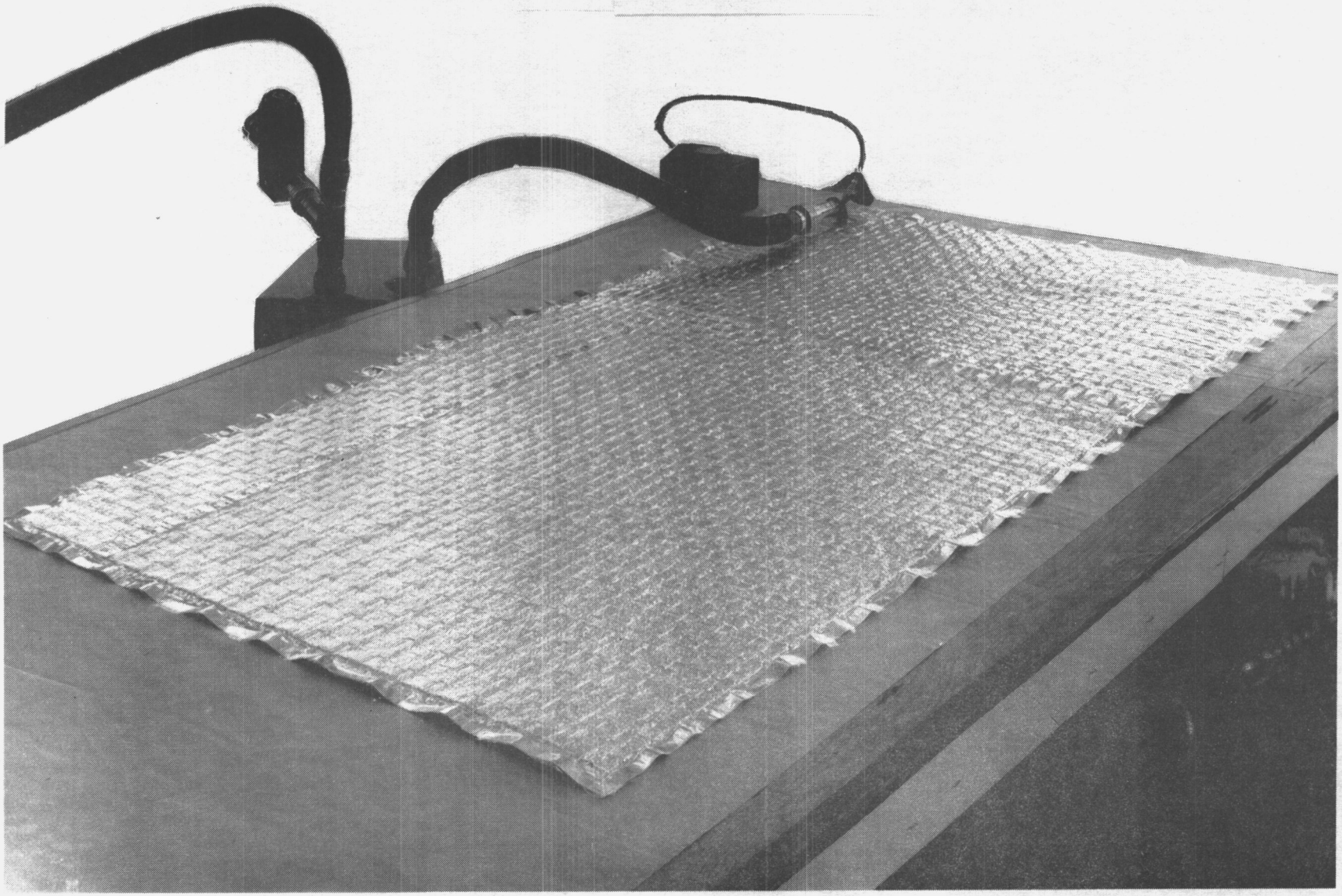

Because of the relatively high helium permeability of the 4-ply casing material ($.33 \times 10^{-5}$ atm.cm^3/sec.-ft.^{2} atm.) as compared to the MAAM (2×10^{-9} atm.cm^3/sec.-ft.^{2} atm.), a mixture of nitrogen gas containing slightly less than 2% by volume of helium gas was used for helium leak checking. By using this method, a helium leak rate can be established for a relatively permeable material, by a ratio of the measured indicated leak rate to the concentration of helium in the trace gas. For the SEMI panels, the panel leak rate approaches the established leak rate of the parent 4-ply casing material.

Each SEMI panel contained an evacuation manifold located at the warm end. The copper manifold contained a large port (3/4" Ø pipe size) for a General Electric type 22 GT-103 hot ionization gauge, and also a bellows sealed needle valve. The needle valve was required for panel evacuation and carbon dioxide backfill. However, in order to provide a greater transmittance path for the initial panel cleanup, each panel was evacuated through the gauge port for approximately 48 hours. The panel was then back filled with Coleman grade CO_2, theGeneral Electric gauge installed and the panel continuously re-evacuated through the needle valve until the second CO_2 backfill was completed just prior to installing the panels on the calorimeter tank.

The SEMI panels, backfilled with one atmosphere of Coleman Grade carbon dioxide immediately prior to installation, were bonded to the calorimeter tank and to each other with a contact adhesive applied in discontinuous vertical strips at approximately 20" intervals around the circumference of the tank. The completed insulation system is shown in Figure 45.

In order to achieve the desired shingled system of panels wherein each panel contacts the calorimeter tank and is also exposed to ambient conditions, it was necessary to install all eight panels in rotation around the tank. Twenty-four thermocouples were attached to panels A-1 and D-1 during panel installation. Thermocouple locations are shown in Figure 46. The thermocouples were routed between the insulation panels and exited through the upper guard insulation as shown in Figure 47. The checkerboard appearance of the panels results from using the punched hole spacer to separate the aluminized Mylar radiation shields. The readily apparent edges of the sealing tapes between panels and the panel to guard insulation joint are RTV silicone rubber. Silicone rubber having been found satisfactory for this application was applied in a small bead to all tape edges to affect a vacuum seal.

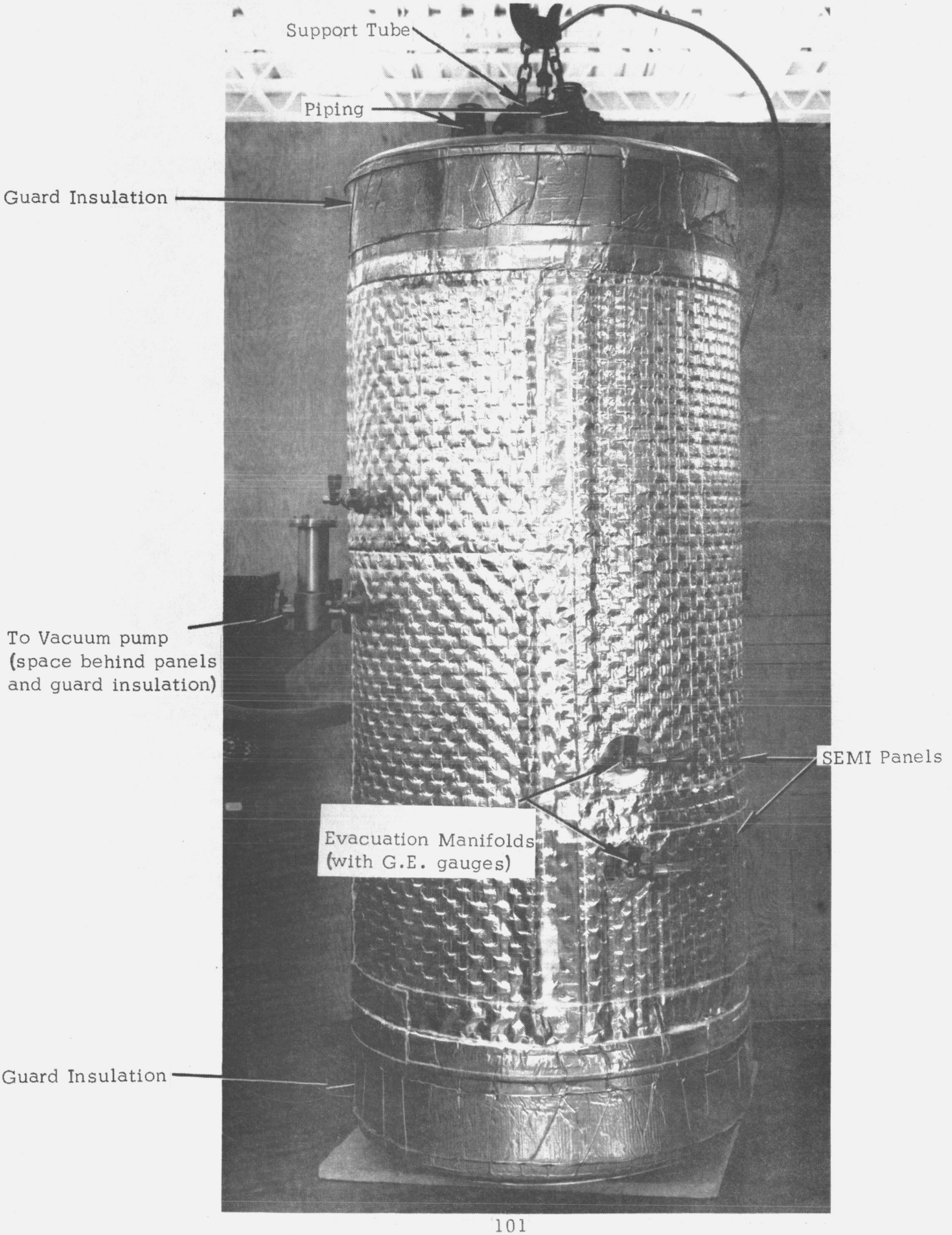

INSULATED CALORIMETER TANK WITH GUARD INSULATION EVACUATED FIGURE 45

Figure 46

Panel Sizes and
Thermocouple Locations
Calorimeter Test Contract NAS3-7953
Total - 24 Couples (30 ga. Copper Constantan)
Total - 8 Panels (4 each)

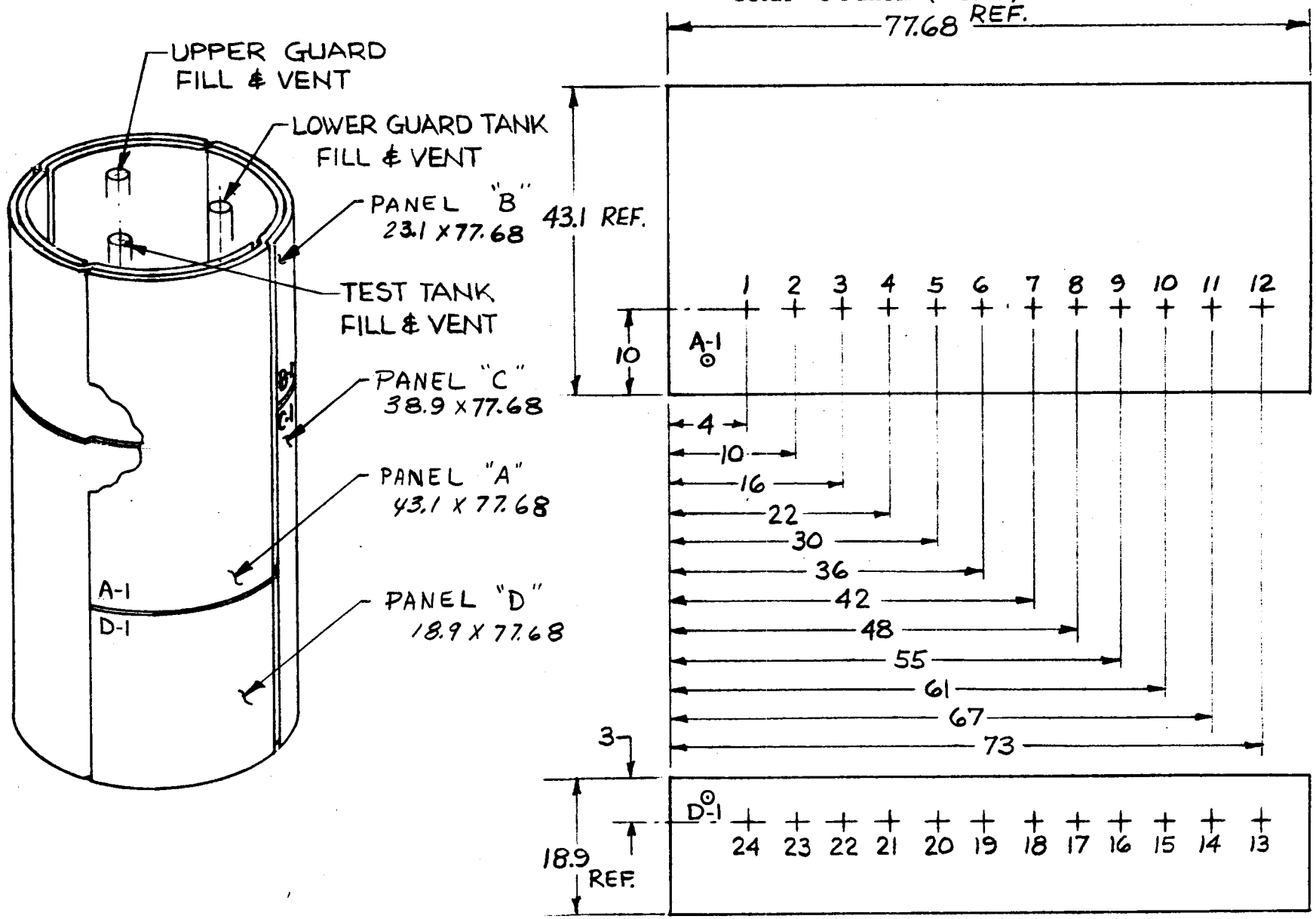

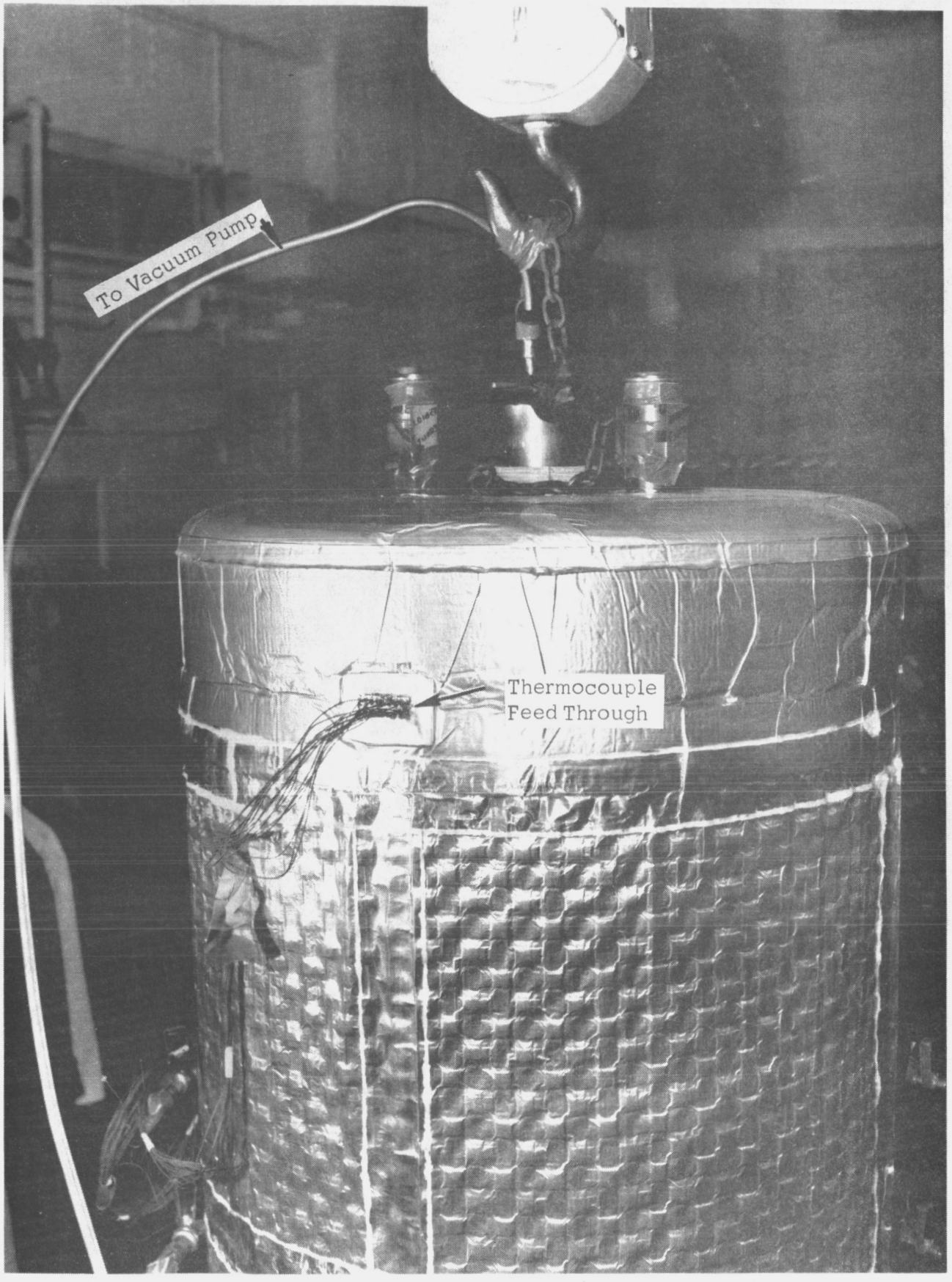

CALORIMETER TANK THERMOCOUPLE FEED THROUGH FIGURE 47

Evacuation of the space behind the panels was accomplished by placing a flat plate on the large support tube which runs the full length of the tank. This pipe is in communication with the space behind the panels via various holes along its length and also at the opposite end of the pipe. This plate attachment was necessary to complete leak testing at Linde Tonawanda. After the tank was returned to Plumbrook Station, Sandusky, Ohio, a permanent welded connection was attached which mated directly to the lid of the space chamber. The entire weight of the tank was supported via a chain bolted to the support pipe. This method permitted leak checking the entire guard insulation system prior to shipment to Sandusky, Ohio. Figure 48 is a view of the completed upper head insulation while Figure 49 is a close-up showing a G.E. 22 GT 103 miniature hot ionization gauge installed in the evacuation port. The handles on all of the panel valves were taped after the CO_2 backfill as a precaution against inadvertent valve openings.

Upon completion of the leak checking at Linde Tonawanda, an 8" diameter foam plug was removed from the lower guard insulation to permit the entire insulated calorimeter tank to be installed in the shipping dolly for transport to Plumbrook Station.

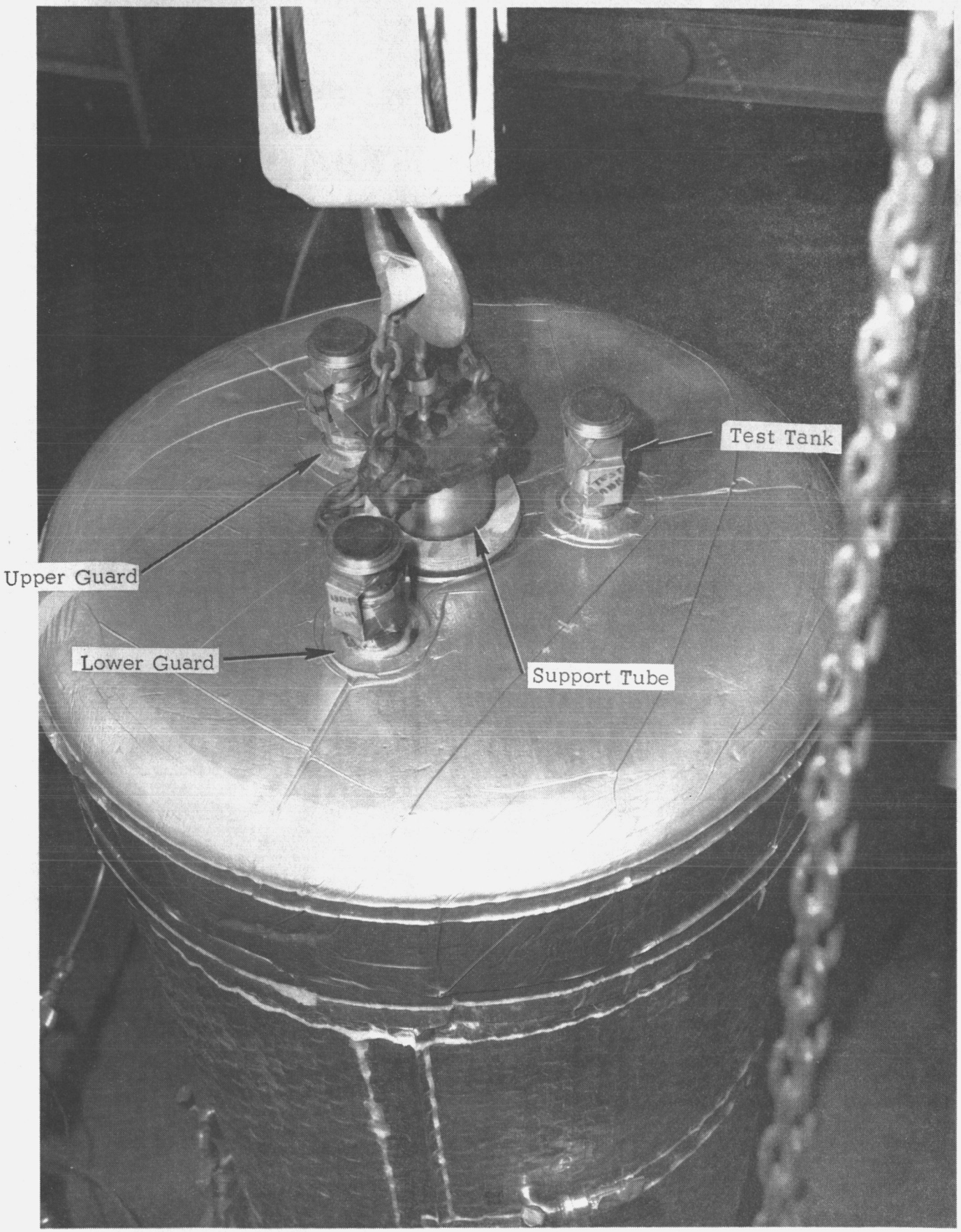

CALORIMETER TANK UPPER GUARD INSULATION FIGURE 48

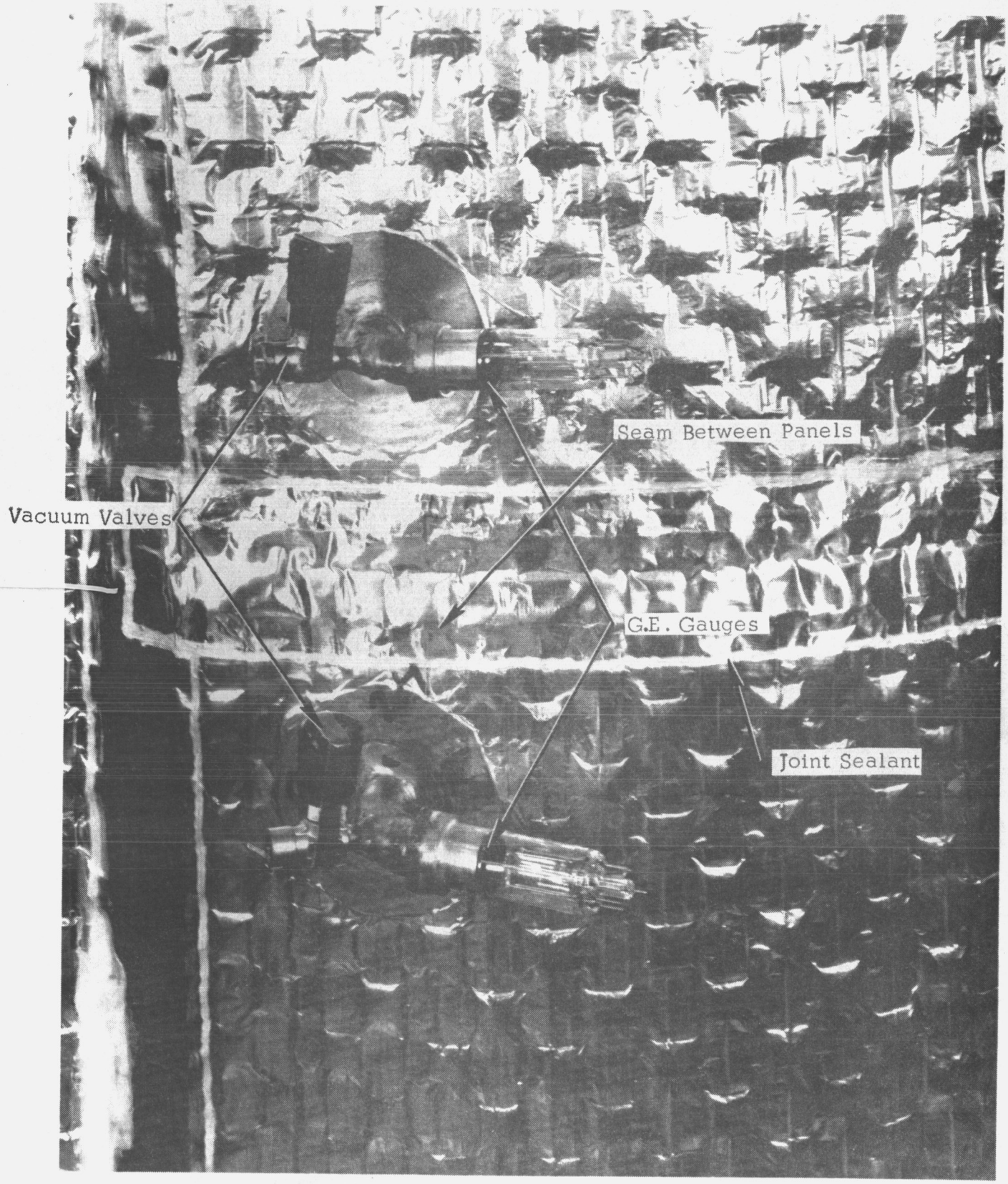

CALORIMETER TANK PANEL EVACUATION PORTS AND G.E. GAUGES FIGURE 49

4.4.3 Calorimeter Thermal Tests

The calorimeter tank insulation was completed at Plumbrook Station by Linde personnel after the calorimeter was mated to the top of the space chamber. This final set up phase included replacement of the foam plug, and application of a patch to the lower head vacuum jacket after the tank had been removed from the lower shipping support structure. A Mylar-lead-Mylar patch was temporarily held in position with a contact cement while an inner band of Narmco 7343/7139 adhesive was curing. The pressure for this cure was achieved by evacuating the area behind the panels. A bead of silicone rubber sealant was immediately applied around the edge of the patch to further reduce the possibilities of a vacuum leak.

After approximately 12 hours of vacuum pumping with an 8-cfm roughing pump through ten feet of 1/2 inch copper tubing, the pressure behind the panels was down to 200 microns. When helium leakage could not be detected, the space behind the panels was backfilled to 1 atm with Coleman grade carbon dioxide and valved off in preparation for the installation of the calorimeter in the chamber.

A series of three tests was conducted. The first two, separated by a 30-day period to demonstrate storage in air after installation on a tank, consisted of a simulated ground hold (panels compressed under a 1 atm pressure), launch trajectory (rapid chamber evacuation), and the space condition (panels recovered). A third test was conducted with the panels and the space behind them vented to the chamber with the chamber evacuated.

Hydrogen gas flow was measured using a dry gas meter calibrated from 10 to 365 cfh. Liquid level in the tanks was determined by means of discrete level sensors, a high level and low level sensor being installed in each of the three tanks. For part of the third test a pressure control system was installed on the test tank vent to eliminate the effects of change in barometric pressure.

All three tests were successful in achieving good thermal performance in spite of the fact that the panels did not cryopump to less than 1×10^{-4} torr panel pressure which was considered desirable for a multilayer insulation system. Time histories of the heat flux,panel pressure and

cold side panel temperature, for the first test are shown in Figure 50. It will be seen that in the termination of the ground hold phase the heat flux was in the order of 11.5 Btu/hr./ft.^{2}, and it was improving. This was essentially repeated in the second test.

Figure 51 shows time histories of the panel pressure and heat flux for all three tests superimposed. It will be seen that an overall heat flux in the order of 0.65 Btu/hr/ft.^{2} was attained, although the panel pressures were somewhat higher than had been desired. It can also be seen that a heat flux of 1 Btu/hr/ft.^{2} can be attained at 30-40 hours after simulated launch.

In an effort to determine the ultimate performance of the shingle panel system as a function of residual gas pressure, the panel pressure and heat flux data were correlated in Figure 52. This represents reasonably good correlation with the exception of the two high points taken early in the third test. It must be remembered, however, that the third test was conducted with the valves between the panels and the chamber opened. Thus, in this particular case the vacuum gauges on the panels were looking directly at the chamber and would be expected to read a lower pressure than when the valves are closed. Apparently then it can be concluded that the effects of residual gas pressure in the steady-state condition were nil.

Atmospheric pressure had considerable effects on the flow rates. In one case a variation of at least 20% was observed. However, these variations could be masked by fairing the data. It is felt that the data shown in Figure 50 are representative of the true conditions and that the atmospheric effects have been eliminated.

The panel temperature profile is shown in Figure 53. The data shown there were taken from the first test, but the other test data were similar. At periods further into the tests than are shown there, a temperature profile from the outside of the panels took the form of a more smooth curve. The coldest temperature measured (thermocouple no. 13) never got as low as -300°F. This indicates a steady-state temperature gradient across the first section of panel of at least 120°F.

In order to get an approximate order of magnitude assessment of the relative contributions of jacket heat leak, radiation and residual solid (or gaseous) conduction, one can compare the computer results with the experimental data. Data from the computer program (section 4.4.1 above) indicate that the effects of heat losses through the jackets and longitudinally along the radiation shields amount to 0.16 Btu/hr/ft.^{2}. From the test data then, the contribution of heat flow normal to the insulation itself is the

Figure 50

Calorimeter Test #1

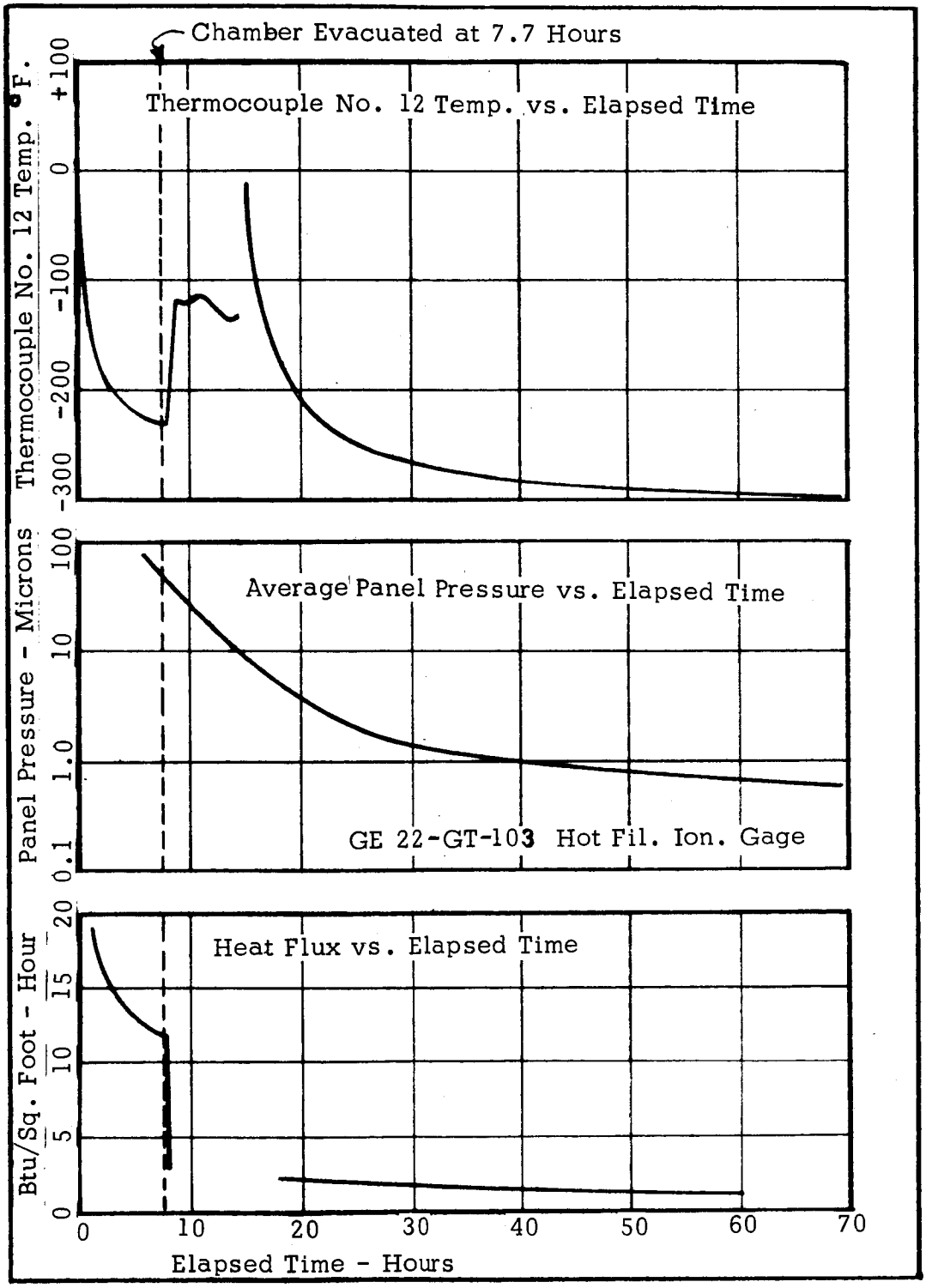

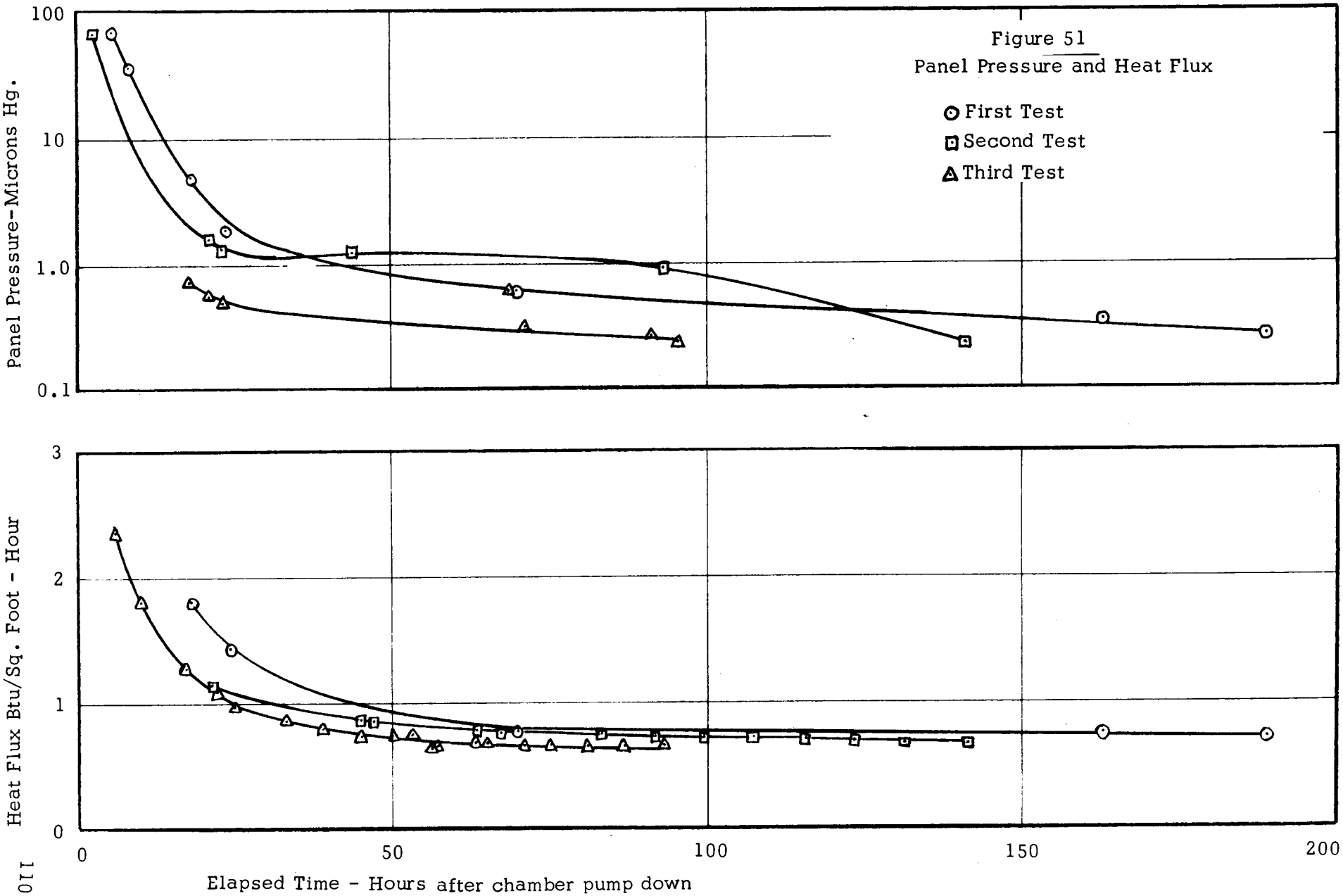

Figure 51
Panel Pressure and Heat Flux

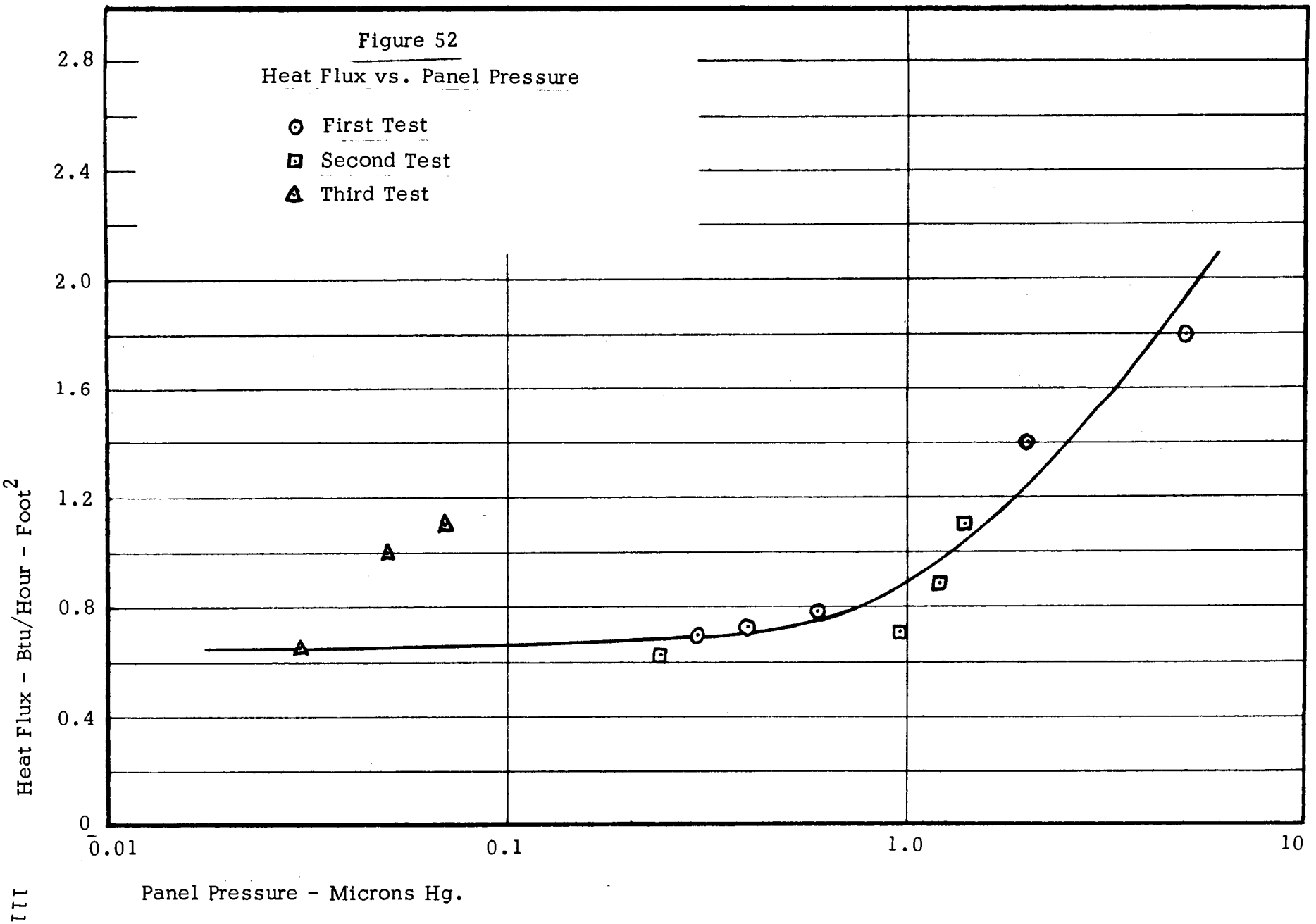
Figure 52
Heat Flux vs. Panel Pressure
First Test
Second Test
Third Test
2.8
2.4
2.0
1.6
1.2
0.8
0.4
0
Heat Flux - Btu/Hour - Foot^2
0.01
0.1
1.0
10
Panel Pressure - Microns Hg.

FIGURE 53 Temperature Profile
Panel No. D1 (Test No. 1)

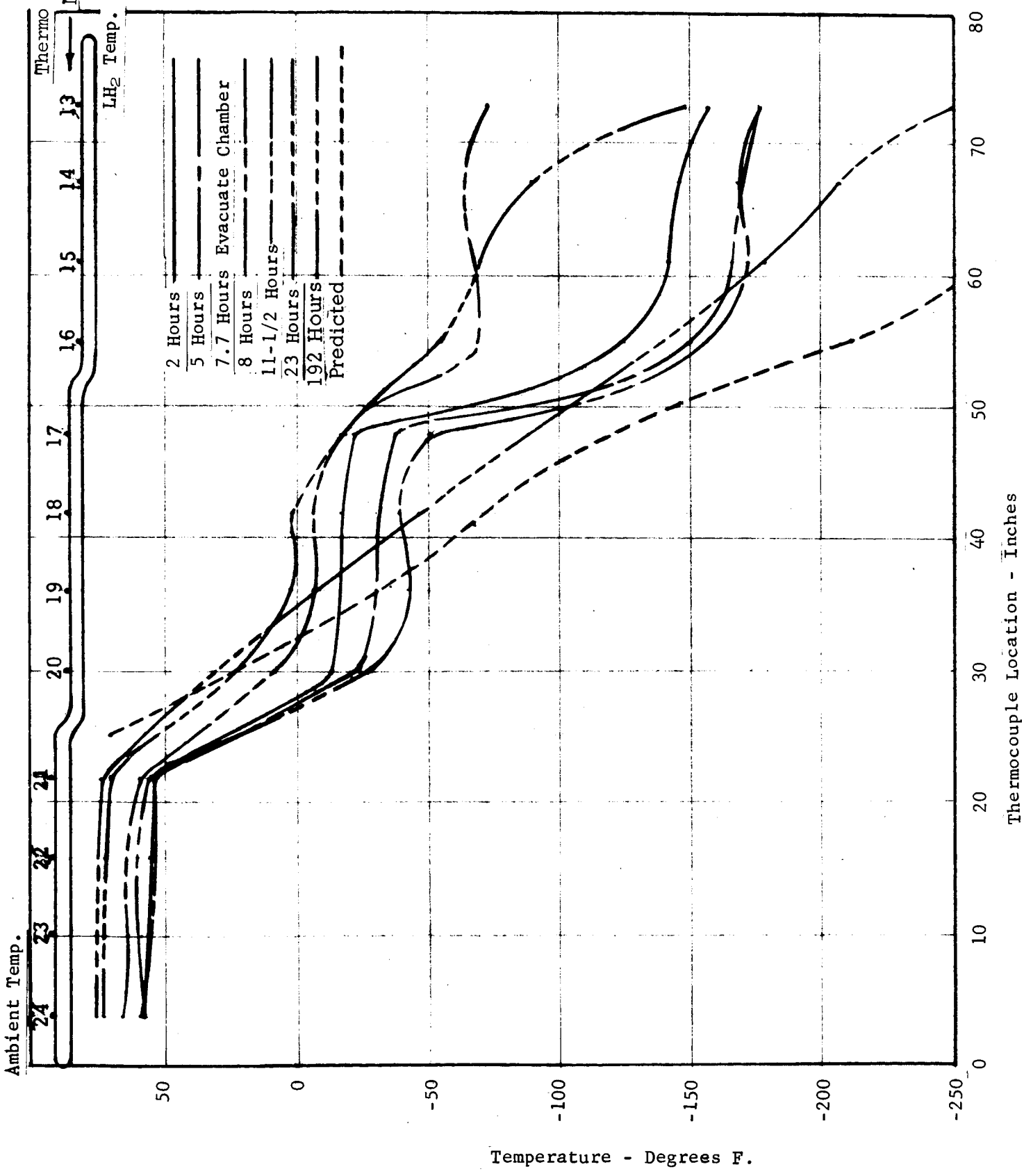

remaining 0.47 Btu/hr/ft.^{2}. The calculations shown in Figure 54 indicate that the radiation contribution amounts to 15% of this. Therefore, solid conduction through the foam amounts to about 85% of the heat leak through the insulation. This may be inherent in the foam material, the result of residual compression due to the jacket configuration; or some residual gaseous conduction within the cells. This area should be the subject of further investigation.

Figure 54

CALCULATION OF INSULATION PERFORMANCE

Heat transport by radiation for a multishield system is given by

$$\left[Q/A\right]_R = \frac{\sigma \epsilon (T_1^4 - T_2^4)}{2 (n + 1)}$$

where:

σ = Stephan Boltzmann Constant = 0.174×10^{-8}

ϵ = Emissivity of reflectors = 0.02 (measured previously)

T_1 = Warm boundary temperature = 520°R

T_2 = Cold boundary temperature = 36°R

n = Number of shields in system = 18

$$\left[Q/A\right]_R = \frac{0.174 \times 10^{-8} \times 0.02 (520^{-4} - 36^{-4})}{2 (18 + 1)} = 0.07 \text{ Btu/hr.-ft.}^2$$

Radiation as a proportion of total = $\frac{0.07}{0.47}$ = 15%

4.5 Concept Application

4.5.1 Application Design Analysis

Application of self-evacuating multi-layer insulation panels (SEMI panels) to tankage other than cylindrical shapes such as spherical and ellipsoidal is envisioned. Therefore, as part of the development activities for the SEMI system, a design study of the problem areas involved in installation and basic panel geometry encountered in insulating these various shapes was initiated. However, since ellipsoidal and cylindrical tankage can be considered as a special case of spherical tankage as far as installation problems are concerned, the investigation was limited to spherical tankage only, although the results would be equally applicable to the previously mentioned special cases.

Three ideas were analyzed: SEMI panels having a cold leg extension for cryopumping; SEMI panels applied in a double shingled fashion and a combination of SEMI panels and pre-evacuated panels installed in true isotherm layers without shingling. Panel size was limited to 6 feet, a maximum dimension for practical handling reasons in a vehicle. The three layered panel concept of previous work was retained to assure that radiation windows resulting at the panel joints are minimized. At the current stage of development the punched hole spacer concept with 20% support area and the impermeable outer casing (Mylar/aluminum/aluminum/Mylar) are recommended.

Panels using the cold leg method would be installed in a three layered shingled fashion with the exception that only a small portion of the total panel, i.e. "cold leg", actually presents a heat path from ambient to the cryogenic surface. The "cold leg" would be a tab like section attached to the edge of each panel. Each tab would then be routed through a penetration in the preceeding layers of insulation panels during installation. The "cold leg" would be sized to assure that the panel is able to cryopump to an acceptable pressure within a reasonable length of time. Further design effort would be needed to define these dimensions. This method may present slightly lower heat flux due to a reduction in heat path at the joints although in the full shingle concept which was tested, conduction through the casing amounted to only 25% of the total heat flux.

The double shingle method (see Figure 55) is extension of the single shingling method used to install SEMI panels on a cylindrical vessel such as the calorimeter tank insulation in which the panels were shingled horizontally. For a sphere, in addition to installing panels shingled vertically around the equator, other panels will be shingled around the pole. The equator panels most likely will be banana peel sections of unsymmetrical design to minimize circumferential overlap. Three layers of pole caps of different diameters would be shingled radially around the pole.

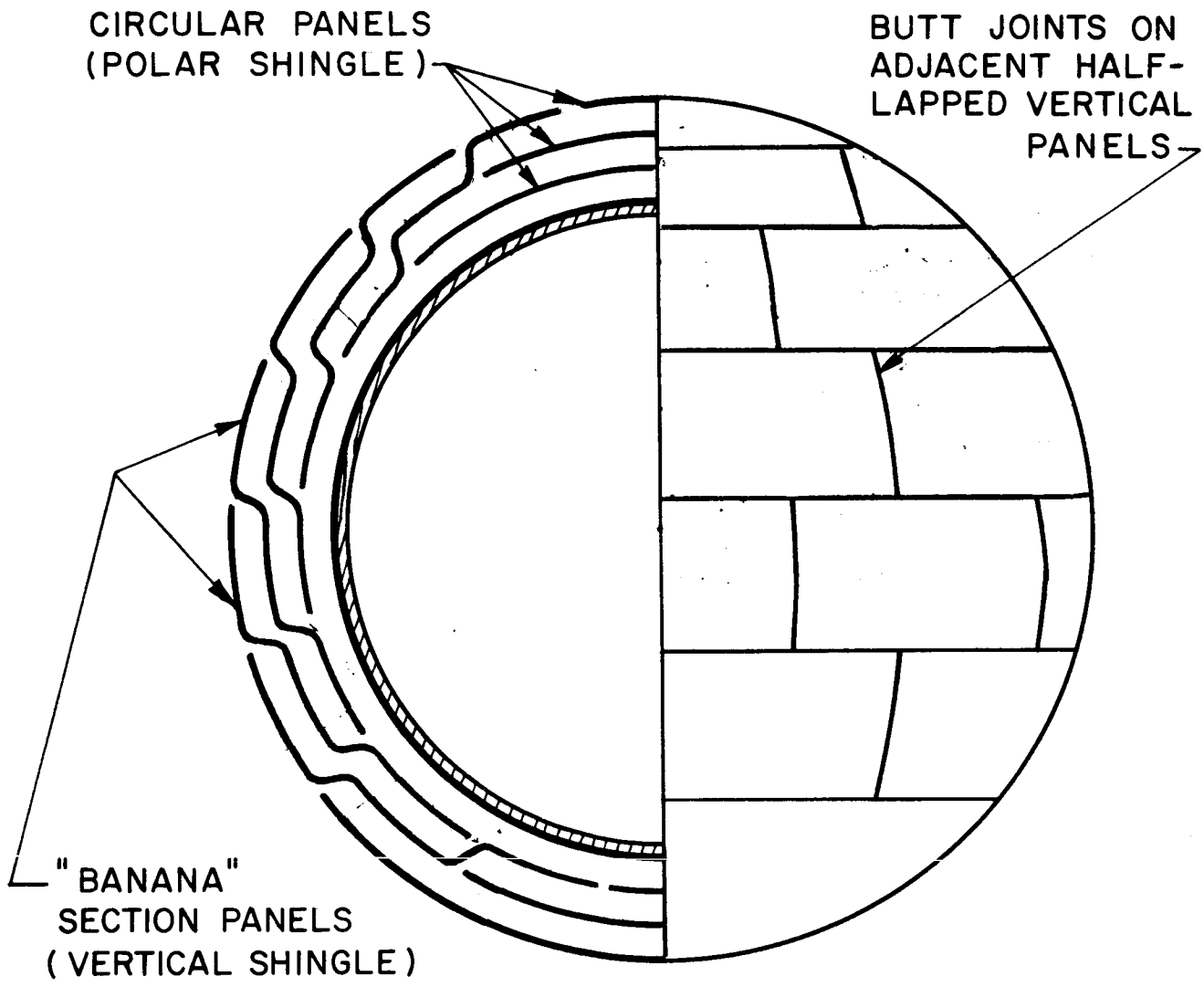

FIGURE 55

DOUBLE SHINGLED INSULATION SYSTEM FOR SPHERICAL, ELLIPSOIDAL OR CYLINDRICAL TANKAGE

The number of both circumferential panels and pole panels will, of necessity, be dictated by the size of the vessel being insulated, bearing in mind that a maximum panel length of six feet is deemed practical.

The third method of insulating vessels with SEMI panels attempts to install the panels in discreet layers, i.e. no shingling. In this method only the inner most panels are exposed to liquid hydrogen temperatures. Therefore, it would be necessary to backfill the second and third layer panels with a gas such as a Ucon which would condense to an acceptable pressure at the higher panel in temperatures (in the order of -100°F) encountered in the outer panels. The outer most panel would most likely be a permanently evacuated panel.

Of the three proposed methods, only the double shingled system appears to be workable with presently developed techniques. The "cold leg" method would not be critically transmittance limited as evidenced by the testing of transmittance samples but practical installation problems of interleaving the "cold leg" cryopumping tabs with the inner layers of SEMI panels would be excessive. Installing the SEMI panels in discrete layers as proposed would require additional development work to determine a condensible gas which has the necessary properties and is compatible with the insulation materials. The advantages of this system lie in the ease of installation and some improvement in overall thermal performance because of elimination of the heat transfer through the jacket. However, vacuum maintenance is a severe problem.

Continuing therefore with the double shingled arrangement, the side (vertical) panels for all three layered systems would be installed as shown in Figure 55 with the pole panels installed as shown in Figure 56. Approximate panel sizes were determined for spheres having diameters of 48 inches, 82 inches and 192 inches employing a three layered, double shingled system. The results of this analysis are presented in Table 16. As noted in Table 16 various panel arrangements were determined for an 82 inch diameter tank, preliminary to the more detailed design effort. These variations consist of changing panel overlap, including reducing the pole cap to a two layer panel, with the side (vertical) panels completely overlapping the upper pole panels to form the third layer.

A similar approach would be followed in insulating cylinders and ellipsoids with a double shingled system as illustrated in Figures 57 and 58.

Of immediate concern is the physical size of the panels in regards chiefly to length and width dimensions, although increased thickness is also of interest because of the requirements for deep-drawing or forming the vacuum casing. Casing material splices have resulted in achieving

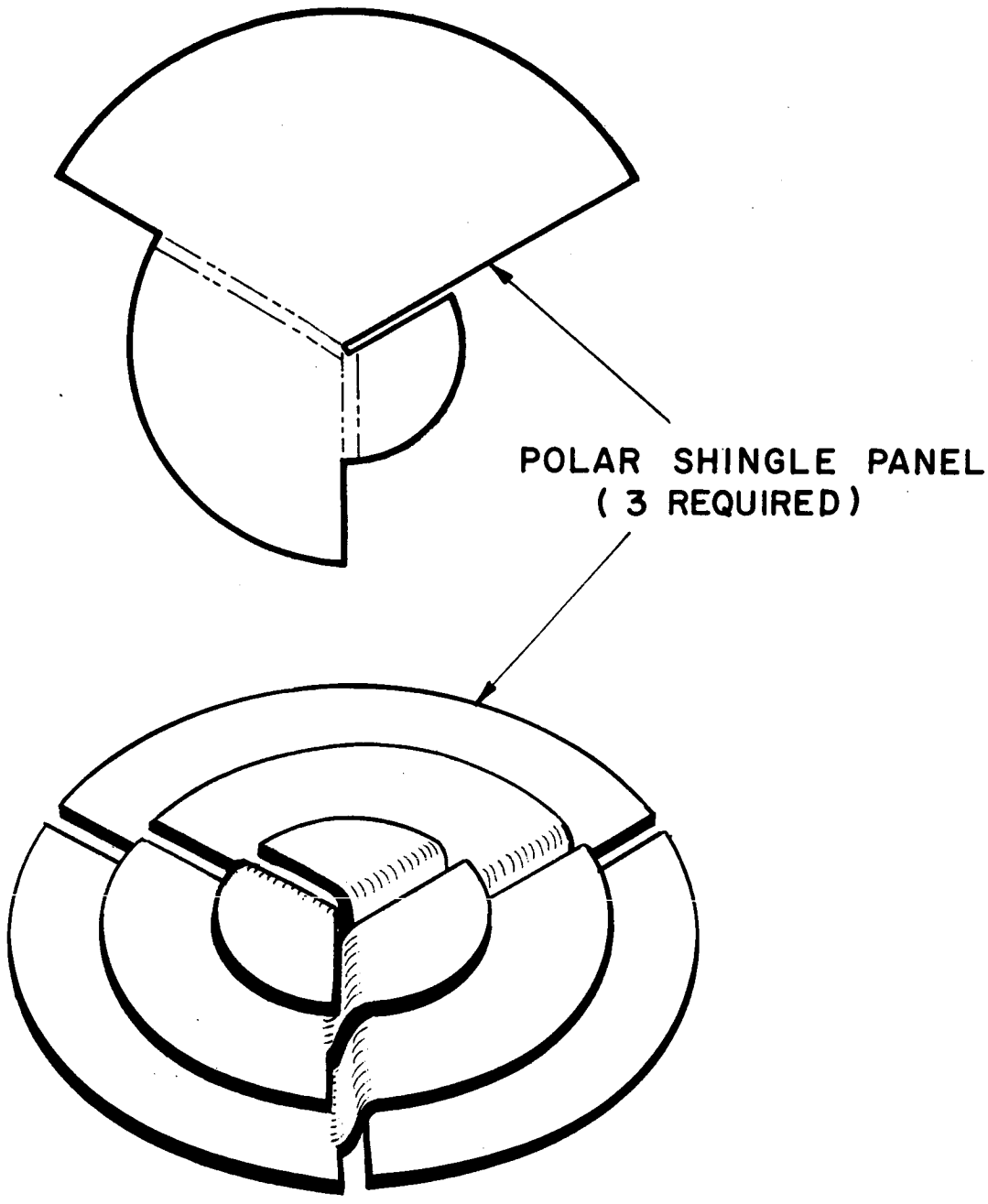

FIGURE 56

POLAR SHINGLE SYSTEM

TABLE 16

TYPICAL PANEL SIZES FOR SPHERICAL TANKAGE

Tank Diameter	Panel Style*		No. Req'd.	Dimension Inches X	Dimension Inches Y	Minimum Heat Path Length-Inches
48" Diameter	Scheme No. 1	A	4	38.5	32.0	12.8
		B	8	38.5	38.5	12.8
		C	4	38.5	38.5	12.8
		D	3	38.5	44.4	6.4
		E	3	38.5	44.4	12.8
82" Diameter	Scheme No. 1	A	12	43.3	53.0	15.0
		B	12	43.3	61.0	23.0
		D	6	69.0	72.5	15.0
	Scheme No. 2	A	6	43.3	59.0	21.5
		B	12	43.3	65.5	22.0
		C	6	43.3	65.0	21.5
		D	3	64.5	74.5	15.5
		E	3	64.5	74.5	21.5
	Scheme No. 3	A	12	41.1	38.5	12.0
		A	12	43.3	41.0	14.5
		B	12	43.3	43.5	14.5
		D	6	60.0	62.5	12.0

TABLE 16 (cont'd)

TYPICAL PANEL SIZES FOR SPHERICAL TANKAGE

Tank Diameter	Panel Style*		No. Req'd.	Dimension Inches X	Dimension Inches Y	Minimum Heat Path Length-Inches
82" Diameter	Scheme No. 4	A	12	43.3	59.0	18.0
		B	12	43.3	64.0	23.0
		D	6	66.0	72.8	18.0
192" Diameter	Scheme No. 1	A	20	41.1	56.8	15.2
		A	28	40.3	67.2	26.5
		A	28	41.6	79.5	26.5
		A	28	43.3	79.5	26.0
		B	28	43.3	79.5	26.5
		D	6	75.8	78.6	15.2

* Panel Styles

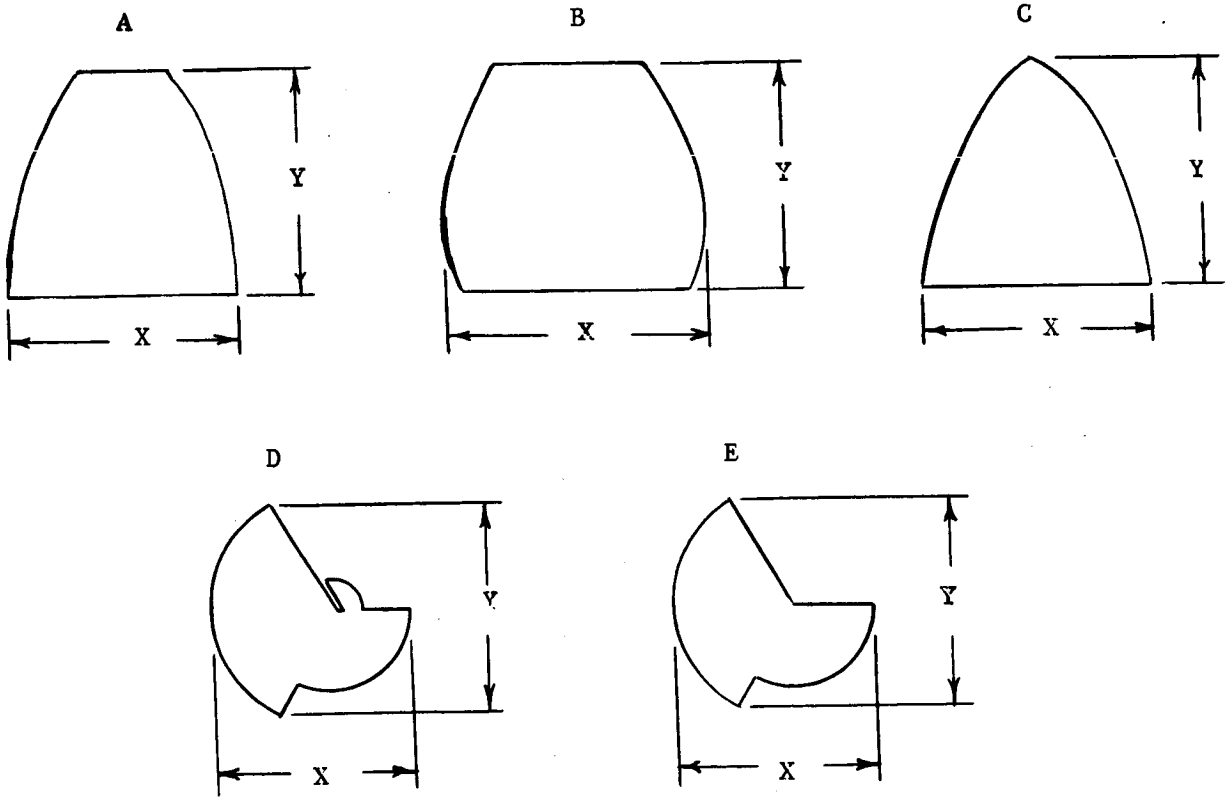

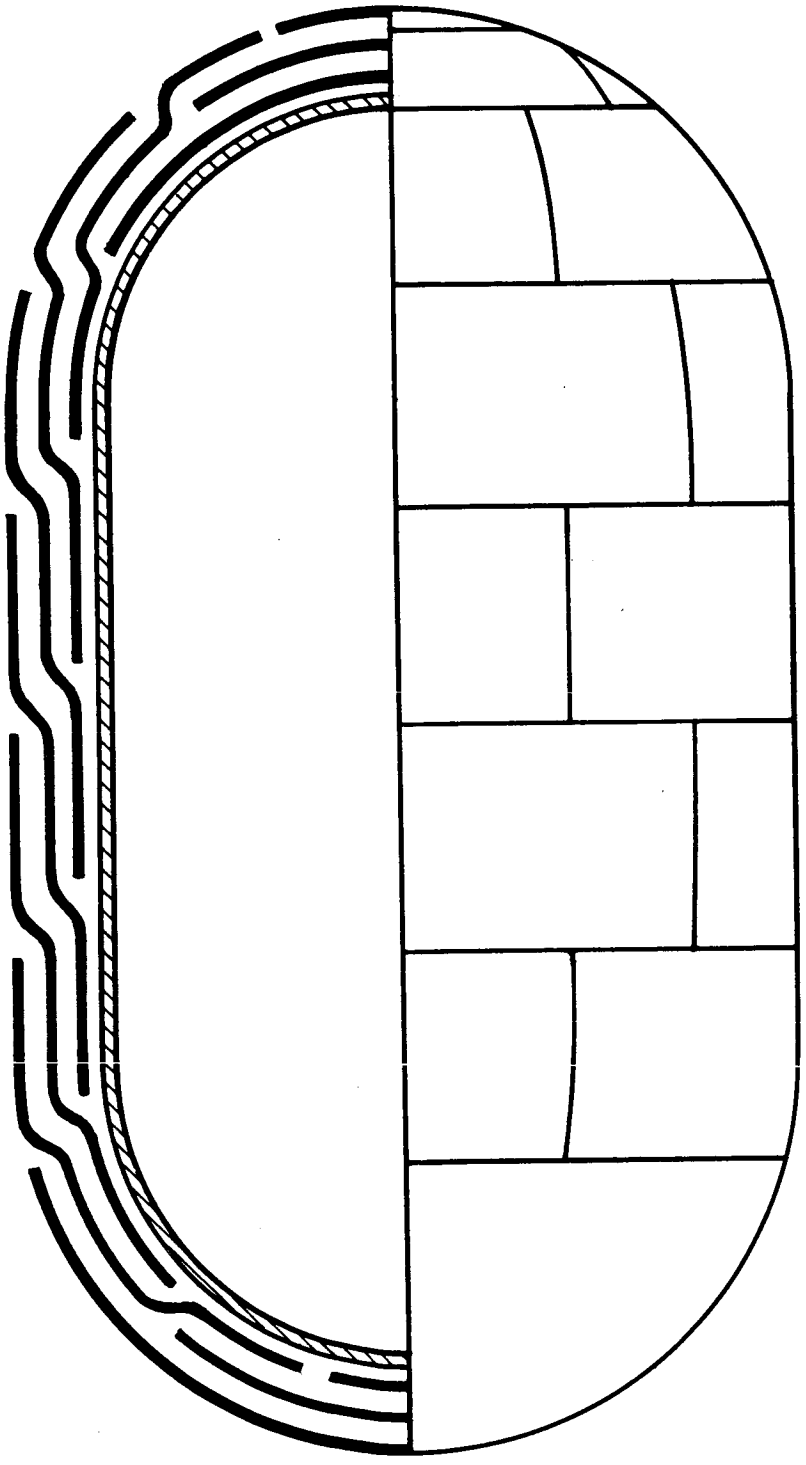

FIGURE 57

DOUBLE SHINGLED INSULATION SYSTEM FOR CYLINDRICAL TANKAGE

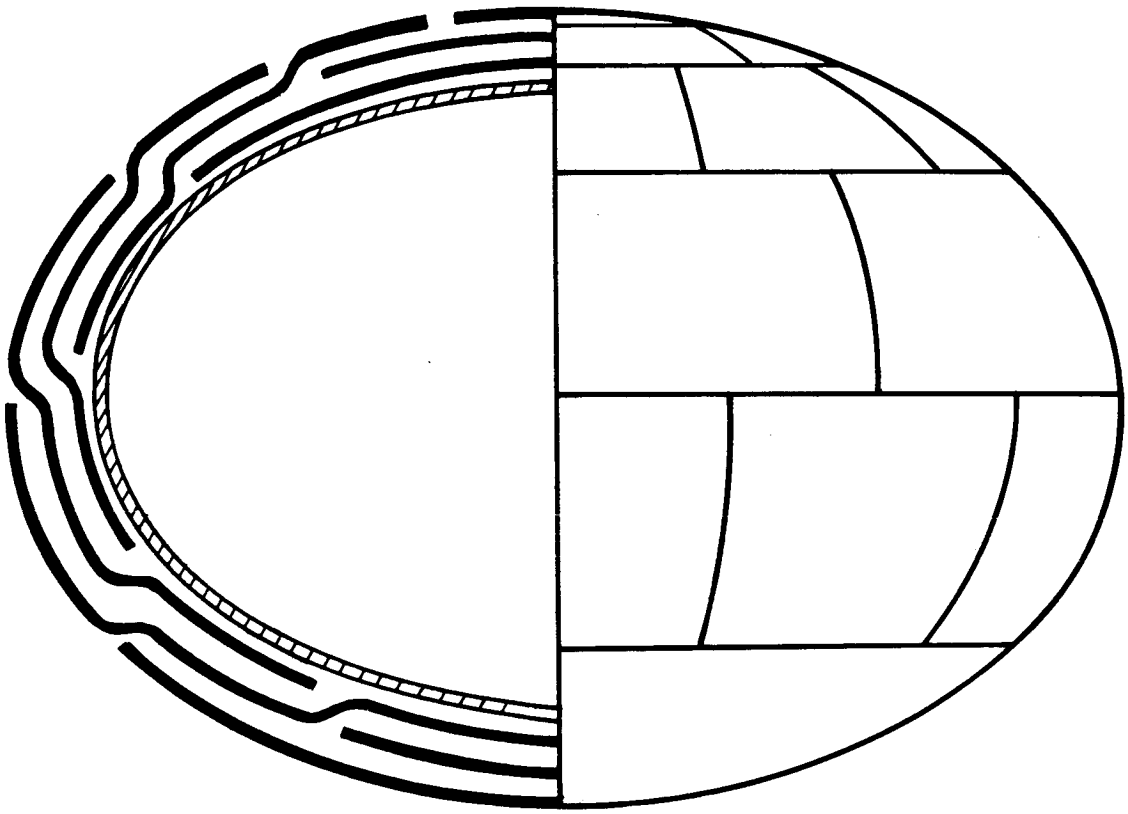

FIGURE 58

DOUBLE SHINGLED INSULATION SYSTEM FOR ELLIPSOIDAL TANKAGE

leak tight joints, although the joints are more prone to structural failure than the parent material, since the joint strength is dependent upon the bond strength of only one layer of the 4-ply laminate. Limitations in regards to widths of open cell foam spacer and aluminized Mylar radiation shield materials would not appear to be insurmountable. Therefore practical panels do not appear to be limited in size because of material availability. However, practicality may dictate that panels be limited by such factors as the maximum number of people within the confines of the fabrication area, or more importantly the actual installation area. Physical size of the panels would be limited by the size of the access doors within the vehicle shrouds, etc. Increased panel thickness, although troublesome, would not appear to be a severe impediment to panel fabrication although this increased thickness would probably require additional development work including an investigation into the use of preformed corner/edge and/or transition joints, and extra length allowance, or perhaps a vacuum formed "step" to permit the panel layers to be shingled.

Regardless of panel size, means to achieve the necessary clamping pressures for adhesives other than heat sealable types will require investigation. This clamping problem will be encountered since the shape of the panels will require adhesive joints along compound curved surfaces.

Installation of the shingled pole caps may present assembly problems which most likely could be overcome by preassembling the separate pole panels into a single 360° pole cap prior to final assembly on the tankage. This preassembly operation would most likely be performed on a mandrel that allows access to both the inside and outside surfaces of the pole cap.

4.5.2 82.6 inch Tank Design

Because of the complex, "shingled" arrangement of the insulation panels, a three-dimensional thermal analysis was required to evaluate accurately the thermal characteristics of the insulation system.

The steady state thermal behavior of the two spherical-shell sections is governed by the Fourier equation of heat conduction. In spherical coordinates, this equation is:

$$\frac{\partial}{\partial r}\left(k_r r^2 \sin\theta \frac{\partial T}{\partial r}\right) + \frac{\partial}{\partial \theta}\left(k_\theta \sin\theta \frac{\partial T}{\partial \theta}\right) + \frac{1}{\sin\theta}\frac{\partial}{\partial \varphi}\left(k \frac{\partial T}{\partial \varphi}\right) = 0$$

In the above equation, the coordinates r, θ, φ represent, respectively the radial distance outward from the sphere center, the angular distance from a pole measured along a meridian, and angular distance measured along a parallel. The thermal conductivities along these directions are k_r, k_θ, and $k\varphi$, and T is the temperature.

The thermal behavior of the conical support structure is governed by a differential equation of similar form, in which the coordinates are taken to be the distance, S measured along intersections of the conical surface with planes normal to its base, the perpendicular distance Z from the surface, and the angular distance φ measured along intersections of the surface with planes parallel to the base. Coordinates Z and φ are equivalent to the r and φ spherical coordinates.

Because of the complex boundary conditions introduced by the shingling and the presence of the conical structure, an exact thermal analysis is impractical. Therefore, the differential equations have been discretized in each of the three coordinate directions. The resulting finite difference equations combined with the boundary conditions, give a non-homogeneous set of simultaneous linear equations.

The computing mesh used results in a total of 344 similtaneous equations in 344 unknown temperatures. Solution of such a large system of equations ordinarily would require much computer core storage and use of double precision arithmetic. However, by suitable manipulation 40 of the unknown temperatures can be split off, reducing the number of equations and unknowns to 304. Furthermore, the resulting 304 x 304 coefficient matrix is block-tridiagonal, of block size 16 x 16 and block order 19. This system can be solved by a block-elimination technique which is merely the matrix analogue of the familiar Gaussian elimination method. Once the 304 temperatures are found, the 40 other unknown temperatures can be evaluated and heat fluxes calculated.

A Fortran program was written to perform this analysis on the IBM 360/40 computer located at the Tonawanda Laboratories. A more complete discussion is included in appendix 5. Besides the temperatures, this program also calculated heat fluxes to and from all system components. The analysis was performed for three different designs similar to that shown on Linde Drawing D/SK 102425, Figure 59. In the design depicted there, six panels are installed around the girth of the tank (Details A through G). In order to determine quantitatively the effect of panel size, systems of three panels, six panels and twelve panels around the girth were analyzed by computor. The bulkhead panels for all cases were as shown. For the initial examination, a basic thermal conductivity of the insulation of 3.5×10^{-5} Btu/hr.ft.°R was assumed. Subsequently conductivity values of 1.5×10^{-5} and 2.5×10^{-5} Btu/hr.ft.°R were run, and the effects of the conductivity of 7.1×10^{-5} Btu/hr.ft.°R experienced on the calorimeter tank estimated (the heat flux based on this data would be 0.67 Btu/hr.ft.^{2}). The results are shown in Table 17.

The data are broken down into three areas of the tank to show the effect of the conical support. In all cases this accounts for 1/3 to 1/2 the total heat leak. The range in heat leak for the cone area is due primarily to the panel joints over the cone and secondarily to interaction with the insulation system. The differences between lower and upper bulkhead sections is due to the location of the break points between the matrices chosen to account for the conical section and resulting different areas involved.

Review of this data as plotted on Figure 60 indicates the importance of minimizing the number of panels. However, it can be seen that a six panel system with a thermal conductivity of 3.5×10^{-5} Btu/hr.ft.°F has a heat leak of 151 Btu/hr. If there were no edge effects, the heat flux based on a 1.35 inch thick (18 radiation shields) three panel system would be 0.153 Btu/hr.ft.^{2}, as compared with 0.62 Btu/hr.ft.^{2} for the installed insulation system, or 0.80 Btu/hr.ft.^{2} if the effect of the support cone in included. This points up the need to emphasize reduction of edge effects.

If possible it would be desirable from a fabrication standpoint to limit the system to a six panel configuration in order to reduce fabrication problems associated with as large a panel size that would be required for the three panel system.

Consideration and some development work should be given to breaking of the radiation shields at each layer of shingling. Indications are that the

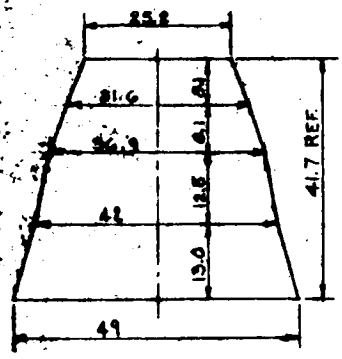

A
6 REQ'D.

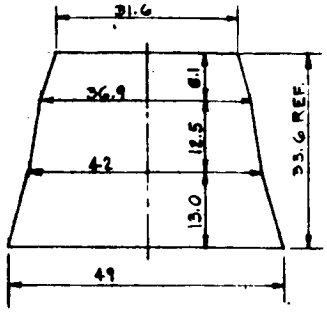

B
6 REQ'D.

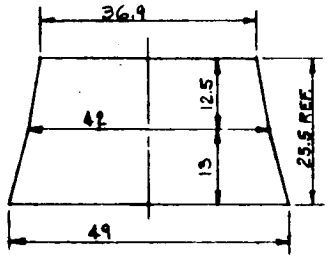

C
6 REQ'D.

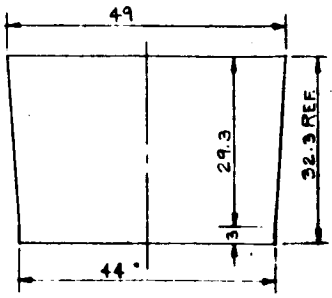

D
6 REQ'D.

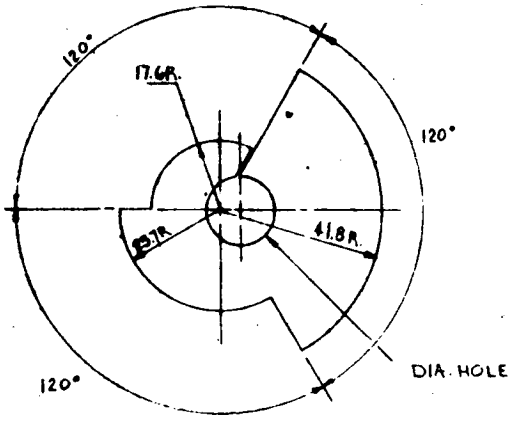

J
1 REQ'D. AS SHOWN
1 REQ'D. WITH HOLE 120° CLOCK-WISE
1 REQ'D. WITH HOLE 120° COUNTER-CLOCK-WISE

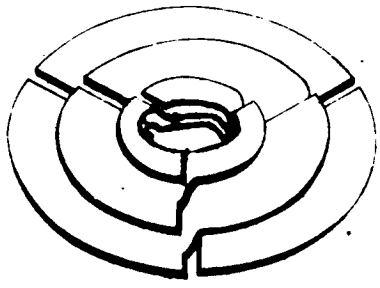

NOTE:
PANELS SHOWN ASSEMBLED IN FLAT PLANE FOR CLARITY

ASSEMBLY OF "J" PANELS
ASSEMBLY OF "H" PANELS (SIMILAR)

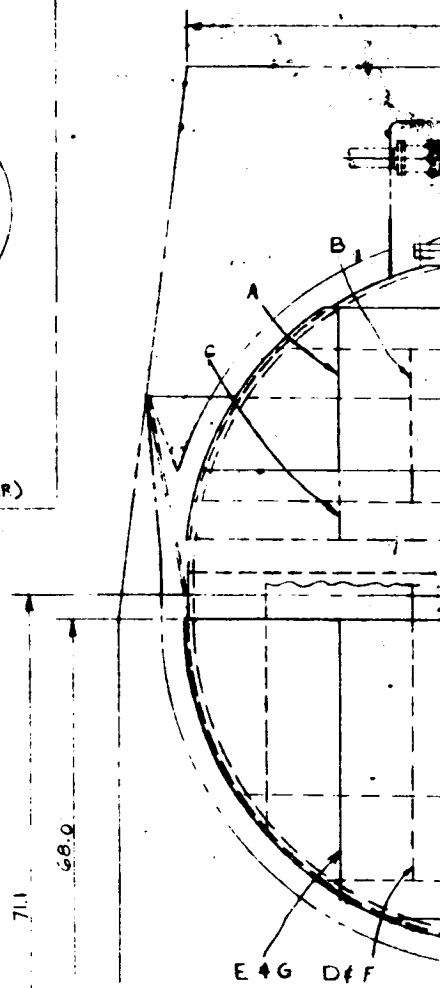

PANELS STAGGERED AS SHOWN

FOLDOUT FRAME 1

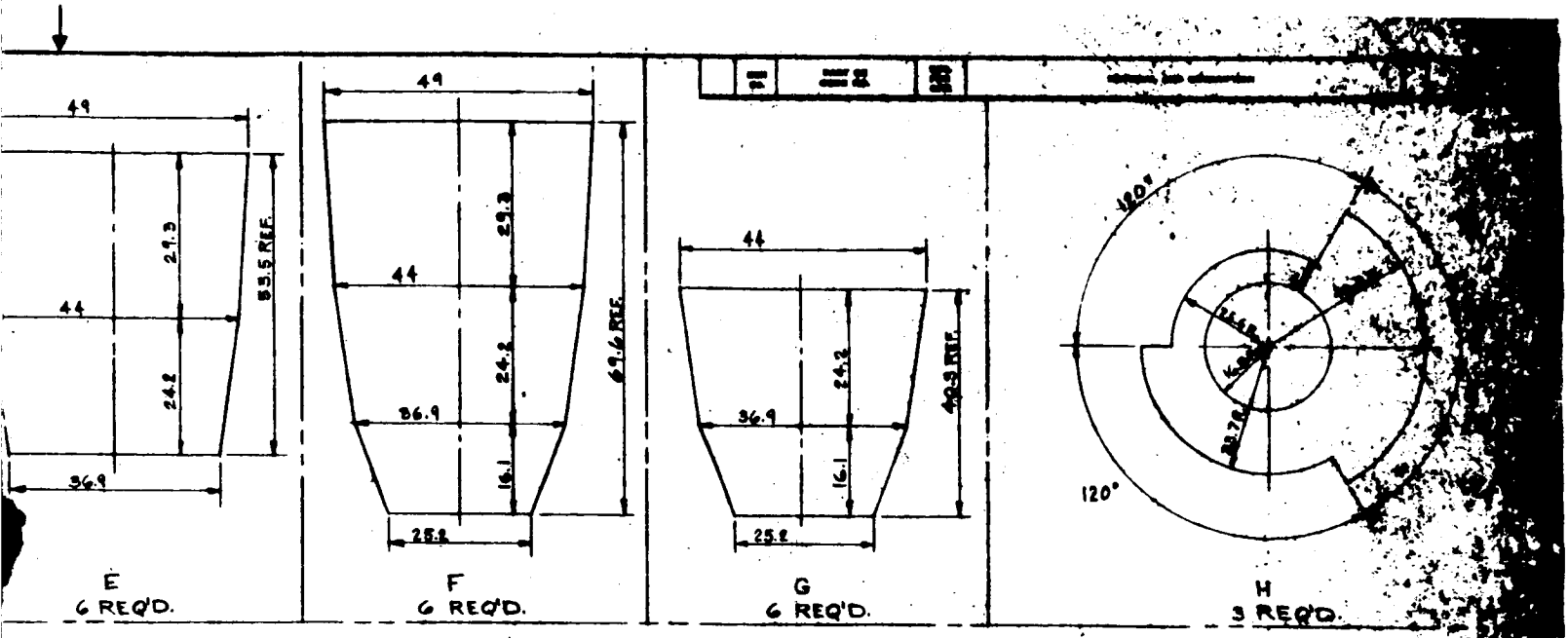

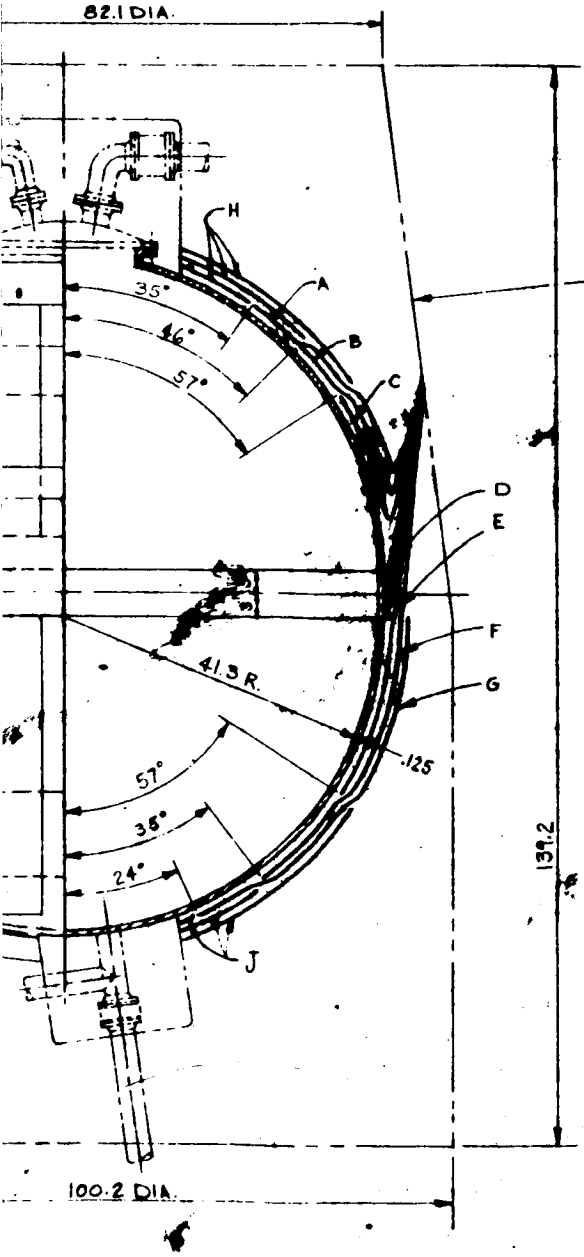

(REF.)
NASA DWG. CF 620533

FOLDOUT FRAME 2

FIGURE 59

TITLE:
CRYOPUMP PANEL LAYOUT
82.6" DIA. TANK
NAS 3-7953

UNION CARBIDE CORPORATION
LINDE DIVISION

TABLE 17

RESULTS OF COMPUTER ANALYSIS

82.6-inch diameter tank
3 layer shingled system
including conical support
Spherical Area = 149 ft.^{2}
Conical Support Area = 40 ft.^{2}

Thermal Conductivity Btu/hr.ft.°F	No. of Panels*	Heat From Top Spherical Section Btu/hr.	Heat From Bottom Spherical Section Btu/hr.	Heat Through Conical Support Btu/hr.	Total Heat Leak Btu/hr.	Heat Flux Sphere Only Btu/hr.ft.^{2}	Heat Flux Total Area Btu/hr.ft.^{2}
1.5×10^{-5}	3	30.3	27.4	47.2	104.9	.39	.56
	6	38.4	39.3	52.3	129.9	.52	.69
	12	-	-	-	-	-	-
2.5×10^{-5}	3	33.4	32.2	49.4	115.1	.44	.61
	6	41.5	44.5	54.8	140.1	.58	.74
	12	-	-	-	-	-	-
3.5×10^{-5}	3	36.5	37.0	51.6	125.0	.49	.66
	6	44.6	49.5	57.2	151.3	.62	.80
	12	87.9	126.3	108.2	314.4	1.43	1.67

* Refers to number of vertical panels per layer.

Total Panels Per System
3	27
4	34
6	48
12	90

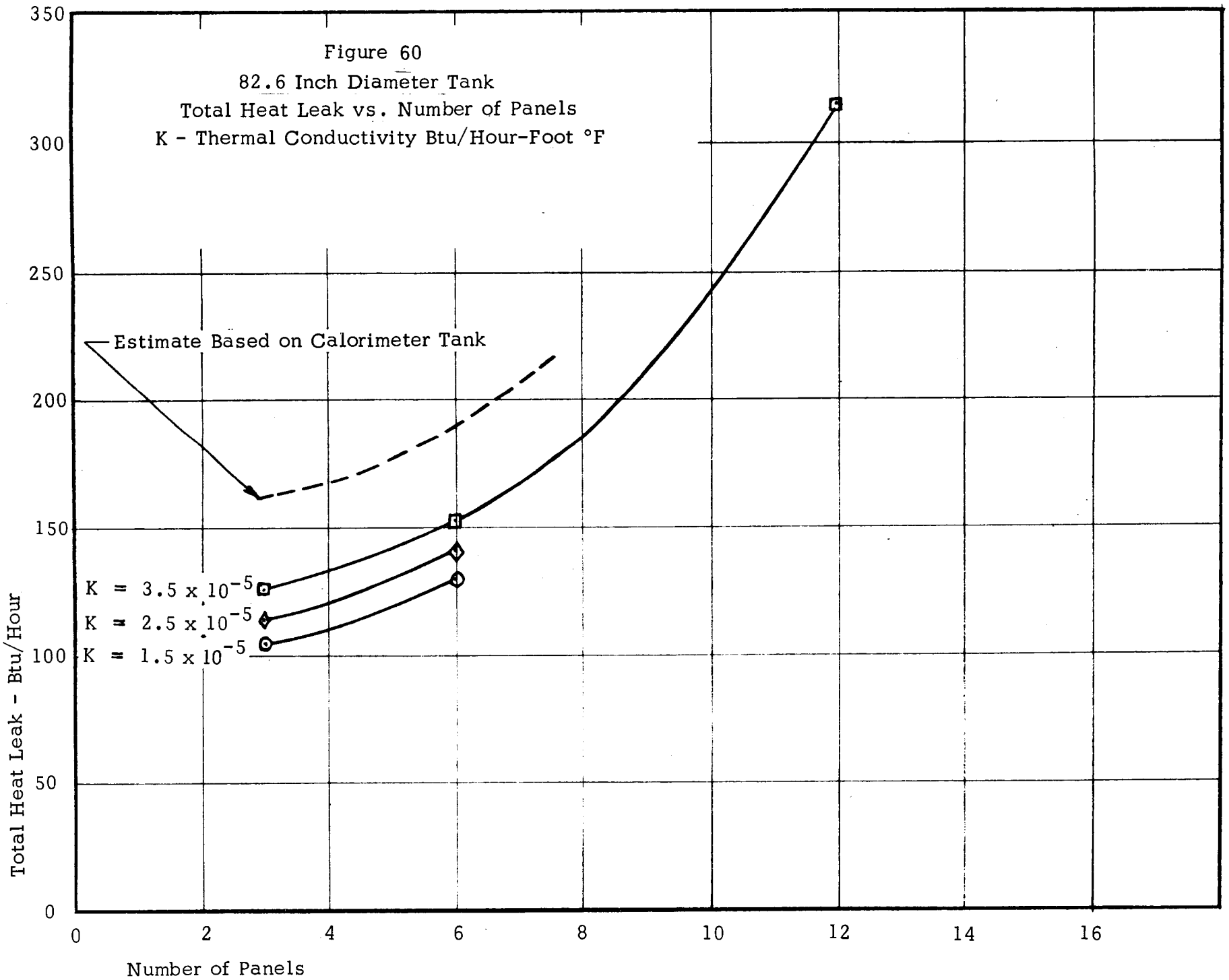
Figure 60
82.6 Inch Diameter Tank
Total Heat Leak vs. Number of Panels
K - Thermal Conductivity Btu/Hour-Foot °F
Estimate Based on Calorimeter Tank
K = 3.5 x 10-5
K = 2.5 x 10-5
K = 1.5 x 10-5
Total Heat Leak - Btu/Hour
Number of Panels
0
50
100
150
200
250
300
350
0
2
4
6
8
10
12
14
16

total heat transfer could be reduced by as much as 20% if the resulting radiation windows could be eliminated.

Following completion of the preliminary design study to establish concepts for insulating spherical tankage with SEMI panels, a design using the three layered double shingled panel insulation system concept was made for the 82.6 inch diameter tank. Since the conical support system must also be insulated, it was decided that the length of the SEMI panels would be extended to include these areas. To accomplish this and in order to achieve the maximum panel thermal length, it was necessary to invert the original polar shingle panel concept, that is to place the smaller segment of the polar panel in contact with the cryogenic surface, rather than using the largest segment of the polar panel in contact with the cryopumping surface as originally intended. This available area should still provide sufficient cryopumping surface although it may cause additional cryopumping problems due to the poor gas conductance,since the surfact is further removed.

The preliminary design requires a total of 48 panels for a three layered system. The maximum dimensions on the vertical panels are 49 inches wide by 70 inches long. Maximum overall dimensions of the polar panels are 68 inches wide by 74 inches long. This system as shown in Figure 59 (Linde dwg. No. D-SK-102425) divides the tank circumference into six equal spaces, i.e. requires six vertical panels per layer (60° system). On each adjacent layer the butt joints are half lapped to reduce system edge losses via radiation windows. In addition to the case shown, the computer analysis was programmed to permit varying the width of the verical panels, thus obtaining solutions for a system requiing three panels around the tank circumference (120° system), and for a system requiring 12 vertical panels around the equator (30° system). Plotting the results of these cases then, permitted interpolating for the expected results using a four panel system (90° system). The four panel system was not evaluated directly by computer because of the difference in symmetry in panels encountered in a four panel system as compared to the six panel system. Using a 60° reference system the panel symmetry repeats every 120°. Therefore, using a 60° system as the reference, by symmetry the 30° system panels being one half the size of the 60° panels, and the 120° panels being twice the size of the 60° panels, contributed a proportionate increase/decrease in heat leak due to the increase/decrease in the number of panel edge losses. Configuration and size of the polar shingled panels and the length of the vertical shingle panels remained the same for all panel combinations, i.e. for 30°, 60°, 90°, or 120° system.

Meaningful size variations for computer analysis were not possible for either the polar panels or vertical lengths because of restrictions imposed by the tank configuration and necessary cryopumping areas required for panels. Overall panel sizes for the various configurations are shown in Table 18. All panels are of a compound curvature rather than a single plane and therefore the noted panel depth is presented as a means of gauging the apparent curvature of each panel. It is readily apparent that in a system using a greater number of vertical panels, the panels are more easily handled. However, as noted in Table 18 , the maximum depth (curvature) for a 12 panel system is 28 inches as compared to 36for the three panel system; and therefore this problem is probably no more acute in either system.

TABLE 18.

Panel Dimensions - 82.6-Inch Diameter Tank

Three Layered Shingled System Including Conical Support

Panel Style - see Figure 58	Approximate Overall Panel Dimensions (inches)									
	Length "L"	Width "W"				Depth "D"				
Number of vertical panels per layer →		3	4	6	12	3	4	6	12	
A	42	98	74	49	25	34	29	25	23	
B	34	98	74	49	25	31	25	20	17	
C	26	98	74	49	25	29	21	16	12	
D	32	98	74	49	25	26	17	10	6	
E	54	98	74	49	25	29	21	16	12	
F	70	98	74	49	25	34	29	25	23	
G	40	88	66	44	22	36	32	29	28	
H	68	——	74	——		——	17	——		
J	68	——	74	——		——	17	——		

* Number of vertical panels per layer	Total number of panels per system
3	27
4	34
6	48
12	90

5.0 References

1. CR-72017 Investigation of a Lightweight Self-Evacuating Prefabricated Multilayer Insulation System for Cryogenic Space Propulsion Stages by L. R. Niendorf and G. E. Nies.

2. CR-54929 Advanced Studies on Multilayer Insulation Systems by Staff, Arthur D. Little, Inc.

3. Carslaw, H. S., and Jaeger, J. C., Conduction of Heat in Solids, Oxford Clarendon Press, 2nd ed., 1959.

4. Dushman, S., Scientific Foundations of Vacuum Technique, John Wiley and Sons, 1962.

5. Honig, R. E., and Hook, H. O., RCA Rev., Vol. 21, p. 360, 1960.

6. Cryogenic Engineering News, Jan., 1967.

7. Selected Values of Properties of Hydrocarbons and Related Compounds API Research Project 44, Carnegie Institute of Technology.

6.0 Acknowledgements

This contract work was performed under the direction of the National Aeronautics and Space Administration, Lewis Research Center. Mr. J. R. Faddoul of the Liquid Rocket Technology Branch was the LeRC Project Manager. In addition, the assistance of Messrs. L. D. Potts, R. L. Ried, and D. Sukow of Union Carbide Corporation, Linde Division is also gratefully acknowledged.

Appendix 1

PRESSURE DEFLECTION DATA - ROOM TEMPERATURE EVACUATED BAG TEST - *
4-PLY ALUMINIZED MYLAR CASING MATERIAL 12 INCH X 18 INCH PANEL SIZE

PANEL DESCRIPTION	CYCLE	COMPRESSIVE LOAD-(psi)	AVERAGE PANEL THICKNESS (inch) (SUPPORT AREA)	
1. Panel contained two foam maze on silk spacers with one aluminized Mylar radiation shields. Each spacer consists of two layers of foam maze on silk mismatched by one half space (13%Support Area). 25 inch wide web with 13/16 inch square holes.		.01	.048	
	2	.22	.048	
		.42	.047	
		13.02	.036	
		14.40	.034	
		.01	.043	
	3	14.4	.033	
		.01	.041	
	4	14.4	.032	
		.01	.041	
	5	14.4	.032	
		.01	.041	
	6	14.4	.033	
		.01	.040	
2. Dimpled Casing Material Panel constructed with 7 foam spacers and 6 aluminized Mylar radiation shields. 7/8 inch diameter dimples on 60° pattern located on 1-1/2 inch centers.			Support Zone	Free
	1	.01	.176	.235
		.23	.163	.195
		.62	.158	.175
		1.0	.153	.169
		2.94	.148	.157
		4.88	.144	.152
		8.75	.134	.141
		14.45	.118	.128
		13.55	.130	.143
		.01	.146	.179
	2	14.45	.114	.122
		.01	.138	.175
	3	14.45	.110	.119
		.01	.136	.172
	4	14.45	.108	.115
		.01	.130	.175
	5	14.45	.107	.117
		.01	.127	.165
	6	14.45	.106	.115
		.01	.127	.165

*Refer to Section 4.1.1 for discussion

PANEL DESCRIPTION	CYCLE	COMPRESSIVE LOAD-(psi)	AVERAGE PANEL THICKNESS (inch) (SUPPORT AREA)
3. Panel contained 7 foam spacers and 6 aluminized Mylar radiation shields. Each .02 inch thick spacer criss-crossed with two layers of .020 inch thick by 3/4 inch wide foam strips, located on 2-1/4 inch centers (13% support area).	1	.01	.545
		.14	.497
		.34	.502
		.54	.495
		.74	.511
		.94	.508
		2.94	.498
		4.94	.489
		6.94	.479
		8.94	.463
		10.94	.459
		12.94	.452
		14.35	.447
		.01	.491
	4	14.35	.430
		.01	.470
	5	14.35	.422
		.01	.464
	6	14.35	.430
		.01	.469
4. Panel constructed of 7 foam spacers and 6 aluminized Mylar radiation shields. Each spacer consisted of 3 sheets of .02 inch thick foam. Two of the three sheets contained 13/16 inch square holes, with 5/16 inch web spacing, assembled mismatched by one half hole. (15% support area)	1	.01	.479
		.14	.439
		.34	.443
		.54	.439
		.74	.431
		.94	.424
		2.94	.401
		4.94	.385
		6.94	.378
		8.94	.371
		10.94	.364
		12.94	.354
		14.25	.340
		.01	.389

PANEL DESCRIPTION	CYCLE	COMPRESSIVE LOAD (psi)	AVERAGE PANEL THICKNESS (inch) (SUPPORT AREA)
Panel # 4 Continued	4	14.35	.340
		.01	.395
	5	14.35	.337
		.01	.389
	6	14.35	.330
		.01	.375

Appendix 2

PANEL GAS TRANSMITTANCE*

The following equations were used to reduce the transmittance data of the one-foot wide by three-foot long test panels.

WET DRUM METHOD:

To obtain panel throughput Q_s in atm. cfm

$$Q_s = \frac{\Delta V_{WD} \times T_{STD}}{\Delta t \; \bar{T}} \cdot \frac{(P_{atm} - P_{WV})}{P_{STD}}$$

where: ΔV_{WD} = increment of gas ($ft.^3$) passing through wet drum meter in time increment Δt

Δt = time increment - (minutes)

$\bar{T}$ = average gas supply temperature (°R)

T_{STD} = 530°R

P_{STD} = 760 mm Hg abs.

P_{WV} = vapor pressure of water at wet drum temperature. (mm Hg. abs.)

P_{atm} = barometric pressure (mm Hg)

And to obtain unit transmittance F in $\frac{\text{(cfm) (foot length)}}{\text{(foot width) (inch thickness)}}$

$$F_t = \frac{Q_s \times L}{\Delta P} \times \frac{P_{STD}}{W \times t} \times 10^{+3} \frac{\text{microns}}{\text{mm Hg}}$$

where: L = panel length - (ft.)
W = panel width - (ft.)
t = panel thickness (inches)
ΔP = pressure frop across panel - (microns)

*Refer to Section 4.1.3 for discussion

Example - Panel SC-6 at 30,000 micron average pressure.

	Initial	Final	Increment
Wet Drum Reading	.234	.253	.019 ft.^{3}
Time	12:58 PM	13:25 PM	27 Minutes

$L = 3$ ft. $\quad w = 1$ ft. $\quad t = 0.242$ in.

$\bar{T} = 531°R$

$T_{gas} = 75°F \quad \therefore \quad P_{WV} = 22$ mm Hg

$P_{atm} = 750$ mm Hg

$\Delta P = 22.8 \times 10^{+3}$ microns

$$\text{and } Q_s = \frac{(.019)\ (530)\ (750 - 22)}{(27)\ (5.31 \times 10^{+2})\ (760)} = 6.7 \times 10^{-4} \text{ atm. cfm}$$

$$\text{and } F_t = \frac{(6.7 \times 10^{-4})\ (3)\ (7.6 \times 10^{+2})\ (10^{+3})}{(22.8 \times 10^{+3})\ (1)\ (0.242)}$$

$$= 279.0 \times 10^{-3}\ \frac{\text{(cfm) - (foot length)}}{\text{(foot width)(inch thickness)}}$$

STANDARD VOLUME METHOD:

To obtain throughput Q_s in atm. cfm

$$Q_s = \frac{T_{STD}\ (V_{Co_2})\ \Delta P_s}{P_{STD}\ \bar{T}\ \Delta t}$$

where

V_{Co_2} = Fixed Supply Volume (.075 ft.^{2})

Δp_s = Change in Co_2 supply pressure during Δt time increment (mm Hg).

Δt = Time increment (minutes)

and unittransmittance $F_t = \frac{\text{(cfm) (foot length)}}{\text{(foot width) (inch thickness)}}$

$$F_t = \frac{L \times P_{STD} \times Q_s}{W \quad P} \times 10^{+3} \quad \frac{\text{micron}}{\text{mm Hg}}$$

Example - Panel SC-5 at 300 microns average pressure

Δp_s = 64 mm Hg - 62 mm Hg = 2 mm Hg

Δt = 28 minutes

L = 3 ft. (length)

W = 1 ft. (width)

t = 0.211 in. (thickness)

Δp = 500 microns

$$\text{then } Q_s = \frac{(5.30)\ (.075)\ (2)\ (10^{+2})}{(7.60)\ (5.38)\ (28)\ (\times 10^{+4})} = 6.95 \times 10^{-6} \text{ atm. cfm}$$

$$\text{and } F_t = \frac{(3)\ (7.60)\ (6.95 \times 10^{-6}) \times 10^{+3+2}}{(1)\quad 5.00 \times 0.211 \quad \times 10^{+2}}$$

$$= 150.0 \times 10^{-3} \frac{\text{(cfm) - (ft. length)}}{\text{(ft. width) (inch thickness)}}$$

Appendix 2

PANEL GAS TRANSMITTANCE DATA

Panel	% Support	MEASURED THICKNESS (INCH) Support Area	Open Area	Avg.	GAS TRANSMITTANCE ($\frac{\text{cfm-ft. length}}{\text{ft.width-inch thick}}$) F_t	PANEL PRESSURE (MICRONS) ΔP	Avg. P
PC-1	22	.392	.262	.290	.0915	330	185
					.2000	6350	5650
					1.6950	6350	115650
					7.4450	5080	403650
					14.0800	5080	594650
PC-2	19	.394	.263	.291	.2005	660	420
					.2200	8600	9400
					.4255	10160	21000
					1.5900	6350	99650
					7.8400	10414	396600
					20.3900	4440	597560
PC-2 (Retest data)	19	.394	.263	.291	.1385	64	72
					.1241	153.4	108
					.1380	195	227
PC-3	20	.401	.267	.293	.1028	315	210
					.1126	8890	272
					.1010	6350	2650
					.1830	6350	13700
					.7920	5720	96000
					3.7200	7620	394370
					7.3000	5080	596910

Appendix 2 (Cont'd)

Panel	% Support	MEASURED THICKNESS (INCH) Support Area	Open Area	Avg.	GAS TRANSMITTANCE ($\frac{\text{cfm-ft. length}}{\text{ft.width-inch thick}}$) F_t	PANEL PRESSURE (MICRONS) ΔP	Avg. P
PC-4	11	.372	.248	.262	.2110	450	275
					.2290	6350	4650
					2.7900	6350	117650
					10.7000	6350	410650
					18.3000	6350	600650
PC-5	20	.363	.242	.266	.0725	130	80
					.1900	6350	4750
					2.6200	7620	117380
					9.2900	5080	414920
					17.0500	5080	615900
PC-6	28	.388	.258	.294	.1710	525	337.5
					1.7870	7620	114380
					7.4900	6350	409650
					14.7500	8890	613000
SC-1	11	.315	.210	.222	.1000	6985	1800
					1.1090	7620	118580
					5.0000	9525	416570
					11.3100	7620	616980
SC-2	11	.318	.212	.224	.1458	525	290
					.1220	6350	8650
					1.1840	10160	113340
					4.7750	6350	428650
					8.9400	5080	622420

Appendix 2 (Cont'd)

Panel	% Support	MEASURED THICKNESS (INCH) Support Area	Open Area	Avg.	GAS TRANSMITTANCE ($\frac{\text{cfm-ft. length}}{\text{ft.width-inch thick}}$) F_t	PANEL PRESSURE (MICRONS) ΔP	Avg. P
SC-3	11	.307	.2045	.216	.1142	5080	4820
					1.3100	11430	113170
					5.3000	7620	413470
					11.8100	6350	620450
SC-4	10	.315	.21	.220	.0768	245	138
					.1058	390	285
					.1295	4400	5560
					.1672	4440	15560
					.4910	6980	51520
					.9370	5080	96920
					4.7100	5080	395920
					4.1550	3175	398830
					6.1500	3175	597820
SC-5	20	.288	.192	.211	.1500	490	300
					.1800	3170	12000
					.2746	2540	16000
					1.1890	8890	118000
					3.1300	7620	338000
					7.1100	7620	596000
SC-6	30	.315	.21	.242	.0943	5715	5000
					.2790	11430	30000
					.9430	8255	97000
					1.7500	11430	423000

Panel	% Support	MEASURED THICKNESS (INCH) Support Area	Open Area	Avg.	GAS TRANSMITTANCE ($\frac{\text{cfm-ft. length}}{\text{ft.width-inch thick}}$) F_t	PANEL PRESSURE (MICRONS) ΔP	Avg. P
P-1	-	.281	-	.281	.1505	440	280
					.2919	6350	5850
					2.5300	10160	113340
					9.4600	5715	419280
					18.800	5080	620920
P-2 (NAS3-6289)	-	.06	-	.06	.1145	-	167
					.0785	-	192
					.0668	-	207
					.0968	-	550
					.0899	-	850
					.1580	-	6440
					.4890	-	18300
					1.2840	-	119600
					2.0900	-	199500
					4.7200	-	401300
					8.3800	-	600000
S-1	-	.375	-	.375	.0200	10160	13600
					.0585	9525	64560
					.2530	10160	293000
					.5710	7620	512380

* Transmittance $F_t = \frac{F}{\text{Panel Avg. Thickness (Inch)}} = \frac{\text{CFM - Foot Length}}{\text{Foot Width - inch thickness}}$

Appendix 3

STORAGE LIFE CALCULATIONS*

The following equations were used to determine panel pressures for various time periods due to a function of panel area exposed to atmospheric air, casing permeability, and offgassing of the various insulation materials. Permeability data, offgassing data, and the partial pressure of hydrogen for the various materials were obtained from development work performed under Contract NAS3-6289.

To calculate offgassing contribution

$$\text{Total Offgassing Based on pressure rise data} = \frac{\Delta \text{Pressure} \times \text{Test Chamber Volume}}{\Delta \text{ Time} \times \text{Sample Area}}$$

or Hydrogen Offgassing Rate = (Total Offgassing Rate) x (H_2 partial pressure of sample)

Example

40" x 72" 4-ply panel, 30 days, 14 foam layers, 6 radiation shields

Open cell foam contribution	=	35.5 atm. cc H_2
Aluminized Mylar contribution	=	2.3 atm. cc H_2
Casing material & joints contribution	=	8.4 atm. cc H_2
	=	46.2 atm. cc H_2

To calculate casing permeability contribution

= Helium permeability rate x area x time x helium partial pressure

Example

40" x 72" 4-ply panel with H_2 getter, 100% of panel exposed to air for five days.

= 3.504×10^{-4} atm. cc helium

* Refer to Section 4.2.3 for discussion

Permeability Rates

4-ply aluminized Mylar	=	$.338 \times 10^{-5}$	$\frac{\text{atm cc helium}}{\text{Sec. ft}^2 \text{ atm. helium}}$
Mylar lead Mylar laminate	=	2×10^{-9}	"
Mylar tri laminate	=	1.22×10^{-5}	"
Mylar aluminum Mylar	=	2×10^{-9}	"

Then to determine final panel pressure

$$= \text{Pressure Initial} + \frac{\text{Additional Gas Load}}{\text{panel volume}} = \text{Torr}$$

Where additional gas load results from offgassing and/or casing permeability.

Example

Using offgassing data from above assuming the initial panel pressure to be 5×10^{-5} torr, panel volume = 14,000 cc (40" x 72" x .3" thick) without H_2 getter -

$$P_{30 \text{ days}} = 5 \times 10^{-5} \text{ torr} + \frac{(46.2 \text{ atm. cc}) \ 760 \text{ torr}}{14{,}000 \text{ cc atm.}}$$

$$= 5 \times 10^{-5} \text{ torr} + 2.5 \text{ torr}$$

Appendix 4

PRESSURE HISTORY DATA - CRYOPUMPED STORAGE LIFE*

TEST PANELS AT LH_2 TEMPERATURE

Test No. 1

Panel No. 1 - 14 layers of open cell foam, 6 aluminized Mylar radiation shields, 0.5 gms of hydrogen getter enclosed in 4-ply aluminized Mylar with the air exposed area laminated with "MAAM"**

Panel No. 2 - Same as Panel No. 1 except that outer air exposed area is CO_2 purged rather than laminated with "MAAM."

Time	Panel No. 1		Panel No. 2		
	Pressure***	Temperature	Pressure***	Temperature	
Minutes	Torr	°F	Torr	°F	Remarks
0	750	55	750	55	Start LN_2 Fill
10	496	-	367	-	
11	242	-	113	-	
12	138	-	63	-	
13	88	-	37	-	
14	63	-	37	-	
24	34	-	31	-	
53	-	-	-	-	Stop LN_2 Fill
61	.075	48.2	.150	48.2	
71	.060	43.3	.175	46.2	
85	.055	-	.145	-	
201	.070	35.8	.175	40.8	
211	-	-	-	-	Start LH_2 Fill
228	-	22.8	-	27.1	Stop LH_2 Fill
236	<.005	-	<.005	-	
243	<.005	24.8	<.005	30.6	
271	<.005	24.6	<.005	40.7	Start LH_2 Fill
274	<.005	-	<.005	-	Open Gas Sample Bulbs
281	<.005	-	<.005	-	Stop LH_2 Fill
289	<.005	22.1	<.005	33.6	
321	<.005	32.0	<.005	33.6	Close Gas Sample Bulbs

* Refer to Section 4.2.3 for discussion.

** "MAAM" - Mylar-Aluminum-Aluminum-Mylar Laminate

*** Vacuum pressure measured with thermocouple gauge unless noted in remarks.

PRESSURE HISTORY DATA - CRYOPUMPED STORAGE LIFE TEST PANELS AT LH_2 TEMPERATURE

Test No. 2

Panel No. 1 - 14 layers of open cell foam, 6 aluminized Mylar radiation shields, 0.5 gms of hydrogen getter, enclosed in 4-ply laminate of aluminized Mylar with air exposed area laminated with "MAAM."

Panel No. 2 - Same as Panel No. 1 except that air exposed area is CO_2 purged rather than laminated with "MAAM."

	Panel No. 1		Panel No. 2		
Time Minutes	Pressure Torr	Temperature °F	Pressure Torr	Temperature °F	Remarks
0	750	-	750	-	Start LN_2 Fill
0.5	701	-	727	-	
7	625	-	650	-	
10	431	63.4	120	60.1	
12	142	-	42	-	
16	17	-	17	-	
18	-	61.2	-	60.3	
29	1	-	1	-	
36	-	-	-	-	Stop LN_2 Fill
54	-	-	-	-	Start LN_2 Fill
57	.5	-	.5	-	
64	-	-	-	-	Stop LN_2 Fill
69	.4	-	.4	-	
169	.174	44.4	.174	50.9	Start LH_2 Fill
198	-	22.1	-	23.9	Stop LH_2 Fill
199	.150	-	.08		
219	-	-	-	-	Open gas sample bulbs

Appendix 4 (Cont'd)

Test No. 2

Time Minutes	Pressure Torr	Temperature °F	Pressure Torr	Temperature °F	Remarks
221	.150	-	.060		
232	-	41.9	-	41.9	
244	.150	-	.060	-	
289	.250	46.4	.250	46.4	Close gas sample bulb
297	.250	-	.250	-	
312	.300	-	.300	-	
322	.400	-	.400	-	

PRESSURE HISTORY DATA - CRYOPUMPED STORAGE LIFE TEST PANELS AT LH_2 TEMPERATURE

Test No. 3

Time (Minutes)	Panel No. 1 Pressure (Torr)	Panel No. 2 Pressure (Torr)	Remarks
0	735	735	Start LN_2 Fill
10	634	480	
11	455	255.0	
12	177	50.7	
15	50.7	25.3	
35	-	-	Stop LN_2 Flow
187	-	-	Start LH_2 Fill
195	.035	.035	
205	< .001	< .001	
207	-	-	Stop LH_2 Fill

TEST NO. 3 (CONTINUED)

Time (Minutes)	Panel No. 1 Pressure (Torr)	Panel No. 2 Pressure (Torr)	Remarks
220	2.5×10^{-4}	7×10^{-4}	Cold cathode gauges operative
227	3×10^{-4}	9×10^{-4}	
234	-	-	Begin LH_2 Topping
236	-	-	Stop LH_2 Fill
239	1.8×10^{-4}	5.5×10^{-4}	
255	-	-	Resume LH_2 Topping
263	-	2.5×10^{-4}	Stop LH_2 Fill
269	1.3×10^{-4}	1.5×10^{-4}	Resume LH_2 topping
272	-	-	Stop LH_2 Fill
275	-	1×10^{-4}	
281	1.1×10^{-4}	-	
288	1.05×10^{-4}	-	

TEST NO. 4

0	735	735	Start LN_2 Flow
10	660	660	
20	25.3	25.3	
27	-	-	Stop LN_2 Fill
120	-	-	Start LH_2 Fill
138	.040	.003	Stop LH_2 Fill
146	-	-	Start LH_2 Topping

TEST NO. 4 (CONTINUED)

Time (Minutes)	Panel No. 1 Pressure (Torr)	Panel No. 2 Pressure (Torr)	Remarks
150	<.001	<.001	Stop LH_2 Fill
197			Resume LH_2 Topping
206	<.001	<.001	Stop LH_2 Transfer
300			Resume LH_2 Fill
313			Stop LH_2 Fill
	.005 +	.005+	Cold Cathode gauges off scale Open gas sample bulbs
314	1.0	.005+	Gas sample bulb leaking on Panel No. 1
350	<.001	<.001	Close gas sample bulbs

Appendix 5

Computer Program - Thermal Analysis of a Self Evacuated Insulation System for Use on Spherical Tankage

A. INTRODUCTION

An effort was undertaken to analyze the temperature profile and the heat flow through the self evacuating insulation panels on an 82.6 inch diameter spherical tank employing a continuous conical support member. The object was to provide a means for evaluating the insulation performance for various panel configurations of different panel widths, and panel conductivities. This insulation system of panels, achieves self evacuation by cryopumping the gas within the panels, which in this case, is carbon dioxide. However in order to achieve this self-evacuation feature, each panel must be installed such that some portion is in contact with the cryogenic surface, and therefore, the thermal analysis of such a system, becomes highly complex. A three layered system of shingled insulation panels was designed for the 82.6 inch diameter tank, including not only the spherical portion but also the conical support systems as well. Some typical results are given.

B. SUMMARY AND CONCLUSIONS

A Fortran IV computer program for thermal analysis of a spherical container-insulation system has been written and used to predict system temperature profiles and heat fluxes for different insulation-panel thermal conductivities and dimensions. The container is essentially spherical, with a cone-shaped support structure attached at its equator. The insulation system, which encloses the entire container-support system, consists of vertical and polar insulation panels combined in a "shingled" three-layer pattern that repeats itself at every 120-degree interval measured along a parallel of latitude. The program provides for an angular width $\emptyset$ of 30, 60, or 120 degrees in the latitudinal direction for the vertical panels.

To date, the program has been used to solve nine different cases on the IBM-360/40 computer. For the typical parameter values used, the results indicate that:

1. The total system heat flux decreases markedly, by a factor of about 2, when $\emptyset$ is increased from 30 to 60 degrees, because of the reduced number of radial butt-joint heat leaks. The decrease resulting from increasing $\emptyset$ from 60 to 120 degrees is much less--a factor of about 1.2.

2. Halving the normal thermal conductivity of the insulation decreases the total system heat flux by less than 15%; halving the lateral conductivity decreases the flux by about 20%.

3. Variation of $\emptyset$ has less effect upon the heat flux from the conical portion of the insulation (30-40% of total flux) than upon the spherical portion, probably because of the relatively constant heat leak provided by the metal cone.

C. DISCUSSION

1. Geometry of Insulation-Container System

The insulation-container system to be analyzed thermally, shown in detail in Linde Drawing No. D/SK-102425, can be described as follows:

The container consists of two hemispherical shells joined to the ends of a short cylindrical shell of length 6 inches, with inlet-outlet pipe flanges centered near the spherical poles. The nominal radius of the hemispheres and the cylinder is 42 inches. A support structure, in the shape of a thin-walled (0.016-inch thick) frustum of a cone, attaches to the container at the midplane (the plane normal to the container's polar axis and midway between the poles). The entire unit is housed in a three-layer shingled insulation system consisting of insulation panels of nine different shapes, a polar shingled panel and three vertical shingled panels each for both the upper and lower hemispherical sections plus an additional vertical panel on the underside of the cone. The lapping arrangement of the panels is shown in Figures A1 and A2.

The reader will note that the total number of both polar panels is three apiece. Moving around a parallel of latitude for each hemisphere in a counter-clockwise sense viewed from above the container, a given polar panel occupies the top layer position for the first 120 degrees of angular distance, the middle layer position for the next 120 degrees, and the bottom layer position for the final 120 degrees. The total number of each of the seven different vertical panels is

assumed to be 3 x I, where I is an integer. For the purpose of this analysis, we restricted ourselves to the cases I = 1, 2, and 4 which correspond to angular panel widths, measured along a parallel of latitude, of 120, 60, and 30 degrees, respectively. Since panel butt joints leak heat radially by conduction through the butt casing, the heat flux into the system will depend critically upon the angular width $\emptyset$ of the vertical panels. Analysis for the indicated three panel widths allows us to assume temperature periodicity of period 120 degrees in the latitudinal direction and to estimate the heat leak for intermediate panel widths by interpolation. Distribution of the butt-joint heat leaks in the latitudinal direction for all seven vertical panels is shown schematically in Figure A-8.

As shown in Figures A1 & A6 we assume that insulation contacts the cone along its entire length on the bottom surface and down to the location of the "bend" in the top insulation layer on the top surface. At the juncture of the upper hemisphere and cone, we assume loose "bends" in the middle and lower insulation layers, so that there is no heat conduction normal to the layers in this small region. Cone-insulation lap lengths given in FigureA-6were used in the program calculations as typical values and should not be regarded as final design values.

2. Theory

a. Basic Equations

At steady state, the flow of heat in the hemispherical sections of the insulation is governed by the (time-independent) Fourier equation in spherical coordinates,

$$\frac{\partial}{\partial r}\left(k_r \cdot r^2 \cdot \sin\theta \cdot \frac{\partial T}{\partial r}\right) + \frac{\partial}{\partial \theta}\left(k_\theta \cdot \sin\theta \cdot \frac{\partial T}{\partial \theta}\right) + \frac{1}{\sin\theta}\frac{\partial}{\partial \varphi}\left(k_\varphi \frac{\partial T}{\partial \varphi}\right) = 0 \qquad (1)$$

where r, θ, and φ, shown in Figure A-3, are defined as follows:

(1) r = displacement from center of sphere

(2) θ = angular displacement, along a meridan of longitude, from upper pole of sphere

(3) φ = angular displacement, along a parallel of latitude, in a counter-clockwise sense when viewed from above the upper pole.

In terms of the conical coordinates shown in Figure 3, the Fourier equation governing the heat flow in the conical support structure and attached insulation is

$$\frac{\partial}{\partial S}\left(k_S \cdot R \cdot \frac{\partial T}{\partial S}\right) + \frac{\partial}{\partial Z}\left(k_Z \cdot R \cdot \frac{\partial T}{\partial Z}\right) + \frac{\partial}{\partial \varphi}\left(\frac{k_\varphi}{R}\frac{\partial T}{\partial \varphi}\right) = 0 \qquad (2)$$

where R is the perpendicular distance from the conic axis (in this case coincident with the polar axis of the sphere).

The conical coordinates are defined as follows:

(1) Z = displacement in direction normal to conic surface

(2) S = displacement along intersections of the conic surface with a family of planes having a common intersection at the conic axis

(3) φ = angular displacement along intersections of the conic surface with a family of planes normal to the conic axis.

In equations (1) and (2), T is the temperature and k_r, k_θ, k_φ, k_z, k_s, are the thermal conductivities in the coordinate directions denoted by the subscripts.

In this particular problem, $k_\theta = k_\varphi = k_s = k_p$ and $k_r = k_z = k_n$, where both k_p and k_n are assumed constant and $k_p \gg k_n$. Therefore, (1) and (2) become

$$k_n \cdot \sin\theta \cdot \frac{\partial}{\partial r}\left(r^2 \frac{\partial T}{\partial r}\right) + k_p \cdot \left[\frac{\partial}{\partial \theta}\left(\sin\theta \frac{\partial T}{\partial \theta}\right) + \frac{1}{\sin\theta}\frac{\partial^2 T}{\partial \varphi^2}\right] = 0 \qquad (3)$$

$$k_n \frac{\partial}{\partial Z}\left(R \frac{\partial T}{\partial Z}\right) + k_p \cdot \left[\frac{\partial}{\partial S}\left(R \frac{\partial T}{\partial S}\right) + \frac{\partial}{\partial \varphi}\left(\frac{1}{R}\frac{\partial T}{\partial \varphi}\right)\right] = 0 \qquad (4)$$

The lateral thermal conductivity k_p is an effective value found by adding the contributions due to the panel casing, spacer, and radiation shields.

The temperature distribution in the insulation system results from solving (1) and (2) subject to the following boundary conditions:

(1) Temperature of inner surface of sphere insulation ($r = R_o = 42"$) and at void space within cone is cryogenic (40°R).

(2) Temperature of outer surface of sphere insulation ($r = R_o + 3.dr = 43.35"$) and outer surface of cone insulation is ambient (530°R).

(3) Temperature at insulation-flange interface varies linearly with r, for both upper and lower spherical sections, according to the relation

$$T(r) = 40 + \frac{(r - R_o)(490)}{3 \cdot dr} = 40 + \frac{(r - 42)"(490)}{1.35"}$$

(r in inches ("))

Because of the pole geometry and constraints imposed upon the angular widths of the non-polar panels, there is an additional, symmetry, condition:

$$T(\Phi) = T(\Phi + 120°) = T(\Phi + 240°)$$

That is, there is temperature periodicity in the Φ direction of period 120 degrees. Thus, only 1/3 of the system need be analyzed and the resulting heat fluxes tripled to obtain the total system fluxes.

b. Finite Difference Mesh

Because of the highly anisotropic "shingle" structure of the insulation, an analytical solution of (3) and (4) is impractical. However, the true temperature profile can be approximated by setting up an integration network within the insulation system, writing (3) or (4) in finite difference form at each resulting mesh point. There results a system of simultaneous linear equations that can be solved uniquely for the unknown temperatures.

As shown on Figures A-4-A-7a 344-point mesh was chosen. This mesh was set up in the following manner.

Each spherical section has four θ-regions. Referring to Figure A-1, these regions have arc lengths, at r = 42", of 8.8", 8.1", 8.1" & 12.5" for the upper section and 8.0", 8.1", 16.1" & 24.2" for the lower section. If each region is split into two parts of equal arc length, with mesh points centered in each part, there result 16 θ-positions for the two spherical sections. There are two r-positions for the spherical sections, at the upper-middle and middle-lower layer interfaces. Also, eight φ- positions, with 15-degree angular spacing, were chosen for a total φ-width of 120 degrees (the period of the repeating temperature pattern). Therefore, the total number of mesh points in the two spherical sections is 16 x 2 x 8 = 256.

The same eight φ-positions were chosen for the conical section. However, the need for determining the temperature profile of the metal cone plus the changing number of insulation layers moving up the cone dictates a different network in the other two coordinate directions. As shown on Figure 6, there are 11 mesh points per φ-position for a total of 88 for the cone. The 88-cone mesh points plus the 256 sphere mesh points equal a total of 344.

Finite difference approximation of (3) or (4) at each mesh point results in 344 simultaneous equations that must be solved. Because of the relative lack of symmetry in the insulation system, the resulting equations often vary in form from one mesh point to another. Typical examples are given below for a vertical panel width Ø = 60 degrees.

At mesh point (7,1) on the upper sphere (see Figures A-4 & A-7) the finite difference approximation to Equation (3) becomes

$$(k_n/d_p)\cdot(A_{RT1}\cdot(T_w - T(7,1)) - A_{RM1}\cdot(T(7,1) - T(15,1)))$$

$$+ k_p\cdot((A_{\theta 1}/\Delta\theta_1)(T' - T(7,1)) - (A_{\theta_2}/\Delta\theta_2)(T(7,1) - T(7,2)))$$

$$+ (k_p\cdot A_{\varphi 1}/d\varphi)\cdot(T(6,1) - 2\cdot T(7,1) + T(8,1)) = 0$$

where
T_w = ambient temperature (530°R)
T' = flange temperature = $2/3\cdot T_w + 1/3\cdot T_c$ = 366.7°R
$\Delta\theta_1$ = $d\theta_1/2$
$\Delta\theta_2$ = $(d\theta_1 + d\theta_2)/2$
A_{RT1} = $(R_o + 2.5dr)^2\cdot\sin\theta_1\cdot d\theta_1\cdot d\varphi$
A_{RM1} = $(R_o + 1.5dr)^2\cdot\sin\theta_1\cdot d\theta_1\cdot d\varphi$

$$A_{\theta 1} = \sin(\theta_1 - (d\theta_1/4)) \cdot dr \cdot d\varphi$$
$$A_{\theta 2} = \sin((\theta_1 + \theta_2)/2) \cdot dr \cdot d\varphi$$
$$A\varphi_1 = dr \cdot d\theta_1/\sin\theta_1$$

One should note that, prior to discretization, all terms in Equation (3) were multiplied by $dr \cdot d\theta \cdot d\varphi$ so that the temperature coefficients in the difference equation will be in units of Btu-hr^{-1}-°R^{-1}. These coefficients can then be used directly, once the difference equations have been solved, to calculate the system heat fluxes.

As shown in the preceding example and the other two examples of sphere-mesh-point heat balances that follow, each unknown temperature T(I,J) has two subscripts. The subscript I indicates the mesh point position in the r - φ plane: I varies from 1 through 8 for mesh points in the middle-upper layer interface and from 9 through 16 in the middle-lower layer interface, increasing with increasing φ (from left to right in Figures A-7 & A-8). The subscript J indicates the θ-position of the mesh point and varies from 1 through 19 for the entire system: J = 1 - 8 for the upper sphere, 9 - 11 for the cone, and 12 - 19 for the lower sphere. J = 1 represents the θ-position closest to the upper flange in the upper spherical section; J = 19 represents the θ-position closest to the lower flange in the lower spherical section.

As a second example, the finite difference equation for mesh point (16,3) is

$$(k_n/dr)\cdot(A_{RM3} \cdot (T(8,3) - T(16,3)) - (A_{RB3} + Z)\cdot(T(16,3) - T_c))$$
$$+ k_p \cdot ((A_{\theta 3}/\Delta\theta_3)\cdot(T(16,2) - T(16,3)) - (A_{\theta 4}/\Delta\theta_4)\cdot(T(16,3) - T(16,4)))$$
$$+ (k_p \cdot A_{\varphi 3}/d\varphi)\cdot(T(15,3) - 3 \cdot T(16,3) + 2 \cdot T_c) = 0$$

where
T_c = cryogenic temperature = 40°R
$\Delta\theta_3 = (d\theta_2 + d\theta_3)/2$
$\Delta\theta_4 = (d\theta_3 + d\theta_4)/2$
$A_{RM3} = (R_o + 1.5dr)^2 \cdot \sin\theta_3 \cdot d\theta_3 \cdot d\varphi$
$A_{RB3} = (R_o + 0.5dr)^2 \cdot \sin\theta_3 \cdot d\theta_3 \cdot d\varphi$
$Z = (k\cdot t)_c \cdot (R_o + 0.5dr) \cdot \sin(\theta_2 + \frac{1}{2} \cdot d\theta_2) \cdot d\varphi$
$(k\cdot t)_c$ = thermal conductivity - thickness product for insulation panel casing

$$A_{\theta 3} = \sin((\theta_2 + \theta_3)/2) \cdot dr \cdot d\varphi$$
$$A_{\theta 4} = \sin((\theta_3 + \theta_4)/2) \cdot dr \cdot d\varphi$$
$$A_{\varphi 3} = dr \cdot d\theta_3 / \sin\theta_3$$

The reader will note in this example the additional heat leak in the normal direction through the bottom panel due to the butt joint between the upper pole panel and Panel No. 1, as indicated by the quantity Z. Also of interest is the thermal "shorting" to cryogenic in the φ-direction, as indicated by the larger weights (3 and 2 rather than 2 and 1) assigned to T (16,3) and T_c in the third term on the left, because the distance between point (16,3) and cryogenic is only 1/2 the distance between points (16,3) and (15,3) (since the mesh points are centered within each increment).

A third, and final, example of a sphere difference equation is the equation for mesh point (3,5):

$$(k_n/dr) \cdot (A_{RT5} \cdot (T_w - T(3,5)) - (A_{RM5} + Z') \cdot (T(3,5) - T(11,5)))$$
$$+ k_p \cdot ((A_{\theta 5}/\Delta\theta_5) \cdot (T(3,4) + T(11,4) - 2 \cdot T(3,5))$$
$$- (A_{\theta 6}/\Delta\theta_6) \cdot (T(3,5) - T(3,6)))$$
$$+ (k_p \cdot A_{\varphi 5}/d\varphi) \cdot (T(2,5) - 2 \cdot T(3,5) + T(4,5)) = 0$$

where
T_w = ambient temperature = 530°R
$\Delta\theta_5 = (d\theta_4 + d\theta_5)/2$
$\Delta\theta_6 = (d\theta_5 + d\theta_6)/2$
$A_{RT5} = (R_o + 2.5dr)^2 \cdot \sin\theta_5 \cdot d\theta_5 \cdot d\varphi$
$A_{RM5} = (R_o + 1.5dr)^2 \cdot \sin\theta_5 \cdot d\theta_5 \cdot d\varphi$
$Z' = (k \cdot t)_c \cdot (R_o + 1.5dr) \cdot d\theta_5 / k_n$
$A_{\theta 5} = ((A_4 \cdot A_5)/(2 \cdot A_4 + A_5)) \cdot dr \cdot d\varphi$
$A_4 = \sin(\theta_4 + 1/2\, d\theta_4)$
$A_5 = \sin(\theta_5 - 1/2\, d\theta_5)$
$A_{\theta 6} = \sin((\theta_5 + \theta_6/2) \cdot dr \cdot d\varphi$
$A_{\varphi 5} = dr \cdot d\theta_5 / \sin\theta_5$

In this example, the reader will note the additional heat leak in the normal direction through the bottom panel due to the butt joint between adjacent no. 1 Panels. This butt joint lies along a spherical meridian, whereas the pole panel to no. 1 Panel butt joint influencing the

previous sample equation lies along a parallel of latitude. Also of interest is the unusual form of the term involving $A_{\theta 5}$. However, one can see from Figures A-1& A-4 that between the fourth and fifth θ-positions Panel No. 1 changes levels, from bottom panel at J = 4 to middle panel at J = 5. Also, the middle section of the pole panel ends here. Therefore, the temperature at the top radial position for J = 5 will be influenced by temperatures at <u>both</u> radial positions for J = 4.

Similar difference equations can be derived from Equation (4) for the cone mesh points. The heat flow paths assumed in the mathematical model of the cone structure are shown in Figure A-6. For example, discretization of Equation (4) around cone mesh point (7,3), where 7 denotes the Φ-position and 3 the position in the S-Z plane, gives

$$(k_n/dr)\cdot((A_{Z3}\cdot(T_w - T_3'(7)) - (A_{Z34} + Z'')\cdot(T_3'(7) - T_4'(7)))$$

$$+ k_p \cdot \left(\frac{A_{S310}\cdot(T_{10}'(7) - T_3'(7))}{((S_2 + S_3)/2)} - \frac{A_{S35}\cdot(T_3'(7) - T_5'(7))}{((S_0 + S_1 + S_2)/2)}\right)$$

$$+ (k_p \cdot A_{\varphi 3}/d\varphi)\cdot(T_3'(6) - 2\cdot T_3'(7) + T_3'(8)) = 0$$

where

$A_{Z3} = S_2 \cdot R_3 \cdot d\varphi$

$A_{Z34} = S_2 \cdot R_{34} \cdot d\varphi$

$Z'' = S_2 \cdot (k\cdot t)_c/k_n$

$A_{S310} = \dfrac{(S_2 + S_3)\cdot dr \cdot d\varphi}{(S_2/R') + (S_3/R'')}$

$A_{S35} = \dfrac{(S_0 + S_1 + S_2)\cdot dr \cdot d\varphi}{((S_0 + S_1)/R''') + S_2/R''''}$

$A_{\varphi 3} = S_2 \cdot dr/R_3$

$R_3 = R_o + (S_1 + \frac{1}{2}\cdot S_2)\cdot \cos X + 2.5 \cdot dr \cdot \sin X$

$R_{34} = R_3 - dr \cdot \sin X$

$R' = R_o + (S_1 + (0.75)S_2)\cdot \cos X + 2\cdot dr \cdot \sin X$

$R'' = R' + (0.25)(S_2 + S_3)\cdot \cos X - dr \cdot \sin X$

$R''' = R_o + (0.25)(3\cdot S_1 - S_0)\cdot \cos X + 2\cdot dr \cdot \sin X$

$R'''' = R''' + (0.25)(S_1 + S_2)\cdot \cos X$

X = inclination of conic surface with horizontal

The reader will note the compound structure of the terms A_{S310} and A_{S35}, which reflects the variation of heat conduction cross-section area with S. The terms are derived by splitting each region into two parts and assuming that the total thermal resistance (or reciprocal conductance) is the sum of the resistance of the parts. The two parts influencing A_{S310} extend in the S direction between mesh point (7,9) and increment boundary (3), and between boundary (3) and mesh point (7,3); the parts influencing A_{S35} extend between (7,3) and increment boundary (4), and between boundary (4) and mesh point (7,5). One should also note again the radial heat-leak term Z".

c. Evaluation of Temperatures

Once Equations (3) and (4) have been cast into difference form for all 344 mesh points, as shown in the examples given in the preceding section, the resulting linear equations can be solved directly for the unknown temperatures. However, direct solution of 344 simultaneous equations by conventional methods would require the inversion of a 344 x 344 coefficient matrix. Inversion of such a large matrix would be very expensive in terms of computation time and, since most of the matrix elements will be zeros, wasteful of computer core storage, particularly since the effects of round-off error on the accuracy of the results would probably dictate the use of double precision arithmetic. However, the structure of the equation is such that the temperatures can be obtained by inverting, not one 344 x 344 matrix, but nineteen 16 x 16 matrices plus one 40 x 40 matrix. Therefore, the number of arithmetic operations (proportional to the matrix order cubed) is greatly reduced and standard precision arithmetic can be used.

One will note from Figures A-4 &A-5 that the unknown temperatures at any θ-position in either hemispherical section are influenced only by neighboring temperatures in that particular plane plus temperatures in the two r-φ planes on either side (except θ-positions 1 and 19, where a prescribed-temperature pipe-flange boundary replaces one of the r-φ planes). Therefore, the 256 equations for the two spherical sections can be represented matrically by the top 8 and bottom 8 rows of the matrix equation shown schematically in Figure A-9. Each matrix row in the schematic diagram corresponds to a different θ-position, with θ-position 1 occupying the top row. Each of the quantities $\underline{A_{i,j}}$ is a 16 x 16 matrix representing the mutual influence of the temperatures in the ith r-φ plane (or θ-position) with themselves (i = j) or with the temperatures in an adjacent r-φ plane (i ≠ j),* since the coefficient matrix is symmetric, $\underline{A_{i,j}} = \underline{A_{j,i}}$. Each quantity $\overline{T}_j$ is a 16-element

*The reader should note here the distinction in notation between a matrix ($\underline{X}$) or vector ($\overline{X}$) and an element of a matrix or vector (X(I,J) or X(I)).

vector of unknown temperatures in the jth r-φ plane. Each quantity $\overline{B}_i$ is a 16-element vector of constant terms, involving the known ambient, cryogenic, and flange temperatures. All blank squares represent 16 x 16 null (zero) matrices.

In Figure A-9, only 48 unknown temperatures (the middle three rows) are assumed for the cone so that the order of the matrix equation is 304 instead of 344. Although there are actually 88 unknown cone temperatures, the structure of the 88 equations is not consistent with the "block-tridiagonal" structure of the sphere equations. The cone equations, however, can be cast into a form that is consistent with this structure.

Referring again to Figure A-9, let $\overline{T1}$ represent a 48-element vector of the unknown temperatures $T_1'(I)$, $T_2'(I)$, $T_3'(I)$, $T_4'(I)$, $T_5'(I)$, $T_6'(I)$, and $\overline{T2}$ a 40-element vector of the unknown temperatures $T_7'(I)$, $T_8'(I)$, $T_9'(I)$, $T_{10}'(I)$, $T_{11}'(I)$, where I = 1 - 8. The equations centered about the first 48 temperatures can be written in matrix form as

$$\underline{A11} \cdot \overline{T1} + \underline{A12} \cdot \overline{T2} = \overline{B1} \qquad (5)$$

where $\underline{A11}$ is a 48 x 48 matrix, $\underline{A12}$ a 48 x 40 matrix, and $\overline{B1}$ a 48-element vector. Likewise, the equations centered about the last 40 temperatures can be written as

$$\underline{A21} \cdot \overline{T1} + \underline{A22} \cdot \overline{T2} = \overline{B2} \qquad (6)$$

where $\underline{A21}$ is a 40 x 48 matrix (equal to the transpose of $\underline{A12}$), $\underline{A22}$ is a 40 x 40 matrix, and $\overline{B2}$ is a constant vector dependent only upon the known ambient and cryogenic boundary temperature. ($\overline{B1}$ also depends upon the unknown temperatures of the adjacent sphere mesh points, as implied by the presence of matrices $\underline{A_{9,8}}$ and $\underline{A_{11,12}}$ in block rows 9 and 11 of the coefficient matrix shown in Figure A-8.)

Solving (6) for $\overline{T2}$, we get

$$\overline{T2} = \underline{A22}^{-1} \cdot (\overline{B2} - \underline{A21} \cdot \overline{T1}) \qquad (7)$$

Substitution of (7) into (5) gives

$$\underline{A}' \cdot \overline{T1} = \overline{B}' \qquad (8)$$

where $\underline{A}' = \underline{A11} - \underline{A12} \cdot \underline{A22}^{-1} \cdot \underline{A21}$ and $\overline{B}' = \overline{B1} - \underline{A12} \cdot \underline{A22}^{-1} \cdot \overline{B2}$ are of the same order as $\underline{A11}$ and $\overline{B1}$, respectively. The matrix $\underline{A}'$ divides into nine 16 x 16 submatrices. However, the submatrices in the upper right-hand and lower left-hand corners of $\underline{A}'$ are null (all 256 elements of each are zero), reflecting the lack of mutual interaction of the temperatures T'1(I) and T'2(I) with T'5(I) and T'6(I). Therefore, $\underline{A}'$ is block-tridiagonal, of block order 3 and block size 16 x 16, and the system of equations denoted matrically by equation (8) is consistent in structure with the sphere equations.

In Figure A-9, the elements of the submatrices and subvectors corresponding to the cone are now given, for I = 1 - 16 and J = 1 - 16, by

$$A_{9,8}(I,J) = A_{8,9}(J,I) \qquad \text{(from symmetry)}$$

$$A_{9,9}(I,J) = A'(I,J)$$

$$A_{9,10}(I,J) = A'(I,J+16)$$

$$A_{10,9}(I,J) = A'(I+16,J)$$

$$= A_{9,10}(J,I) \qquad \text{(from symmetry)}$$

$$A_{10,10}(I,J) = A'(I+16,J+16)$$

$$A_{10,11}(I,J) = A'(I+16,J+32)$$

$$A_{11,10}(I,J) = A'(I+32,J+16)$$

$$= A_{10,11}(J,I) \qquad \text{(from symmetry)}$$

$$A_{11,11}(I,J) = A(I+32,J+32)$$

$$A_{11,12}(I,J) = A_{12,11}(J,I) \qquad \text{(from symmetry)}$$

$$B_9(I) = B'(I)$$

$$B_{10}(I) = B'(I+16)$$

$$B_{11}(I) = B'(I+32)$$

and for I = 1 - 8,

$$T_9\ (I) = T'_1\ (I)$$

$$T_9\ (I + 8) = T'_2\ (I)$$

$$T_{10}\ (I) = T'_3\ (I)$$

$$T_{10}\ (I + 8) = T'_4\ (I)$$

$$T_{11}\ (I) = T'_5\ (I)$$

$$T_{11}\ (I + 8) = T'_6\ (I)$$

We can now solve the system of 304 equations shown schematically in Figure A-9. The block-elimination solution technique, which is the matrix analogue of the familiar Gauss elimination method used for solving scalar linear equations, has been described by L. D. Potts in an earlier analysis (see Ref. 1, Sec. 5.0) and is outlined schematically in Figure A-11.

The solution gives us the 304 unknown temperatures and therefore the 48 elements of the vector $\overline{T1}$. The elements of $\overline{T2}$, representing the remaining 40 temperatures, can now be found from equation (7).

d. Evaluation of Fluxes

Once the 344 temperatures have been determined, the desired system heat fluxes can be calculated. Twelve heat fluxes are calculated and printed out by the computer program. They are listed below, along with the variable name assigned to each in the computer program.

1. Flux into upper sphere from pipe (or flange) - FIUSFP
2. Flux into upper sphere from surroundings - FIUSFS
3. Flux into upper sphere from cone - FIUSFC
4. Flux into lower sphere from cone - FILSFC
5. Flux into lower sphere from surroundings - FILSFS
6. Flux into lower sphere from pipe (or flange) - FILSFP
7. Flux into cone from surroundings - FICFS
8. Flux from upper sphere (to cryogenic) - FFUS
9. Flux from lower sphere (to cryogenic) - FFLS
10. Flux from cone (to cryogenic) - FFC
11. Total flux into system - FTI
12. Total flux to cryogenic - FTO

The first ten fluxes are calculated by summation over all the pertinent sphere and/or cone mesh points. For example, the flux FILSFP is found from the relation

$$FILSFP = (k_p \cdot A_{\theta 19}/\Delta\theta_{19}) \sum_{I=1}^{8} ((T(I,19) - T') + (T(I+8,19) - T''))$$

where $A_{\theta 19} = \sin(\theta_{19} + (d\theta_{19}/4)) \cdot dr \cdot d\Phi$

$\Delta\theta_{19} = d\theta_{19}/2$

$T' = (2 \cdot T_w + T_c)/3$

$T'' = (T_w + 2 \cdot T_c)/3$

The total fluxes FTI and FTO are then evaluated from:

FTI = FIUSFP + FIUSFS + FILSFP + FILSFS + FICFS

FTO = FFUS + FFLS + FFC

The required equality of FTI and FTO provides a useful check on the accuracy of the calculations. In all the cases run with the computer program, FTI and FTO agreed within a closure error of less than 0.005%.

3. Description of Computer Program

The Fortran IV computer program written to solve the heat conduction equations consists of a main program and fifteen subroutines. These subroutines are described, within the context of the overall program, in the program flow diagrams shown in Figures A-10 & A-11. The program provides for printout of the twelve system heat fluxes described earlier. The temperatures at all 344 mesh points can also be printed out, if desired.

In Figures A-10 & A-11 subroutine names are underlined. The MINV subroutine (see Figure A-11) which is a standard IBM library routine for matrix inversion, is also called by CONEQ to invert the 40 x 40 matrix A22 (see preceding section). All other subroutines are called only as indicated in the flow diagrams.

4. Input Format and Typical Results

Data input to the program consists of four cards per problem, preceded by a header card giving the total number of problems. Input variables, and values assigned to same (where applicable) for cases run to date, are listed in Table A5-1.

Table A5-1

Input Parameters

Card	Variable Name	Unit (and Magnitude, if applicable)	Description
Header	NTOT	≥ 1	Number of problems
1	SU(1)	(16.8) in.	Arc lengths, at outer surface of container, of θ-regions of upper (SU(I)) and lower (SL(I)) spherical sections. I = 1 represents arc length occupied by flange.
	SL(1)	(9.6) in.	
	SU(2)	(8.8) in.	
	SL(2)	(8.0) in.	
	SU(3)	(8.1) in.	
	SL(3)	(8.1) in.	
	SU(4)	(8.1) in.	
	SL(4)	(16.1) in.	
	SU(5)	(12.5) in.	
	SL(5)	(24.2) in.	
2	TCN	Btu-hr^{-1}-ft^{-1}-°R^{-1}	k_n: insulation thermal conductivity normal to the layers.
	TKC	(0.0053333) Btu-hr^{-1}-°R^{-1}	k·t product for cone ((thermal conductivity) x (thickness)).
	TKLC	(0.000321) Btu-hr^{-1}-°R^{-1}	$(k \cdot t)_c$: k·t product for insulation panel casing.
	TKL	Btu-hr^{-1}-°R^{-1}	kp·dr: k·t product for insulation, parallel to the layers (dr in ft).
	RO	(42.0) in.	Radius of container.
	DR	(0.45) in.	Insulation panel thickness (equal to 12·dr).
3	SO	(3.0) in.	Cone - insulation lap lengths.
	S1	(13.227) in.	
	S2	(7.0) in.	
	S3	(3.0) in.	
	S4	(3.0) in.	

Table A5-1 (Cont.)

Card	Variable Name	Unit (and Magnitude, if applicable)	Description
	RC	(46.737) in.	Distance of top end of cone from conic axis.
	SC	(26.227) in.	Slant height of conic surface.
	INDEX	1, 2, or 3	Index to determine angular width of vertical panels. $\emptyset = 30^{o}, 60^{o}, 120^{o}$ for INDEX = 1, 2, 3, respectively.
	IND	---	If IND = 0, fluxes and temperatures are printed out. If IND > 0, fluxes only are printed out.
4	SIM	(3.0) in.	Length of upper hemisphere-cone insulation "bend" for panels #2 (SIM) and #3 (SIB).
	SIB	(6.0) in.	
	TW	(530.0) ^{o}R	Ambient temperature
	TC	(40.0) ^{o}R	Cryogenic temperature.

System heat fluxes for nine cases run with the program, for different values of $\emptyset$, TCN, and TKL, are given in Table A5-2. The flux names in the left-hand column correspond to the names listed in section "Evaluation of Fluxes".

Table A5-2

Typical Values for Calculated Fluxes

	Case								
	(1)	(2)	(3)	(4)	(5)	(6)	(7)	(8)	(9)
Ø (degrees)	30	60	120	60	120	60	120	60	120
TCN ($Btu\text{-}hr^{-1}\text{-}ft^{-1}\text{-}°R^{-1}$) x 1000	0.035	0.035	0.035	0.025	0.025	0.015	0.015	0.035	0.035
TKL ($Btu\text{-}hr^{-1}\text{-}°R^{-1}$) x 1000	1.2866	--	--	--	--	--	--	0.64463	--
Fluxes ($Btu\text{-}hr^{-1}$)									
FIUSFP	3.7	3.2	3.0	3.3	3.0	3.3	3.1	1.8	1.7
FIUSFS	75.7	33.7	25.6	30.5	22.5	27.2	19.3	24.9	19.4
FIUSFC	8.7	7.9	7.9	7.8	7.9	7.8	8.0	4.1	4.0
FICFS	112.4	68.9	62.9	66.5	60.8	64.0	58.6	58.1	53.4
FILSFC	3.5	3.9	3.4	3.9	3.4	3.9	3.4	2.1	1.8
FILSFS	120.1	43.3	31.4	38.2	26.7	33.0	21.7	33.7	25.2
FILSFP	2.7	2.3	2.2	2.4	2.2	2.4	2.2	1.3	1.2
FFUS	88.2	44.8	36.5	41.6	33.4	38.4	30.3	30.8	25.1
FFC	100.1	57.2	51.6	54.8	49.4	52.2	47.2	51.8	47.5
FFLS	126.3	49.5	37.0	44.5	32.2	39.3	27.4	37.1	28.2
FTI	314.6	151.5	125.0	140.9	115.1	129.9	104.9	119.75	100.9
FTO	314.6	151.5	125.0	140.9	115.1	129.9	104.9	119.75	100.9

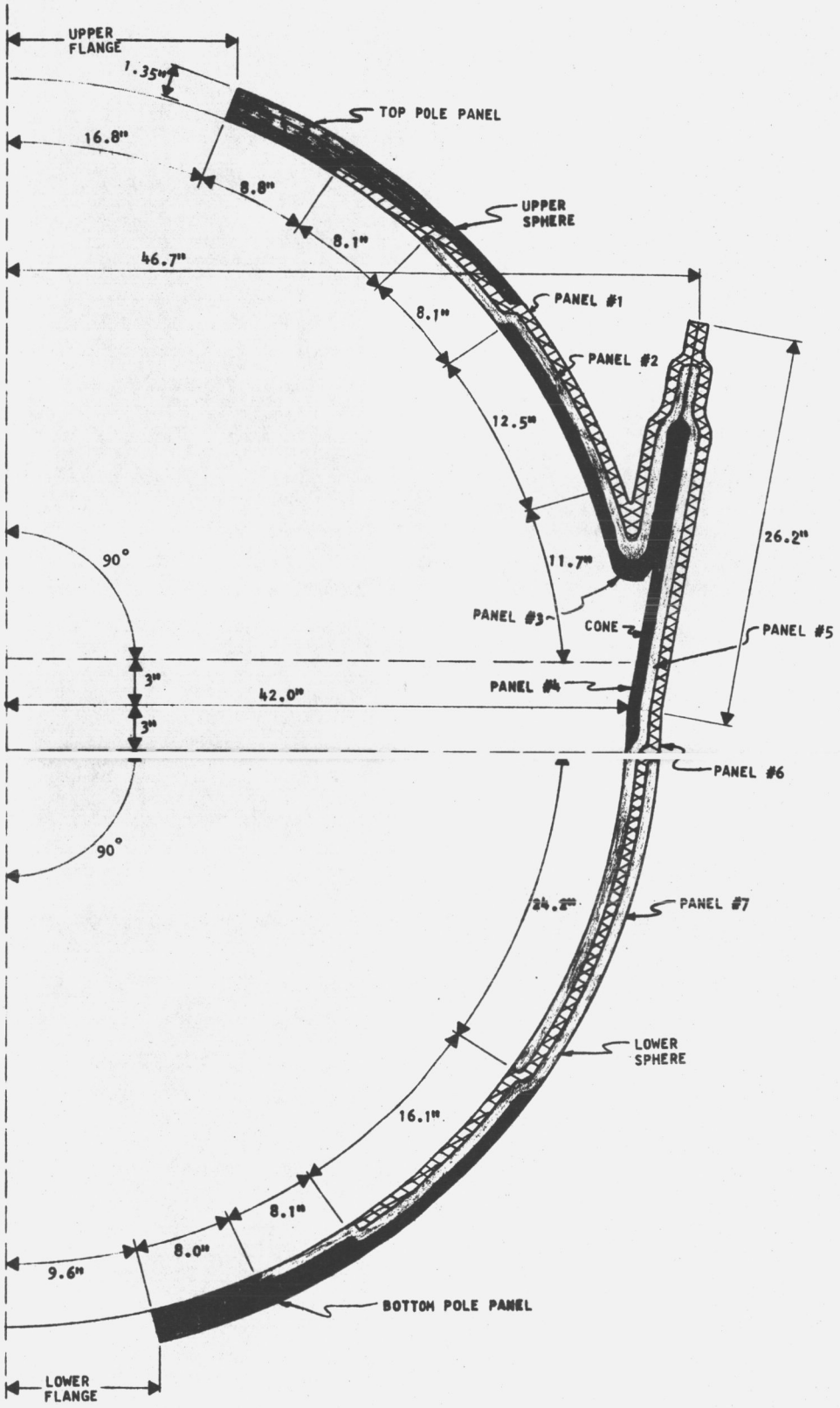

TITLE FIGURE *A-1
ARRANGEMENT OF INSULATION LAYERS FOR ENTIRE SYSTEM IN r-θ PLANE

BY	DATE	CHK'D	
APPV'D		SHEET	SHEETS

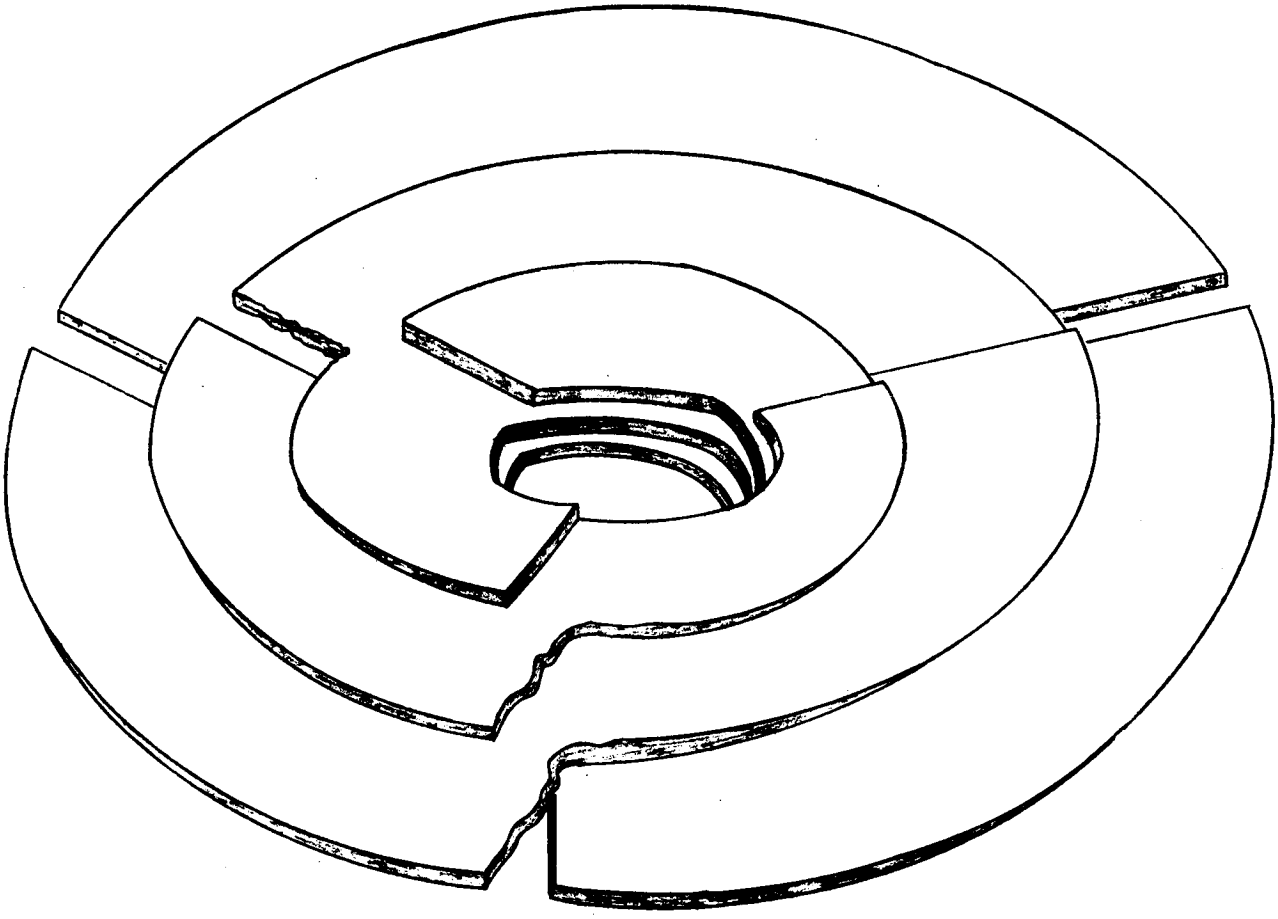

TITLE FIGURE* A-2 POLAR PANEL ARRANGEMENT (CRYOGENIC SURFACE FACING UP)	BY DATE	CHK'D	
	APPV'D	SHEET	SHEETS

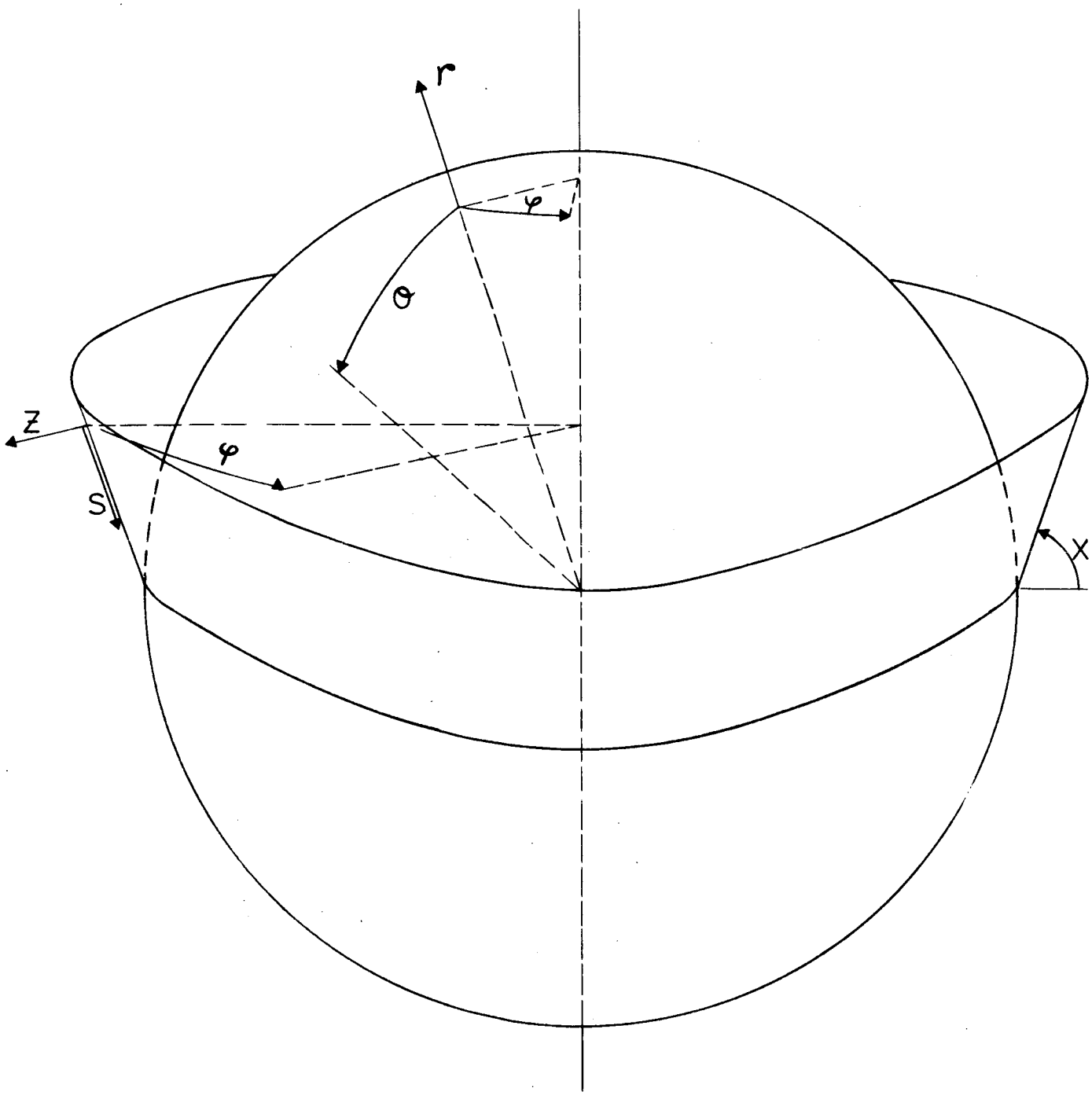

TITLE FIGURE # A-3

DISPLACEMENT COORDINATES FOR SPHERE AND CONE

BY	DATE	CHK'D	
APPV'D		SHEET	SHEETS

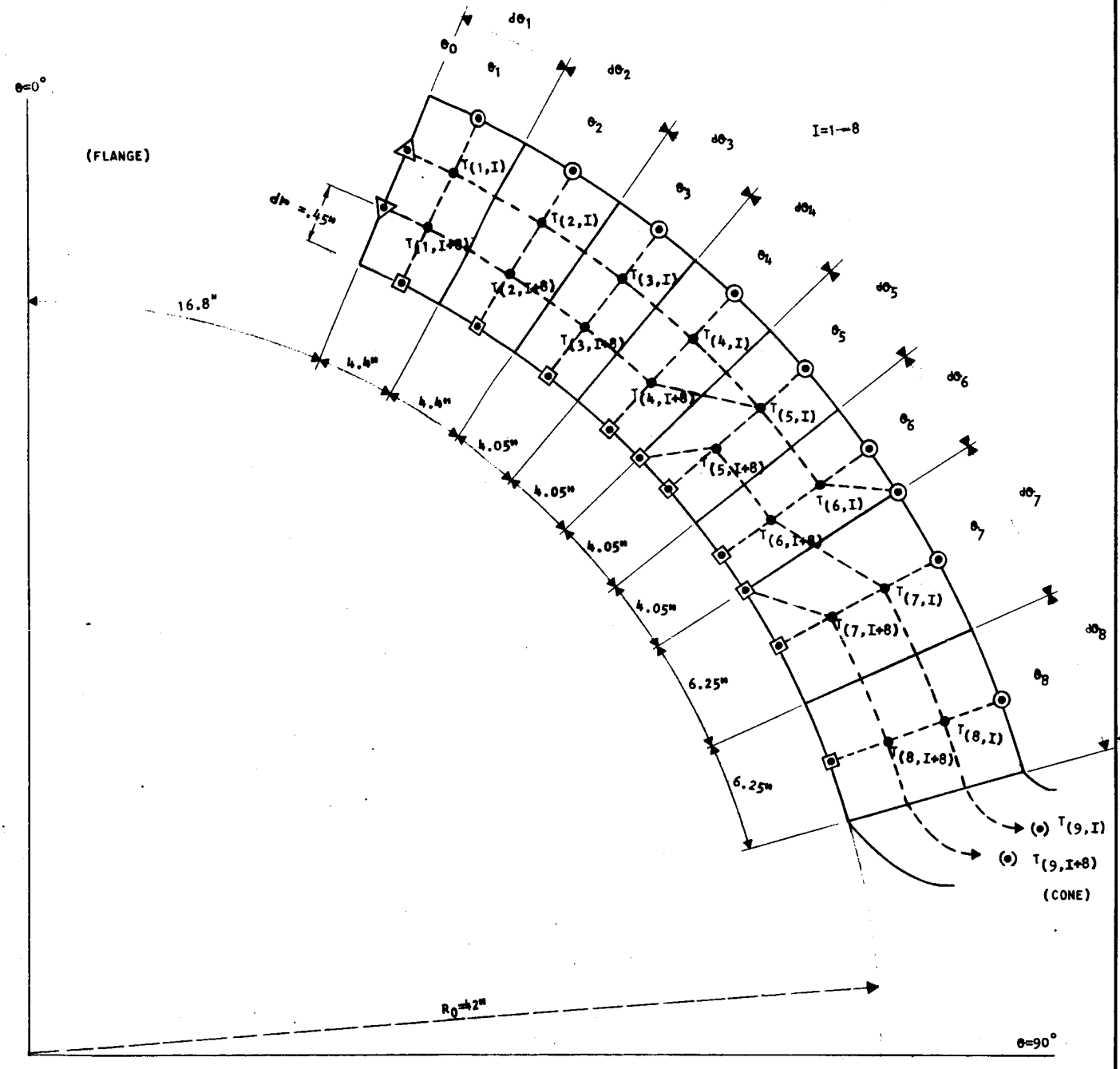

NOTATION

- INCREMENT BOUNDARIES
- HEAT FLOW PATHS
- UNKNOWN TEMPERATURES
- $T = T_W$ (AMBIENT)
- $T = \frac{2}{3} T_W + \frac{1}{3} T_C$
- $T = \frac{1}{3} T_W + \frac{2}{3} T_C$
- $T = T_C$ (CRYOGENIC)
- "PHANTOM" TEMPERATURES

TITLE FIGURE* A-4
INTEGRATION NETWORK IN r-Θ PLANE
(UPPER HEMISPHERE)

BY	DATE	CHK'D	
APPV'D		SHEET	SHEETS

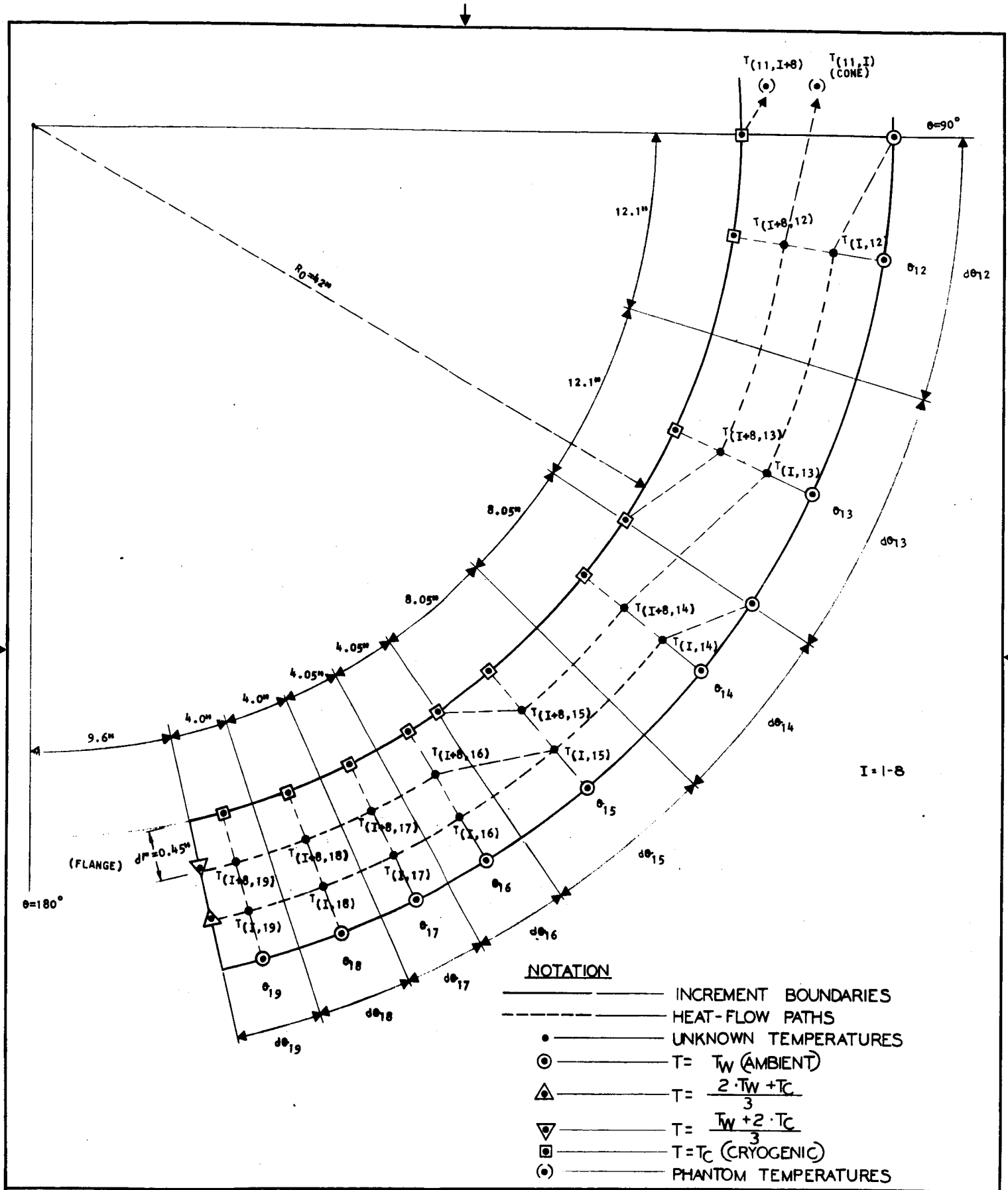

TITLE FIGURE* A-5

INTEGRATION NETWORK IN r-θ PLANE
(LOWER HEMISPHERE)

BY	DATE	CHK'D	
APPV'D		SHEET	SHEETS

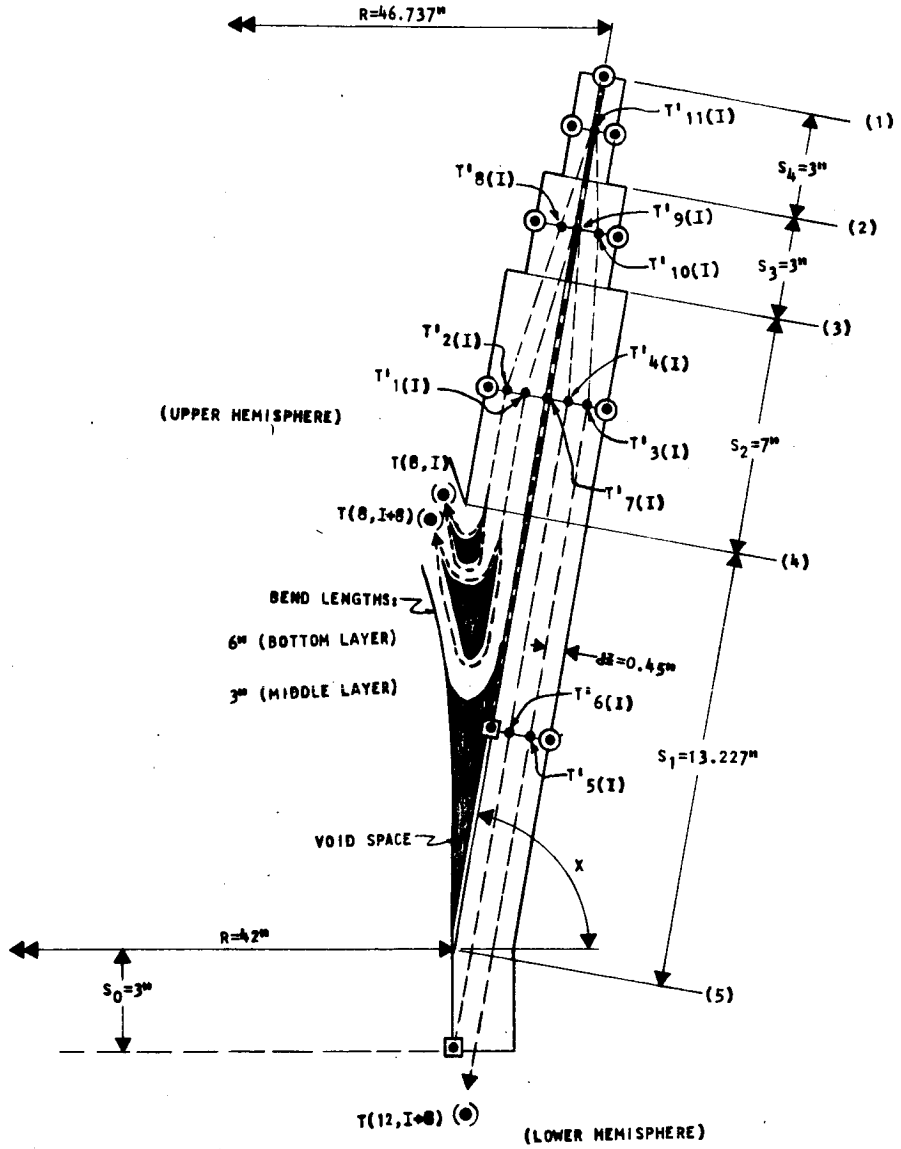

NOTATION

- INCREMENT BOUNDARIES
- HEAT-FLOW PATHS THROUGH INSULATION ONLY
- HEAT-FLOW PATHS THROUGH CONICAL SHELF ONLY
- HEAT-FLOW PATHS THROUGH CONICAL SHELF PLUS ADJOINING INSULATION
- ● UNKNOWN TEMPERATURES
- ◉ $T = T_W$ (AMBIENT)
- ▣ $T = T_C$ (CRYOGENIC)
- (●) "PHANTOM" TEMPERATURES

TITLE FIGURE* A-6

INTEGRATION NETWORK IN S-Z PLANE FOR CONE

BY	DATE	CHK'D	
APPV'D		SHEET	SHEETS

FOR NOTATION: SEE FIGURE #6

A) HEMISPHERE NETWORK -

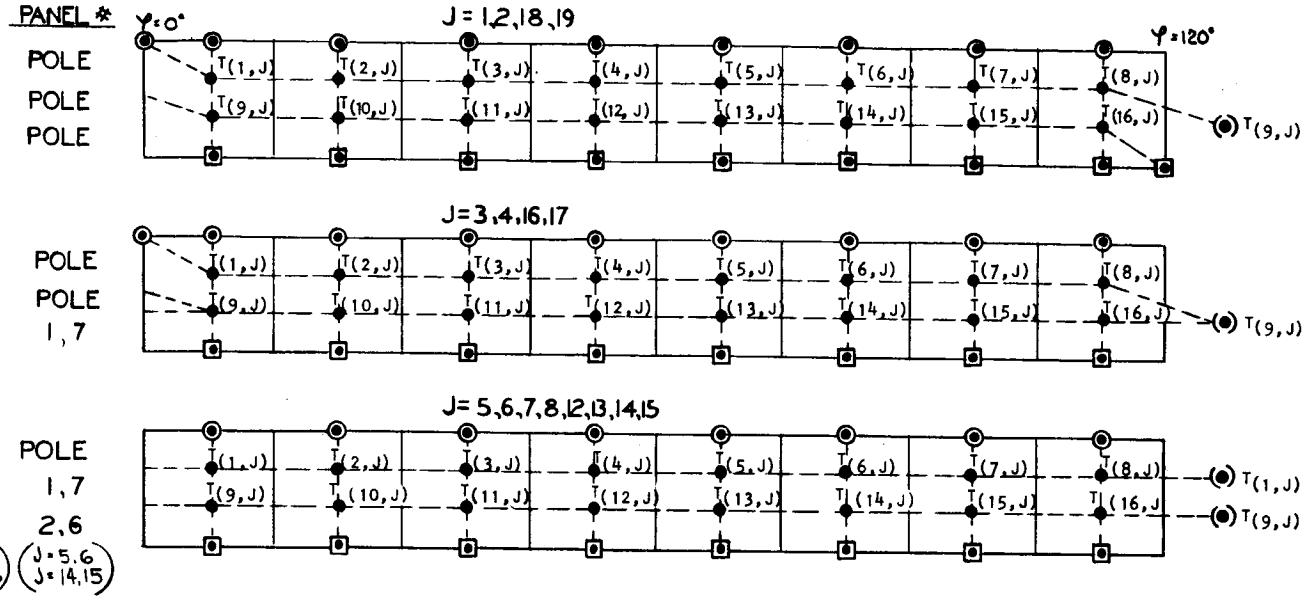

B) CONE NETWORK (MOVING DOWN CONE - TOP SURFACE AT TOP)

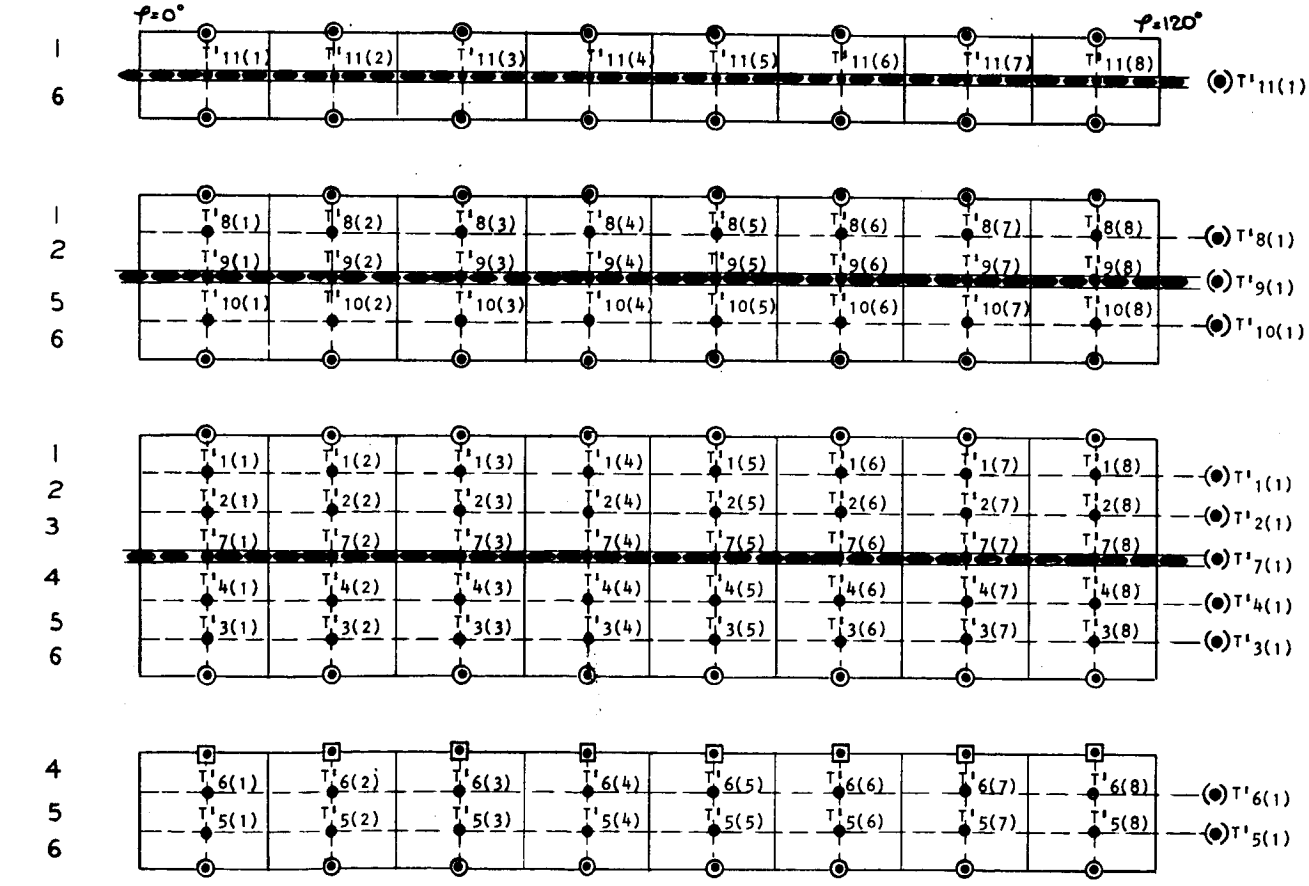

TITLE FIGURE # A-7

INTEGRATION NETWORKS IN r-φ PLANE (FOR BOTH HEMISPHERES) AND IN z-φ PLANE (FOR CONE) (ANGULAR INCREMENT WIDTH = 15°)

BY	DATE	CHK'D	
APPV'D		SHEET	SHEETS

PANELS* 1,3,5,7

$\Phi = 30^\circ$

$\Phi = 60^\circ$

$\Phi = 120^\circ$

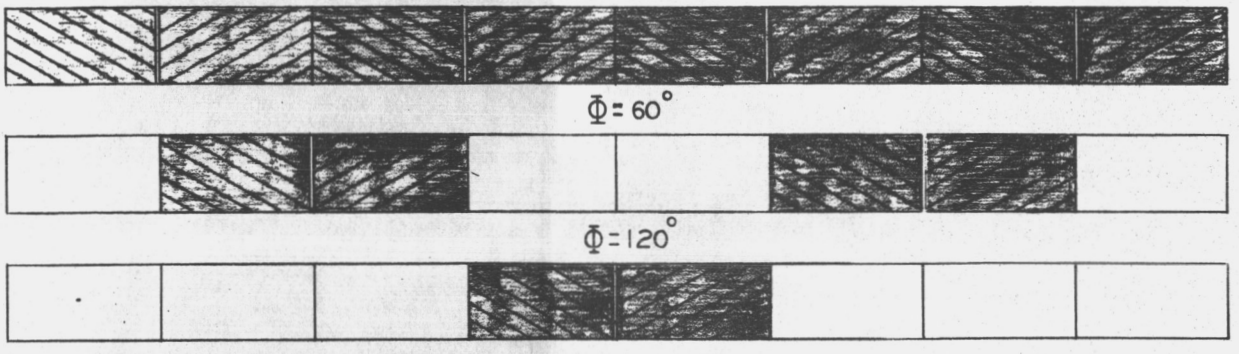

PANELS* 2,4,6

$\Phi = 30^\circ$

$\Phi = 60^\circ$

$\Phi = 120^\circ$

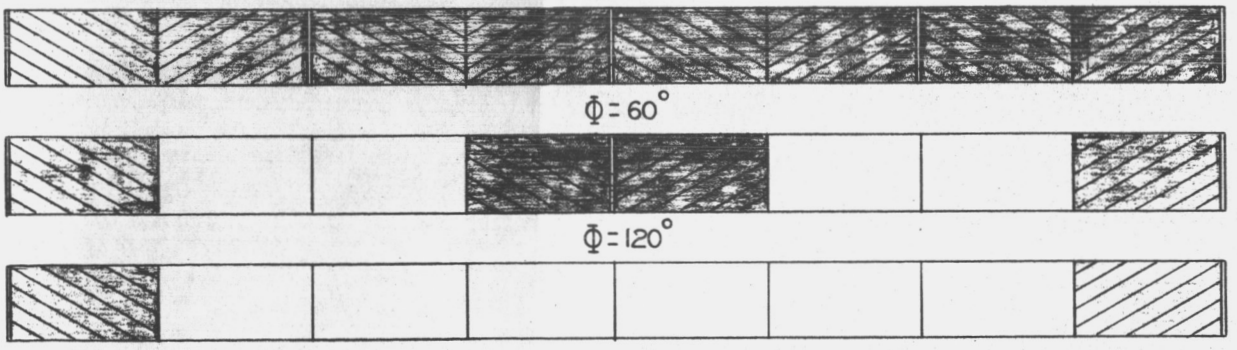

HEAT LEAKS ARE INDICATED BY A DOUBLE LINE. AFFECTED INCREMENTS ARE SHADED.

TITLE FIGURE* A-8
DISTRIBUTION OF VERTICAL PANEL BUTT-JOINT HEAT LEAKS IN r-y (OR z-y) PLANE FOR DIFFERENT VALUES OF ANGULAR PANEL WIDTH Φ

BY DATE	CHK'D	
APPV'D	SHEET	SHEETS

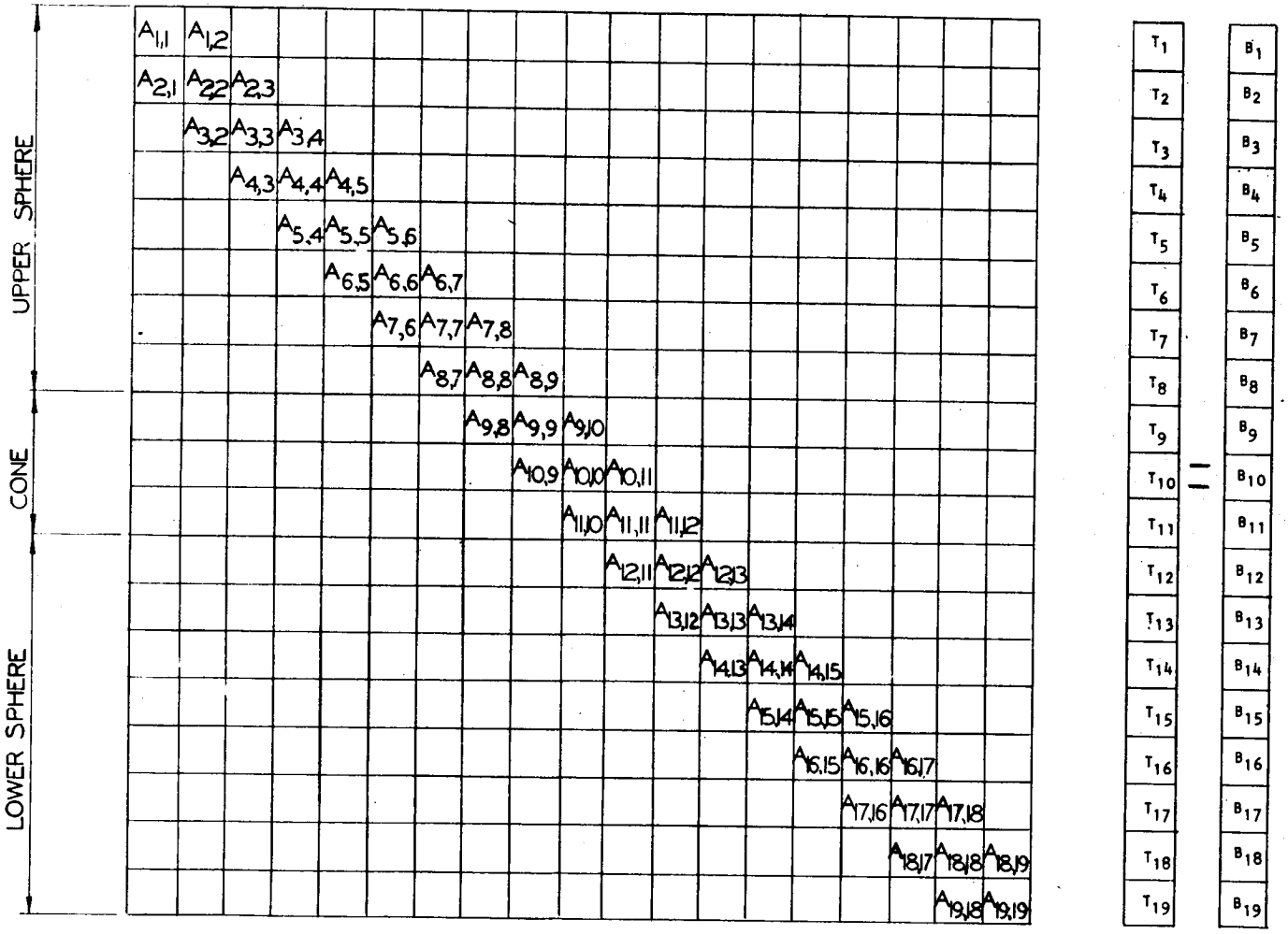

TITLE FIGURE A-9

FORM OF MATRIX EQUATION CORRESPONDING TO REDUCED SET OF DIFFERENCE EQUATIONS (304 IN NO.)

BY	DATE	CHK'D	
APPV'D		SHEET	SHEETS

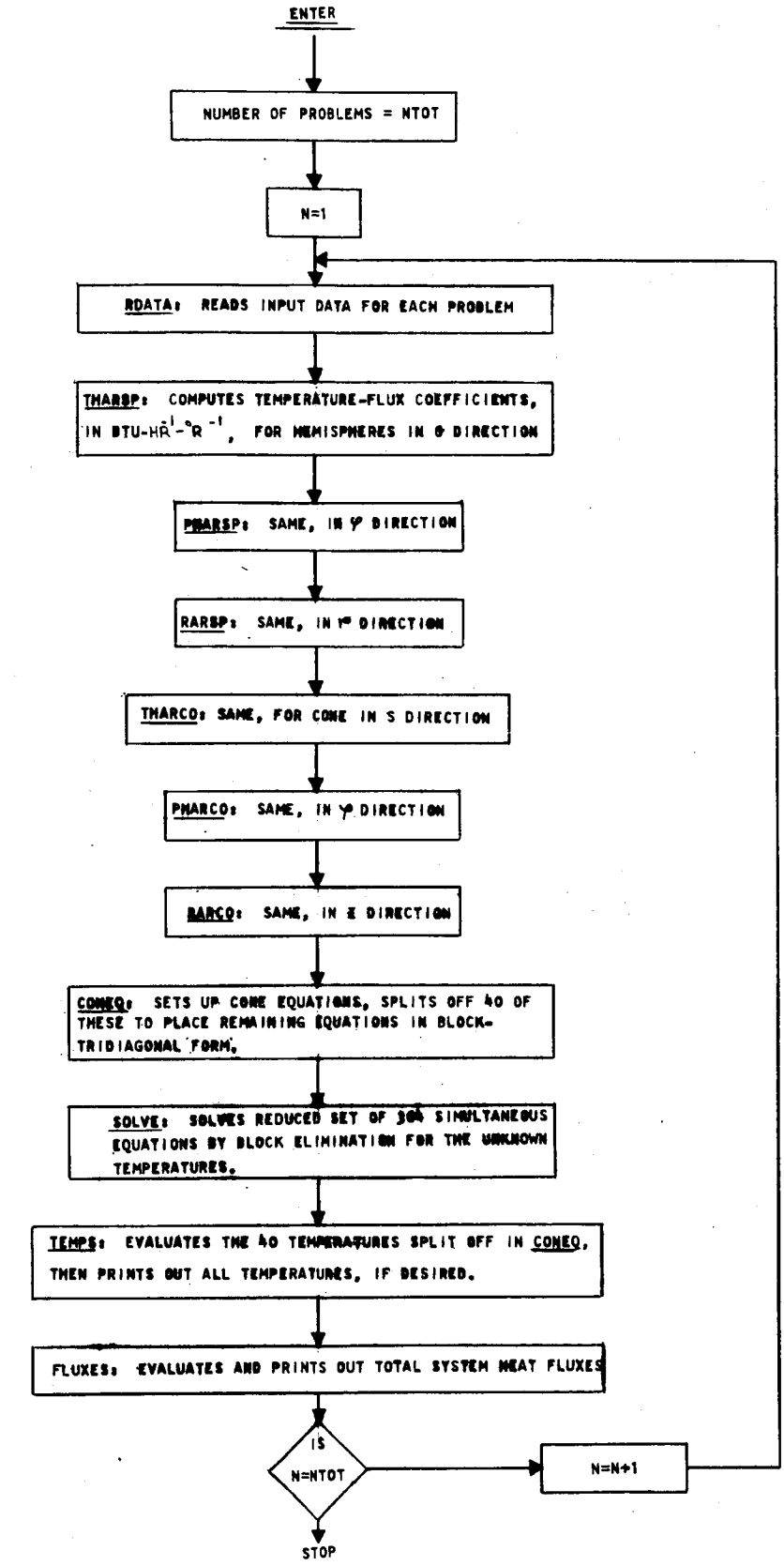

TITLE	BY DATE	CHK'D	
FIGURE* A-10 FLOW DIAGRAM OF MAIN PROGRAM	APPV'D	SHEET	SHEETS

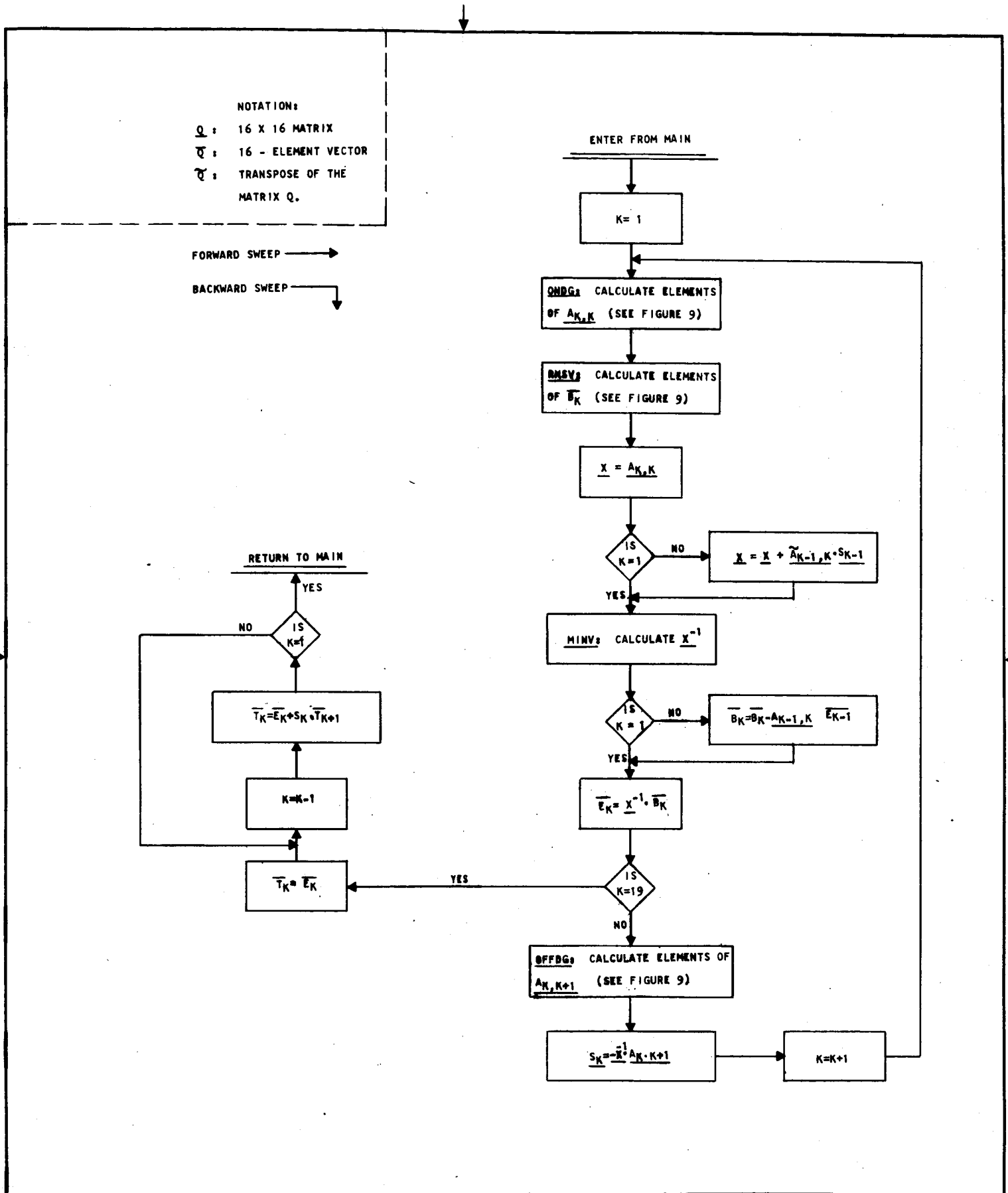

TITLE

FIGURE* A-11

FLOW DIAGRAM OF "SOLVE" SUBROUTINE

BY	DATE	CHK'D	
APPV'D		SHEET	SHEETS